2009

Generic two-phase coexistence in the quadratic contact process

Xiaofang Guo
Iowa State University

Generic two-phase coexistence in the quadratic contact process

by

Xiaofang Guo

A dissertation submitted to the graduate faculty

in partial fulfillment of the requirements for the degree of

DOCTOR OF PHILOSOPHY

Co-majors: Condensed Matter Physics; Applied Mathematics

Program of Study Committee:
Jim Evans, Co-major Professor
Alex Travesset, Co-major Professor
Ryan Martin
Michael Smiley
Edward Yu

Iowa State University

Ames, Iowa

2009

TABLE OF CONTENTS

ABSTRACT

This thesis focuses on the demonstration of the existence of and analysis of phenomena related to the discontinuous non-equilibrium phase transition between an active (or reactive) state and a poisoned (or extinguished) state occurring in a stochastic lattice-gas realization of Schloegl's second model for autocatalysis. This realization, also known as the Quadratic Contact Process, involves spontaneous annihilation, autocatalytic creation, and diffusion or hopping of particles on a square lattice, where creation at empty sites requires a suitable nearby pair of particles. The poisoned state exists for all annihilation rates $p>0$ and is an absorbing particle-free "vacuum" state. The populated active steady state exists just for p below a critical value, p_e. Our initial studies without particle hopping demonstrated a dependence on orientation or slope, S, of the equistability or stationary point $p=p_{eq}(S)$ for a planar interface separating active and poisoned states. They also showed that $p_e = p_{eq}(S=1)$ for diagonal interfaces. This orientation dependence was shown to extend to non-zero hop rates $h>0$, but to quickly weaken with increasing h. If p_f denotes the critical value below which a finite population can survive, then we show that $p_f = p_{eq}(S=0)$ and that $p_f < p_e$. This strict inequality contrasts a postulate of Durrett, and is a direct consequence of the occurrence of coexisting stable active and poisoned states for a finite range $p_f \le p \le p_e$. Although this so-called generic two-phase coexistence (2PC) contrasts behavior in thermodynamic systems. However, one still finds metastability and nucleation phenomena similar to those in discontinuous equilibrium transitions. We also provide a theoretical framework for analysis of such metastability phenomena. Extensions of the basic model are considered to different lattices and to introduce tricritical behavior. Most precise analysis was performed with

kinetic Monte Carlo simulation. However, we also developed exact hierarchical master equations and performed approximate truncation analysis of these equations.

CHAPTER 1. GENERAL INTRODUCTION

Introduction

Non-equilibrium phase transitions have attracted the interest of the statistical physics community for many decades. Lattice-gas (LG) models provide one framework within which to describe and analyze such behavior for non-equilibrium many-particle systems [1]. In many of these models, the spatial structure of the system is described by a lattice (typically, square, triangular, hexagonal or cubic), the sites of which are specified to be in one of two states. Here, we will refer to these states as either occupied or vacant. The evolution of the LG model for a process of interest includes specification of all possible transitions between different configurations of particles on the lattice together with assignment of the associated rates. In the mathematical statistics community, such models are called Interacting Particle Systems (IPS), and they correspond to stochastic Markov processes for evolution between different possible configurations of the system [2]. Behavior for an infinite lattice is typically of primary interest. However, in order to analyze model behavior by computer simulation, it is necessary to use a finite lattice and invariably periodic boundary are imposed to minimize edge effects.

Specification of the evolution of stochastic spatial models for non-equilibrium processes often is not based on a Hamiltonian and may incorporate irreversible steps [3]. Thus, the microscopic rates governing evolution are not constrained by detailed-balance conditions. Such conditions are based on first specifying a Hamiltonian describing the energy of all possible configurations of the system. Then, the ratio of the rates for forward and reverse processes is determined by the energy difference between initial and final states.

Significantly, in part due to the lack of this detailed-balance constraint, these non-equilibrium models can display a richer variety of spatiotemporal behavior than traditional Hamiltonian systems. Such models have been broadly applied in describing dynamics and pattern formation in systems including, i.e., adsorption-desorption phenomena, chemical reactions, population dynamics, spread of epidemics or information, and other ecological and sociological phenomena [1, 3-6].

A specific feature of non-equilibrium models is the possible occurrence of "absorbing states" (using the language of Markov processes) from which the system can never escape [1, 3, 5, and 7]. One example is for a reaction model where particle can spontaneously annihilate at some specified rate, p, but are also created autocatalytically in the presence of another nearby particle or particles. For this system, it is clear that the particle-free "vacuum" state is an absorbing state (since it is impossible to create particle without preexisting particles). A related example is for epidemic models where sick individuals recover at a specified rate, r, but healthy individuals are infected by sick neighbor(s). Here, it is clear that the completely healthy population is an absorbing state.

In addition, the steady-states of such non-equilibrium models often exhibit continuous (second-order) and discontinuous (first-order) phase transitions as some control parameter is varied, which are similar to the very familiar equilibrium phase transitions in Hamiltonian systems [1, 3, 5, and 7]. For continuous non-equilibrium transitions, this analogy has been explored in most detail. In fact, the concept of universality carries over from equilibrium transitions: universality mean that fundamental features of behavior near the transition are independent of the details of the model (i.e., they are the same or "universal" for a broad class of models). A robust universality class for continuous non-equilibrium transitions to

absorbing states (described above) has been identified. Technically, this is described as the universality class of directed percolation or Reggeon field theory [3, 5, and 7].

To provide two examples, consider the reaction and epidemic models above. For the reaction model, one can imagine that the reaction is extinguished (and the system is particle-free) when the particle annihilation rate exceeds a critical value p_c. If the model exhibits a continuous transition to this extinguished state, one anticipates that the steady-state particle concentration has the form $C \sim (p_c - p)^{\beta 1}$ as p approaches p_c from below. For $p>p_c$, the system always evolves to the vacuum absorbing state with C=0. For the epidemic model, one can imagine that the epidemic always dies out recover rate exceeds a critical value r_c. If the model exhibits a continuous transition to the completely healthy state, one anticipates that the steady-state fraction of sick individuals has the form $S \sim (r_c - r)^{\beta 2}$ as r approaches r_c from below. However, both models lie the directed percolation universality class, and one finds that $\beta_1 = \beta_2 \approx 0.583$ [1].

Less attention has been paid to discontinuous non-equilibrium transitions for which universality does not apply [8-13]. Perhaps the most extensive studies have been for two-component or three-state reaction models (see below), including the Ziff-Gulari-Barshad (ZGB) model [8], which do display discontinuous transitions. The ZGB model is introduced by Ziff, Gulari, and Barshad in 1986 to mimic the oxidation of carbon monoxide (CO) on a catalytic surface, and it is often described as a monomer-dimer surface reaction model. The model involves the following steps: random adsorption of monomers (representing CO) at single empty sites of a two-dimensional lattice (d=2); random adsorption of dimers (representing O_2) at neighboring empty pairs of sites followed by immediate dissociation into constituent atoms residing on these two sites; and irreversible reaction of adjacent adsorbed

monomer species (CO) and atoms from the dissociated dimer species (O) to form the product (CO_2). Thus the two-components on the surface are CO and O, and the three possible states of surface sites are: (i) occupied by CO; (ii) occupied by O; (iii) unoccupied or empty. Specifically, with increasing CO adsorption rate (or CO partial pressure above the surface), the ZGB model exhibits a discontinuous transition from an active (i.e., reactive) state with a non-zero production rate for CO_2 to an absorbing or poisoned state [8], in which the surface is completely covered or saturated by CO.

Various related phenomena for this non-equilibrium transition have been analyzed in some detail: the steady-state coverage versus partial pressure including the pressure at the discontinuous poisoning transition [8]; propagation and fluctuation behavior of interfaces separating active and CO-poisoned states [8,10,11]; “epidemic properties” related to the survival of an active or reactive “droplet” (i.e., compact region of the active state) embedded in the CO-poisoned absorbing state [9, 12]; and nucleation of droplets of the CO-absorbing state within the metastable reactive state and associated metastability phenomena [10, 13]. Some features of observed behavior are unusual for a discontinuous transition [4], and likely reflect the presence of a weak line tension at the interface between reactive and absorbing states. (Recall that discontinuous equilibrium transitions are always associated with a finite line tension in 2D or surface tension in 3D at interface separating the two coexisting states.) Such simple ZGB-type models are invaluable for elucidating basic issues associated with non-equilibrium phase transitions in reaction systems.

Single-component models (in which the system includes only one type of particle) are even simpler and perhaps more convenient for exploring fundamental issues for discontinuous non-equilibrium transitions. The single-component Bidaux-Boccara-Chaté

(BBC) model [14] is a probabilistic synchronous cellular automaton in which the state of all sites is updated simultaneously at discrete time steps. The state of site x at time t+1 depends on the number of occupied sites in the set comprising x and its eight closest neighbors at time t based on some stochastic rule [14]. The transition in the BBC is discontinuous in $d \geq 2$ dimensions, but continuous for d=1 [1]. Another single-component model is the so-called triplet creation model [15]. Here particles spontaneously annihilate, but are also created autocatalytically in the presence of three nearby particles (a triplet). This triplet creation model may provide an example of a model with a discontinuous transition for d=1 at least for sufficiently rapid particle hopping.

Perhaps, the single-component reaction model considered most often in the context of discontinuous phase transitions is Schloegl's second model (Schloegl 1972). More general versions of Schloegl-type models associated with autocatalytic kinetics [16], when traditionally formulated at the mean-field level, provide classic examples of bifurcation behavior and of synergetics (i.e. spatio-temporal behavior) [17]. Schloegl's first model for autocatalysis in a reactive system of particles, X, includes the following steps: $X \leftrightarrow 2X$ (autocatalytic reaction of a particle by a nearby existing particle), $X \rightarrow \varnothing$ (spontaneous annihilation) and possibly particle diffusion. For this model, the mean-field kinetics is quadratic leading to a continuous transition to the particle-free vacuum steady-state state. Schloegl's second model includes the following steps: $2X \leftrightarrow 3X$ (autocatalytic reaction of particle by a nearby existing pair of particles), $X \rightarrow \varnothing$ (spontaneous annihilation) and possibly particle diffusion, for which the mean-field kinetics is cubic suggesting a discontinuous transition (at least in the presence of fluctuations or in a lattice-gas model realization).

The behavior of lattice-gas versions or realizations of these non-equilibrium reaction models can be rigorously formulated in terms of master equations for the evolution of the probabilities of various configurations. Typically, it is impossible to solve these equations exactly with analytic methods. However, an analytic treatment of model behavior can be developed based on truncation approximations to the exact master equations. The simplest approximation is mean-field site approximation which ignores all spatial correlations. This approximation could be interpreted as describing the exact behavior of the models with particle hopping to nearest-neighbor (NN) empty sites at rate h in the limit $h \to \infty$, since such hopping "stirs" the system destroying spatial correlations. In the pair approximation, one factorizes probabilities for the multi-site configurations into products of probabilities for the constituent pairs, and divides by single-site probabilities for sites shared by the pairs (to avoid over counting). One retains equations for both single-site and pair probabilities and in this way accounts to some extent for correlations between neighboring sites. These two approximations can reveal qualitative features of exact model behavior.

Kinetic Monte Carlo (KMC) simulation is the most common tool for precise analysis of non-equilibrium LG models. This approach uses a random number generator to select and implement various processes with the appropriate relative weights thereby generating evolution of the model through specific sequence configurations [18]. In this dissertation, we perform a KMC simulation analysis for models defined on a rectangular-shaped ($L_x \times L_y$) site square lattice with periodic boundary conditions. The latter limit "edge effects" and allow assessment of behavior for an infinite lattice provided that L_x and L_y are chosen moderately large. Two kinds of simulation: constant-p (CP) simulation and constant-coverage (CC) simulation [19] are adopted for analysis (in the context of models involving

adsorption-desorption or annihilation-creation of particles). In a constant-pressure simulation algorithm, one specifies an adsorption (or annihilation) rate p and runs simulation to implement adsorption (or annihilation), desorption (or creation) and diffusion with the appropriate relative rates to determine both the dynamics and the steady-state behavior. In CC simulations, one specifies a target coverage θ (or concentration C) and then runs the simulation attempting to adsorb or desorb (annihilate or create particles) if the actual coverage (concentration) is below or above the target θ (C), respectively. The adsorption rate $p = p(\theta)$ (annihilation rate $p=p(C)$) is the fraction of adsorption (annihilation) attempts. For a sufficiently large system, these two simulation processes should be equivalent.

In this dissertation, we consider various realizations of Schloegl's second model for the evolution of particle populations on a square lattice (d=2) to analyze the behavior of discontinuous non-equilibrium phase transitions. In the first realization, one can use the language of adsorption-desorption of particles on a square lattice, the following steps are involved [3, 20]: random adsorption of particles at empty sites at a rate or "pressure" p; cooperative desorption of particles at rate k/4 where k = 0, 1, 2, or 4 denotes the number of *diagonally adjacent pairs of NN empty sites*. Thus, one has: k=0 for particles with just 0 or 1 empty NN sites, and also for 2 empty NN sites which are on opposite sides of the particle; k=1 for particles with just 2 diagonally adjacent empty NN sites; k=2 for particles with 3 empty NN sites; and k=4 for particles with all 4 NN sites empty. See Fig.1. We use this realization in Chapters 2 and 3.

In the second realization for Schloegl's second model is formulated in terms of the spontaneous annihilation and autocatalytic creation of particles. This realization interchanges the role of particles and vacancies from that in the above description of adsorption-desorption

model. This realization on a square lattice as a stochastic Markov process involves the following components: **(i)** spontaneous particle annihilation occurring randomly at rate p; **(ii)** autocatalytic particle creation at an empty site requiring one or more diagonally adjacent pairs of occupied sites; specifically, the creation rate is given by k/4, where k is the number of such diagonally adjacent occupied pairs and thus can take the values k = 0, 1, 2,or 4; **(iii)** hopping of particles to any adjacent empty sites at rate h (per target site), a third process which could also be added in the adsorption-desorption realization. See **Fig.2** for a schematic of these processes. We use this realization in Chapters 4, 5, and 6.

In a third realization, Schloegl's second model is regarded as a spatial "contact processes" which can describe the spread of disease (or information) by nearest-neighbor interaction between individuals distributed on a square lattice of site [1, 3]. This realization is most commonly referred to as the Quadratic Contact Processes (QCP). Individuals at each site of the lattice are either sick or healthy. Sick individuals recover spontaneously at a fixed rate and healthy individuals are infected by diagonal pairs of sick neighbors (an "autocatalytic" process) at rates which can be deduced from the above realizations. Thus, the sick (healthy) state corresponds to vacancies or empty sites (particles or filled sites) in the first adsorption-desorption realization, whereas the opposite is true for the second reaction model realization.

Our studies of the above realizations of the QCP or Schloegl second model reveal the feature of generic two-phase coexistence (2PC) or true bistability [21], which means the coexistence of stable active and absorbing states occurring for a finite range of "pressure" parameter, p. This dramatically contrasts behavior for discontinuous equilibrium transitions where coexistence can only occur at a single value of the relevant parameter p

(corresponding to equality of chemical potentials of the two phases). For the QCP, 2PC can be understood in terms of an orientation dependence of propagation, and specifically of the pressure for equistability or stationarity, of planar interfaces separating active and absorbing states [22]. Perhaps the classic example of such a 2PC phenomenon is provided by Toom's synchronous North-East-Center (NEC) stochastic cellular-automata "voting" model [23-26]. In this model, an array of voters on a square grid chooses one of two parties. Votes are updated synchronously at discrete times based on the votes of selected neighbors those to the north (N) and east (E) or the center (C) site under consideration. However, this model introduces an explicit artificial asymmetry in to dynamic voting rules (favoring north and east over south and west neighbors) which helps induce generic two-phase coexistence. In this respect, our realization of the QCP or of Schloegl's second model is more appealing example of this fundamental non-equilibrium phenomenon since there is no artificial asymmetry in the rates.

Thesis Organization

The main body of this Dissertation is based on three published papers (Chapters 2, 3, and 4), and two additional manuscripts (Chapters 5 and 6) which are to be submitted in 2009. A fourth published Letter is not included as it constitutes a condensed version of the material in Ch.2. Additional publications should also result from the material in the appendices.

Chapter 2 reprints the published paper *"Generic two-phase coexistence, relaxation kinetics, and interface propagation in the quadratic contact process: Simulation studies"*, by *X. Guo, D.-J. Liu and J.W. Evans in Physical Review E 75 (2007) 061129*. This paper gives a detailed description and analysis of the first adsorption-desorption realization of the QCP

model on a square lattice, noting a special feature of the dynamics in this model in the absence of particle hopping. It also specifies in detail the kinetic Monte Carlo simulation procedures including constant-p and constant-coverage (CC) simulations. The steady-state behavior for the model, specifically generic two-phase coexistence, is characterized. Simulation results for the kinetics of relaxation to the steady states of the QCP for spatially homogeneous systems are also given.

Further, an "effective" spinodal point terminating a metastable active state for pressures above the two-phase coexistence region is identified, and "rapid" relaxation or poisoning kinetics for pressures above this spinodal pressure are described. This paper also gives analysis of slower nucleation-mediated relaxation or poisoning for pressures in the metastable region below this spinodal but above the PC region, and elucidates the dynamics of poisoned droplets within the two-phase coexistence region. For lower pressures below the two-phase coexistence region, some unusual aspects of relaxation kinetics are elucidated by making a connection to bootstrap percolation models. In addition, the propagation of interfaces with various orientations between the absorbing and active states in spatially inhomogeneous systems is analyzed. The dependence of propagation and equistability on interface orientation underlies the generic two-phase coexistence in the QCP. A condensed version of this study has also been published as *"Quadratic Contact process: Phase-separation with Orientation-dependent Equistability"* by *D.-J. Liu, X. Guo, and J.W. Evans in Physical Review Letters 96 (2007) 050601*.

Chapter 3 reprints the published paper *"Generic two-phase coexistence, relaxation kinetics, and interface propagation in the quadratic contact process: Analytic studies"*, by *X. Guo, J.W. Evans, and D.-J. Liu in Physica A 387 (2008) 177-201*. In this paper, the

hierarchical form of the exact master equations and appropriate truncation approximations for spatially homogeneous states of the QCP are developed. Corresponding predictions for steady-states and kinetics from analytic studies are compared with results from KMC simulations. Further, this analytic treatment is used to treat the spatially non-uniform states. The primary focus is on analysis of the propagation of planar interfaces separating the active and absorbing states for various orientations. In particular, we determine the orientation-dependence of the equistability pressure. We also consider planar perturbations of the active state and determine the critical form of such perturbations above which they grow. In addition, the dynamics of two-dimensional droplets of one phase embedded in the other is explored.

Chapter 4 reprints the published paper *"Schloegl's second model for autocatalysis with particle diffusion: Lattice-gas realization exhibiting generic two-phase coexistence"*, by *X. Guo, D.-J. Liu and J.W. Evans in the Journal Chemical Physics 130, (2009) 074106*. In this paper, we specify the second reaction model realization of Schloegl's second model with particle hopping on a square lattice, as well as outlining related fundamental concepts. We also review previous results for this model in the limiting cases of zero and infinite particle diffusion. We analyze the steady states and their relative stability which leads to a characterization of the discontinuous phase transition in this model and demonstrates the so-called generic two-phase coexistence. We also analyze key aspects of the kinetics elucidating metastability associated with this transition. Generic two-phase coexistence in this model is again tied to an orientation-dependence of the equistability of planar interfaces separating the active and poisoned states. Thus, we are motivated characterize both interface structure and propagation. Exploiting these insights, we present a droplet analysis in order to characterize

both phase stability in generic two-phase coexistence regime and the size and structure of critical droplets in the metastable regime.

Chapter 5 corresponds to the unpublished manuscript "Metastability in Schlogel's second model for autocatalysis: lattice-gas realization with particle diffusion" which we plan to submit for publication to Physical Review E in 2009. This work constitutes a more detailed study of metastability already considered in Chapter 4 for Schloegl's second model with particle hopping. However, Chapter 5 considers larger hops rate and applies both KMC simulation and an analytic approximation. Specifically, we provide a more accurate assessment of the location of ps+ by characterizing the associated poisoning kinetics and interface propagation behavior.

Chapter 6 corresponds to the unpublished manuscript *"Tricritical behavior in a hybrid of standard and quadratic contact process models"* which we also plan to submit for publication to Physica A in 2009. The key strategy here is to explore "perturbations" of the quadratic contact process associated with incorporating or "mixing in" a component of the standard contact process mechanism. Since the former exhibits a discontinuous transition and the latter a continuous transition, one could imagine conversion from a discontinuous to a continuous transition with an increasing relative contribution from the standard contact process. Such a conversion corresponds to a non-equilibrium tricritical point where one might expect unique scaling behavior. We show that this tricritical point does exist and analyze the associated scaling.

At the end of this dissertation, several appendices are included presenting additional analysis and results. Appendix A provides a finite-size scaling analysis for the QCP with particle hopping to assess the dependence of simulation results on system size. For

comparison with our analysis of non-equilibrium models, Appendix B presents pair-approximation analysis for interface evolution in a LG realization of the equilibrium 2D Ising model with Glauber or adsorption-desorption dynamics. Appendix C provides some additional results (supplementing Chapter 5) from our KMC simulation and from analysis of the pair approximation for the QCP with particle hopping. Appendix D provides some additional results (supplementing Chapter 6) of our analysis of tricritical behavior in a generalized Schloegl model. Appendix E provides an analysis based on the site approximation of critical droplets and related phenomena for Schloegl's second model. Appendix F presents some basic analysis of Schloegl's second model for autocatalysis on various lattices, and well as of a modified model.

References

[1] J. Marro and R. Dickman, *Nonequilibrium phase transitions in lattice models* (Cambridge UP, Cambridge, 1999).
[2] T.Liggett, *Interacting Particle Systems*, Springer-Verlag, Berlin, 1985.
[3] R. Durrett, SIAM Rev. **41**, 677 (1999).
[4] E. Loscar and E.V. Albano, Rep. Prog. Phys. **66**, 1343 (2003).
[5] H. Hinrichsen, Adv. Phys. **49**, 815 (2000).
[6] J.D. Gunton, M.S.Miguel, and P.S. Sahni, *phase Transitions and critical Phenomena* (Academic, New York, 1983), Vol. 8.
[7] G. Odor, Rev. Mod. Phys. **76**, 663 (2004).
[8] R.M. Ziff, E. Gulari, and Y. Barshad, Phys. Rev. Lett. **56**, 2553 (1986).
[9] J.W. Evans and M.S. Miesch, Phys. Rev. Lett. **66**, 833 (1991).
[10] J.W. Evans and T.R. Ray, Phys. Rev. E **50**, 4302 (1994).
[11] R. H. Goodman, D. S. Graff, L. M. Sander, P. Leroux-Hugon, and E. Clément Phys. Rev. E **52**, 5904 (1995).
[12] R.A. Monetti and E.V. Albano, J. Phys. A **34**, 1103 (2001).
[13] E. Machado, G.M. Buendia, and P.A. Rikvold, Phys. Rev. E **71**, 031603 (2005).
[14] R. Bidaux, N. Boccara, and H. Chaté, Phys. Rev. A **39**, 3094 (1989)
[15] R. Dickman and T. Tomé, Phys. Rev. A **44**, 4833 (1991).
[16] F. Schloegl, Z. Phys. **253**, 147 (1972).
[17] A.L. Mikhailov, *Foundations of Synergetics I* (Springer-Verlag, Berlin, 1990).
[18] D.P. Landau and K. Binder, *A Guide to Monte Carlo Simulations in Statistical physics*, Cambridge UP, Cambridge, 2000

[19] R.M. Ziff and B.J. Brosilow, Phys. Rev. A **46**, 4630 (1992).
[20] D.-J. Liu, Xiaofang Guo, and J.W. Evans, Phys. Rev. Lett. **98**, 050601 (2007).
[21] M.A. Munoz, F. de los Santos, and M.M.T. da Gama, Euro. Phys. J. B **43**, 73 (2005).
[22] P. Grassberger, Z. Phys. B Cond. Matt. **47**, 365 (1982).
[23] A.L. Toom, in *Multicomponent random systems*, edited by R.L. Dobrushin and Y.G. Sinai Marcel Dekker, New York, 1980).
[24] C.H. Bennett and G. Grinstein, Phys. Rev. Lett. **55**, 657 (1985).
[25] G. Grinstein, IBM J. Res. & Dev. **48**, 5 (2004).
[26] Y. He, C. Jayaprakash, and G. Grinstein, Phys. Rev. A **42**, 3348 (1990).

Figures

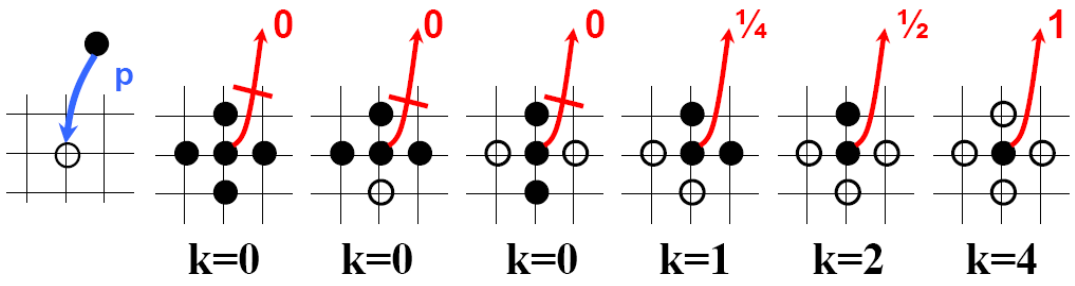

Figure 1. Schematic of desorption rules and rates in the adsorption-desorption model realization of the QCP. Solid (open) circles denote particles (empty sites) on the square lattice. Description rates (k values) for the central particle are indicated above (below) the various configurations.

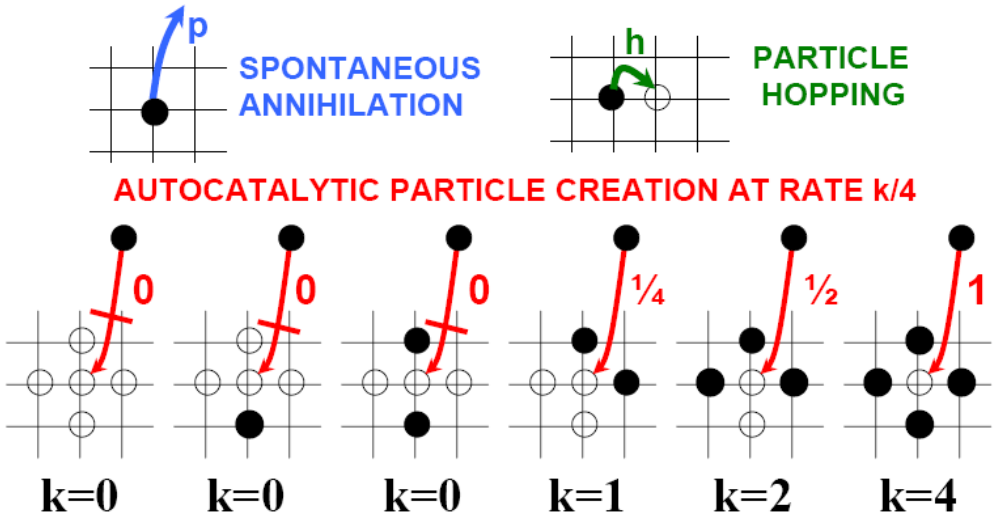

Figure 2. Schematic of particle annihilation, autocatalytic creation, and hopping processes in Schloegl's second model or the QCP on a square lattice. Here particles are denoted by filled circles (•) and empty sites by open circles (o). Rates for the various processes are also indicated, and the bar through the arrow indicates that the process is not allowed.

CHAPTER 2. GENERIC TWO-PHASE COEXISTENCE, RELAXATION KINETICS, AND INTERFACE PROPAGATION IN THE QUADRATIC CONTACT PROCESS: SIMULATION STUDIES

A paper published in Physical Review E[1]

Xiaofang Guo[2, 3, 4], Da-Jiang Liu[2], and J.W. Evans[2, 4]

[2]Ames Laboratory, USDOE, Iowa State University, Ames, Iowa 50011

[3]Department of Physics and Astronomy, Iowa State University, Ames, Iowa 50011

[4]Department of Mathematics, Iowa State University, Ames, Iowa 50011

Abstract

The quadratic contact process is formulated as an adsorption-desorption model on a two-dimensional square lattice. It involves random adsorption at empty sites and correlated desorption requiring *diagonally adjacent pairs of empty neighbors*. We assess model behavior utilizing kinetic Monte Carlo simulations. One finds generic two-phase coexistence between a low-coverage active steady-state and a completely covered or "poisoned" absorbing steady-state, i.e., both states are stable over a finite range of adsorption rates or "pressures". This behavior is in marked contrast to that for equilibrium phase separation. For spatially homogeneous systems, we provide a comprehensive characterization of the kinetics of relaxation to the steady-states. We analyze rapid poisoning for higher pressures above an effective spinodal point terminating a metastable active state, nucleation-mediated poisoning in the metastable region, the dynamics of poisoned droplets within the two-phase coexistence

region, and behavior reminiscent of bootstrap percolation dynamics for lower pressures. For spatially inhomogeneous systems, we analyze the propagation of planar interfaces between active and absorbing states, fully characterizing an orientation-dependence which underlies the generic two-phase coexistence.

PACS 05.70.Fh, 05.50.+q, 02.50.Ey

I. Introduction

Stochastic spatial models for far-from-equilibrium processes incorporating irreversible steps [1] can display a richer variety of spatiotemporal behavior than traditional Hamiltonian systems where microscopic transition rates are constrained to satisfy detailed-balance. One example of a feature specific to non-equilibrium systems is the occurrence of absorbing states, using the parlance of Markov processes, from which the system can never escape [1-4]. Nonetheless, more generally, the steady-states of such non-equilibrium models often exhibit continuous (second-order) and discontinuous (first-order) phase transitions which appear analogous to equilibrium phase transitions in Hamiltonian systems [1-4]. Most effort towards exploring this analogy has focused on continuous non-equilibrium transitions where the concept of universality carries over from equilibrium transitions. In fact, a robust universality class for continuous transitions to non-degenerate absorbing states has been identified as that of directed percolation or Reggeon field theory [2-4].

For non-equilibrium processes, less attention has been paid to discontinuous transitions where universality does not apply [5-11]. However, one such well-known example is provided by the two-component Ziff-Gulari-Barshad (ZGB) model for a monomer-dimer surface reaction [5]. This ZGB model includes the following steps: random

adsorption of monomers at single empty sites of a two-dimensional lattice (d=2); dissociative adsorption of dimers at empty pairs of sites; and irreversible reaction of adjacent monomer and dimer species. In this model, a discontinuous transition from an active (i.e., reactive) state to a monomer-poisoned absorbing state occurs for sufficiently high monomer adsorption rate or "partial pressure" [5]. Various phenomena related to this non-equilibrium transition have been analyzed in some detail: the steady-state coverage versus partial pressure including the pressure at the discontinuous poisoning transition [5]; propagation and fluctuation behavior of interfaces between active and poisoned states [5,7,8]; epidemic properties related to an active droplet embedded in the monomer-poisoned absorbing state [6,9]; and nucleation of droplets of the absorbing state within the metastable active state and associated metastability phenomena [7,11]. Some features of observed behavior are unusual for a discontinuous transitions [10] (e.g., apparent algebraic scaling of epidemic properties [6]), and likely reflect the presence of a weak line tension at the interface between active and absorbing states. We explore this latter issue elsewhere [12].

To facilitate a fundamental understanding of discontinuous non-equilibrium transitions, it is more convenient and natural to search for and analyze single-component models with the desired behavior (as an alternative to further analysis of the more complex two-component ZGB model). Such simpler single-component models which purportedly exhibit discontinuous transitions in low-dimensions have also been developed and analyzed previously. The so-called Bidaux-Boccara-Chaté model [13] is a probabilistic cellular automata which exhibits a discontinuous transition in $d \geq 2$ dimensions, but not for d=1 [2]. The so-called triplet creation model [14] was developed to provide an example of a model with a discontinuous transition for d=1 at least for sufficiently rapid particle hopping. The

issue of existence of this discontinuous transition in this model has also been addressed in more recent studies [15]. Schloegl's second model for autocatalysis, described in more detail below, provides another example of a single-component model designed with the potential to exhibit a discontinuous transition.

There has been considerable interest in the class of Schloegl-type models associated with autocatalytic kinetics [16], where mean-field versions provide classic examples of bifurcation behavior and synergetics [17]. Special cases of this kinetics are as follows: $X \leftrightarrow 2X$ and $X \rightarrow \varnothing$ for Schloegl's first model, and $2X \leftrightarrow 3X$ and $X \rightarrow \varnothing$ for Schloegl's second model, where X denotes a particle (so, e.g., $X \rightarrow \varnothing$ represents particle annihilation). The mean-field kinetics are quadratic for the first model suggesting a continuous transition to the vacuum state, and cubic for the second model suggesting a discontinuous transition. It is indeed the case that various discrete realizations of the first model exhibit a continuous transition in the universality class of directed percolation. However, contrasting early reports, one careful study of a synchronous cellular-automata type realization of the second model [18] reported a continuous transition for spatial dimension d=1-3. A discontinuous transition emerged only for $d \geq 4$. Another study of a lattice-gas model realization confirmed the existence of a continuous transition for d=1 [2]. Both studies actually included particle hopping which should if anything enhance a discontinuous transition reflecting given that bistability is exhibited by the mean-field version of the model. However, within the context of the current study, it should be recognized that model behavior will depend on the specific discrete realization.

In this work, we adopt a realization of Schloegl-type models on a square lattice (d=2) which is in the spirit of adsorption-desorption models. These models are also referred to as a

"contact processes". Roughly speaking, the following adsorption-desorption prescription interchanges the role of particles and vacancies from that in the above description of Schloegl models. In the standard contact process (SCP) which mimics Schloegl's first model, particles adsorb randomly on the empty sites at fixed rate or "pressure", and desorb at a rate proportional to the number of empty nearest-neighbor (NN) sites [2-4]. Not surprisingly, this process exhibits a continuous poisoning transition to a completely covered surface (an absorbing state) which is in the directed percolation universality class. In the quadratic contact process (QCP) which mimics Schloegl's second model, again particles adsorb randomly on the empty sites at fixed rate or "pressure", and desorb at a rate proportional to the number of *diagonally adjacent pairs of empty NN sites* [1,19]. We have recently shown that this QCP exhibits a discontinuous poisoning transition between an active state with a low coverage and a completely covered surface (again an absorbing state) [19]. These models are related to more general threshold contact processes where desorption is allowed (at a single rate) only if M or more adjacent sites are empty [20]. Then, the case M=1 is similar to the SCP, M=2 to the QCP (as discussed further below), and models with M≥3 have no active state for any p>0 on a square lattice. For M=3, particles within completely filled rectangular regions cannot desorb, so these regions spread irreversibly. For M=4, no particles in clusters of any shape cannot desorb, so all clusters spread irreversibly.

The traditional picture for discontinuous transitions to absorbing states is that the active and absorbing states coexist at a unique equistability pressure. Remarkably, for the QCP, coexistence of stable active and absorbing states occurs for a finite range of pressure. This means that for any pressure in this range, droplets of the absorbing state embedded in the active cannot grow indefinitely but rather die out, even though the absorbing state is

stable. Likewise, droplets of the active state embedded in the absorbing state cannot grow indefinitely and instead die out. This feature leads to so-called generic two-phase coexistence (PC) or true bistability [21], which dramatically contrasts behavior for discontinuous equilibrium transitions. For the QCP, PC can be understood in terms of an orientation dependence of the propagation of planar interfaces between active and absorbing states [18], as described in more detail in the following sections.

We should note that the prototype for such PC phenomenon is provided by Toom's synchronous North-East-Center (NEC) stochastic cellular-automata model [22-25]. In this model, individuals located on a square lattice change their votes for one of two parties guided by the majority of their current vote and those of their neighbors to their north and east. However, some biased randomness or noise is also included in the rules for voting. The overall magnitude of this noise corresponds to an effective temperature, and the bias towards one of the two parties is analogous to the application of an external magnetic field in the Ising model. PC occurs below a critical noise amplitude for sufficiently small bias. This behavior is elucidated by a heuristic analysis of the evolution of droplets of preferred party votes embedded in a state dominated by votes for the disfavored party. This analysis reveals that these preferred droplets do not grow, but rather shrink at a finite rate [23,24]. The strong asymmetry in the voting rules is believed to be responsible for PC, which also occurs in continuum analogues of the Toom model [25].

The outline of this paper is as follows. In Sec. II, we first specify our discrete stochastic lattice-gas (LG) model for the QCP on a square lattice, emphasizing a special feature of the dynamics in this model. We also describe our kinetic Monte Carlo simulation procedures. Then, we characterize the steady-state behavior for the model, specifically

generic two-phase coexistence, which was observed in our previous simulation study [19]. Next, in Sec. III, we focus on simulation results for the kinetics of relaxation to the steady states of the QCP for spatially homogeneous systems. We identify an "effective" spinodal point terminating a metastable active state for pressures above the two-phase coexistence region, and describe "rapid" relaxation or poisoning kinetics for pressures above this spinodal pressure. We also analyze nucleation-mediated relaxation or poisoning for pressures in the metastable region, and we characterize the dynamics of poisoned droplets within the two-phase coexistence region. In addition, for lower pressures below the two-phase coexistence region, some unusual aspects of relaxation kinetics are elucidated by making a connection to bootstrap percolation models. In Sec. IV, we analyze the propagation of interfaces with various orientations between the absorbing and active states in spatially inhomogeneous systems. As noted above, the dependence of propagation and equistability on interface orientation underlies the generic two-phase coexistence in the QCP. A summary and discussion of other models with generic two-phase coexistence, and of various generalized QCP-type models, is presented in Sec. V.

II. Adsorption-Desorption Model for QCP: Steady-State Behavior

Our adsorption-desorption model realization of the QCP on a square lattice involves the following steps [1,19]: random adsorption of particles at empty sites at rate or "pressure" p; cooperative desorption of particles at rate k/4 where k = 0, 1, 2, or 4 denotes the number of *diagonally adjacent pairs of NN empty sites*. Thus, one has: k=0 for particles with just 0 or 1 empty NN sites, and also for 2 empty NN sites which are on opposite sides of the particle; k=1 for particles with just 2 diagonally adjacent empty NN sites; k=2 for particles with 3

empty NN sites; and k=4 for particles with all 4 NN sites empty. See Fig.1. Below we use $\theta = \theta(p, t)$ to denote the coverage, i.e., the fraction of filled sites, which generally evolves with time. Also $\theta_{ss} = \theta_{ss}(p)$ denotes the value of θ in the active steady state which, intuitively, one expects to exist at least for low p. In fact, the existence of such a state for sufficiently small p has been proved rigorously [20,26]. In this small p regime, most particles are isolated with a desorption rate of unity. Consequently, evolution is approximately described by Langmuir kinetics,

$$d\theta/dt \approx p(1-\theta) - 1\cdot\theta \text{ for } p<<1, \text{ and } \theta_{ss} = p + O(p^2). \quad (1)$$

For a more systematic expansion of θ with p, one might regard the QCP as a perturbation of a random adsorption-desorption model. Then, one could use a perturbation-theoretic analysis within a creation-annihilation operator formulation of the problem to analyze steady-state behavior [2]. For high *p*, one should expect that adsorption will swamp desorption, so that the system will reach a completely covered or "poisoned" absorbing state with $\theta = \theta(p) \equiv 1$.

Our kinetic Monte Carlo (KMC) simulation analysis of the behavior of this model is performed on "rectangular shaped" ($L_x \times L_y$)-site square lattices with periodic boundary conditions. In conventional constant-p simulations, one specifies an adsorption rate p and then runs the simulation implementing adsorption and reaction with the appropriate relative rates. In this way, one determines both the dynamics and the steady-state behavior including the variation of the steady-state coverage, $\theta_{ss}(p)$, with p. Alternatively, in a constant-coverage (CC) simulation algorithm [27], one specifies a target coverage θ and runs the simulation attempting to adsorb (desorb) if the actual coverage is below (above) the target θ. The fraction of adsorption attempts yields the pressure $p=p(\theta)$. The two simulation approaches

should be equivalent for a sufficiently large system. In previous studies, the CC approach has proven particularly useful for analyzing discontinuous transitions where specifying θ anywhere in the range of the discontinuous jump of θ versus p should give the same "equistability pressure" corresponding to coexistence of the two steady-states. However, for the QCP, the situation proves more complex than for conventional discontinuous transitions where one has a unique equistability pressure.

As indicated in Sec. I, simulations of the QCP demonstrate the existence of a discontinuous transition from active to absorbing states with increasing p. More specifically, starting from an empty lattice, conventional simulations reveal the evolution to a stable active state for $0 \le p \le p_{eq}^* \approx 0.0944$, where θ_{ss} increases monotonically with p to a maximum of $\theta_{ss}(p=p_{eq}^*) \approx 0.17$ (See Fig. 2). In this regime, simulations indicate that droplets of the absorbing state embedded in the active state never grow indefinitely, i.e., the state is stable against local perturbations (See Sec. III C for a detailed discussion). For larger *p*, the system eventually poisons reaching the absorbing state, as shown in Sec. III A and III B. Due to a special feature of the QCP rules described below, the absorbing state is always stable against local perturbations, i.e. droplets of the empty or active state can never grow for any $p \ge 0$. Thus, one might assign generic two-phase coexistence (PC) for $0 \le p \le p_{eq}^*$, although below we will impose a more restrictive definition.

Remarkably, CC simulations reveal that the equistability pressure at which a stationary planar interface is formed between the active and absorbing states depends on the interface orientation, S [19]. We denote this pressure by $p_{eq}(S)$. These simulations were performed in a rectangular system with $L_y = SL_x$ containing an initial perfect strip of the

absorbing state with slope S. The strip quickly equilibrated but remains stable, its overall slope being preserved by the periodic boundary conditions. Specifically, $p_{eq}(S)$ displays a maximum of $p_{eq}(S=1) = 0.09443 \pm 0.00003$ (corresponding to p_{eq}^*) and decreases with increasing S to a minimum of $p_{eq}(S \to \infty) = 0.0869 \pm 0.0005$ [19]. By symmetry, one has that $p_{eq}(S) = p_{eq}(1/S)$. Conventional simulations support these observations: for $p<p_{eq}(S)$, the active state displaces the absorbing state separated from it by a planar interface of slope S, and for $p>p_{eq}(S)$, the opposite is true. See Sec. IV for a comprehensive analysis of interface propagation.

Reformulating the above observations, for $p_{eq}(S=\infty) < p < p_{eq}(S=1)$, the active state will displace the absorbing state separated from it by a planar interface with a slope sufficiently close to unity. Also, the absorbing state will displace the active state separated by a planar interface with a slope sufficiently close to S=∞. Thus, in this regime, both states are stable against certain non-local interfaces, in addition to being stable against local perturbations by embedded droplets. Using this more restrictive definition, we associate PC only with the regime $p_{eq}(S=\infty) < p < p_{eq}(S=1) = p_{eq}^*$. Certainly, we are not providing a rigorous proof of PC for this model. However, we believe that the discussion in Sec.3C provides a clear heuristic picture. Finally we mention that for $0 \le p \le p_{eq}(S=\infty)$, the absorbing state is not stable relative to the active state separated from it by a planar interface with any slope $0<S<\infty$.

At this point, it is appropriate to emphasize that the specific form of the desorption rules in the QCP imply certain special features for the dynamics in this model. First, it is clear that a vertical strip of the poisoned state (or even a single vertical column) can never be

eroded for any $p \geq 0$. The same is true for horizontal strips. Particles in such strips can never have more than one empty NN site, and thus have $k=0$. Consequently, analysis of the evolution of vertical strips, and the determination of $p_{eq}(S=\infty)$ above is quite delicate: while a vertical strip will not expand in an infinite system for $p \leq p_{eq}(S=\infty)$, it will expand in a finite system due to the certainty of completion of additional filled rows of sites (which corresponds to falling into a new absorbing state). Thus, careful analysis of the size-dependence of behavior is required to accurately determine $p_{eq}(S=\infty)$ [19]. Second, an isolated empty patch or an isolated patch of the active state embedded in the absorbing state can never grow outside of a rectangle inscribing that patch. Thus, eventually, the patch must be filled in for any $p>0$; i.e., the system will evolve to the absorbing state with probability of unity [1]. This feature automatically guarantees the above mentioned stability of the absorbing state against local perturbations for any $p>0$.

Finally, having introduced our adsorption-desorption version of the QCP, we mention that one motivation for consideration of such lattice-gas models is application to modeling of catalytic reactions on single-crystal surfaces. Such reactions can exhibit discontinuous poisoning-type transitions. The ZGB model [5] was intended to describe surface science studies of CO-oxidation on single-crystal catalyst surfaces. However, under typical low pressure conditions, CO has high surface mobility which produces strong bistability rather than a discontinuous transition [28]. Thus, the jump in coverage or in the CO_2-production rate observed experimentally upon increasing the CO-partial pressure corresponds to a spinodal point, rather than to the discontinuous transition at an equistability point. In fact, behavior with strong bistability is better captured by hybrid models directly incorporating infinite CO mobility but finite mobility for oxygen [28]. However, for high-pressure

catalysis, CO surface mobility is inhibited which allows strong fluctuations and sharp interfaces to develop. In this regime, basic aspects of behavior could be qualitatively similar to that displayed by simpler ZGB or QCP type models with limited or zero surface mobility [29].

III. Relaxation Kinetics in the QCP

A. "Rapid" Poisoning Kinetics above the Metastable Region

The traditional picture of discontinuous transitions holds that a state which is stable below the transition extends to a metastable state above the transition for a finite region in parameter space which is terminated by a spinodal point. Thus, for the QCP, one would expect a metastable active state to exist for some finite range of $p>p_{eq}(S=1)$. However, the precise nature and even the existence of such metastable extensions is a subtle question. For equilibrium Ising-type interacting lattice-gas models, it has now been demonstrated rigorously that there does not exist a unique analytic metastable extension of the stable state above the transition [30,31]. Consequently, the spinodal point is not uniquely defined. However, instead one can generate a C^{∞} family of metastable extensions in a rather natural and simple way by following the dynamics of the model. The latter approach is adapted for the QCP below in Sec. III B.

For the QCP (and for similar models with discontinuous transitions), one might expect that there exists some "effective" spinodal value $p_s(\text{eff})$ (or narrow range of p-values), such that poisoning for $p>p_s(\text{eff})$ occurs much more quickly than in the metastable region for $p_{eq}(S=1) < p < p_s(\text{eff})$. Based on mean-field theories (see Ref. [32] and Appendix A), for $p>p_s(\text{eff})$, one might expect the rate of poisoning to be controlled primarily by the distance

from the effective spinodal, $\delta p_s = p - p_s(\text{eff})$ at least for sufficiently small δp_s. In this case, one has that $\theta \approx \theta(\delta p_s t)$. Thus, an estimate of $p_s(\text{eff})$ can be made by plotting θ versus $\delta p_s t$ and achieving collapse of curves for suitable choice of $p_s(\text{eff})$. A similar approach was reasonably effective for the ZGB model and its extensions to include surface mobility [7]. Figure 3(a) shows the evolution of θ versus t starting from an empty lattice at t=0 for a range of p=0.110-0.125 expected to be above $p_s(\text{eff})$. Indeed, good collapse of these curves plotted against the rescaled time $\delta p_s t$ is achieved choosing $p_s(\text{eff}) \approx 0.0997 \pm 0.0005$. See Fig.3(b). Similar results are achieved using a higher range of p=0.0130-0.0145 with a value of $p_s(\text{eff})$ in the range specified above yielding the best collapse.

B. Nucleation-Mediated Poisoning in the Metastable Region

To motivate our analysis of nucleation-mediated poisoning for the QCP, it is appropriate to first review the heuristic framework for nucleation in equilibrium models. The basic idea is that there exists a finite free energy barrier, E_{nuc}, to the nucleation of a critical droplet of the stable phase in a background of the metastable phase (where subcritical droplets shrink and supercritical droplets grow). One can show that $E_{nuc} \approx b\sigma^2/\Delta$. Here, $b>0$ is a constant, σ denotes the line tension of the interface between the coexisting states at the transition, and Δ is a measure of the (small) distance from the transition, i.e., the driving force for creation of the stable phase [31]. Then, critical droplets of the stable state are nucleated at a rate $k_{nuc} \propto \exp(-\beta E_{nuc})$, where β is the inverse temperature. Once critical droplets are formed, they grow with a velocity $v \propto \Delta$ [31] ignoring finite-curvature corrections. We consider a large system where the nucleation-mediated transition from the metastable to the stable state occurs by the spontaneous formation and growth of many

supercritical droplets. The kinetics of this process is reasonably described within a continuum two-dimensional Avrami formulation [33]. In such formulations, droplets are nucleated at random locations in the plane at a fixed rate, and thereafter expand at constant velocity with a fixed shape. If θ_m (θ_s) denotes the density in the metastable state (stable state), then it follows that

$$\theta(t) \approx \theta_m + (\theta_s - \theta_m)\{1 - \exp[-a\,(t/\tau_{char})^3]\}, \text{ where } \tau_{char} \propto v^{-2/3}\, k^{-1/3}. \quad (2)$$

Using the results above, the characteristic time for nucleation satisfies $\tau_{char} \propto \Delta^{-2/3} \exp(\lambda_{nuc}/\Delta)$ where $\lambda_{nuc} \approx 1/3\ b\ \beta\ \sigma^2$. The procedure for generating a C^∞ family of metastable states (labeled by λ) is to run the dynamics starting from a suitable state near the metastable state for a time τ_{run} or the order of $\exp(\lambda/\Delta)$ where $\lambda<\lambda_{nuc}$ [30,31]. Since τ_{run} diverges exponentially as $\Delta\rightarrow 0$, it is not surprising that one obtains a C^∞ extension of the stable state. However, such extensions can vary strongly with λ and somewhat have limited physical significance. Thus, they may provide limited insight into the location of any effective spinodal point. Extensions with the most physical significance presumably correspond to choosing λ close to λ_{nuc}.

For the non-equilibrium QCP, it is reasonable to propose that the rate of nucleation of critical droplets of the absorbing state within a background for the metastable state for $p>p_{eq}(S=1)$ satisfies

$$k_{nuc} \propto \exp(-c_{nuc}/\delta p), \text{ where } \delta p = p - p_{eq}(S=1)>0, \quad (3)$$

noting that $\delta p>0$ replaces $\Delta>0$ above (cf. Ref. [11] which considers the ZGB model). The parameter c_{nuc} should encode information about the effective line tension between coexisting active and absorbing states in the QCP. These critical droplets will grow with a velocity $v \propto$

δp [7,8,28] at least if one ignores corrections due to finite-curvature. Then, (2) should apply to this non-equilibrium system defining a characteristic time

$$\tau_{char} = (\delta p)^{-2/3} \exp[c_{nuc}/(3\delta p)], \quad (4)$$

and setting θ_s=1 corresponding to the stable absorbing state. To obtain a C^{∞} family of extensions of the active state (labeled by $c<c_{nuc}$), one can naturally run the QCP starting from an empty lattice for a time $\tau_{run}(c) \propto (\delta p)^{-2/3}\exp[c/(3\delta p)]$. More practically, a natural extension might be obtained by choosing τ_{run} as some fixed small fraction of τ_{char}. One such metastable extension is shown in Fig. 2.

Our focus here is on analyzing the Avrami-like nucleation-mediated poisoning kinetics in the QCP for suitably small δp, and in extracting a value for the key parameter c_{nuc}. The value of $p>p_{eq}(S=1)$ (determining δp) cannot be chosen too high since one must remain within the metastable region. On the other hand, δp cannot be too small since then simulations for a finite size system would generate only a single droplet rather than the multiple droplets assumed in our Avrami analysis [11]. The value $p = 0.098$ (or $\delta p \approx 0.0036$) for a 1024×1024 site system meets these requirements, and Fig. 4 shows the corresponding evolution during poisoning. To quantify the kinetics, Fig. 5(a) shows the evolution of θ versus t starting from an empty lattice at t=0 for a range of $p = 0.0975$-0.0990 in the metastable region above $p_{eq}(S=1) \approx 0.0944$. Collapsing these curves by plotting against a rescaled time t/τ_{char} indicates an optimum choice of c_{nuc} in the range $c_{nuc} = 0.02$-0.03, as shown in Fig. 5(b). We also confirm that the shape of these collapsed curves is well described by the Avrami form (2).

Of course, the detailed evolution of configurations in the QCP, as shown in Fig.4, is somewhat different than in classic continuum Avrami models. This partly due to discrete lattice effects, and partly due to fluctuations in the shapes of growing droplets. It is thus appropriate to note that discrete lattice versions of the Avrami model with deterministic droplet growth have been developed for which the kinetics is also exactly solvable and significantly for which the kinetics have essentially the same form as in the continuum model [34]. Perhaps, even more relevant is the observation that lattice versions of the Avrami model with stochastic droplet growth have also been developed. These are usually referred to as cooperative sequential adsorption (or filling) models [34,35]. Evolving configurations in these simple irreversible models do resemble those for the QCP shown in Fig.4.

C. Dynamics of Poisoned Droplets in the Two-Phase Coexistence Region

Next, we further elucidate the unusual generic two-phase coexistence or true bistability exhibited by the QCP. For $p_{eq}(S=\infty) < p < p_{eq}(S=1)$, we consider the evolution of poisoned droplets of the absorbing state which are embedded in the active state. Such droplets form spontaneously, although in our study it is more convenient to embed such droplets “by hand”. Since the absorbing state is stable, we must rationalize why such droplets ultimately disappear rather than growing until the (stable) absorbing state takes over the system.

To characterize such droplet dynamics, it is instructive to focus on a “worst case scenario”. Imagine that a square-shaped droplet is formed or created with sides orientated with the principal lattice directions (i.e., with slopes S=0 and S=∞). Then, since p >

$p_{eq}(S=\infty)$, the sides of this droplet should initially tend to grow outwards with finite velocity. Assuming that growth at the corners of this droplet is inhibited, one expects a tendency towards the development of a roughly octagonal shaped droplet. Then, since $p < p_{eq}(S=1)$, the facets with slope $S= \pm 1$ at the corners will tend to shrink, and the sides with slopes $S=0$ or ∞ will grow out yielding a diamond shaped droplet. Thereafter, this diamond shaped droplet will naturally shrink. From standard simulations, we can readily explore the progression of droplet shapes for various p. Such analyses reveal that the simple progression in geometric shapes mentioned above is somewhat concealed due to large fluctuations. Fig.6 shows simulations with an initial 128×128 site droplet and with p=0.0940. Even with this large size and "high" p close to $p_{eq}(S=1)$, fluctuations in droplet shape are significant and shrinkage of clusters starting at the corners is perhaps more evident that growth of the S=0 and S=∞ sides. However, analysis of the total coverage of the system during this simulation (not shown) does reveal an initial increase corresponding to the regime of net growth from a square to diamond shaped droplet. Then, a fairly sudden transition occurs to a regime of nonlinear decrease of the total coverage consistent with the picture of a diamond shaped cluster shrinking with constant velocity.

Of course the above analysis of droplet evolution is heuristic rather than rigorous, and the understanding of behavior at droplet corners is limited. However, as droplets become larger, a simple deterministic geometric picture of evolution becomes more applicable where behavior is controlled by the orientation dependence of the propagation of planar interfaces. In contrast, for smaller clusters, simple geometric evolution is largely concealed by fluctuations.

D. Relaxation Kkinetics for p=0 or p=0+: Bootstrap Percolation

Relaxation behavior for p below the two-phase coexistence regime is strongly impacted by the special feature of the QCP which makes the absorbing state stable against localized perturbations (i.e., an isolated active or empty droplet embedded in the absorbing state can never survive). In general, to systematically analyze relaxation kinetics in models with unstable or metastable absorbing states, typically one might start with a state corresponding to a lattice partially filled by a random distribution of particles with initial coverage θ_i. Then, for low initial vacancy concentrations, $\theta_v = 1-\theta_i << 1$, the system is initially close to the absorbing state, and one can follow evolution to the active state [7].

However, there is some deviation from this simple scenario for the QCP. First, consider the simplest case for p=0 where particles with k>0 irreversibly desorb in the absence of adsorption. For a strictly finite ($L_x \times L_x$)-site system (i.e., $L_x=L_y=L$, say), one might expect the following scenario described in terms of "small" critical value for $\theta_v=\theta_v^*(L)$. For $\theta_v<\theta_v^*$, empty square or rectangular patches will be formed and grow around any clusters of vacant sites. However, typically the system will eventually "freeze" into a distribution of small isolated non-overlapping empty rectangles. (This distribution will include vacant squares and single vacant sites.) In this case, the system would never reach the active state for p=0 which corresponds to an empty lattice. For $\theta_v>\theta_v^*$, these growing vacant rectangular patches can link sufficiently to percolate, and this leads to the ultimate removal of all particles from the lattice.

More generally, for infinitesimal non-zero pressure p=0+, it then follows that this system of size L would typically reach the active state only for $\theta_i < \theta_i^*(L) \equiv 1-\theta_v^*(L)$, and

would eventually reach the absorbing state for $\theta_i > \theta_i^*(L) \equiv 1-\theta_v^*(L)$. Indeed, simulations indicate that there does exist such a critical value for the initial vacancy coverage, although behavior as $L=L_x\rightarrow\infty$ is more subtle as we describe below.

A detailed characterization of the above critical behavior follows from recognizing that the dynamics of the p=0 QCP model maps onto that of a specific bootstrap percolation (BP) model. In the standard BP model on a square lattice, one culls particles which have a two or more neighboring empty sites [36,37]. This standard BP model is isomorphic to that of so-called 2n diffusion percolation (2n DP) on a square lattice where one adds particles at empty sites if any two or more neighboring sites are occupied [36]. The QCP dynamics for p=0 is actually isomorphic to a variant of 2n DP denoted by s2n DP which requires at least two of the occupied neighbors of the empty site be diagonal neighbors [36].

We translate the key result for these types of BP or DP models into the language used in the current paper where one starts with a "small" random distribution of vacancies of density θ_v on an otherwise occupied lattice, and progressively removes particles according to the prescribed QCP rules. Then, there exists a constant γ such that the critical value $\theta_v^*=\theta_v^*(L)$ of the vacancy density satisfies $\theta_v^* \approx \gamma/\ln(L)$, as $L\rightarrow\infty$. Thus, one has $\theta_v^*\rightarrow 0$ and $\theta_i^*\rightarrow 1$, as $L\rightarrow\infty$, i.e., an infinite system will always reach the active state no matter how close is the initial coverage, $\theta_i<1$, to unity. A more common presentation of this result is that for a fixed initial θ_v, there exists a critical linear system size $L = L^*(\theta_v) \sim \exp[\gamma/\theta_v]$, such that when $L<<L^*$, typically frozen distributions of isolated empty rectangular patches result. However, for L considerably in excess of L*, the lattice will typically completely empty. The above relationships have been demonstrated rigorously for the standard BP or 2n DP model

[38,39], and are supported by numerical simulations for several variants (including s2n DP). The dynamics of interest for small θ_v relies on rare bottleneck events, i.e., the linkage of large clusters of vacant sites, which has also been described as "capture of a critical droplet" [38].

A key conclusion from the above results is that there are very strong finite-size effects on the dynamics as reflected by the exponential increase of L* with the inverse of θ_v. Simulation results indicate that $\gamma \approx 0.25$ for standard BP considering sizes up to $L \approx 2\times10^4$ (although this γ-value is far from the true asymptotic value [39]), and $\gamma \approx 0.47$ for s2n DP or the p=0 QCP considering sizes up to $L \approx 800$ [37]. The larger value of γ in the latter case should be expected since desorption is more difficult for the p=0 QCP than for standard BP. Thus, for a given size L, a larger value of $\theta_v^* \sim \gamma/\ln(L)$ is required for percolative removal of all particles in the p=0 QCP compared to standard BP. Equivalently, for a given θ_v, a larger size $L^*(\theta_v) \sim \exp(\gamma/\theta_v)$ is required for such percolation in the p=0 QCP.

E. Relaxation Kinetics for Lower p: Simulation Results

Next, we turn to the issue of characterizing the relaxation kinetics in the QCP for general lower (but non-zero) p starting with a random distribution of vacancies of coverage θ_v. Here, we select a finite system size, e.g., L = 256 or 512. Then, in our standard analysis for each fixed p>0, we run simulations for various θ_v to determine the critical value $\theta_v^*(p, L)$ which separates evolution to a poisoned state (for $\theta_v < \theta_v^*$) and to the active state for ($\theta_v > \theta_v^*$). In the former case, the system evolves to produce an array of separated active droplets which can be inscribed within a distribution of non-overlapping isolated rectangles. Once

such a state is achieved, it is clear that the system must eventually evolve to an absorbing state just as for p=0+. For the latter case, the active droplets link sufficiently to percolate, leading to evolution to the active state. Strictly speaking, for θ_v sufficiently close to θ_v^*, there can be a significant probability for the system to reach either absorbing or active state. Thus, more precisely, we should state that the system reaches the poisoned state with probability above (below) 0.5 for $\theta_v < \theta_v^*$ ($\theta_v > \theta_v^*$). From a series of such analyses for various p, we can map out the dependence of $\theta_v^*(p, L)$ versus p. See the inset to Fig.7(b) which actually plots a closely related quantity (see below).

The above analysis strictly applies only for $p < p_{eq}(S=1)$. However, with some ambiguity, one can extend the analysis into the metastable region at least for p slightly above $p_{eq}(S=1)$. Here, the critical coverage $\theta_v = \theta_v^*(p, L)$ separates evolution to the absorbing state and to the metastable state. See Fig. 7(a).

Choosing $\theta_v = \theta_v^*(p, L)$ for large L, one finds that after some transient period, the coverage evolves from the initial value of $\theta_i^*(p, L) = 1 - \theta_v^*(p, L)$ to a final value of $\theta_f^*(p, L)$ which is quasi-stationary for 1000's of time units and is typically somewhat different from $\theta_i^*(p, L)$. For example, Fig. 7(a) shows that $\theta_i^* \approx 0.57$ versus $\theta_f^* \approx 0.4$ when p=0.0950 and L=256. We naturally map out $\theta_f^*(p, L)$ versus p, which is actually the quantity shown in the inset to Fig.7. We regard this dependence as more fundamental than that of $\theta_i^*(p,L)$ versus p, which should depend more strongly on the specific choice of the random initial conditions. The form of the θ_f^* versus p curve is somewhat reminiscent of the variation of the unstable steady-state coverage with p in mean-field-type treatments of the QCP (see Ref. [32] and

Appendix A). However, we shall see below that this behavior is not associated with an unstable steady-state.

It should be emphasized that the form of $\theta_f^*(p, L)$ versus p shown in Fig.7 exhibits significant finite-size effects. This is most obvious for p=0+ where $\theta_f^*(0+, L) \sim 1- \gamma/\ln(L) \to 1$, as $L\to\infty$. For moderate p, no significant finite-size effects are evident from our simulations (and this is consistent with the picture below for evolution with a quasi-steady state coverage). However, it is difficult to rule out finite-size effects since they are weak and subtle. Nonetheless, one can say that as $L\to\infty$, at least the portion of the $\theta_f^*(p, L)$ versus p curve near p=0 will rise to go smoothly through $\theta_f^*(p=0, L=\infty) = 1$.

We also note that the variation of $\theta_f^*(p, L)$ with p can be determined by an alternative analysis where simulations are performed in an $(L\times L)$-site system where one fixes $\theta_v > \theta_v^*(L)$ — i.e., $\theta_i < 1 - \theta_v^*(L)$—and explores evolution for various p. There exists a critical pressure, $p^*(\theta_v, L)$, such that for $p < p^*(\theta_v, L)$, the system will evolve to the active state, and for $p > p^*(\theta_v, L)$ the system will poison (since evolution produces an array of active droplets which can be inscribed within a distribution of non-overlapping isolated rectangles). See Fig. 7(b). When $p = p^*(\theta_v, L)$, after a transient period, the coverage evolves from its initial value $\theta_i = 1 - \theta_v$ of to a final quasi-stationary value of θ_f^*. Plotting this θ_f^* versus θ_i recovers the curve shown in the inset to Fig.7.

Finally, we characterize in more detail the evolution of states with quasi-stationary coverage $\theta = \theta_f^*$ observed for pressure p upon choosing an initial $\theta_v = \theta_v^*(p, L)$. As noted above, such behavior is reminiscent of unstable steady-states in mean-field models. In fact, robust unstable steady-states can exist in lattice-gas models in the hydrodynamic limit of

rapid hopping of some species [28]. However, such states are not expected for models with finite mobility. Indeed, monitoring the evolution of the system from the initial random distribution of vacancies (or filled sites) as shown in Fig. 8 reveals a complex and persistent coarsening process. Just as for BP slightly above the percolation threshold, one finds slow coalescence of overlapping rectangular clusters of the active state to form progressively larger inscribing rectangular clusters. This coarsening process (which tends to reduce the coverage) is exactly counterbalanced by the filling and disappearance of isolated clusters of the active state (which tends to increase the coverage).

IV. Propagation of Interfaces Separating Active and Absorbing States

A. Analysis for a Vertical Interface with Slope S=∞

Analysis of the propagation vertical interfaces in the QCP, and thus determination of $p_{eq}(S=\infty)$, is delicate for reasons outlined below. For a finite $(L_x \times L_y)$-site system with periodic boundary conditions which includes a vertical filled strip of length L_y, particles within completely filled columns of the strip can never desorb. Consequently, the strip (and in particular its core) can never shrink. Consider the partially completed columns adjacent to the completed columns of the strip. Completion of each such column corresponds to falling into a new absorbing state. Consequently, this event must eventually occur with probability unity in conventional simulations (for any $p>0$) in a finite system. It must also occur in CC simulations provided there are sufficient particles in the system to allow column completion. In this sense, either conventional or CC simulations in finite systems are potentially

"corrupted". This is why our previous CC simulations provided a careful analysis of finite-size effects [19]. The potential problem is that this "artificial" finite-size propagation can lead to an underestimate of $p_{eq}(S=\infty)$ if the latter is determined by the absence of any expansion of the absorbing state. We are thus motivated to systematically explore finite-size effects in standard simulations for the propagation of vertical interfaces.

One strategy to systematically assess finite-size effects is to perform simulations for a sequence of system sizes with $L_y = 2^n L_x$ for increasing n containing a vertical interface of length L_y. The tendency for finite-size corruption corresponding to "artificial" column completion should decrease as $n \to \infty$. To explore this phenomenon, we show in Fig. 9 the dependence on L_y of the number of completed columns as a function of time starting with a single complete vertical column. For a lower pressure of p =0.087, columns are artificially completed for small L_y, but this rate of column completion appears to vanish as $L_y \to \infty$, consistent with the choice of $p \approx p_{eq}(S=\infty) \approx 0.087$. For a higher pressure p=0.092 satisfying $p_{eq}(S=\infty) < p < p_{eq}(S=1)$, columns are completed artificially quickly for small L_y. The rate of completion does decrease for increasing L_y, but now saturates at a finite value for $L_y \to \infty$. This is consistent with the choice $p > p_{eq}(S=\infty)$.

Finally, it is instructive to analyze the non-zero propagation velocity of a vertical interface, $V(S=\infty, p) < 0$ versus $p > p_{eq}(S=\infty)$ for a large system (where finite size corruption is negligible). Results from our standard constant-p simulation are shown below in Fig.10.

B. Analysis for Interfaces with Slopes $1 \leq S < \infty$

It is appropriate to present a comprehensive analysis of the dynamics of interfaces separating active and absorbing states with various prescribed slopes S. This behavior can be

obtained from standard constant-p simulations. Again, the orientation dependence of propagation underlies the generic two-phase coexistence or true bistability of the QCP. Here, we consider systems with $L_y = S \cdot L_x$ and with periodic boundary conditions starting from an initial filled strip of slope S. After a possible initial transient, the total number of filled sites in the system changes linearly in time. By monitoring this change and accounting for the different local coverages of the absorbing state, $\theta=1$, and the active state, $\theta=\theta_{ss}(p)$, as described above, one can readily extract the propagation velocity, V(S,p), as a function of p.

Results for V(S,p) versus p with S = 1, 2, and 4 are shown in Fig.10 for a broad range of $p \geq 0$. For $0 \leq p \leq p_{eq}(S)$, the active state is more stable than the absorbing state and displaces the latter (for $0<S<\infty$). We assign $V(S,p)>0$ in this case. Since $V(S,p)=0$ when $p=p_{eq}(S)$, this feature allows an independent check on the results for equistability pressures from CC simulations. Estimates of $p_{eq}(S)$ from this analysis are consistent with those presented in Sec.2. As p increases above $p_{eq}(S)$, the absorbing state becomes more stable and displaces the active state, so $V(S,p)<0$. Interface configurations corresponding to the equistability pressure are shown in Fig.11 for various slopes S. These were obtained from CC simulations.

Some more detailed discussion is appropriate for the regime where $p > p_{eq}(S)$ and $V(S,p)<0$ as the associated interface propagation may not be well-defined. First, consider the case S=1 where the active state is only metastable for $p>p_{eq}(S=1)$, and so interface propagation is transient, i.e., propagation only persists until spontaneous nucleation-mediated decay of the active state. Just as for the active state coverage, $\theta_{ss}(p)$ versus p, one does not expect there to exist a unique analytic extension of V(S=1,p) versus p into the metastable region $p>p_{eq}(S=1)$. However, presumably there does exist a C^{∞}-family of extensions obtained

by simulation of transient front propagation for times on the order of $\tau_{run}(c)$ given in Sec.3A with and $c<c_{nuc}$. Second, consider the case $S>1$ where there is a finite range of pressure, $p_{eq}(S>1) < p < p_{eq}(S=1)$, where propagation of the absorbing state into the active state is persistent since the active state is stable against nucleation. In this regime, propagation and the associated velocity, $V(S,p)<0$, are well-defined. Again, a unique analytic extension will not exist for $p > p_{eq}(S=1)$.

An expanded view of the behavior of $V(S,p)$ versus p in this regime of $p \approx p_{eq}(S)$ is shown in the inset to Fig.10. It appears that there is a confluence of the curves for different S at some p-value above $p_{eq}(S=1)$. Examination of interface propagation in mean-field treatments of the QCP extended to treat spatially non-uniform systems also indicate a tendency for such velocity curves to merge quite close together at a spinodal point [32]. (This spinodal point is well-defined in mean-field treatments.) Thus, Fig.9 indicates an effective spinodal point for the active metastable state in the QCP somewhat above p=0.098, consistent with the analysis in Sec. III A.

C. Irreversible Shrinkage of the Absorbing State for p=0

Although not central to the analysis of generic two-phase coexistence, for a complete analysis of interface propagation in the QCP, we consider in more detail the special case when p=0. Here, surprisingly, we are able to present exact results for the non-trivial propagation behavior. For $0<S<\infty$, this case corresponds to irreversible shrinkage of a strip of the absorbing state. The exact analysis is perhaps most readily achieved by recognizing that the dynamics of shrinkage the interface of the absorbing state in the p=0 QCP model maps exactly onto the dynamics of irreversible growth of an interface in the 1+1 dimensional

bridge-site deposition model [40], or equivalently onto the single-step deposition model [40-42]. Both these models involve random deposition at specific allowed sites. The dynamics in these models is in turn equivalent to that of a fully asymmetric spin exchange model (i.e., an up-spin can exchange with a neighboring down-spin only on the left, say), where spin up (down) corresponds to a step up (down) in the single-step model. See Fig.12 where an interface with mean slope S=1 in the QCP is drawn aligned horizontally and corresponds to a flat interface in the single-step models with mean slope, σ, of zero. This in turn corresponds to the spin exchange model in the case of equal populations of up and down spins, i.e., with zero net magnetization (also denoted by σ) of zero. More generally, the equivalence of these models extends to interfaces and surfaces with more general orientations. Specifically, an interface with mean slope $S = (1+\sigma)/(1-\sigma) > 1$ in the QCP corresponds to a surface with mean slope $0 < \sigma = (S-1)/(S+1) < 1$ in the single-step deposition models, and visa versa (as the natural axes differ by 45°).

In the exact analysis, one considers systems with a finite width of interface (specifically, a finite width in the horizontal direction in Fig.12 corresponding to S=1 or σ=0) where regular or skewed periodic boundary conditions preserve the mean slope. Then, in the reference frame moving with the interface or growing surface, there are a finite number of possible configurations. A simple but critical observation for the deposition models is that each configuration has the same number of local valleys and peaks [41]. Thus, for the prescribed deposition dynamics, each configuration can be destroyed or created in the same number of ways. Destruction occurs by deposition which can occur only at a local valley, and creation occurs starting from a configuration which differs only by removal of a particle at

one peak to create a local valley (and by deposition at that valley). This observation implies that in the steady-state, all allowed configurations have the same weight [40-42]. Given this information, one can immediately calculate the steady-state values of various quantities of interest such as the density of local valleys which determines the propagation velocity. Then, one can extract values of these quantities in the limit of infinite system width (which is of primary interest).

The central result from this analysis for the single-step deposition model on an infinite surface with a deposition rate of unity is that the film growth velocity in the direction orthogonal to $\sigma=0$ satisfies $V_{\perp}(\sigma) = ½ (1-\sigma^2)$ for orientations $0\leq\sigma\leq1$ [40,42]. Thus, the growth velocity normal to the mean orientation of the film surface satisfies $V(\sigma) = V_{\perp}(\sigma)/(1+\sigma^2)^{1/2}$. Translating the result into the language of the QCP for p=0, one must note that all particles desorbing from the eroding interface have exactly 2 empty NN sites, so k=1 and the desorption rate is ¼. Also, inspection of Fig.12 indicates that distances must be rescaled by a factor of $1/\sqrt{2}$. This, it follows that infinite interfaces in the p=0 QCP has a propagation velocity

$$V(S\geq1, p=0) = V(\sigma)/(4\sqrt{2}) = ¼\ S(S+1)^{-1}(S^2+1)^{-1/2} \sim 1/(4S), \text{ as } S\rightarrow\infty. \qquad (5)$$

In particular, we note that $V(S=1, p=0) = 1/(8\sqrt{2}) \approx 0.0884$, $V(S=2, p=0) = 1/(6\sqrt{5}) \approx 0.0745$, and $V(S=4, p=0) = 1/(5\sqrt{17}) \approx 0.0485$, consistent with simulation results. As an aside, we mention that the above exact analysis also determines finite-size corrections to the result (5).

V. Summary and Discussion

Our realization of the quadratic contact process (QCP) as an adsoption-desorption model on a square lattice displays generic two-phase coexistence (PC) or true bistability

between an active state and an absorbing state for a range of adsorption rates of pressures. This feature derives from the dependence on interface orientation of the equistability pressure for these two states. This behavior of the QCP is in marked contrast to that for discontinuous transitions in equilibrium systems where equistability occurs at a single pressure.

Indeed, it is natural to compare behavior of the QCP with the equilibrium states of a reversible adsorption-desorption model on a square lattice with random adsorption at rate p and correlated desorption at rate $\exp[n\beta\phi]$. Here, $\beta=1/(kT)$ denotes the inverse temperature, n denotes the number of occupied NN sites, and $\phi<0$ denotes a NN attractive adspecies interaction. The equilibrium properties of this reversible adsorption-desorption model correspond to the 2D Ising model. For low pressures, the steady-state coverage satisfies $\theta_{ss}(p) = p + O(p^2)$, just as in the QCP. Below a critical temperature, $T_c=0.57\phi/k$, increasing p reveals a unique equistability pressure, p_{eq}, where $\theta_{ss}(p)$ undergoes a discontinuous jump corresponding to a transition from a dilute to a dense 2D phase with $\theta_{ss}(p)$ closer to unity. The discontinuous transition disappears as T approaches T_c.

From a broader perspective, generic two-phase coexistence (PC) can never occur in conventional equilibrium models such as the Ising model. This is readily understood since coexistence requires equality of the chemical potentials for the coexisting phases, and this occurs only for a single pressure. One perspective on PC in non-equilibrium models in d spatial dimensions is that the stationary distribution of histories in these models can be regarded as a constituting “generalized Ising models” in d+1 dimensions [23]. For these higher dimensional systems, the free energy can be identically zero in a finite region of parameter space.

As noted in Sec. I, perhaps the prototype of generic two-phase coexistence or true bistability is provided by Toom's NEC stochastic cellular-automata model [22]. The origin of PC in this model derives from the strong broken symmetry of the dynamic voting rules. This results in an obvious strong anisotropy in interface propagation. The dynamic adsorption-desorption rules of the QCP do not incorporate broken symmetry and the anisotropy in interface propagation underlying PC is more subtle. One could speculate that PC in the QCP is related to the presence of an absorbing state, an intrinsically non-equilibrium feature absent in Toom's model. However, this is not the case, as shown in our discussion in Appendix B of generalizations of the QCP [19]. We should emphasize that PC has been observed in a variety of other non-equilibrium models. One such class models pertain to interface motion in the presence of pinning sites, where both pinned and propagating states exist [21]. Bistability derives from the feature that a greater driving force is required to depin an interface rather than to just maintain motion. Another class of examples derives from non-equilibrium adsorption-desorption models with enhanced binding at the substrate [47]. Under suitable conditions, PC exists between a non-wetting phase (corresponding to the film surface pinned to the substrate) and a growing phase. Although not described in Ref. [47], one can relate PC in this model to anisotropy in propagation of the growing phase. Another class of stochastic cellular automata models has been applied to explore generic stability of temporally periodic states (against the expected desynchronization of spatially separated regions) [48]. Again analysis of the evolution (and shrinkage) of temporally out-of-phase droplets is instructive. Currently, we are exploring the hypothesis that PC is a very general phenomenon in non-equilibrium adsorption-desorption or reaction models with discontinuous

transitions, but that it is typically difficult discern due to a combination of weak orientation-dependence of interface propagation and due to weak metastability.

In all of the above analyses, consideration of the evolution (and shrinkage) of droplets of one phase embedded in another is invaluable in understanding the origin of PC. Of course, the concept of critical droplets has long proved a valuable tool for characterizing metastability and nucleation-mediated kinetics in classic equilibrium models [43]. Here, the same framework is shown to extend to the consideration of nucleation-mediated kinetics in the metastable regime just outside the two-phase coexistence regime in the non-equilibrium QCP model. We also note that this approach has been applied previously for ZGB-type models [7,11].

Finally, it is natural to consider several modifications or generalizations of the QCP: (i) introduction of an additional random desorption pathway which removes the absorbing state but preserves PC; (ii) introduction of hopping at rate h which allows connection with the mean-field QCP in the limit as $h \to \infty$; (iii) consideration of the QCP on different two-dimensional lattices which can change the nature of the phase transition to the adsorbing state; (iv) “relaxing” the constraint on desorption in the QCP so that all particles with two or more empty neighbors can desorb (i.e., the M=2 threshold contact process). See Appendix B for further discussion.

Acknowledgements

Work at the Ames Laboratory was supported by the U.S. Department of Energy (Basic Energy Sciences, Division of Chemical Sciences) under Contract No. DE-AC02-07CH11358. XG was also partly supported for this work by NSF Grant CHE-0414768.

Appendix A: Mean-Field QCP in the Limit of Rapid Stirring

The QCP is naturally generalized to allow hopping of particles to NN empty sites at rate h. Introducing any degree of hopping removes the special feature of standard QCP rules which prohibits growth of isolated empty droplets embedded in the absorbing phase and which prohibits the shrinkage of vertical strip of the absorbing state (as noted in Ref. [1]).

Here, we focus on behavior in the $h\rightarrow\infty$ rapid-stirring hydrodynamic limit. We note that for this single-component model with the conventional prescription of hopping to NN empty sites, one will recover a simple description of chemical diffusion with constant diffusion coefficient D=h (where spatial units are in lattice constants) [44]. In contrast, for multi-component models, typically chemical diffusion is non-trivial in the hydrodynamic limit (even in the absence of inter-particle interactions beyond site exclusion) [28]. Below, the coverage $\theta = \theta(\underline{x}, t)$ at site $\underline{x} = (i, j)$ regarded as a continuous variable, and its evolution for spatially non-uniform systems is described exactly by the mean-field reaction-diffusion equation [1]

$$\partial/\partial t\ \theta = f(\theta) + D\ \partial^2/\partial \underline{x}^2\ \theta, \qquad \text{(A1)}$$

$$f(\theta) = p(1-\theta) - \theta(1-\theta)^2.$$

It is convenient to write $f(\theta) = -\partial/\partial\theta\ U(\theta)$ with "potential"

$$U(\theta) = \tfrac{1}{2}\, p(1-\theta)^2 - 1/3\ (1-\theta)^3 + \tfrac{1}{4}\ (1-\theta)^4. \qquad \text{(A2)}$$

The stable steady states correspond to the minima of U, i.e., $\theta=\theta_{absorb}= 1$ for all p (the absorbing state) and $\theta = \theta_{active}(p) = \tfrac{1}{2} - \tfrac{1}{2}\ (1-4p)^{1/2}$ for $p< p_s(mf) = \tfrac{1}{4}$ (the stable active state). These are separated by an unstable steady-state with $\theta = \theta_{unstable}(p) = \tfrac{1}{2}+ \tfrac{1}{2}\ (1-4p)^{1/2}$ for $p< p_s(mf) = \tfrac{1}{4}$, corresponding to a local maximum of U.

To analyze propagation of planar interfaces with velocity V between active and absorbing states, one considers solutions of the form $\theta=\theta(x-Vt)$ [47,48]. Substitution into Eq. (A1) yields

$$D\,\theta'' = -\,\partial/\partial\theta\,[-U(\theta)] - V\,\theta', \qquad \text{(A3)}$$

where the prime denotes derivative with respect to the single variable. This Newton-type equation describes the motion of a pseudo-particle with position θ subject to a two-hill potential $-U(\theta)$ and subject to a drag force with drag coefficient V. The physical interface corresponds to motion from one hill to the other with (almost) vanishing initial and final velocities. Equistability corresponds to the case V=0, which by conservation of energy requires that the two hills have equal height. A simple calculation shows that this corresponds to $p = p_{eq}(mf) = 2/9 \approx 0.222$ (mean-field) [1,48]. This result also follows as a special case of the analysis of the general mean-field Schloegl model of the second kind [17], where it is shown that

$$V \propto (\theta_{absorb} + \theta_{active} - 2\theta_{unstable}). \qquad \text{(A4)}$$

This expression also shows that V has a finite value, V_s, say, at the spinodal $p=p_s(mf)= ¼$, and that $V\text{-}V_s \sim (1\text{-}4p)^{1/2}$, as $p\rightarrow p_s(mf)$. The non-linear behavior as p approaches p_s is reminiscent of the behavior shown in our simulation results for V(S, p) for the QCP in Fig.10.

Appendix B. Modifications and Generalizations of the QCP

We consider the following modifications or generalizations of the standard QCP:

(i) Addition to the QCP of a separate random desorption pathway associated with a "small" desorption rate $d\geq 0$ [19]. Making an analogy with the conventional equilibrium Ising

model, d corresponds to a temperature-like variable, with d=0 recovering the standard QCP. This generalized model removes the special feature of standard QCP rules which prohibits growth of isolated empty droplets and which prohibits the shrinkage of vertical strip of the absorbing state. However, we find that generic two-phase coexistence (PC) persist in this generalized model extending to a range of d>0. PC terminates at an Ising–like critical point $d=d_c$ [19]. A detailed analysis of this generalized model will be provided elsewhere. This observation supports the claim made above that the presence of an absorbing state in the QCP should not be regarded as producing PC. It should also be noted that this generalized model constitutes just one way of perturbing the desorption rates in the QCP, and we find that various other perturbations will also preserve generic two-phase coexistence.

(ii) An adsorption-desorption version of the QCP on a triangular lattice (with coordination number 6): adsorption occurs randomly at rate p, and cooperative desorption of particles occurs at rate k/4 where k = 0, 1, 2, 3, 4, or 6 denotes the number of adjacent pairs of NN empty sites. Interestingly, the mean-field kinetics remains unchanged from the case of the square lattice in contrast to the conversion of the type of transition. CC simulation studies reveal a continuous transition to the absorbing state occurs at $p \approx 0.177$. The simulated steady-state coverage in the active state actually follows the mean-field value from Appendix A more closely and for higher p than for the QCP on the square lattice. This feature is presumably a consequence of the higher coordination number for the triangular lattice. However, eventually the steady-state coverage for the QCP on the triangular lattice departs strongly from MF behavior in the vicinity of the continuous transition.

(iii) Relaxation of the constraint on desorption in the QCP so that now any particle with two or more empty neighbors can desorb. Choosing the desorption rate to always equal

unity, this process corresponds to the threshold contact process for M=2 [20]. A previous study proved the existence of a phase transition, but did not determine its nature [20]. Our own simulation study reveals the existence of a discontinuous transition at $p_{eq}^* \approx 0.36$ (starting from an empty lattice) which should be compared with $p_{eq}^* \approx 0.0944$ for the QCP. The generic two-phase coexistence also occurs. The substantial increase in adsorption rate p_{eq}^* from its value for the standard QCP is readily understood since the effective desorption rate is also significantly higher than in the standard QCP. An additional perspective comes from applying a mean field analysis wherein

$$d\theta/dt = p(1-\theta) - \theta(1-\theta)^2(1+2\theta+3\theta^2), \qquad \text{(B1)}$$

for the M=2 threshold contact process.

From Eq. (B1), one finds a spinodal pressure $p_s \approx 0.678$ for this process versus $p_s \approx 0.25$ for the QCP, so the increase in the mean-field p_s mimics the increase in p_{eq}^*. Some other features of this threshold contact process should be noted. Like the QCP, one still has the special feature that vertical (or horizontal) strips of the absorbing phase cannot be eroded, and that empty patches embedded in the absorbing state cannot grow outside of a rectangular region inscribing them. The irreversible erosion of planar interfaces for p=0 is identical to that in the QCP. Relaxation kinetics for p=0 or p=0+ is described by the standard BP model.

References

[1] R. Durrett, SIAM Rev. **41**, 677 (1999).
[2] J. Marro and R. Dickman, *Nonequilibrium phase transitions in lattice models* (Cambridge UP, Cambridge, 1999).
[3] H. Hinrichsen, Adv. Phys. **49**, 815 (2000).
[4] G. Odor, Rev. Mod. Phys. **76**, 663 (2004).
[5] R.M. Ziff, E. Gulari, and Y. Barshad, Phys. Rev. Lett. **56**, 2553 (1986).
[6] J.W. Evans and M.S. Miesch, Phys. Rev. Lett. **66**, 833 (1991).

[7] J.W. Evans and T.R. Ray, Phys. Rev. E **50**, 4302 (1994).
[8] R. H. Goodman, D. S. Graff, L. M. Sander, P. Leroux-Hugon, and E. Clément Phys. Rev. E **52**, 5904 (1995).
[9] R.A. Monetti and E.V. Albano, J. Phys. A **34**, 1103 (2001).
[10] E. Loscar and E.V. Albano, Rep. Prog. Phys. **66**, 1343 (2003).
[11] E. Machado, G.M. Buendia, and P.A. Rikvold, Phys. Rev. E **71**, 031603 (2005).
[12] Da-Jiang Liu, Xiaofang Guo, D. Unruh, and J.W. Evans, unpublished.
[13] R. Bidaux, N. Boccara, and H. Chaté, Phys. Rev. A **39**, 3094 (1989)
[14] R. Dickman and T. Tomé, Phys. Rev. A **44**, 4833 (1991).
[15] G.A. Cardozo and J.F. Fontanari, Eur. Phys. J. B **51**, 555 (2006).
[16] F. Schloegl, Z. Phys. **253**, 147 (1972).
[17] A.L. Mikhailov, *Foundations of Synergetics I* (Springer-Verlag, Berlin, 1990).
[18] P. Grassberger, Z. Phys. B Cond. Matt. **47**, 365 (1982).
[19] D.-J. Liu, Xiaofang Guo, and J.W. Evans, Phys. Rev. Lett. **98**, 050601 (2007).
[20] S. J. Hanjini, J. Theor. Probability **10**, 737 (1997).
[21] M.A. Munoz, F. de los Santos, and M.M.T. da Gama, Euro. Phys. J. B **43**, 73 (2005).
[22] A.L. Toom, in *Multicomponent random systems*, edited by R.L. Dobrushin and Y.G. Sinai Marcel Dekker, New York, 1980).
[23] C.H. Bennett and G. Grinstein, Phys. Rev. Lett. **55**, 657 (1985).
[24] G. Grinstein, IBM J. Res. & Dev. **48**, 5 (2004).
[25] Y. He, C. Jayaprakash, and G. Grinstein, Phys. Rev. A **42**, 3348 (1990).
[26] M. Bramson and L. Gray, in *Random Walks, Brownian Motion, and Interacting Brownian Motion*, R. Durett and H. Keston, ed.s (Birkhauser, Boston, 1991).
[27] R.M. Ziff and B.J. Brosilow, Phys. Rev. A **46**, 4630 (1992).
[28] J.W. Evans, D.-J. Liu, and M. Tammaro, Chaos **12**, 131 (2002).
[29] D.-J. Liu and J.W. Evans, J. Phys.: Cond. Matt. **19**, 065129 (2007).
[30] R.H. Schonmann and S.B. Shlosman, Comm. Math. Phys. **194**, 389 (1998).
[31] S. Shlosman, Physica A **263**, 180 (1999).
[32] Xiaofang Guo, J.W. Evans, and Da-Jiang Liu, Physica A (2008).
[33] M. Avrami, J. Chem. Phys. **7**, 1103 (1939); **8**, 212 (1940); **9**, 177 (1941).
[34] J.W. Evans, Rev. Mod. Phys. **75**, 1296 (1993).
[35] D.E. Sanders and J.W. Evans, Phys. Rev. A **38**, 4186 (1988).
[36] J. Adler and A. Aharony, J. Phys. A **21**, 1387 (1988).
[37] J. Adler, D. Stauffer, and A. Aharony, J. Phys. A **22**, L297 (1989).
[38] M. Aizenman and J.L. Lebowitz, J. Phys. A **21**, 3801 (1988).
[39] An exact analysis of standard BP indicates that there must exist a crossover in γ for larger L to a precise asymptotic value of $\gamma = \pi^2/18 \approx 0.55$. See A. Holroyd, Prob. Th. and Related Fields, **125**, 195 (2003).
[40] J.W. Evans and H.C. Kang, J. Math. Phys. **32**, 2918 (1991).
[41] P. Meakin, P. Ramanlal, L.M. Sander, and P.C. Ball, Phys. Rev. A **34**, 5091 (1986).
[42] J. Krug and H. Spohn, Europhys. Lett. **8**, 219 (1989).
[43] H. Hinrichsen, R. Livi, D. Mukamel, and A. Politi, Phys. Rev. E **61**, R1032 (2000).
[44] C.H. Bennett, G. Grinstein, Y. He, C. Jayaprakash, and D. Mukamel, Phys. Rev. A **41**, 1932 (1990).

[45] J.D. Gunton and M. Droz, *Introduction to the theory of metastable and unstable states*, Springer Lecture Notes in Physics, Vol. 183 (Springer, Berlin, 1983).
[46] R. Kutner, Phys. Lett. **81A**, 239 (1981).
[47] P.C. Fife and J.B. McLeod, Arch. Rat. Mech. Anal. **65**, 335 (1977).
[48] C. Noble, Ann. Probab. **20**, 724 (1992).

Figures

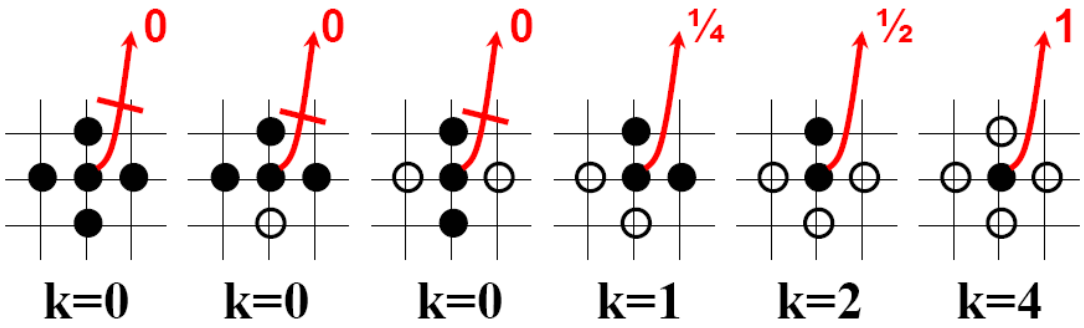

Figure 1. Schematic of desorption processes and rates in the QCP. Filled (empty) circles denote particles (empty sites) on the square lattice. Desorption rates (k-values) for the central particle are indicated above (below) the various configurations.

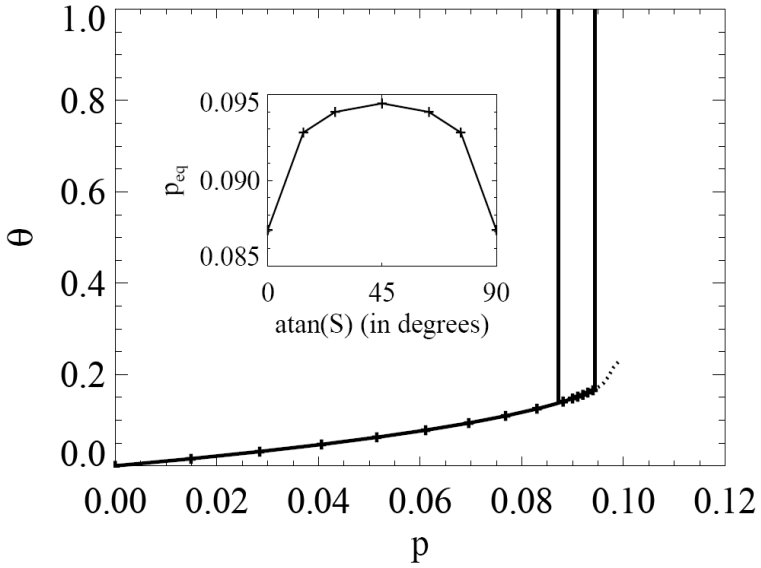

Figure 2. Equation of state for the QCP: steady-state coverage, $\theta=\theta_{ss}$, versus p. The lower solid curve is the active steady-state for which a metastable extension is indicated. The solid vertical lines denote the boundaries of the generic two-phase coexistence region. Inset: equistability pressure, $p_{eq}(S)$, versus interface slope, S.

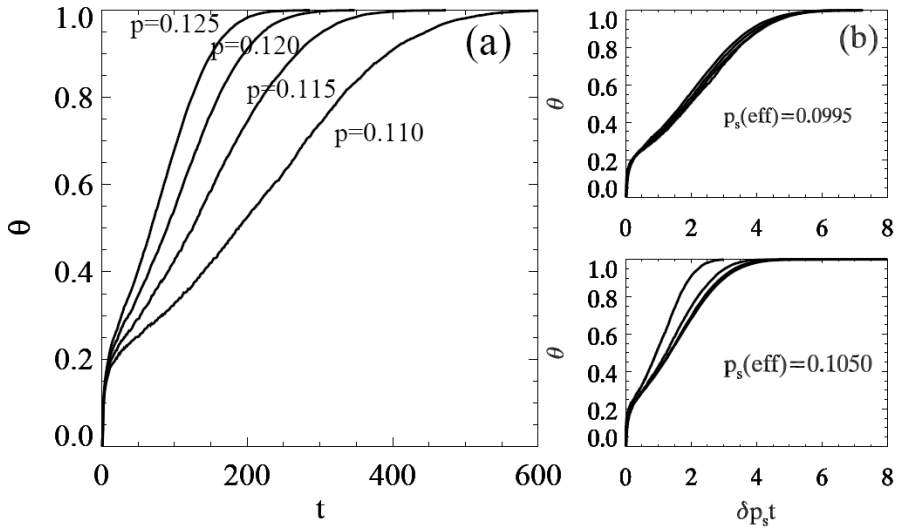

Figure 3. (a) Rapid poisoning kinetics above the effective spinodal point, $p_s(eff)$, for a range of p = 0.110, 0.115, 0.120, and 0.125 (b) Scaled poisoning kinetics for the above p-values indicating that $p_s(eff) = 0.0995 \pm 0.0005$.

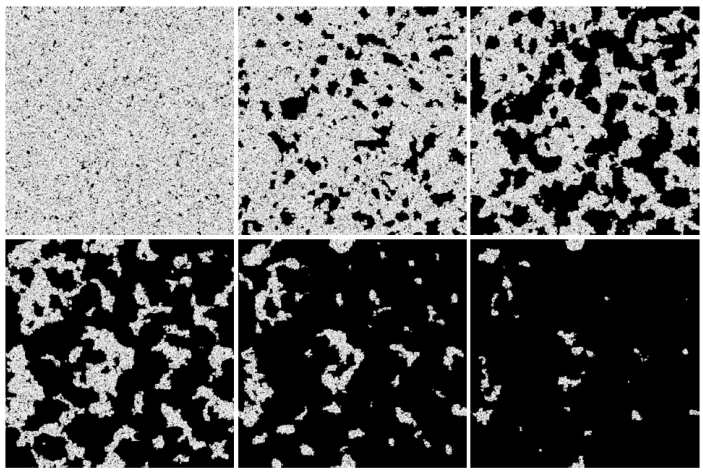

Figure 4. Images of QCP configurations in a 1024×1024 site system during nucleation-mediated poisoning for p=0.098 in the metastable region. Images correspond to unevenly spaced times but roughly equal coverage increments (time increasing from left to right, top then bottom rows, with coverages of 0.20, 0.35, 0.57, 0.76, 0.90, and 0.97).

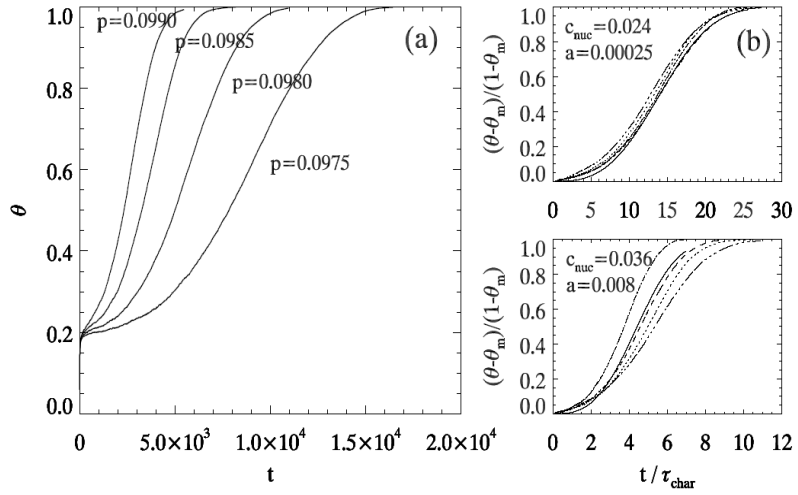

Figure 5. (a) Nucleation-mediated poisoning kinetics in the metastable region for a range of p = 0.0975, 0.0980, 0.0985, and 0.0990. Data is taken from simulations on a large 1024×1024 site lattice to ensure the system is in the multi-droplet regime and to reduce significant statistical fluctuations. (b) Scaled poisoning kinetics for the above p-values in terms of the characteristic time, τ_{char}, given in the text. The best data collapse is for c_{nuc}=0.024. Also shown as solid curves are the Avrami kinetics (1) with best-fit values of a=0.0002 (c_{nuc} =0.024) and a=0.008 (c_{nuc}=0.036).

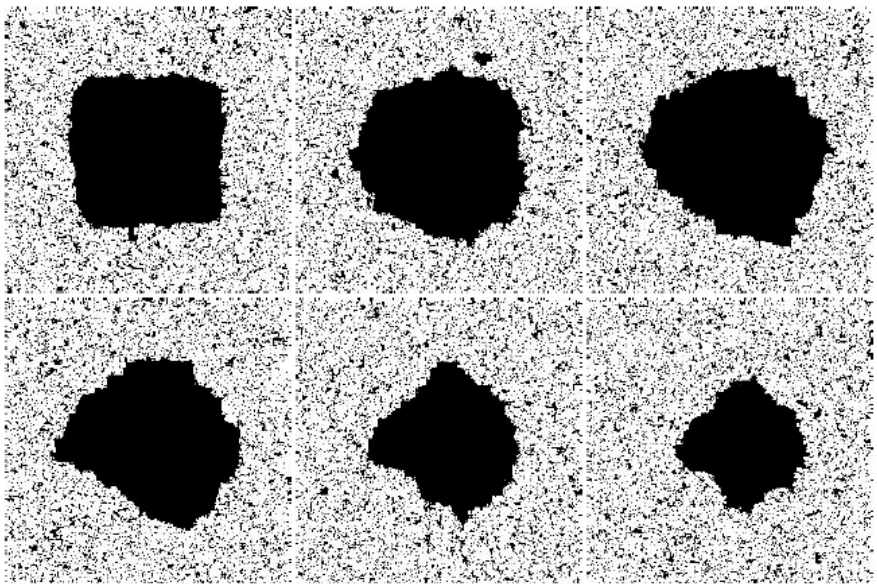

Figure 6. Dynamics of a large initially square poisoned droplet in the two-phase coexistence region for p = 0.0940. The system size is 256×256 sites and the initial droplet size is 128×128 sites. Images are shown for equal time increments of ~4000 time units (time increasing from left to right, top then bottom rows).

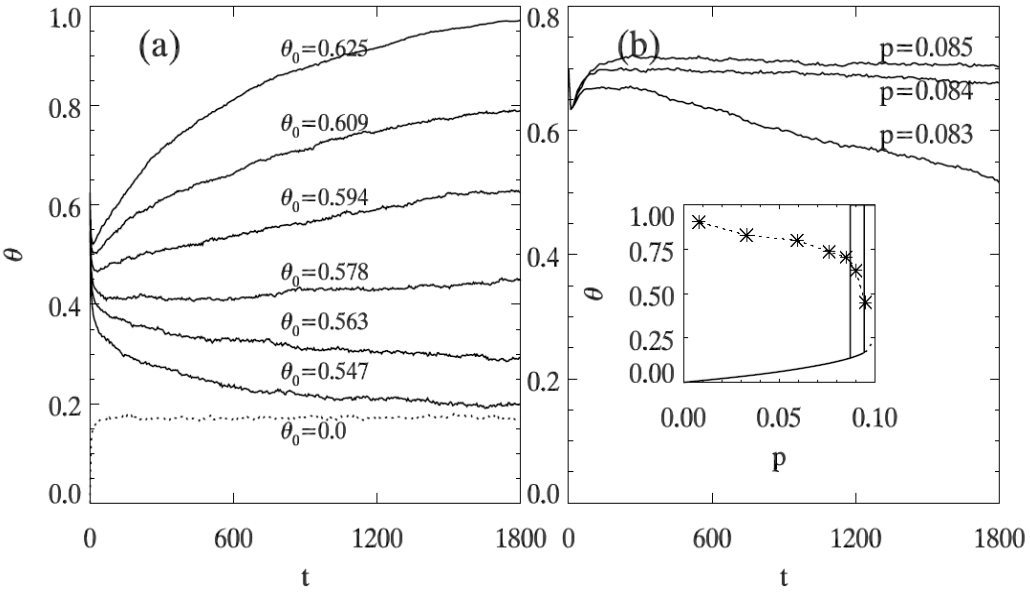

Figure 7. (a) Relaxation kinetics for fixed p = 0.0950 and L=256 in the metastable region just above the two-phase coexistence region, and for varying the initial coverage θ_i (shown). The critical initial coverage separating evolution directly to the absorbing state and to the metastable state is θ_i^*(p=0.0950, L=256) ≈ 0.57 for which θ_f^*(p=0.0950, L=256) ≈ 0.4. Shown for comparison as a dotted line is evolution to the metastable state for θ_i =0. (b) Relaxation kinetics for fixed initial coverage, θ_i = 0.7, varying p (shown). Inset: θ_f^*(p, L) versus p (shown as * symbols) for L=256.

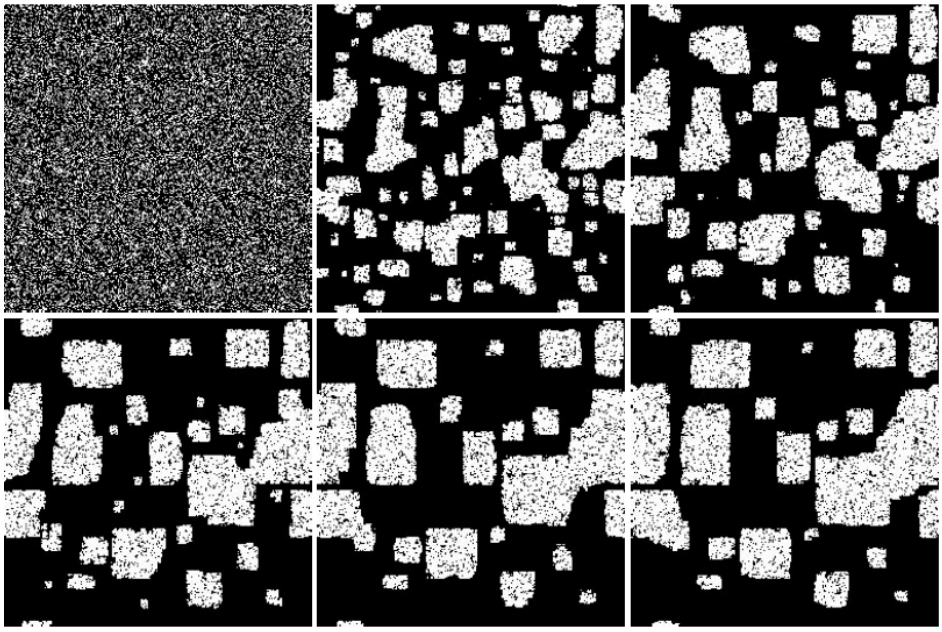

Figure 8. Images of QCP configurations for a 256×256 site system during the coarsening process choosing $\theta_v=\theta_v^*(p, L=256) = 0.3$ (so $\theta_i=0.7$) for p = 0.084. These parameters correspond to the central curve in Fig.7b. Images are shown for equal time increments of 400 time units (time increasing from left to right, top then bottom rows).

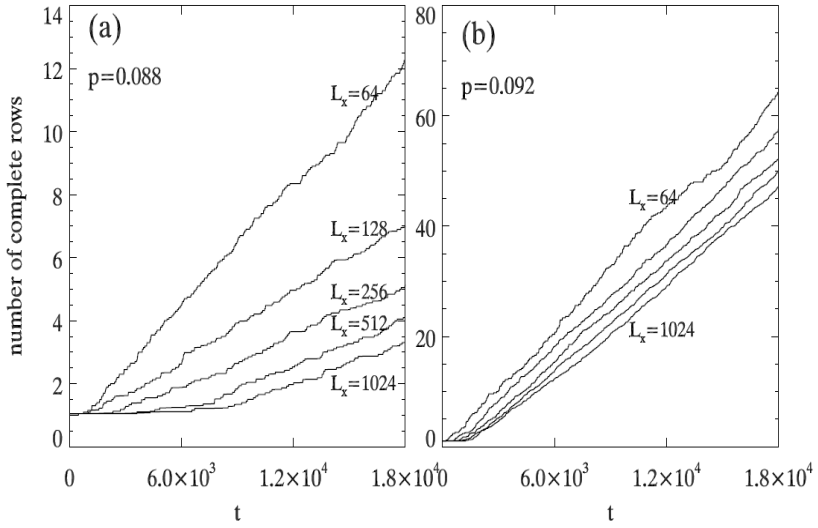

Figure 9. Number of completed columns versus time for vertical interfaces of various lengths, L_y = 64, 128, 256, 512, 1024 (shown). Results are presented for: (a) p=0.088; and (b) p=0.092.

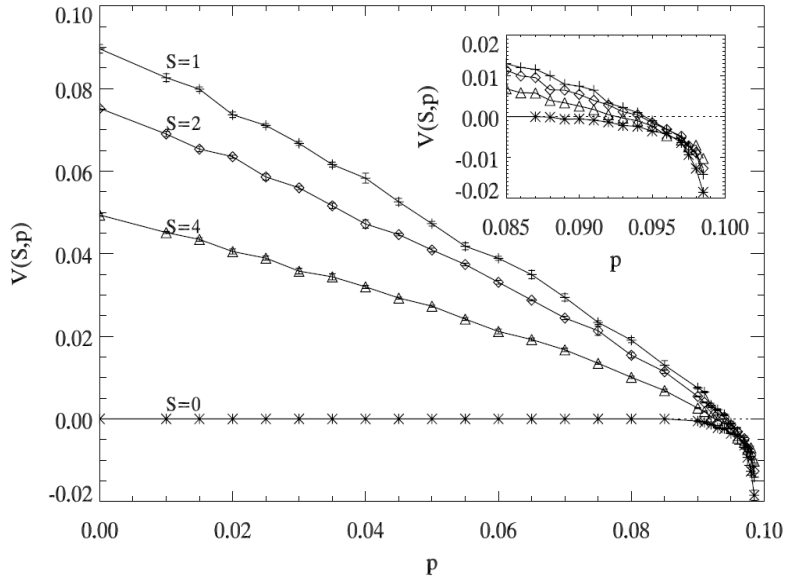

Figure 10. Interface propagation velocity, V(S, p) versus p, in the QCP for broad range of p. Behavior is shown for interface slopes S=1, 2, 4, and ∞. Inset: Behavior near the equistability pressures and approaching the effective spinodal point. Note that V(S=∞, p) ≡ 0 for $p<p_{eq}(S=\infty) \approx 0.0869$, and that V(S=∞, p)<0 only for $p>p_{eq}(S=\infty)$.

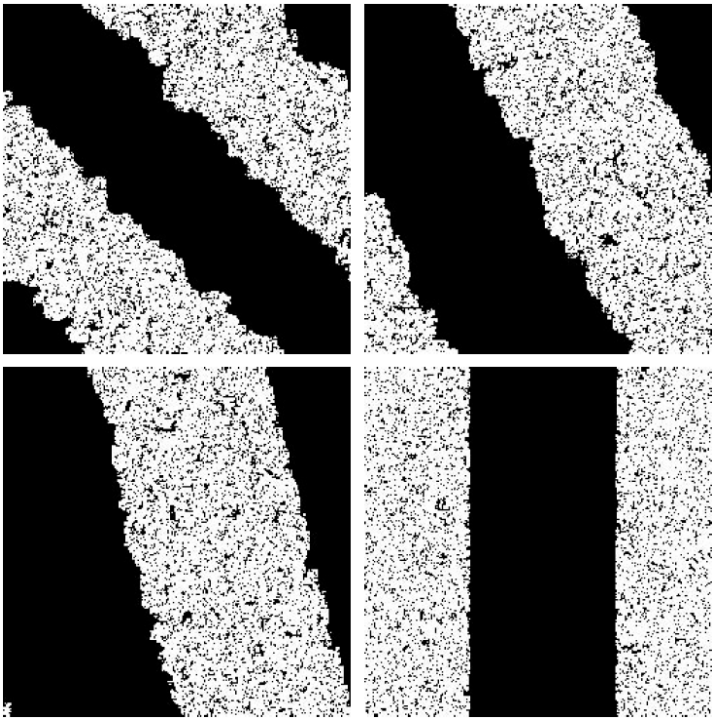

Figure 11. Configurations of equistable interfaces between the active and absorbing states in the QCP for various interface slopes S = 1 (top left), 2 (top right), 4 (bottom left), and ∞ (bottom right). Images sizes are 256×256 sites.

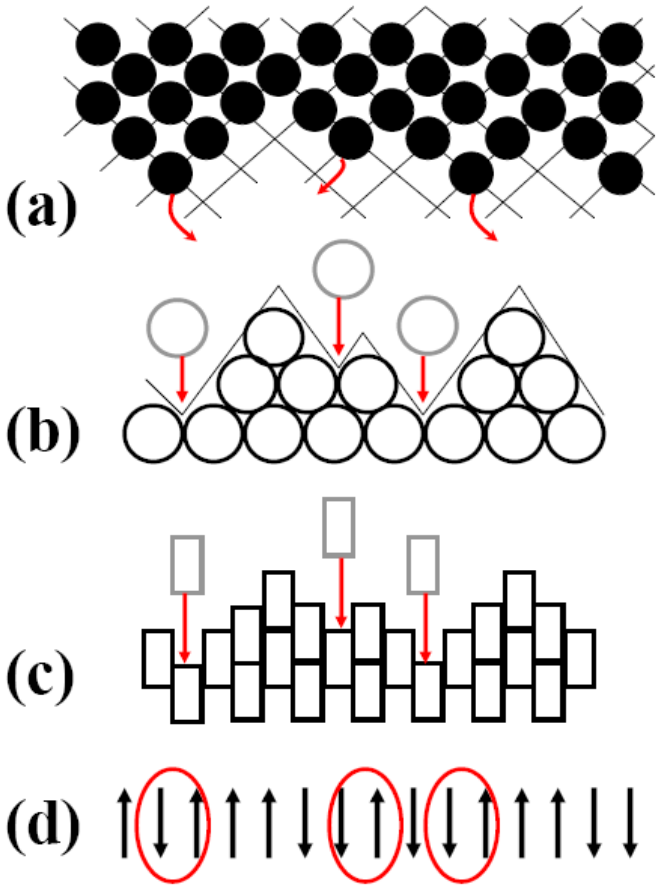

Figure 12. Schematic demonstrating the equivalence of: (a) irreversible erosion of the absorbing state in the QCP with p=0; (b) interface growth in the 1+1 dimensional bridge-site; (c) interface growth in the single-step deposition models; and (d) evolution in a fully asymmetric spin exchange model. We indicate the active sites for erosion by desorption in the QCP (a), and for deposition in models (b) and (c). The active sites for spin exchange are circled in (d). The thin diagonal lines in (b) guide the eye in identifying local peaks and valleys of the growing interface.

CHAPTER 3. GENERIC TWO-PHASE COEXISTENCE, RELAXATION KINETICS, AND INTERFACE PROPAGATION IN THE QUADRATIC CONTACT PROCESS: ANALYTIC STUDIES

A paper published in Physica A

Xiaofang Guo, J.W. Evans, and Da-Jiang Liu

Ames Laboratory – USDOE and Departments of Physics & Astronomy and Mathematics,
Iowa State University, Ames, Iowa, 50011

Abstract

The quadratic contact process is implemented as an adsorption-desorption model on a two-dimensional square lattice. The model involves random adsorption at empty sites, and correlated desorption requiring *diagonal pairs of empty neighbors*. A simulation study of this model [Phys. Rev. Lett. **98**, 050601 (2007)] revealed the existence of generic two-phase coexistence between a low-coverage active steady-state and a completely covered absorbing state. Here, an analytic treatment of model behavior is developed based on truncation approximations to the exact master equations. Applying this approach for spatially homogeneous states, we characterize steady-state behavior as well as the kinetics of relaxation to the steady-states. Extending consideration to spatially inhomogeneous states, we obtain discrete reaction-diffusion type equations characterizing evolution. These are employed to analyze an orientation-dependence of the propagation of planar interfaces between active and absorbing states which underlies the generic two-phase coexistence. We

also describe the dynamics and critical forms of planar perturbations of the active state and of droplets of one phase embedded in the other.

PACS 05.70.Fh, 02.50.Ey, 05.45.-a, 05.50.+q,

1. Introduction

Stochastic spatial models for far-from-equilibrium processes [1] often display a richer variety of spatiotemporal behavior than traditional Hamiltonian systems. However, they can also exhibit some intriguing similarities. The steady-states of such non-equilibrium models often exhibit continuous and discontinuous phase transitions which appear analogous to equilibrium phase transitions in Hamiltonian systems [1-4]. Most effort towards exploring this analogy has focused on continuous non-equilibrium transitions where the concept of universality carries over from the equilibrium case. Instead, our interest here is in discontinuous non-equilibrium transitions which have received less attention. A commonly studied example is provided by the two-component Ziff-Gulari-Barshad (ZGB) model for a monomer-dimer surface reaction [5]. However, for a fundamental understanding of discontinuous non-equilibrium transitions, it is more convenient and natural to search for and analyze single-component models with the desired behavior. This observation motivates our consideration of a so-called quadratic contact process (QCP).

A familiar realization of a QCP is referred to as Schloegl's second model for autocatalysis [1,6,7]. In the most relevant special case of this model, particles X either spontaneously annihilate ($X \rightarrow \varnothing$) at a rate k, or are autocatalytically created and destroyed via a trimolecular reaction ($2X \leftrightarrow 3X$). For low k, an active steady state with finite particle density is expected to exist, in addition to the vacuum steady state with no particles.

However, for high enough k, only the vacuum state should exist. In another realization of a QCP for epidemic spread on a periodic lattice, sick individuals recover spontaneously at some rate k_r, and healthy individuals become infected at rate k_i if they have two suitably configured sick neighbors. For low k_r/k_i, a sustained epidemic steady state should exist, in addition to a completely healthy steady-state. For high enough k_r/k_i, only the completely healthy steady state should exist. Here, we realize a QCP as an adsorption-desorption model on a two-dimensional lattice representing a single-crystal surface [1,8]. Particles absorb randomly at empty sites at rate or "pressure" p, and desorb from the surface provided there exist suitable *pairs of empty neighbors*. For low p, an active lower coverage steady-state is expected to exist, in addition to a completely covered or "poisoned" state. For high enough p, only the poisoned state should exist.

All of these model realizations have cubic mean-field kinetics and thus display the same mean-field behavior including bistability disappearing at a fold bifurcation. This feature suggests that discrete stochastic implementations of these models might exhibit discontinuous transitions. However, behavior of such implementations depends on the specific realization [7,8], and often continuous (instead of discontinuous) transitions are observed in lower spatial dimensions.

We adopt a specific prescription of the QCP on a square lattice which is motivated by a formulation of Durrett [1]: particles adsorb randomly at empty sites at rate or pressure p; particles desorb cooperatively at rate k/4 where k = 0, 1, 2, or 4 denotes the number of *diagonally adjacent pairs of nearest neighbor (NN) empty sites*. Thus, one has: k=0 for particles with just 0 or 1 empty NN sites, and also for 2 empty NN sites which are on opposite sides of the particle; k=1 for particles with just 2 diagonally adjacent empty NN

sites; k=2 for particles with 3 empty NN sites; and k=4 for particles with all 4 NN sites empty. See Fig.1. Now, we describe a special feature of this QCP following immediately from the above rules [1,8]. This special feature, which impacts our analysis below, is manifested to two ways. First, a filled vertical strip (or single column) spanning the system can never be eroded by desorption for any $p \geq 0$. The same is true for filled horizontal strips or rows. Particles within such strips can never have more than one empty NN site, and thus have k=0. Second, an isolated non-poisoned droplet embedded in an otherwise covered lattice can never grow outside of a rectangle inscribing that droplet. Thus, eventually, the droplet must be filled in and perish for any $p>0$. This latter feature was noted by Durrett [1].

One could consider various modified adsorption-desorption prescriptions of the QCP, e.g., allowing desorption for particles with two or more neighboring empty sites on the square lattice irrespective of their configuration. Such a prescription is in the spirit of so-called threshold contact processes [9], and preserves the cubic mean-field kinetics and bistability. Analysis of such modified models reveal qualitatively similar behavior to that for the above Durrett-type prescription including a discontinuous transition and generic two-phase coexistence [10]. Below we consider exclusively the Durrett-type prescription outlined above. One minor advantage of this prescription, which will become clear in Sec.2, is a simplification of the exact master equations resulting from the specific form of the desorption rates, and an associated simple condensed form for the mean-field kinetics.

Kinetic Monte Carlo (KMC) simulation studies of our Durrett-type QCP [8] suggest that for an infinite system, there exists an active steady state with low coverage satisfying $\theta = \theta_{active}(p) = p + O(p^2)$ for sufficiently small p. More specifically, simulations suggest that an infinite system starting with an empty lattice will evolves to this active steady state for $p <$

$p_{eq}^* \approx 0.09443$, but will undergo a discontinuous transition and evolve to a completely covered lattice with $\theta = \theta_{absorb}(p) \equiv 1$ for $p > p_{eq}^*$. The latter is an absorbing or poisoned state from which the system can never escape. More detailed analysis reveals that the equistability pressure, $p_{eq} = p_{eq}(S)$, for which a planar interface separating the active and absorbing states or phases is stationary, depends on the interface slope, S. This is in marked contrast to equilibrium systems. Specifically, $p_{eq}(S)$ displays a maximum of $p_{eq}(S=1) = p_{eq}^* \approx 0.09443$ for diagonal interfaces, and decreases with increasing S to a minimum of $p_{eq}(S\rightarrow\infty) \approx 0.0869$ for vertical interfaces [8]. Recalling that vertical strips cannot shrink, it follows that vertical interfaces are stationary for $p< p_{eq}(S=\infty)$ in an infinite system, whereas the absorbing state expands for $p> p_{eq}(S=\infty)$. As an aside, in a finite system, columns adjacent to the completely filled columns at the interface invariably fill, so the absorbing state expands for any $p>0$. Thus, determination of $p_{eq}(S=\infty)$ avoiding such finite-size effects is delicate [8].

Another perspective on the unusual behavior of the QCP relative to equilibrium systems is that each of the active and absorbing states are stable against local perturbations by the other state for a finite range of p. This phenomenon is called generic two-phase coexistence [11-13] or “true bistability” [8]. It contrasts behavior in equilibrium systems where coexistence of stable phases can occur only at a single p corresponding to equal chemical potentials. To more fully characterize of this generic two-phase coexistence phenomenon for the QCP and to elucidate its origins, first consider the evolution an isolated droplet of the absorbing state embedded in the active state. This droplet will certainly shrink and perish for $p < p_{eq}(S=\infty)$. It will grow for $p > p_{eq}(S=1)$, at least if it is sufficiently large [10]. For $p_{eq}(S=\infty) < p < p_{eq}(S=1)$, the situation is less clear [8,10]. Simulations have been

applied to monitor the evolution of a square absorbing droplet. Its sides initially grow outward since $p > p_{eq}(S=\infty)$. However, growth at the corners is inhibited, and so soon facets with slope $S = \pm 1$ develop and dominate the droplet which becomes diamond shaped. Subsequently, this droplet shrinks and disappears since $p < p_{eq}(S=1)$ [10]. Thus, the active state is stable against local perturbations for $p < p_{eq}(S=1)$. Second, we recall the special feature of the QCP described above which ensures that an isolated droplet of the active state embedded in poisoned state will perish with certainty for any $p>0$.

Thus, we conclude that both the active and absorbing phases in the QCP are stable against local perturbations by the other phase for $0 < p < p_{eq}(S=1)$, which might reasonably be identified as the regime of two-phase coexistence. Our characterization above of equistability pressures for planar interfaces demonstrates that for the narrower regime of $p_{eq}(S=\infty) < p < p_{eq}(S=1)$, both the active and absorbing states are also stable against non-local perturbations, i.e., either can displace the other separated by a planar interface of suitable orientation. For the QCP, we have used the latter more restrictive condition to identify generic two-phase coexistence with the regime $p_{eq}(S=\infty) < p < p_{eq}(S=1)$ [8,10]. One motivation of this more restrictive choice is in part that various perturbations of the QCP to include particle hopping or random desorption [8] with infinitesimal rates remove the above special feature of the QCP and reduce two-phase coexistence to the latter narrower regime.

The classic example of generic two-phase coexistence is provided by Toom's synchronous cellular automata model for the stochastic dynamics of an array of voters distributed on a square lattice. In this model, only voters to the north and east are considered when an individual changes votes [12,13]. Thus, in contrast to the QCP, Toom's dynamic rules incorporate strong symmetry-breaking which helps induces two-phase coexistence. It

should be noted that considerations of droplet dynamics and anisotropy in interface propagation, analogous to those above, were used to elucidate behavior in Toom's model [12,13]. Finally, from a broader perspective, it is appropriate to mention that occurrence of two-phase coexistence and the associated orientation-dependence of interface propagation and equistability has been postulated to occur for broad classes of lattice-gas adsorption-desorption or reaction models exhibiting discontinuous transitions [10].

The focus of our study in this paper is on the development of an analytic treatment for our adsorption-desorption realization of the QCP. This treatment will be based on truncation of the hierarchical form of the corresponding exact master equations. The reader is refereed to Ref. [14] for a more general discussion of this strategy. While such an approach does involve approximations, it can provide insight into model behavior which is lacking in Kinetic Monte Carlo (KMC) simulation studies. Indeed, this type of approach, as typically applied to spatially homogeneous systems, has enjoyed some success in analysis of kinetics and steady-state behavior for the ZGB model and other lattice-gas adsorption-desorption or surface reaction type models [15,16]. However, effective and comprehensive analysis of current model requires extension to treat spatially non-uniform states, e.g., for analysis of interface propagation. This extension has been considered only rarely in previous analyses of lattice-gas models [17]. It naturally produces novel types of discrete reaction-diffusion equations (RDE's). For higher order truncation approximations, these discrete RDE's involves both site coverages and various local spatial correlations, and they also incorporate complex prescriptions of "diffusive coupling". These features contrast with commonly studied discrete RDE's [18-20].

The outline of paper is as follows. In Sec.2, we develop the hierarchical form of the exact master equations and appropriate truncation approximations for spatially homogeneous states of the QCP. We compare predictions for steady-states and kinetics with results from KMC simulations. In Sec.3, we extend the above analysis to treat spatially non-uniform states. The primary focus is on analysis of the propagation of planar interfaces separating the active and absorbing states for various orientations. In particular, we determine the orientation-dependence of the equistability pressure. We also consider planar perturbations of the active state and determine the critical form of such perturbations above which they grow. In addition, we explore the dynamics of two-dimensional droplets of one phase embedded in the other. Finally, Sec.4 provides some further discussion and conclusions.

2. Exact Master Equations & Approximations: Spatially Homogeneous Case

The exact master equations for our QCP (or for any other lattice-gas adsorption-desorption model) can be written in the form of an infinite coupled hierarchy. See Ref. [14]. Let x (o) denote a filled (empty) site, and let P's denote probabilities of various configurations of such sites. Then, for example, one has for the coverage that $\theta = P[x]$. Exploiting rotational symmetry of the model, the first two equations in the hierarchy for the evolution of these quantities with time, t, for a spatially uniform system have the form

$$\begin{aligned} d/dt\, P[x] &= p \cdot P[o] - 4 \cdot \frac{1}{4} \cdot P\begin{bmatrix} & o & \\ x & x & o \\ & x & \end{bmatrix} - 4 \cdot \frac{1}{2} \cdot P\begin{bmatrix} & o & \\ x & x & o \\ & o & \end{bmatrix} - 1 \cdot 1 \cdot P\begin{bmatrix} & o & \\ o & x & o \\ & o & \end{bmatrix} \\ &= p \cdot P[o] - P\begin{bmatrix} o & \\ x & o \end{bmatrix} \end{aligned} \qquad (1)$$

$$\begin{aligned} d/dt\ P\begin{bmatrix} x & x \end{bmatrix} &= 2\{\, p \cdot P\begin{bmatrix} x & o \end{bmatrix} - 2 \cdot \frac{1}{4} \cdot P\begin{bmatrix} & o & \\ x & x & o \\ & x & \end{bmatrix} - 1 \cdot \frac{1}{2} \cdot P\begin{bmatrix} & o & \\ x & x & o \\ & o & \end{bmatrix} \} \\ &= 2 \cdot p \cdot P\begin{bmatrix} x & o \end{bmatrix} - P\begin{bmatrix} & o & \\ x & x & o \\ & & \end{bmatrix} \end{aligned} \qquad (2)$$

The gain (loss) terms correspond to adsorption (desorption). In the first line on the right-hand-side of (1), integer factors reflect the number of equivalent contributing configurations or terms due to rotational or reflection symmetries. Fractions reflect desorption rates of the form k/4. The first line on the RHS of (2) has an extra symmetry factor of 2. The second line on the right-hand-side of (1) and (2) is obtained by <u>exact simplification</u> using conservation of probability relations, and the specific form of the QCP desorption rates. Below, we apply various approximate truncation procedures to this hierarchy. We will also utilize the exact relation

$$P[xx] = 1 - 2\,P[o] + P[oo] = 2\theta - 1 + P[oo] \geq 2\theta - 1. \qquad (3)$$

Thus, from (3), the conditional probability, $Q = P[x\,x]/P[x]$, for finding a filled site adjacent to a specified filled site (a key quantity utilized below) satisfies $Q \geq (2\theta-1)/\theta$ which is a non-trivial constraint for $\theta \geq ½$.

2.1. Site-, Pair-, and Higher-Order Approximations

The simplest mean-field <u>site approximation</u> ignores all spatial correlations. It could be interpreted as describing exactly behavior in a modified QCP with particle hopping to NN empty sites at rate h in the hydrodynamic limit $h \to \infty$. However, it does <u>not</u> exactly describe the case h=0 of interest here. The site approximation completely factorizes the above multi-

site configuration probabilities in terms of single-site quantities P[x] = θ and P[o] = 1-P[x]. One thus obtains the kinetic equation

$$d/dt\ P[x] = p \cdot P[o] - P[x]\ P[o]^2 \quad \text{or} \quad d/dt\ \theta = p(1-\theta) - \theta(1-\theta)^2, \tag{4}$$

$$\text{so } \theta(1-\theta) = p \text{ or } \theta = 1 \text{ in the steady-states.} \tag{5}$$

As expected for mean-field approximations, rather than a discontinuous transition, equation (5) reveals bistability for $0 < p < p_s(\text{site}) = ¼ = 0.25$ (the upper spinodal), where $\theta(p_s) = \theta_s(\text{site}) = ½$. In this regime, a stable active state with

$$\theta = \theta_{active}(p) = ½ - ½\ (1-4p)^{1/2} = p + O(p^2) \tag{6}$$

coexists with a stable absorbing state with $\theta = \theta_{absorb}(p) \equiv 1$. These two stable states are separated by an unstable steady state with $\theta = \theta_{unstable}(p) = ½ + ½\ (1-4p)^{1/2}$. The absorbing state is the only steady-state for $p > p_s = ¼$. Analysis within the site approximation of the propagation of an interface between active and absorbing states with slope S=1 (see Sec.3) yields an equistability pressure, $p_{eq}(S=1) \approx 0.2113$ (site) which as expected is somewhat below p_s(site). However, these values of $p_s(\text{site}) = 1/4$, $\theta_s(\text{site}) = 1/2$, and $p_{eq}(S=1) \approx 0.2113$ (site) are well above the precise simulation values of $p_s(\text{eff}) \approx 0.0995 \pm 0.0005$, $\theta_s \approx 0.22 \pm 0.02$, and $p_{eq}(S=1) \approx 0.09443$ [8,10]. This inaccuracy might be expected as the site approximation is quite severe.

A significantly improved description comes from applying the pair approximation. This approximation suitably factorizes probabilities for the above multi-site configurations in the desorption terms of (1) and (2) into products of probabilities for the m constituent pairs, and divides by $P[x]^{m-1}$ to avoid over-counting the central shared filled site [14,15,21]. One thus obtains

$$d/dt\ P[x] = p\cdot P[o] - P[x\ \ o]^2/P[x], \text{ and} \tag{7}$$

$$d/dt\ P[x\ \ x] = 2p\cdot P[x\ \ o] - P[x\ \ x]\ P[x\ \ o]^2/P[x]^2. \tag{8}$$

Since one has P[x o] + P[x x] = P[x], one can use P[x o] = P[x] – P[x x] and P[o] = 1-P[x] to close these equations. In terms of conditional probability, Q = P[x x]/P[x], for finding a filled site adjacent to a specified filled site, (7) and (8) become

$$d/dt\ \theta = p(1-\theta) - (1-Q)^2\,\theta\ , \text{ and} \tag{9}$$

$$d/dt\ (\theta Q) = [2p - Q(1-Q)]\ (1-Q)\ \theta. \tag{10}$$

Note that one can rearrange (9) and (10) to obtain

$$d/dt\ Q = 2p\ [1 - Q(1+\theta)/(2\theta)]. \tag{11}$$

These equations also immediately yield the <u>steady-state relations</u>

$$p(1-\theta) - (1-Q)^2\theta\ = 0 \text{ and } Q(1-Q) = 2p, \quad \text{or} \quad \theta = Q = 1. \tag{12}$$

Either eliminating p from (12), or examining the steady-state form of (11), one obtains the simple steady-state relation [22]

$$Q = 2\theta/(1+\theta) \geq \theta, \tag{13}$$

which applies for <u>both</u> stable and unstable steady-states. This inequality demonstrates that all steady-states exhibit particle clustering, noting that Q = θ applies for a random distribution of particles.

From the second equation in (12), it is clear that the bistability regime in the pair approximation is $0 < p < p_s(\text{pair}) = 1/8 = 0.125$ (the upper spinodal), where $Q(p_s) = Q_s(\text{pair}) = 1/2$ and $\theta(p_s) = \theta_s(\text{pair}) = 1/3$. In this regime, a stable active state with

$$Q = Q_{\text{active}}(p) = \tfrac{1}{2} - \tfrac{1}{2}\,(1-8p)^{1/2} = 2p + O(p^2), \tag{14}$$

and $\theta = \theta_{active}(p) = p+O(p^2)$, coexists with a stable absorbing state with $Q = Q_{absorb}(p) \equiv 1$ and $\theta = \theta_{absorb}(p) \equiv 1$. These states are separated by an unstable steady state with $Q = Q_{unstable}(p) = ½ + ½ (1-8p)^{1/2}$. These values for $p_s(pair)=1/8$, $Q_s(pair)=1/2$, and $\theta_s(pair)=1/3$ are not far above the precise simulation values of $p_s(eff) \approx 0.0997\pm0.0005$, $Q_s \approx 0.38\pm0.03$ (see below) and $\theta_s \approx 0.22\pm0.02$ [8,10]. Analysis within the pair approximation of the propagation of interface with slope S=1 (see Section 3) yields an equistability pressure of $p_{eq}(S=1) \approx 0.1083$ (pair) somewhat below $p_s(pair)$. This value is quite close to the simulation value of $p_{eq}(S=1) \approx 0.09443$ [8]. The effectiveness of the pair approximation is further illustrated below in Sec.2.2 and 2.3.

Given the success of the pair approximation, it is natural to explore higher-order approximations. To systematize such approximations, it is convenient to first rewrite multi-site configuration probabilities in terms of filled site configurations, then to factorize these exactly in terms of conditional probabilities, and finally to apply a truncation approximation to the conditional probabilities [14]. These approximations are called m-NN corresponding to ignoring the influence of sites which are further than m^{th} nearest neighbor (NN) to the site of interest. The lead to closed coupled non-linear sets of N(m) equations. Further details are provided in Appendix A.

2.2. Results for Steady-State Behavior: Approximation VS Simulation

The 0-NN approximation recovers the site-approximation evolution equation (4) for P[x] so N(0) = 1. The 1-NN approximation recovers the pair-approximation equations (7) and (8) for P[x] and P[xx] so N(1) = 2. The 2-NN approximation produces a closed set of N(2) = 5 equations for the evolution of P[x], P[x x], and P's for a bent triple, a T-shaped quartet, and

a square quartet of filled sites [23]. The 3-NN approximation produces a closed set of N(3) = 11 equations for the evolution of the above five P's, plus P's for two more connected configurations (a linear triple, a cross-shaped quintuple), and four more disconnected configurations (a 2NN pair, a 3NN pair, a T and cross with the central site missing).

Predictions for the steady-state $\theta(p)$ versus p in the active state for the pair and higher-order approximations, as well as from simulations, are shown in Fig.2. We do not show results for the site approximation which reasonably describes behavior for lower p, but not near the spinodal point. An expanded view of the small difference between the simulated and approximate coverages, $\Delta\theta(p)$, versus p is shown in the inset to Fig.2. The higher-order approximations describe somewhat better exact behavior (although this offset by poorer predictions for equistability as discussed below). Since the conditional probability, Q, is a basic quantity describing correlations, we compare predictions for the steady-state Q(p) versus p from analytic 1-NN, 2-NN and 3-NN approximations with simulation results. See Fig.3. The 0-NN site approximation $Q=\theta$ fails to describe behavior even for low p.

2.3. Pair-Approximation Results for Relaxation Kinetics

One can also apply the various m-NN approximations above to assess relaxation kinetics in the QCP. We focus on pair-approximation predictions. We first show in Fig.4a pair-approximation predictions for the evolution of $\theta(t)$ versus t starting with an empty lattice for a range of $\delta p_s = p - p_s(\text{pair}) > 0$ above the spinodal. The rate of poisoning is roughly controlled by δp_s, so evolution is described by the form $\theta(t) \approx f(\delta p_s\, t)$. This behavior and the form of f is qualitatively similar to precise simulation results for kinetics of the QCP in Ref. [10] for the corresponding range of $\delta p = p - p_s(\text{eff})$. Fig.4b shows the evolution of $Q-\theta$ which

is positive during the intermediate stages of poisoning indicating the development of clustering.

Henceforth, we focus on pair-approximation predictions for the evolution of $\theta(t)$ versus t for fixed p below the spinodal starting from a partially randomly filled lattice with various initial coverages, $\theta_i = Q_i$. See Fig.5a. For each fixed p, there exists a special value of the initial coverage, $\theta_i^* = \theta_i^*(p)$, so that for $\theta_i > \theta_i^*$ the system poisons, and for $\theta_i < \theta_i^*$ it reaches the active steady-state. A more complete picture of behavior comes from examination of phase-portrait for flow in the (θ, Q)-plane which describes evolution starting from any pair of values of θ and Q. See Fig. 6 for behavior for p=0.10 which is below $p_s(\text{pair}) = 1/8$. Recall from the introduction to Sec. 2 that physical states are restricted to $Q \geq (2\theta-1)/\theta$ for $\theta \geq 1/2$. For initially random states, the system starts at a point on the line $(\theta, Q) = (\theta_i, \theta_i)$. When $\theta_i = \theta_i^*$, this point lies on the separatrix delineating domains of attraction for the active state (denoted by A) and the absorbing or poisoned state (denoted by P). The system then evolves to the unstable steady-state (denoted by U) by flowing along this separatrix. In this case, the coverage decreases from $\theta_i = \theta_i^*$ as the system moves along the separatrix to the unstable steady-state which lies in the region $Q > \theta$ corresponding to states with particle clustering [cf. (10)]. This explains the initial decrease of coverage in Fig.5a for θ_i close to θ_i^*.

The kinetics in higher-order approximations exhibit similar behavior (not shown). For relaxation at fixed p below the spinodal starting from a partially randomly filled lattice, again there is a special value of $\theta_i=\theta_i^*$ for which the system evolves to the unstable steady-state. Now, the initial states for various θ_i lie on a one-dimensional curve in the N(m) dimensional

space of the configurational probability variables. For $\theta_i=\theta_i^*$, this curve crosses the N(m)-1 dimensional separatrix hypersurface delineating domains of attraction for the active and absorbing states, and evolution corresponds to flow on this hypersurface to the unstable state.

2.4. Comparison with Simulation Results for Relaxation Kinetics

Here, we compare pair-approximation predictions for relaxation kinetics for lower p with simulation results. Fig.5b shows simulation results for the evolution of $\theta(t)$ versus t for fixed p=0.08 starting from a partially randomly filled lattice with various initial coverages, θ_i. This choice of p=0.08 is not only <u>below</u> the spinodal, $p_s(\text{eff}) \approx 0.0995$, but also below the regime of two-phase coexistence. Behavior is qualitatively similar to pair-approximation kinetics in Fig.5a in that there appears to exist a value θ_i^* of θ_i such that the system poisons for $\theta_i>\theta_i^*$ and approaches the active state for $\theta_i<\theta_i^*$. However, the transient kinetics is distinct from that of the pair approximation. More significantly, it should be emphasized that for $\theta_i = \theta_i^*$, the system does <u>not</u> evolve to an unstable steady state, but rather to a "coarsening state". In this state, there is a balance between shrinkage and disappearance of isolated quasi-rectangular regions of the active state, and coalescence and growth of other generally larger active regions [10]. See the inset to Fig.5b.

A more complete picture of simulation predictions for relaxation kinetics when p=0.08 and comparison with pair-approximation behavior comes from examination of phase-portrait for flow in the (θ, Q)-plane. Rather than just starting from random states (θ, Q) = (θ_i, θ_i), we generate a more expansive portrait by starting with states on the "anti-clustering" boundary of the physical phase space. Specifically, we generate Q=0 states with no NN pairs of particles by Random Sequential Adsorption (RSA) with NN exclusion when $0 \le \theta \le \theta_J \approx$

0.3641 (RSA jamming coverage) [14], and by adding relaxation mechanisms to RSA for $\theta_J < \theta \leq ½$ [24]. For the boundary with $Q = (2\theta-1)/\theta$ and $½ \leq \theta \leq 1$, we start with a perfect checkerboard c(2×2)-structure of alternating filled and empty sites, and randomly occupy a suitable fraction of the remaining empty sites. The phase-portrait for evolution starting from these states obtained from simulations of the QCP is shown in Fig.7. All states with Q=0 and $0 \leq \theta \leq 1/2$ evolve to the active steady state. States with $Q = (2\theta -1)/\theta$ and $\theta > 1/2$ evolve to the active state for initial coverages $\theta < \theta^* \approx 0.78$ and poison for $\theta > \theta^*$. We estimate that the "coarsening state" occurs at $(\theta_c, Q_c) \approx (0.80, 0.97)$ for p=0.08. Simulated behavior has overall qualitative similarities with the pair-approximation predictions. However, there are significant differences near the coarsening state (versus near the unstable state), as well as in the evolution towards the steady states.

The trajectories starting from the anti-clustering boundaries in the (θ, Q)-plane tend to follow a well-defined upper envelope which leads to the steady states. The states along this envelope, like the coarsening state, display some degree of phase separation between the active and absorbing states. Thus, one can determine Q as a function of θ by taking a suitable average of the values for the absorbing state $Q_{absorb} = 1$ and the active state $Q_{active} \approx 0.23$. This average should be weighted by the fractional area of the phases and also by the local coverage yielding for this envelope

$$Q_{envelope} = Q_{envelope}(\theta) = \theta^{-1} [1 - (1-\theta_{active}Q_{active})(1-\theta)(1-\theta_{active})^{-1}], \quad (15)$$

which interpolates between the active and absorbing states. In particular for $\theta = \theta_c \approx 0.80$, this relation yields $Q_c \approx 0.97$ entirely consistent with the estimate above. This envelope corresponds to significantly higher Q-values than for the flow trajectories predicted by the

pair approximation from the unstable to the stable active states. This reflects the feature that the pair approximation does not accommodate a tendency for phase-separation [25]. Of course, simulated evolution near the coarsening state is also more complex than pair approximation evolution near the unstable state. Furthermore, simulated evolution in this regime is subject to finite-size-effects (when the size of the coarsening features becomes comparable to the system size) and to large fluctuations. Thus, our simulations were performed for a large 1000×1000 site system.

3. Master Equations and Approximations for Interface Evolution

In this section, we are primarily interested in analyzing the propagation of interfaces separating stable active and absorbing phases, and in application of this analysis to the determination of equistability pressures. To implement this analysis, one must first extend the master equation formulation to treat spatially non-uniform states. For such states, the configuration probabilities in hierarchical master equations depend on the site location. Also, symmetry-equivalent terms collected together in (1) and (2) must typically be enumerated separately. However, some exact simplification is still possible using conservation of probability relations and the specific form of desorption rates for the QCP [cf. (1) and (2)]. This simplification leads to the following exact form for the first two hierarchical equations

$$\begin{aligned} d/dt\, P[x_{i,j}] = p \cdot P[o_{i,j}] - \frac{1}{4} \cdot P\begin{bmatrix} o_{i,j+1} & \\ x_{i,j} & o_{i+1,j} \end{bmatrix} - \frac{1}{4} \cdot P\begin{bmatrix} x_{i,j} & o_{i+1,j} \\ o_{i,j-1} & \end{bmatrix} \\ - \frac{1}{4} \cdot P\begin{bmatrix} o_{i-1,j} & x_{i,j} \\ & o_{i,j-1} \end{bmatrix} - \frac{1}{4} \cdot P\begin{bmatrix} & o_{i,j+1} \\ o_{i-1,j} & x_{i,j} \end{bmatrix} \end{aligned} \qquad (16)$$

$$
\begin{aligned}
d/dt\, P\begin{bmatrix} x_{i-1,j} & x_{i,j} \end{bmatrix} &= p \cdot P\begin{bmatrix} x_{i-1,j} & o_{i,j} \end{bmatrix} + p \cdot P\begin{bmatrix} o_{i-1,j} & x_{i,j} \end{bmatrix} \\
&- \frac{1}{4} \cdot P\begin{bmatrix} & o_{i,j+1} & \\ x_{i-1,j} & x_{i,j} & o_{i+1,j} \end{bmatrix} - \frac{1}{4} \cdot P\begin{bmatrix} x_{i-1,j} & x_{i,j} & o_{i+1,j} \\ & o_{i,j-1} & \end{bmatrix} \\
&- \frac{1}{4} \cdot P\begin{bmatrix} & o_{i,j+1} & \\ o_{i-1,j} & x_{i,j} & x_{i+1,j} \end{bmatrix} - \frac{1}{4} \cdot P\begin{bmatrix} o_{i-1,j} & x_{i,j} & x_{i+1,j} \\ & o_{i,j-1} & \end{bmatrix}
\end{aligned}
\qquad (17)
$$

where filled and empty sites are also labeled by their position (i,j) on the square lattice. Thus, $\theta_{i,j} = P[x_{i,j}]$ denotes the coverage of site (i,j). For the special case of a system with translational invariance, it is clear that (16) and (17) reduce to the equations (1) and (2) of Sec. 2.

Despite the additional complexity of the equations (16) and (17) relative to the spatially homogeneous case, the truncation procedures described above can still be implemented, but now with all probabilities labeled by site location. As a result, one obtains a coupled set of discrete reaction-diffusion type equations (RDE's) for a finite number of different types of configurational probabilities. An analogous procedure was implemented for the ZGB model on a square lattice, but only at the level of the site approximation and only for vertical interfaces [17]. In a broader context, there has been considerable interest in discrete RDE's of the Nagumo-type for bistable systems [18-20]. Most focus has been on assessing the phenomenon of propagation failure [18-20], a feature not seen in analogous continuum RDE's [26,27].

As indicated above, our primary interest here is in determining equistability pressures for coexisting stable active and absorbing phases. Here, it suffices to consider the evolution of planar interfaces between active and inactive states where the spatial non-uniformity is

only in a single direction. In particular, our focus is on determining the propagation velocity, V(p) = V(p, S), versus p, for various interface slopes, S. Unless otherwise stated, we use the convention that V>0 corresponds to the active state displacing or eroding the absorbing state, and V<0 corresponds to the opposite case. Then, the equistability pressure, $p_{eq} = p_{eq}(S)$, is determined from the condition $V(p = p_{eq}(S), S) = 0$. For planar interfaces, there is considerable simplification of the discrete RDE's which reduce to a one-dimensional form. This case will be considered exclusively in Sec.3A-3E. In Sec.3F, we consider two-dimensional droplet dynamics necessarily starting from the general form of (16) and (17).

3.1. Site-Approximation Formulation for Planar Interfaces

First, we consider <u>vertical interfaces with S=∞</u> separating active and absorbing states for $p < p_s$(site). Then, the site occupancies in (16) are just labeled by the column index, i, so that $\theta_i = P[x_{i,j}] = 1 - P[o_{i,j}]$. See Fig. 8. In the site approximation, these equations reduce to

$$d/dt\ P[x_i] = p \cdot P[o_i] - ½\ P[x_i]\ P[o_i]\ P[o_{i+1}] - ½\ P[x_i]\ P[o_i]\ P[o_{i-1}]. \quad (18)$$

Equation (18) can be written in a discrete RDE form as

$$d/dt\ \theta_i = p(1-\theta_i) - ½\ \theta_i(1-\theta_i)(2 - \theta_{i-1} - \theta_{i+1}) = p(1-\theta_i) - \theta_i(1-\theta_i)^2 + D(\theta_i)\ \Delta\theta_i, \quad (19)$$

with discrete Laplacian $\Delta u_i = u_{i+1} - 2u_i + u_{i-1}$ (noting that columns are separated by one lattice constant) and the pseudo-diffusion coefficient satisfies $D(\theta) = ½\ \theta(1-\theta)$. From (19), it follows that a poisoned column with $\theta_i=1$ will remain poisoned for all later times, so that absorbing vertical strips cannot be eroded within this approximation (preserving exact behavior).

Second, we consider <u>diagonal interfaces with slope S=1</u> separating active and absorbing states for $p<p_s$(site). Now, each diagonal row of sites labeled by m, say, will have its own coverage, $\theta_m = P[x_m] = 1 - P[o_m]$. These diagonal rows are separated by a distance

$d_1=1/\sqrt{2}$ lattice constants (in the direction orthogonal to the rows), a feature which impacts determination of propagation velocities from solution of the discrete RDE's. Factorizing the exact master equations (16) within the site approximation incorporating the reduced symmetry yields the equations

$$d/dt\ P[x_m] = p\cdot P[o_m] - 1/4\ P[x_m]P[o_{m-1}]^2 - \tfrac{1}{2}\ P[x_m]P[o_{m-1}]P[o_{m+1}] - 1/4\ P[x_i]P[o_{m+1}]^2. \quad (20)$$

These can be simplified and written in discrete RDE-type forms as

$$d/dt\ \theta_m = p(1-\theta_m) - \tfrac{1}{4}\ \theta_m(2 - \theta_{m-1} - \theta_{m+1})^2$$

$$= p(1-\theta_m) - \theta_m(1-\theta_m)^2 + D(\theta_{m-1}, \theta_m, \theta_{m+1})\ \Delta_1\theta_m$$

$$= p(1-\theta_m) - \theta_m(1-\theta_m)^2 + D(\theta_m)\ \Delta_1\theta_m - \theta_m\ (\Delta_1\theta_m)^2/16, \quad (21)$$

where $\Delta_1 u_m = (u_{m+1} - 2u_m + u_{m-1})/(d_1)^2$ is a discrete Laplacian, $D(\theta_{m-1}, \theta_m, \theta_{m+1}) = \theta_m(4 - \theta_{m-1} - 2\theta_m - \theta_{m+1})/8$ is a pseudo-diffusion coefficient, and $D(\theta)$ is as above.

This analysis is readily extended to consider <u>interfaces with general integer slope $S\geq 1$</u> for $p<p_s$(site). Now, off-diagonal rows with slope S, labeled by m, will each have distinct coverages, θ_m. See Fig.8. These rows are separated by a distance $d_S = 1/\sqrt{(1+S^2)}$. Factorizing (16) within the site approximation yields

$$d/dt\ \theta_m = p(1 - \theta_m) - \tfrac{1}{4}\ \theta_m\ (2 - \theta_{m-1} - \theta_{m+1})\ (2 - \theta_{m-S} - \theta_{m+S})$$

$$= p(1-\theta_m) - \theta_m(1-\theta_m)^2 + D(\theta_m)\ \Delta_{1,S}\ \theta_m - \tfrac{1}{4}\ S^2(1+S^2)^{-2}\ \theta_m\ \Delta_1\theta_m\ \Delta_S\theta_m, \quad (22)$$

where $\Delta_S u_m = (u_{m+S} - 2u_m + u_{m-S})/(Sd_S)^2$ and $\Delta_{1,S}\ u_m = [(1+S^2)^{-1}\ \Delta_1 u_m + S^2(1+S^2)^{-1}\ \Delta_S u_m]$ are refined discrete Laplacians, and $D(\theta)$ is as above. Thus, (22) reduces to (21) for S=1. Discrete diffusion terms involving Δ, Δ_1, Δ_S, or $\Delta_{1,S}$ naturally vanish for a linear coverage profile.

3.2. Site-Approximation Analysis and Numerics: Vertical Interfaces

It is instructive to first consider separately the special case of a vertical interface with $S=\infty$ for $p < p_s$(site). As noted in Sec.3A, analysis of the evolution equations (19) within the site approximation shows that the absorbing state can never be eroded, preserving a basic property of the QCP. This special feature significantly impacts behavior, e.g., ensuring that $V(p, S=\infty) \leq 0$ for all $p \geq 0$ according to our sign convention. Numerical integration of (19) further reveals that the vertical absorbing strip is stationary, i.e., it does not erode or grow, so that $V(p, S=\infty) \equiv 0$ for $p \leq p_{eq}(S=\infty) \approx 0.2071$ (site). Only for $p > p_{eq}(S=\infty)$ (site) does the absorbing state expand into the active state with $V(p, S=\infty) < 0$. Numerical results for $V(p, S=\infty)$ versus p will be presented in Sec.3C which indicate an apparent non-linear decrease in the magnitude of $V(p, S=\infty) < 0$ to zero as $p \to p_{eq}(S=\infty)$ (site) from above. This feature is reminiscent of behavior approaching threshold for propagation failure in Nagumo-type discrete RDE's [19].

Here, we provide a more detailed analysis of the stationary regime $p < p_{eq}(S=\infty)$, including a characterization of the transition point at $p = p_{eq}(S=\infty)$. For $p < p_{eq}(S=\infty)$, the interface profiles corresponding to stationary solutions of (18) are chosen to satisfy

$$\theta_0 = \theta_{-1} = \ldots = 1, \text{ and } 1 > \theta_1 > \theta_2 > \ldots \text{ with } \theta_i \to \theta_{active}(p) \text{ (site approx.) , as } i \to \infty. \quad (23)$$

From the steady-state form of (19), these coverages satisfy the recurrence relations

$$\theta_2 = 1 - 2p/\theta_1, \text{ and } \theta_{i+1} = 2 - \theta_{i-1} - 2p/\theta_i \text{ for } i>1. \quad (24)$$

Selection of $\theta_1=\theta_1(p)$, which determines the entire profile, must produce the desired asymptotic behavior, $\theta_i \to \theta_{active}(p)$, as $i \to \infty$, and is thus non-trivial.

It is clear that for p=0, the stationary profile corresponds to a sharp jump from the absorbing state to the active empty state with $\theta_1 = \theta_2 = \ldots = 0$. Furthermore, as p increases, one expects that the profile becomes broader. This feature is illustrated by linearization of (24) for large i using $\theta_i(p) = \theta_{active}(p) + \delta\theta_i(p)$ with small $\delta\theta_i$ to show that

$$\delta\theta_i(p) \sim \lambda^i, \text{ as } i\to\infty, \text{ where } \lambda=\lambda(p)=[1-\sqrt{(1-r^2)}]/r \text{ with } r=r(p)=\theta_{active}/(1-\theta_{active}). \qquad (25)$$

Broadening of the interface is a consequence of the feature that both r(p) and $\lambda(p)$ increase monotonically with p from zero when p=0 to unity when $p = p_s(\text{site})$. The latter follows from the observation that $\theta_{active} \to 0$, as $p \to 0$, and $\theta_{active} \to \theta_s = ½$, as $p \to p_s(\text{site}) = ¼$. Note, however, that the stationary interface exists only for $p \le p_{eq}(S=\infty) \approx 0.2071 < p_s(\text{site})$.

While instructive, the above analysis of the behavior of the stationary profile does not provide much insight into the transition from a stationary to a propagating vertical interface at $p=p_{eq}(S=\infty) \approx 0.2071$ (site). To achieve such insight, it is convenient to recast the 3-term recurrence relation (24) for i>1 into the form of an iterated map [28], $(u_i, v_i) \to (u_{i+1}, v_{i+1})$, in a two-dimensional phase space $(u_i, v_i) = (\theta_{i-1}, \theta_i)$. This iterated map has the form

$$u_{i+1} = v_i, \text{ and } v_{i+1} = 2 - u_i - 2p/v_i, \qquad (26)$$

with a the fixed point, $(u, v) = (\theta_{active}, \theta_{active})$. Linearizing the map (26) about this fixed point shows that the two eigenvalues of the associated Jacobian sum to $2(1-\theta_{active})/\theta_{active} \ge 2$ for $p \le p_s(\text{site})$. Thus, the magnitude of at least one eigenvalue must be larger than unity implying that this fixed point is unstable [28]

As the <u>first component</u> in of our numerical analysis of this iterated map, we start at points $(u, v) = (\theta_{active}+\varepsilon, \theta_{active}+\varepsilon')$ slightly perturbed from the fixed point ($\varepsilon, \varepsilon' << 1$) and

iterate. Points from these different iterations together generate a continuous curve. Fig.9 shows these curves of the iterated points for three p-values: for smaller p, the curve connects the unstable fixed point to the physical boundaries u=1 and v=1 of the phase space. This corresponds to a physical stationary profile where θ_i varies from $\theta_0 = 1$ to $\theta_{i\to\infty} = \theta_{active}$. For p $\approx$ 0.2071, the curve reaches the physical boundaries tangentially corresponding to $p=p_{eq}(S=\infty)$. For larger p, the curve never reaches these boundaries corresponding to the lack of a stationary solution.

The second component in our analysis is motivated by the observation from Fig.9 that at the threshold value of $p=p_{eq}(S=\infty)$, the continuous curve generated from the orbits reaches the physical boundaries of the phase space at (u, v) = (1-p, 1) or (1, 1-p) [29]. A key consequence of this observation and the recurrence relations (24) is that at the threshold, $p=p_{eq}(S=\infty)$, the stationary profile has the form

$$\theta_{i\le 0}(p)=1,\ \theta_1(p)=1-p,\ \theta_2(p)=(1-3p)/(1-p),\ \theta_3(p)=(1-4p-p^2)/(1-3p),\ \text{etc.}, \qquad (27)$$

Thus, knowledge of the form of $\theta_1(p) = 1-p$ in this special case allows determination of the form of all the $\theta_{i>1}(p)$. Of course, it remains to determine the value of $p=p_{eq}(S=\infty)$. However, this can be done efficiently with numerical simulations by adjusting estimates of p to satisfy the requirement that $\theta_i(p) \to \theta_{active}(p)$, as $i\to\infty$, yielding the precise estimate of $p_{eq}(S=\infty) \approx 0.2071068$. Insight into the relation $\theta_1(p) = 1-p$ when $p = p_{eq}(S=\infty)$ is provided in Sec.3.4.

3.3. Site-Approximation Analysis and Numerics: Interfaces for 1≤S≤∞:

Results within the site approximation for the interface propagation velocity, V(p, S), versus p with $p<p_s$(site) are shown in Fig.10. These results are obtained from numerical analysis of (21) and (22) for a diagonal and off-diagonal interfaces with slopes S≥1. The active state displaces the absorbing state for $p < p_{eq}(S)$, so that V(p, S) > 0, and the opposite applies for $p > p_{eq}(S)$. We determine that $p_{eq}(S=1) \approx 0.2113$ (site) as mentioned in Sec.2A, $p_{eq}(S=2) \approx 0.2100$, $p_{eq}(S=4) \approx 0.2074$, $p_{eq}(S=8) \approx 0.2057$, etc. (site). Note that the limiting value $p_{eq}(S\to\infty) \approx 0.2055$ is below $p_{eq}(S=\infty) \approx 0.2071$ obtained from analysis of behavior for a vertical interface in Sec.3B. To emphasize this point, Fig. 10 also shows the behavior of V(p, S= ∞) versus p for a vertical interface. The curves for V(p, S) versus p for large S pivot around the point ($p=p_{eq}(S\to\infty)$, V=0) and appear to converge uniformly to the curve V(p, S=∞) versus p, as S→∞. This feature is shown most clearly in the inset to Fig.10. Such detailed behavior likely does not reflect the exact behavior of the QCP. Based on these results, the site-approximation prediction for the regime of <u>generic two-phase coexistence</u> is $p_{eq}(S\to\infty) \approx 0.2055 < p < p_{eq}(S=1) \approx 0.2113$ in the sense described in Sec.1.

The trends in these site-approximation results are qualitatively consistent with exact QCP behavior as determined in simulation studies [8,10]. Two specific features should be noted. <u>First</u>, for moderate S≥1, the site approximation yields reasonably accurate values for V(p, S) if one compares simulation to approximation for the same $\delta p = p - p_{eq}(S)$. <u>Second</u>, and perhaps more significantly, just as for exact QCP behavior observed from simulations [10], one finds a tendency of the V(p, S) curves for different S to merge for increasing p approaching the spinodal point. Actually, our numerical analysis indicates that these

velocities are not exactly equal when $p=p_s$. However, from a broader perspective, a tendency for the V(p, S) curves to merge provides a new characterization of the metastable regime.

One simple perspective on the tendency for V(p, S) curves to merge comes examination of the discrete RDE's given in Sec.3A. Let x denote the physical distance in the direction of propagation (measured in lattice constants), so that $x = d_S\, m = m/\sqrt{(1+S^2)}$ in terms of the diagonal or off-diagonal row number m for interfaces of slope $1 \le S < \infty$, and x = i in terms of column number i for vertical interfaces. Then, for profiles with slowly varying coverages, all of the forms Δ, Δ_S, and $\Delta_{1,S}$ of the discrete Laplacian reduce to $\partial^2/\partial x^2$. Consequently, setting $D(\theta) = \frac{1}{2}\,\theta(1-\theta)$ as in Sec.3A, the discrete reaction-diffusion equations (21) and (22) for $1 \le S < \infty$, as well as the equations (19) for $S=\infty$, reduce to the same continuum RDE

$$\partial\theta/\partial t \approx p(1-\theta) - \theta(1-\theta)^2 + D(\theta)\,\partial^2\theta/\partial x^2, \qquad (28)$$

provided that we neglect higher-order terms which are quadratic in profile curvature. This feature together with the observation that interface profiles become broader for increasing p explains the tendency for the V(p, S) to merge for different S. As an aside, we note that the continuum RDE (28) does not have a mass-conserving form for the diffusion term. It is also distinct from the RDE describing behavior in a modified QCP with particle hopping to NN empty sites at rate h in the hydrodynamic limit $h \to \infty$ in which D=h=constant [1, 17].

Given the feature that merging of velocity curves occurs both in the site approximation and in simulations of exact model behavior, further elucidation is appropriate. Examination of terms dropped in going from the discrete RDE's to (28) suggests that the difference between the V(p, S) for different S scales like the inverse 4^{th} power of a suitable

measure of the interface profile width. Indeed, we find a linear variation of the difference $\delta V = V(p, S=1) - V(p, S=2)$ with the 4^{th} power of a measure of the maximum gradient of the profile (the inverse of this quantity measuring interface width). See Fig.11. Numerical evidence indicates that δV oscillates weakly and does not exactly reach zero as $p \rightarrow p_s$. Another perspective comes from the development of "dispersion relations" for interface propagation in Appendix B.

3.4. Site-Approximation Analysis of Planar Critical Perturbations

For $p < p_s(\text{site})$, one can consider planar vertical perturbations of the active state where again coverages and correlations depend only on column index i. One might expect that such a perturbation of the active state will always decay for sufficiently small p. However, at least for p sufficiently close to $p_s(\text{site})$, there should exist a critical size above which the perturbation will survive and grow. In the latter case, a localized region of the absorbing state will develop, and spread by propagation of two interfaces traveling outwards in opposite directions. These concepts have analogues for continuum RDE's which provide mean-field descriptions of bistable systems. In the continuum case, the unique shape of the planar critical perturbation or "critical nucleus" is readily determined, including its maximum or peak coverage [27]. The size and shape of the unstable steady-state profile of this critical perturbation obtained from the discrete RDE's for the site approximation is of primary interest here.

Clearly, the maximum (peak) coverage of the critical perturbation must be strictly less than unity for $p > p_{eq}(S=\infty)$. Otherwise, a propagating front would develop spreading the absorbing state across the system. Furthermore, one might expect that this peak coverage

should increase continuously and approach unity as p decreases to $p_{eq}(S=\infty)$. In this case, the profile of each side of the critical perturbation will correspond to the stationary interface between active and absorbing states at $p=p_{eq}(S=\infty)$. The possibility of an unstable critical perturbation with the peak coverage less than unity for some $p < p_{eq}(S=\infty)$ would seem to contradict the feature that the active state is more stable. Such a perturbation larger than this critical size could not grow indefinitely. However, it could grow transiently creating a local region of the absorbing state bordered by stationary interfaces separating the active state. Its stability is ensured by the special feature of the QCP that vertical poisoned strips cannot be eroded. This "discrete anomaly" is realized within the site approximation, but has no analogue in the continuum case.

Another feature of our analysis of critical perturbation behavior for the discrete RDE's is that we can select different symmetry classes for the perturbation, contrasting the continuum case. We first consider the case of profiles which have reflection symmetry about i=0 so that $\theta_i = \theta_{-i}$ and $\theta_i \rightarrow \theta_{active}$, as $i\rightarrow\infty$, where θ_0 is the maximum coverage in the profile. Analysis of the steady-state form of (19) for the critical perturbation reveals that

$$\theta_1 = 1 - p/\theta_0, \text{ and } \theta_{i+1} = 2 - \theta_{i-1} - 2p/\theta_i \text{ for } i\geq 1. \qquad (29)$$

Selection of $\theta_0 = \theta_0(p)$, which determines the entire profile, is non-trivial as it must produce the desired asymptotic behavior, $\theta_i \rightarrow \theta_{active}(p)$, as $i\rightarrow\infty$. The forms of critical perturbations symmetric about i=0 determined in this way are shown in Fig.12a for various $p \geq p_{eq}(S=\infty)$. We now comment further on two limiting cases. First, as p decreases towards $p_{eq}(S=\infty)$, the peak coverage, θ_0 does approach unity, so the profile of each side of the critical profile approaches the stationary interface described in Sec.3B. From (29), $\theta_0(p) = 1$ implies

that $\theta_1(p) = 1-p$ at $p = p_{eq}(S=\infty)$, a result utilized in Sec.3B. Second, as p increases towards p_s(site) from below, the size of the critical perturbation should decrease and ultimately vanish. Consistently, choosing $\theta_0 = \theta_{active} = ½$ (site) at $p = p_s = ¼$ (site) in (29) implies that all $\theta_i = \theta_{active} = ½$ for all i>0.

Next, we consider perturbations which are reflection symmetry about i= -½. Now, $\theta_0 = \theta_{-1}$ is the maximum coverage, and $\theta_i = \theta_{-i-1}$ for i≥1, where $\theta_i \rightarrow \theta_{active}$, as $i \rightarrow \infty$. Analysis of the steady-state form of (19) for the critical perturbation now reveals that

$$\theta_1 = 2 - \theta_0 - 2p/\theta_0 \rightarrow 1-2p, \text{ as } \theta_0 \rightarrow 1, \tag{30}$$

which yields distinct behavior from that associated with (29). See Fig.12b. A more complete analysis reveals that the size of the critical perturbation vanishes at $p = p_s = ¼$ (site), and increases as p decreases towards $p_{eq}(S=\infty)$. However, $\theta_0 = \theta_{-1}$ only reaches a value of $\theta_0 \approx 0.9417$, rather than unity, at $p= p_{eq}(S=\infty)$. Furthermore, a critical perturbation with $\theta_0<1$ exists for a range $p_0 < p < p_{eq}(S=\infty) \approx 0.2071$, where $p_0 \approx 0.1962$. One finds that $\theta_0 \rightarrow 1$, as $p \rightarrow p_0$. Thus, for critical perturbations in this symmetry class, we have realized the "discrete anomaly" mentioned above. For $p_0 < p < p_{eq}(S=\infty) \approx 0.2071$, perturbations exceeding the critical size grow transiently.

Another perspective on these critical perturbations comes from representing their profiles in terms of the vertices of polygons inscribed by continuous curves generated from the orbits of the iterated map (26) as shown in Fig.9. In Fig.13, we represent both symmetry classes of critical perturbations for $p = 0.24 < p_s$(site) = ¼ and for $p = p_{eq}(S=\infty) \approx 0.2071$. In addition, we represent the critical perturbation symmetric about i= -1/2 for $p \approx 0.1962 < p_{eq}(S=\infty)$. Here, the continuous curve extends beyond the physical phase space, $0 \leq u, v \leq 1$.

Finally, we note that one can extend the above concept of critical perturbations to situations where the coverages and spatial correlations are constant along rows of finite slope S. The basic features are illustrated by the case S=1 where coverages are labeled by the diagonal row number m as in Sec.3C. Consider perturbations of the active state where the maximum coverage corresponds to θ_0, and where $\theta_m = \theta_{-m} \to \theta_{active}$, as $m \to \infty$. The profile of critical perturbations is determined from analysis of the steady-state form of (21). It follows that

$$\theta_1 = 1 - p^{1/2}(1-\theta_0)^{1/2}(\theta_0)^{-1/2}, \text{ and } \theta_{m+1} = 2 - \theta_{m-1} - 2p^{1/2}(1-\theta_m)^{1/2}(\theta_m)^{-1/2} \text{ for } m>0. \quad (31)$$

As $p \to p_{eq}(S=1)$ from above, one has $\theta_0 \to 1$, so from (31) all $\theta_m \to 1$ for fixed m. The profile of the critical perturbation becomes infinitely broad, each side corresponding to the stationary profile at $p = p_{eq}(S=1)$. As $p \to p_s = 1/4$ from below, one has $\theta_0 \to \theta_{active} = ½$, so from (31) all $\theta_m \to \theta_{active}$, and the critical perturbation decreases in size and vanishes.

3.5. Pair-Approximation Formulation and Analysis of Planar Interfaces and Critical Perturbations

The pair approximation was particularly successful in describing steady-state behavior and kinetics for spatially homogeneous systems in Sec. 2B and 2C. Thus, we naturally extend its application to consider the propagation of planar interfaces separating active and absorbing states for $p < p_s(\text{pair})$, as well as the behavior of associated planar critical perturbations. As for the site approximation treatment, the coverages depend on the column index, i, for vertical interfaces, or on the diagonal or off-diagonal row index, m, for interfaces with finite slope S. In the pair approximation treatment, the same is true for pair

probabilities of which there are now two types: those for neighboring sites in the same column, denoted by ψ's, and those for neighboring sites in the same horizontal row, denoted by φ's. See Fig. 8. The analysis here starts with the exact master equations for a non-uniform system (16) and (17), and factorizes multi-site probabilities in terms of the above site and pair probabilities. This leads to particularly complex sets of coupled discrete RDE's for these quantities. These are presented in Appendix C.

As with site approximation, it is instructive to first consider the special case of vertical interfaces and associated planar critical perturbations. Here, behavior is impacted by the feature incorporated into the discrete RDE's for the pair approximation that filled vertical columns or strips cannot be eroded. Numerical integration of these discrete RDE's reveals that such vertical absorbing strips are stationary for $p \leq p_{eq}(S=\infty) \approx 0.10601$ (pair), and that the absorbing state expands into the active state only for $p > p_{eq}(S=\infty)$ (pair). Analysis of planar vertical critical perturbations reveals a "discrete anomaly" as seen already in the site approximation in Sec.3.4, i.e., a finite perturbation of the active state by the absorbing state with peak coverage less than unity persists for a small range of p below $p_{eq}(S=\infty)$ (pair). A detailed presentation of these results is provided in Appendix D.

Next, in Fig.14, we present results of a comprehensive numerical analysis of the discrete RDE's within the pair approximation for the interface propagation velocity, V(p, S), versus p. We consider diagonal and off-diagonal interfaces with slope $S \geq 1$, and vertical interfaces with slope $S = \infty$. The sign convention of Fig. 8 is used. We determine that $p_{eq}(S=1) \approx 0.1083$ (pair) as mentioned in Sec.2A, $p_{eq}(S=2) \approx 0.1078$ (pair), $p_{eq}(S=4) \approx 0.1070$ (pair), $p_{eq}(S=8) \approx 0.1062$ (pair), etc.. Analogous to behavior in the site approximation, $p_{eq}(S \rightarrow \infty) \approx$

0.1056 (pair) is below the value of $p_{eq}(S=\infty) \approx 0.1060$ (pair). More generally, overall behavior of this family of curves for various S is qualitatively similar to that observed for the site approximation. In particular, this includes a pivoting of the curves around the point ($p=p_{eq}(S\rightarrow\infty)$, V=0) and apparent uniform convergence to the curve V(p, S=∞) versus p, as $S\rightarrow\infty$.

More significantly, the overall behavior and trends in these pair approximation results for V(p, S) versus p are in semi-quantitative agreement with exact QCP behavior as determined in simulation studies. In particular, for moderate S≥1, the pair approximation yields roughly the correct values for V(p, S) if one compares with simulation values for either the same absolute p or the same $\delta p = p-p_{eq}(S)$. For p=0, one can determine exactly the velocity of shrinkage of an absorbing strip with various slopes in the QCP to obtain $V(p=0, S) = ¼\ S(S+1)^{-1}(S^2+1)^{-1/2}$ [8,10]. These values are quite close to pair-approximation predictions. Just as for exact QCP behavior (and in the site approximation analysis), one finds a tendency of the V(p, S) curves for different S to merge approaching the spinodal point. However, as in the site approximation, pair-approximation velocities are not exactly equal when $p=p_s$(pair).

Summarizing the above results, the pair-approximation prediction for the regime of generic two-phase coexistence is $p_{eq}(S\rightarrow\infty) \approx 0.1056 < p < p_{eq}(S=1) \approx 0.1083$ in the sense described in Sec.1. This result should be compared with precise simulation predictions for generic two-phase coexistence in the QCP for $p_{eq}(S=\infty) \approx 0.0869 < p < p_{eq}(S=1) \approx 0.0944$ [8]. In principle, one could extend this analysis to higher-order approximations. See Appendix E.

3.6. Dynamics and Criticality for Two-Dimensional Droplets

For analysis of metastability in the vicinity of discontinuous transitions, as well as for insight into generic two-phase coexistence, it is instructive to analyze the dynamics of two-dimensional droplets of one phase embedded within the other [8,10,12,13].

We first consider behavior in the regime of generic two-phase coexistence, $p_{eq}(S\rightarrow\infty) < p < p_{eq}(S=1)$, where the embedded droplet should eventually disappear since both active and absorbing states are stable against local perturbations. In analyzing the behavior of a droplet of the absorbing phase embedded in the active phase, we consider a "worst case scenario" of a large square-shaped poisoned droplet with edges aligned with the principal lattice directions (S=0 and S=∞). Then, initially the droplet should grow since $p > p_{eq}(S=\infty)$. Numerical integration of the full two-dimensional form of the non-uniform master equations (16) and (17), after applying a truncation approximation, reveals that the droplet does indeed grow initially. However, growth at the corners of the droplet is inhibited, and thus facets with slope S= ±1 develop. Subsequently, these shrink producing an octagonal shaped cluster. Eventually the original sides with slopes S=0 or ∞ grow out producing a diamond-shapes cluster which then shrinks and disappears. See Fig.15 for site-approximation results with p=0.209. Analogous behavior is observed in simulation studies, although fluctuations conceal the simple geometric progression of droplet shapes [8,10]. In analyzing the behavior of a droplet of the active phase embedded in the absorbing phase, we also consider a "worst case scenario" of a large diagonal active or empty droplet with edges having slopes S=±1. Then, initially the droplet will grow since $p < p_{eq}(S=1)$. However, ultimately growth is constrained by the feature of the QCP preserved in truncation approximations that an empty or active

droplet embedded in the absorbing phase cannot grow outside of a rectangle inscribing that droplet. Indeed, the diamond-shaped droplet initially grows outward to form a larger square droplet, but then growth is arrested and the droplet shrinks and disappears. See Fig.15 for site-approximation results for p=0.209.

Second, we discuss the existence of critical droplets of the absorbing phase embedded in the active phase for $p_{eq}(S=1) < p < p_s$ (noting that for smaller p such droplets shrink and perish). Analogous to our discussion of planar perturbations in Sec.3D and 3F, one expects that a small perturbation will decay, and that there exists a critical size only above which a perturbation will survive. In the latter case, a localized region of the absorbing state will develop, and spread by propagation of a curved interface traveling outwards. Of primary interest here is the size and shape of the critical perturbation. This unstable steady-state profile can be obtained by analysis of the time-independent version of (16) and (17) after applying a truncation approximation. Again we must also specify the "symmetry class" of the perturbation. We consider the case of profiles which have a 4-fold symmetry about the site (i, j) = (0, 0), so that $\theta_{i,j} = \theta_{\pm i,\pm j} \to \theta_{active}$, as $|i| + |j| \to \infty$, so $\theta_{0,0}$ is the maximum coverage in the profile. In the site approximation, factorizing the steady-state form of (16) produces a set of recurrence relations for the coverages $\theta_0 = \theta_{0,0}$, $\theta_1 = \theta_{0,\pm1} = \theta_{\pm1,0}$, $\theta_2 = \theta_{\pm1,\pm1}$, $\theta_3 = \theta_{0,\pm2} = \theta_{\pm2,0}$, etc., which have the form

$$p(1-\theta_0) = \theta_0(1-\theta_1)^2,\ 2p(1-\theta_1) = \theta_1(1-\theta_2)(1-\theta_0) + \theta_1(1-\theta_2)(1-\theta_3),\ldots \qquad (32)$$

These are solved (non-trivially) for the $\theta_{m>0}$ in terms of $\theta_0=\theta_0(p)$ and then θ_0 is selected to satisfy the boundary condition for $|i| + |j| \to \infty$.

4. Conclusions

We have developed an approximate analytic treatment for the QCP based on truncation of the exact master equations for both spatially homogeneous and inhomogeneous states. Qualitative features of exact model behavior are recovered even with the simplest site approximation. The pair approximation is even more effective, being capable of semi-quantitative predictions. Analysis is facilitated by exact simplification of the master equations for the QCP before applying the factorization approximations. This simplification is aided by the specific form of the desorption rates in our Durrett-type formulation of the QCP.

We should also emphasize that the strategies developed and applied here are applicable to a broad class of non-equilibrium lattice-gas adsorption-desorption or reaction models. Our approach extends to treat the QCP on other types of lattices as illustrated in Appendix F. Furthermore, these techniques are effective for analysis of generalized QCP models which include other pathways for desorption as well as particle hopping [30]. One could apply this type of analysis to models for the stochastic dynamics of systems described by a Hamiltonian where the steady states are conventional equilibrium states. A close analogue to the QCP is an adsorption-desorption model with random desorption at empty sites at rate p, and correlated desorption at a rate proportional to α^n where n denotes the number of filled nearest neighbors (choosing $\alpha<1$ for attractive interactions). The equilibrium states are described by the Ising lattice-gas model. For sufficiently small $\alpha<1$, site or pair approximations to the exact master equations produce bistability between stable high and low coverage states. Extending this analysis to non-uniform states, one can

determine the equistability pressure. One generally finds an artificial dependence on interface orientation introduced by the approximation, but absent in exact model behavior.

These dynamic mean-field truncation approximations invariably fail to capture certain finer details associated with fluctuation-controlled behavior either for non-equilibrium models or for Hamiltonian-based models. For the QCP, these shortcomings include a failure to describe nucleation-mediated transitions from the active state to the absorbing state for $p>p_{eq}(S=1)$, and as inability to capture existence and subtle dynamics "coarsening states" described in Sec. 2E. The latter are replaced by unstable steady states in dynamic mean-field formulations. These analytic formulations do however provide additional insight into relaxation kinetics and interface propagation beyond that attained with KMC simulations.

One spin-off of our analysis of spatially non-uniform states is the generation of novel classes of discrete RDE's which provide new challenges for mathematical analysis. These involve not just site coverages or concentrations, but also local spatial correlations. Also, the "diffusive coupling" arising from the correlated desorption dynamics (rather than from particle hopping) is more complex than in conventional forms describing discrete diffusion [18-20].

Acknowledgements

Work at the Ames Laboratory was supported by the Department of Energy, Basic Energy Sciences - Division of Chemical Sciences, under Contract No. DE-AC02-07CH11358.

Appendix A: Higher-Order Dynamic Cluster Approximations

Given the success of the pair approximation in describing spatially uniform states as demonstrated in Sec.2, it is natural to explore higher-order approximations. To systematize such approximations, it is convenient to first rewrite multi-site configuration probabilities in terms of filled site configurations, then to factorize these exactly in terms of conditional probabilities, and finally to apply a truncation approximation to the conditional probabilities [14]. An example of the first two steps is as follows:

$$P\begin{bmatrix} & x & \\ x & x & o \\ & o & \end{bmatrix} = P\begin{bmatrix} & x \\ x & x \end{bmatrix} - 2\,P\begin{bmatrix} & x & \\ x & x & x \\ & & \end{bmatrix} + P\begin{bmatrix} & x & \\ x & x & x \\ & x & \end{bmatrix}, \text{ with} \tag{A1}$$

$$P\begin{bmatrix} & x \\ x & x \end{bmatrix} = Q\begin{bmatrix} & x' \\ x & x' \end{bmatrix} P\begin{bmatrix} x \\ x \end{bmatrix} = Q\begin{bmatrix} & x' \\ x & x' \end{bmatrix} Q\begin{bmatrix} x \\ x' \end{bmatrix} P[x] \text{ and} \tag{A2}$$

$$P\begin{bmatrix} & x & \\ x & x & x \\ & & \end{bmatrix} = Q\begin{bmatrix} & x' & \\ x & x' & x' \\ & & \end{bmatrix} P\begin{bmatrix} x & \\ x & x \end{bmatrix} = Q\begin{bmatrix} & x' & \\ x & x' & x' \\ & & \end{bmatrix} Q\begin{bmatrix} x & \\ x' & x' \end{bmatrix} P[x \quad x] = \Lambda \tag{A3}$$

Here, Q's denote conditional probabilities for finding the site denoted x filled <u>given</u> the other sites denoted by x′ are specified filled, so e.g., Q =P[xx]/P[x] = Q[x x′]. A natural truncation procedure for the Q's is to ignore the influence of x′-sites more than a specific suitably-defined distance from the filled x-site of interest [14]. Specifically, our m-NN approximation ignores all x′-sites which are further than m^{th} nearest-neighbors from the x-site. Thus, the 0-NN approximation ignores all x′-sites (the site approximation). The 1-NN approximation considers only NN x′-sites (the pair approximation). The 2-NN considers NN and also diagonal or 2NN x′-sites, etc. Thus, for example, one has that

$$Q\begin{bmatrix} & x' & \\ x & x' & x' \\ & & \end{bmatrix} \approx Q[x] = P[x]\,(0\text{ - NN}),\ \text{or } Q\begin{bmatrix} x & x' \end{bmatrix}\,(1\text{ - NN}),\ \text{or } Q\begin{bmatrix} & x' \\ x & x' \end{bmatrix}\,(2\text{ - NN}) \qquad \text{(A4)}$$

and this Q is left untruncated in the 3-NN approximation. The accuracy of these truncation approximations would benefit from a propensity for specified filled x′-sites to shield the x-site of interest from the influence of more distant x′-sites. For QCP for p=0, i.e, irreversible cooperative desorption, does exhibit a corresponding filled-site Markov field property, i.e., walls of filled sites shield the influence of sites on one side from the other [14]. However, such “complete shielding” is absent in the QCP with p>0.

After implementing the truncation approximation, the Q’s can be rewritten as ratios of P’s. One performs this procedure on a sufficient number of hierarchical equations for P’s to obtain a closed coupled set of N(m) evolution equations, where one expects that N(m) will increase quickly with the order of the approximation, m [14]. These closed evolution equations can then be integrated to determine kinetics, or the corresponding N(m) coupled algebraic equations obtained from dP/dt = 0 can be solved to determine steady-state behavior.

Appendix B: “Dispersion Relations” for V (P, S) in the Site Approximation

Additional characterization of the orientation dependence of interface propagation is possible by focusing on the form of the edge of the front close to the active state. Specifically, one writes $\theta = \theta_{active} + \delta\theta$ where $\delta\theta \to 0$ at this front. Analogous to our treatment of stationary profiles in Sec.3B, we assume that $\delta\theta$ decays exponentially like

$$\delta\theta \sim \lambda^{(x-Vt)} = \exp[-\kappa(x-Vt)],\ \text{as } x \to \infty, \qquad \text{(B1)}$$

where $\lambda=e^{-\kappa}$ and x=i for vertical interfaces, or $x=d_S$ m diagonal or off-diagonal interfaces, is the appropriate physical distance in the propagation direction (cf. Sec.3C). Here, for convenience, we adopt the convention that V>0 when the absorbing state displaces the active state (in contrast to that used in the text). Then, substitution into the discrete RDE's for the site approximation followed by linearization yields "dispersion relations" of the form

$$\kappa V = -(1-2\theta_{active})(1-\theta_{active}) + D(\theta_{active})\, F_S(\kappa), \qquad \text{(B2)}$$

Where, $F_{S=\infty}(\kappa) = 2\cosh(\kappa) - 2$

and $F_{1\le S<\infty}(\kappa) = (1+S^2)^{-1}\,[2\cdot\cosh(\kappa d_S) - 2]/d_S^2 + S^2(1+S^2)^{-1}\,[2\cdot\cosh(\kappa S d_S) - 2]/(Sd_S)^2$.

In the slow decay regime $\kappa<<1$, one has that $F_S(\kappa) \sim \kappa^2$, and (B2) reduces to the relation obtained from analysis of the continuum RDE (28). However, in general for finite decay rate, there is a dependence of κ on interface orientation. Since V>0 for p close to p_s, (B2) has a solution for $\kappa=\kappa_s$ which is non-vanishing at $p=p_s$ satisfying $4\kappa_s V_s = F_S(\kappa_s)$. Since $V_s \approx 0.06$ is quite small, it follows that $F_S(\kappa_s)\approx (\kappa_s)^2$ and $\kappa_s \approx 4V_s$ roughly independent of interface slope S.

Appendix C: Pair-Approximation Formulation for Planar Interfaces

First, we consider propagation of vertical interfaces with slope $S=\infty$ separating active and absorbing states. After factorizing the non-uniform hierarchical master equations (16) and (17), one obtains a coupled set of equations for the coverages, $\theta_i = P[x_i]$, in each column i, and for probabilities of pairs of neighboring filled sites oriented horizontally, $\varphi_{i-1/2}= P[x_{i-1}\, x_i]$, in columns i-1 and i, and vertically, ψ_i, in column i. See Fig.8. These equations have the form

$$d/dt\ \theta_i = p(1-\theta_i) - \tfrac{1}{2}\,(\theta_i - \psi_i)(2\theta_i - \varphi_{i-1/2} - \varphi_{i+1/2})/\theta_i, \tag{C1}$$

$$d/dt\ \psi_i = 2p(\theta_i - \psi_i) - \tfrac{1}{2}\,\psi_i\,(\theta_i - \psi_i)(2\theta_i - \varphi_{i-1/2} - \varphi_{i+1/2})/(\theta_i)^2. \tag{C2}$$

$$d/dt\ \varphi_{i-1/2} = p(\theta_{i-1}+\theta_i - 2\varphi_{i-1/2}) - \tfrac{1}{2}\,\varphi_{i-1/2}(\theta_i-\varphi_{i+1/2})(\theta_i-\psi_i)/(\theta_i)^2$$

$$- \tfrac{1}{2}\,\varphi_{i-1/2}(\theta_{i-1}-\varphi_{i-3/2})(\theta_{i-1}-\psi_{i-1})/(\theta_{i-1})^2, \tag{C3}$$

From this form, it is clear that a poisoned column with $\theta_i = \psi_i = 1$ will remain poisoned for all later times, so that absorbing vertical strips cannot be eroded within this approximation. Also, if columns i and i-1 are poisoned, then it follows that $\varphi_{i-1/2} = 1$ for all later times.

Second, we consider the evolution of diagonal interfaces with slope S=1. As in our site-approximation treatment, each diagonal row of sites is labeled by m and has its own coverage, θ_m. Conveniently, by reflection symmetry in a line orthogonal to these rows, the probability for an NN pair of filled sites in diagonal rows m and m+1 is independent of whether the pair is horizontal or vertical on the square lattice. This probability is denoted here by $\varphi_{m+1/2}$ since the center of this pair is midway between rows m and m+1. Factorizing the non-uniform master equations (16) and (17) and simplifying yields

$$d/dt\ \theta_m = p(1-\theta_m) - \tfrac{1}{4}\,(2\theta_m - \varphi_{m-1/2} - \varphi_{m+1/2})^2/\theta_m, \tag{C4}$$

$$d/dt\ \varphi_{m-1/2} = p(\theta_{m-1} + \theta_m - 2\varphi_{m-1/2})$$

$$- \tfrac{1}{4}\,\varphi_{m-1/2}\,(\theta_{m-1} - \varphi_{m-3/2})(2\theta_{m-1} - \varphi_{m-1/2} - \varphi_{m-3/2})/(\theta_{m-1})^2$$

$$- \tfrac{1}{4}\,\varphi_{m-1/2}\,(\theta_m - \varphi_{m+1/2})(2\theta_m - \varphi_{m-1/2} - \varphi_{m+1/2})/(\theta_m)^2. \tag{C5}$$

Third, we can extend the above analysis to consider interfaces with general integer slope S≥1. As for the site approximation, off-diagonal rows with slope S, labeled by m, will have distinct coverages, θ_m. However, now we must also introduce two probabilities, $\varphi_{m+S/2}$

for NN horizontal pairs of filled sites in rows m and m+S, and $\psi_{m+1/2}$ for NN vertical pairs of filled sites in rows m and m+1. See Fig.8.

The above equations cannot be simply written in the conventional discrete RDE form as for the site approximation. However, our selected notation illustrates that they do effectively have such a form. For example, for linear profiles, the equations reduce to those for the homogeneous pair approximation in Sec.2.1.

Appendix D: Pair-Approximation Analysis of Vertical Interfaces and Planar Critical Perturbations

Here, we analyze stationary vertical profiles within the pair approximation including stationary interfaces for $p \le p_{eq}(S=\infty)$, and planar critical perturbations from the active state for $p \le p_s$ (pair). In both cases, analysis utilizes the steady-state form of (C1)-(C3). It is convenient to introduce the conditional probability, Q_i, for finding a particle or filled site in column i directly above (or below) a specified filled site in the same column, so that $\psi_i = \theta_i Q_i$. Then, noting that $\varphi_{i\pm1/2}$ can be eliminated from (C1) and (C2), one obtains the steady-state relation

$$Q_i = 2\theta_i/(1+\theta_i) \ge \theta_i. \qquad \text{(D1)}$$

(D1) is the analogue of the relation (13) for homogeneous systems. Using (D1) to eliminate ψ_i from (C1) and (C3) yields a closed pair of recurrence relations

$$\varphi_{i+1/2} = 2(1-p)\theta_i - \varphi_{i-1/2} - 2p, \text{ and} \qquad \text{(D2)}$$

$$2p(\theta_{i-1}+\theta_i -2\varphi_{i-1/2}) = \varphi_{i-1/2}(\theta_i -\varphi_{i+1/2})(1-\theta_i)/[\theta_i(1+\theta_i)]$$
$$+ \varphi_{i-1/2}(\theta_i -\varphi_{i-3/2})(1-\theta_{i-1})/[\theta_{i-1}(1+\theta_{i-1})], \qquad \text{(D3)}$$

or alternatively that $\theta_i = \psi_i = 1$ in which case (D2) and (D3) do not apply.

First, we consider stationary vertical interfaces between the absorbing and active states for $p < p_{eq}(S=\infty)$. These stationary solutions are chosen to satisfy

$\theta_0 = \theta_{-1} = \ldots 1$, $\varphi_{-1/2} = \varphi_{-3/2} = \ldots 1$, with

$1 > \theta_1 > \theta_2 > \ldots$ as well as $1 > \varphi_{1/2} > \varphi_{3/2} > \ldots$ (D4)

with $\theta_i \rightarrow \theta_{active}(p)$, and $\varphi_{i+1/2} \rightarrow 2(\theta_{active})^2/(1+\theta_{active})$, as $i \rightarrow \infty$. Then, (D2) and (D3) apply for $i>0$ and can be solved as follows. For i=1, substitution of (D2) into (D3) gives a complex relationship between $\varphi_{1/2}$ and θ_1. However, one can readily check that the solution is $\theta_1 = \varphi_{1/2}$, as is required from basic probability considerations [31]. Then, using (D2) for i=1 immediately gives $\varphi_{3/2} = \varphi_{3/2}(\theta_1)$ as a function of θ_1. For $i>1$, recursive substitution of (D2) into (D3) gives a cubic equation for θ_i in terms of previously determined quantities θ_{i-1}, $\varphi_{i-3/2}$, $\varphi_{i-1/2}$, and $\varphi_{i+1/2}$ which are known functions of θ_1. Thus, one can obtain all $\theta_{i>1} = \theta_{i>1}(\theta_1)$ as functions of θ_1, which is still unknown. The value of θ_1 must be selected to guarantee satisfaction of the desired boundary condition as $i \rightarrow \infty$. The stationary profile is a sharp step function with $\theta_1 = \theta_2 = \ldots = 0$ etc. for p=0, and becomes progressively broader as p increases.

Next, we analyze stationary planar vertical critical perturbations from the active state for $p < p_s(pair)$. First, consider perturbations which have reflection symmetry about i=0, where $\theta_0 < 1$ is the maximum coverage. Then, one has $\theta_i = \theta_{-i}$ as well as $\varphi_{i+1/2} = \varphi_{-i+1/2}$ for $i \geq 0$, together with the boundary conditions $\theta_i \rightarrow \theta_{active}(p)$, as $i \rightarrow \infty$. Analysis of the first equation in (D2) for i=0 yields

$\varphi_{1/2} = \theta_0 - p(1+\theta_0)$, so that $\varphi_{1/2} \rightarrow 1-2p$ as $\theta_0 \rightarrow 1$. (D5)

Perhaps of most significance is that that limiting behavior $\theta_0 \to 1$ [32] occurs when p $\approx$ 0.10598, slightly below $p_{eq}(S=\infty) \approx 0.10601$ (pair). In addition, one can show that $\varphi_{1/2} \to$ 1/6 (the spinodal value of the active steady-state pair probability) as $p \to p_s$ = 1/8 (pair), corresponding to a decrease in size and disappearance of the critical perturbation at the spinodal. One can also consider perturbations which have reflection symmetry about i = -1/2.

Finally, we note that one can explore the recurrence relations (D2) and (D3) in the form of an iterated map, $(u_i, v_i) = (\theta_{i-1}, \theta_i) \to (u_{i+1}, v_{i+1})$, which at each step involves solving a cubic equation for coverage (after specifying an initial value for the horizontal pair probability). As in the site approximation, we can start with values of the coverage and pair probability randomly perturbed from the active steady-state values, and then generate associated orbits. Unlike the pair approximation, these orbits often survive only a finite number of iterations before the solution becomes complex. Also, this procedure does not generate a simple continuous curve symmetric about u=v as in the site approximation, but rather a more complex structure. Longer lived orbits do tend to generate a continuous curve, but it does no pass through the active fixed point and is not tangent to u=1 and v=1 at $p=p_{eq}(S=\infty)$ (pair). These features presumably underlie more complex behavior described above for critical perturbations symmetric about i=0.

Appendix E: Higher-Order Approximations for Planar Interfaces

Rather complicated discrete RDE's describing non-uniform states can be derived for higher-order truncation approximations. One expects to find the same qualitative behavior as within the site and pair approximations. However, one should not expect to find the same degree of improvement in agreement with exact results as observed in going from the site to

the pair approximation. Primarily for this reason, we only describe results for propagation of an interface with slope S=1 in the 2NN approximation. In this case, the reduced symmetry relative to the spatially uniform system means that one must consider probabilities for 8 (rather than 5) quantities for each diagonal row. Numerical analysis of these equations reveals that $p_{eq}(S=1) \approx 0.117$ (2NN). This value is actually higher than the pair-approximation prediction, and thus deviates slightly further from the precise simulation result. This feature might be anticipated from examination of the shape of the equation of state for the 2NN approximation (relative to that for the pair approximation) shown in Fig.2. While it is not possible to simply determine $p_{eq}(S=1)$ from a simple equal-area type construction as for equilibrium systems, this type of analysis suggests a shift of $p_{eq}(S=1)$ to higher values for higher-order approximations.

Appendix F: QCP on a Triangular Lattice

An adsorption-desorption version of the QCP on a triangular lattice (with coordination number 6) has rules analogous to that on the square lattice: adsorption occurs randomly at rate p, and cooperative desorption of particles occurs at rate k/4 where k = 0 to 4, or k=6 denotes the number of adjacent pairs of NN empty sites. Simulation studies reveal a continuous transition to the absorbing state occurs at $p \approx 0.177$ [10]. The steady-state coverage in the active state follows the site-approximation value more closely and for higher p than for the QCP on the square lattice, but it departs strongly in the vicinity of the continuous transition.

It should also be noted that the exact master equations for this model on the triangular lattice can be simplified just as for the square lattice case. In particular, for spatially

homogeneous states, one has that $d\theta/dt = p(1-\theta) - P(x2o)$, where P(x2o) is the probability of finding some site filled and two specific adjacent NN sites both empty. Thus, one recovers exactly the same site-approximation kinetics for this model as for the square lattice. Simplification of the exact master equations also extends to the spatially inhomogeneous case, $d/dt\ \theta_{i,j} = p(1-\theta_{i,j}) - P_{i,j}(x2o)$, where $P_{i,j}(x2o)$ equals one sixth of the sum of the probabilities of finding site (i,j) filled and one of the six possible adjacent NN pairs of sites both empty.

References

[1] R. Durrett, SIAM Rev. **41**, 677 (1999).
[2] J. Marro and R. Dickman, *Nonequilibrium phase transitions in lattice models* (Cambridge UP, Cambridge, 1999).
[3] H. Hinrichsen, Adv. Phys. **49**, 815 (2000).
[4] G. Odor, Rev. Mod. Phys. **76**, 663 (2004).
[5] R.M. Ziff, E. Gulari, and Y. Barshad, Phys. Rev. Lett. **56**, 2553 (1986).
[6] F. Schloegl, Z. Phys. **253**, 147 (1972).
[7] P. Grassberger, Z. Phys. B Cond. Matt. **47**, 365 (1982).
[8] D.-J. Liu, Xiaofang Guo, and J.W. Evans, Phys. Rev. Lett. **98**, 050601 (2007).
[9] S.J. Hanjini, J. Theor. Probab. **10**, 737 (1997).
[10] Xiaofang Guo, D.-J. Liu, and J.W. Evans, Phys. Rev. E, **75**, 061129 (2007).
[11] M.A. Munoz, F. de los Santos, and M.M.T. da Gama, Euro. Phys. J. B **43**, 73 (2005).
[12] A.L. Toom, in *Multicomponent random systems*, edited by R.L. Dobrushin and Y.G. Sinai Marcel Dekker, New York, 1980).
[13] C.H. Bennett and G. Grinstein, Phys. Rev. Lett. **55**, 657 (1985).
[14] J.W. Evans, Rev. Mod. Phys. **65**, 1281 (1993).
[15] R. Dickman, Phys. Rev. A **34**, 4246 (1986).
[16] J.W. Evans and M.S. Miesch, Surf. Sci. **245**, 401 (1992).
[17] P. Fischer and U.M. Titulaer, Surf. Sci. **221**, 409 (1989).
[18] J.P. Keener, SIAM J. Applied Math. **47**, 556 (1987).
[19] G. Fath, Physica D **116**, 176 (1998).
[20] C.E. Elmer, Physica D **218**, 11 (2006).
[21] D.M. Burley, in *Phase Transitions and Critical Phenomena*, Vol.2, Ed.s C. Domb and M.S. Green (Academic, New York, 1972).
[22] In the pair approximation, the conditional probability for finding an empty adjacent to a specified filled site is given by $Q_e = 1-Q = (1-\theta)/(1+\theta)$. This result was used in Ref.[8].

[23] These can be reduced to four equations by further factorizing the probability for the T-shaped configuration. This produces negligible changes to the predicted behavior.
[24] E.W. James, D.-J. Liu, and J.W. Evans, J. Colloids Surf. A **165**, 241 (2000).
[25] We have redefined Q to "deemphasize" phase separation by averaging Q-values for the two phases weighting only by fractional area. Then, the simulated refined (Q, θ)-flow reveals behavior closer to the pair approximation prediction. However, configurations near the coarsening state do tend to evolve to the active or poisoned steady states along a roughly straight line trajectory (as should be expected for phase-separated states).
[26] P.C. Fife and J.B. McLeod, Arch. Rat. Mech. Anal. **65**, 335 (1977).
[27] A.L. Mikhailov, *Foundations of Synergetics I* (Springer-Verlag, Berlin, 1990).
[28] P.G. Drazin, *Nonlinear Systems* (Cambridge University Press, Cambridge, 1992).
[29] Note that the iterated map takes (u, v) = (1-p, 1) into (u, v) = (1, 1-p).
[30] D.-J. Liu, Xiaofang Guo, D. Unruh, and J.W. Evans, unpublished.
[31] If column i is completely filled, so that $\theta_i = \psi_i = 1$, then it immediately follows from basic probability considerations that $\varphi_{i+1/2} = \theta_{i+1}$ and that $\varphi_{i-1/2} = \theta_{i-1}$.
[32] From (D2) and (D3) for i=1, one can determine $\theta_1 = 1-2p$ and $\varphi_{3/2} = 1-6p+4p^2$. Then, one can recursively solves these equations for i>1 to determine all of the θ_i and $\varphi_{i+1/2}$ for i>1 as functions of p (by eliminating $\varphi_{i+1/2}$ and solving a cubic equation for θ_i at each step).

Figures

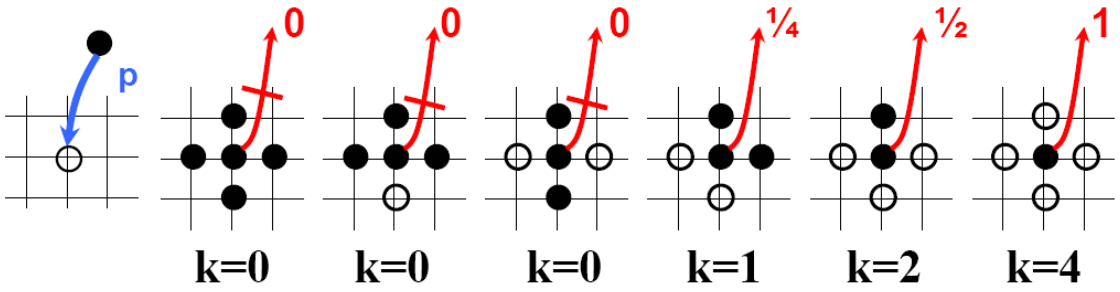

Figure 1. Schematic of desorption rules and rates in the QCP.

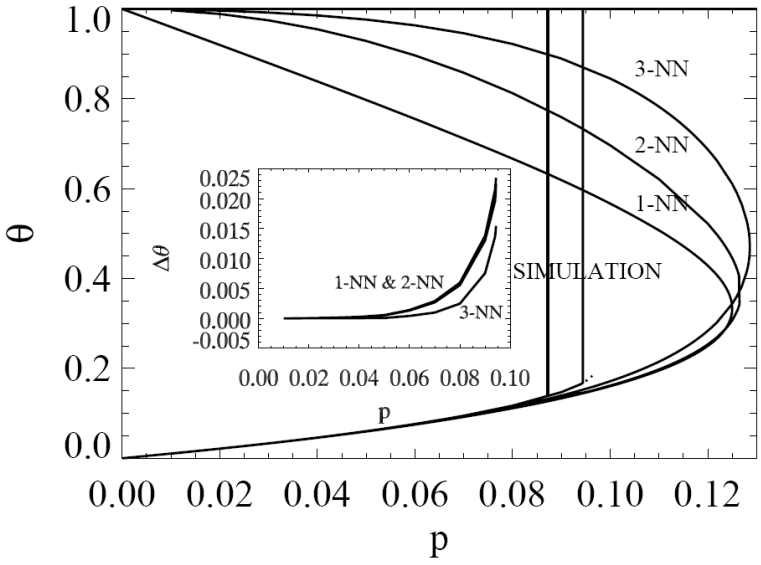

Figure 2. Predictions of m-NN approximations and simulation results for steady-state θ(p) versus p. Inset: Expanded view of differences between approximate and simulated steady-state θ(p).

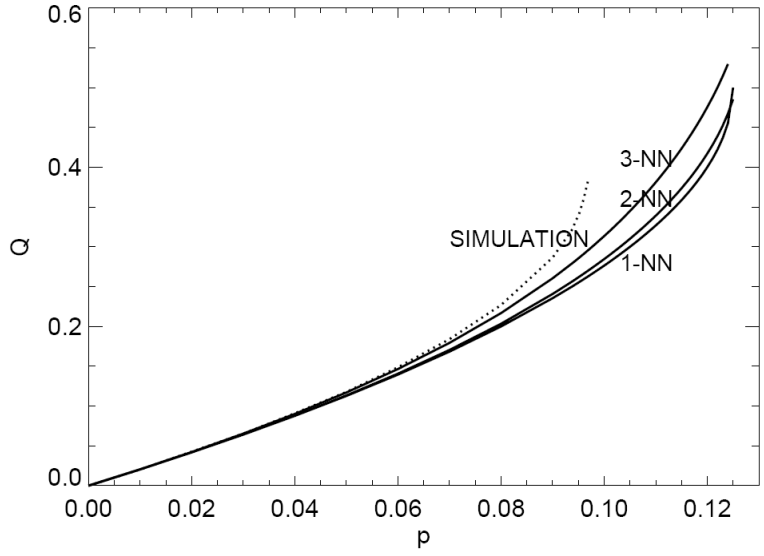

Figure 3. Predictions of m-NN approximations and simulation results for steady-state Q(p) versus p.

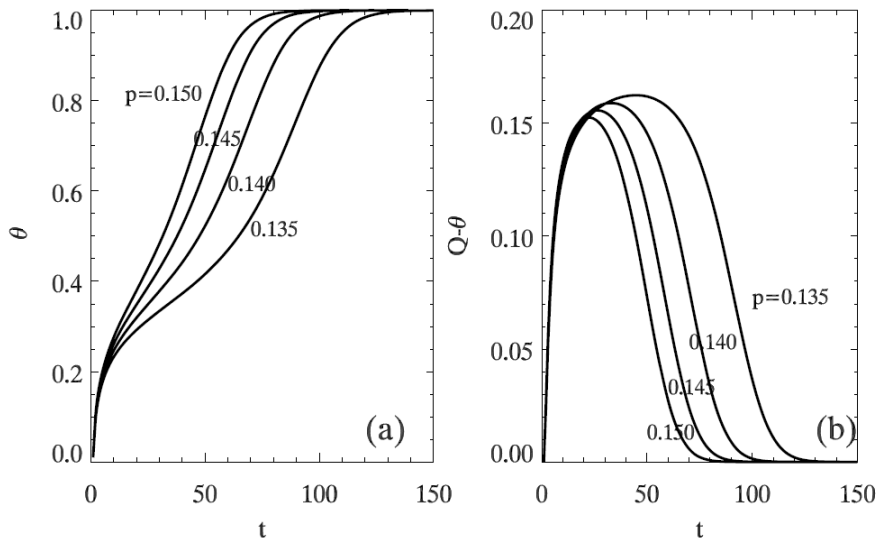

Figure 4. Pair-approximation predictions for relaxation kinetics: (a) poisoning kinetics above the spinodal for $\delta p_s = p - p_s = 0.010$-$0.025$; (b) corresponding evolution of $Q-\theta$ (>0 for clustering)

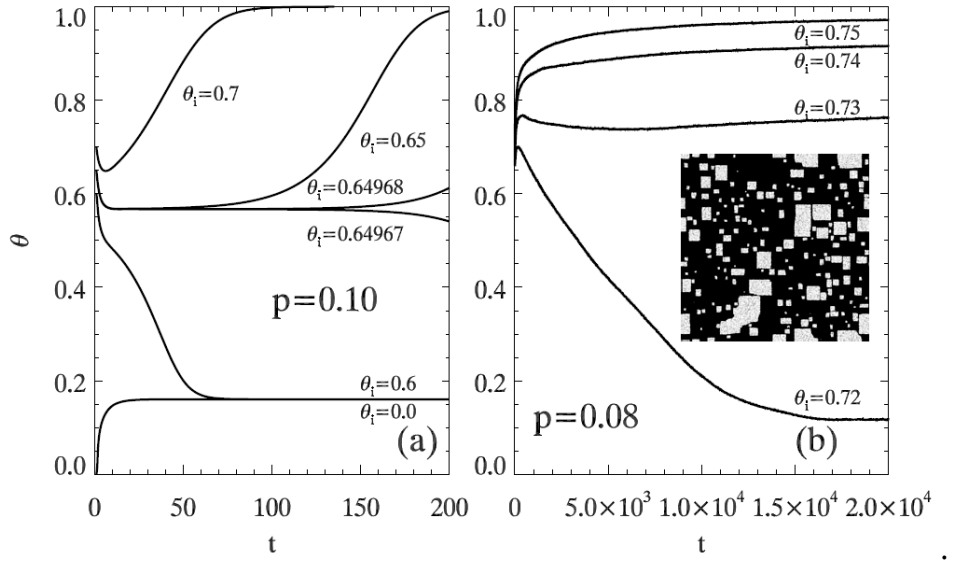

Figure 5. Relaxation kinetics at fixed lower p below p_{eq} and p_s starting from a random state for varying initial $\theta=\theta_i$ (including $\theta_i=0$, an initially empty lattice, shown as a dashed line): (a) pair approximation predictions for p=0.1; (b) simulation predictions for p=0.08. Inset: the "coarsening state" achieved after $t=2\times10^4$ time units starting with $\theta_i \approx 0.76$.

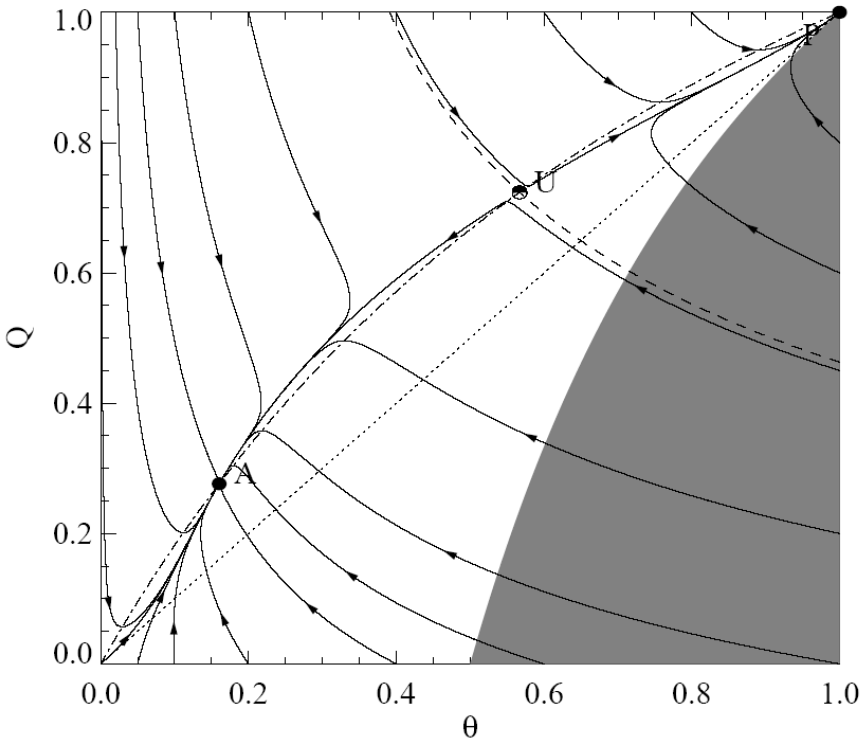

Figure 6. Pair-approximation prediction of the phase-portrait for flow in the (θ, Q)-plane for p=0.10 below p_s=1/8. The shaded region, Q≤(2θ-1)/θ, is not physically accessible. The dotted line, Q=θ, corresponds to random states (cf. Fig.5). The dot-dashed line, Q=2θ/(1+θ), illustrates the steady-state relation (10). Active (A), poisoned (P), and unstable (U) states are indicated.

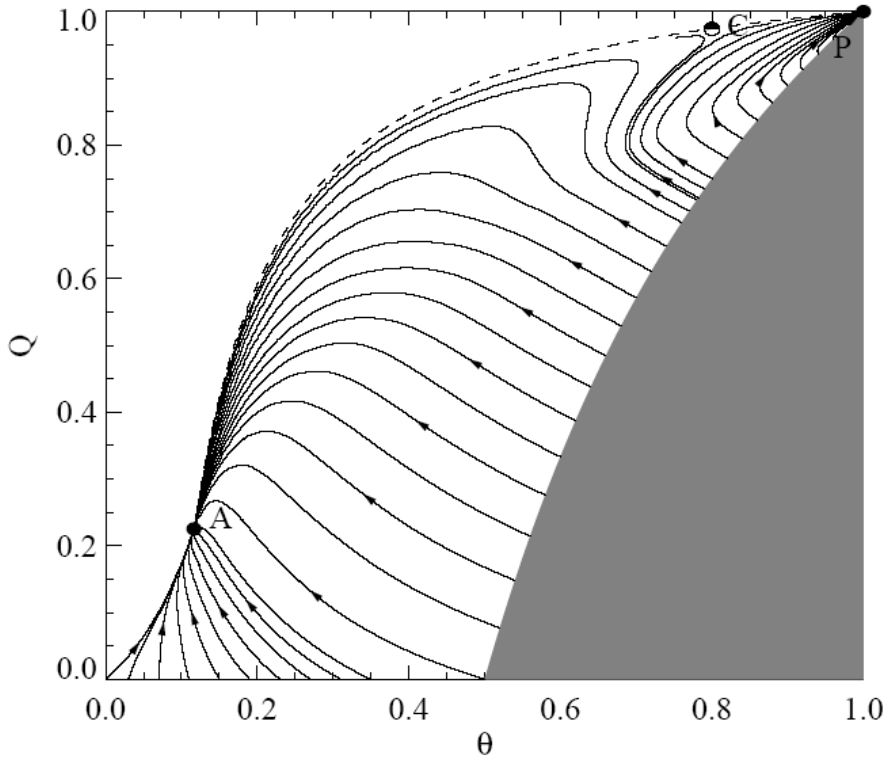

Figure 7. Simulated prediction of the phase-portrait for flow in the (θ, Q)-plane for p=0.08. Trajectories start from the "anti-clustering" boundary of physically accessible (θ,Q)-space with Q=0 for θ≤1/2, and Q=(2θ-1)/θ for θ≥1/2. The location of the active (A) and poisoned (P) states, and the estimated location of the "coarsening state" (C) are also indicated.

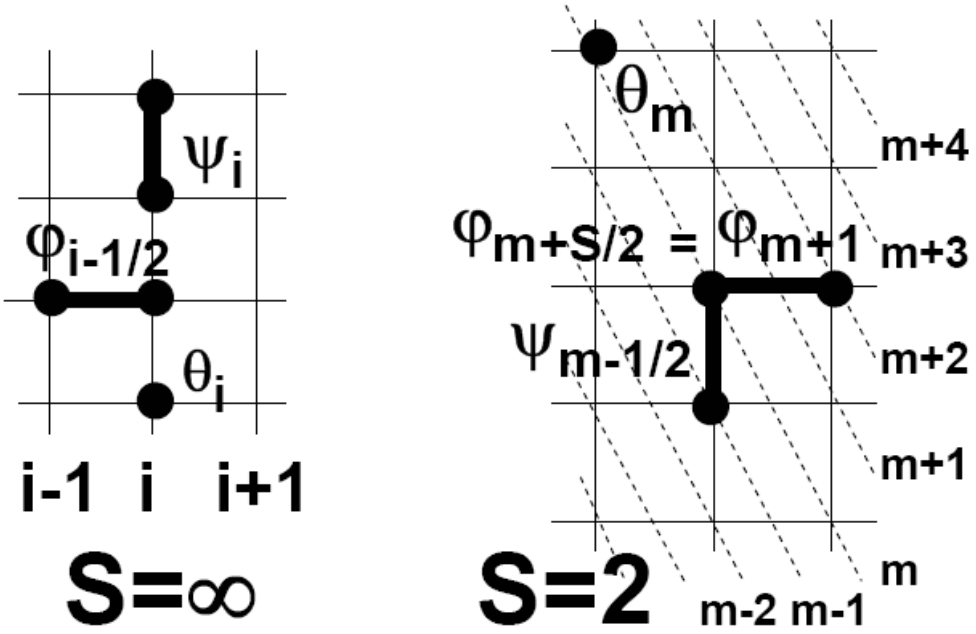

Figure 8. Schematic for labeling of rows in the non-uniform master equations and associated truncation approximations.

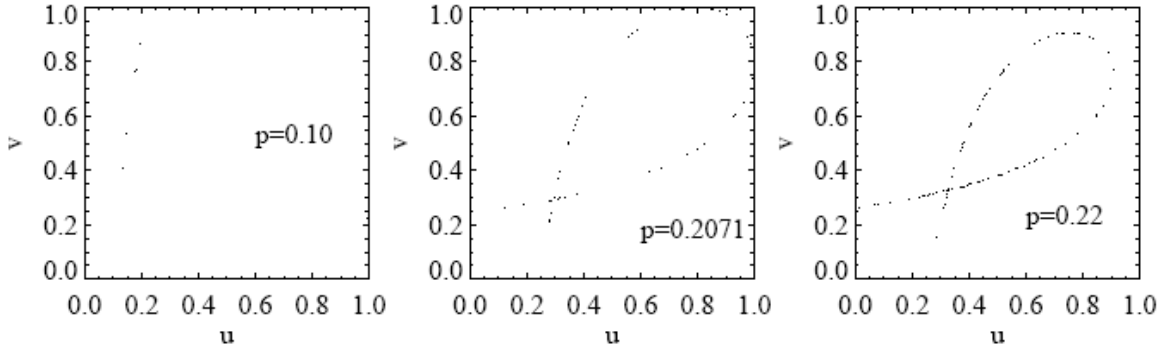

Figure 9. Orbit of iterated map $(u_i, v_i) \rightarrow (u_{i+1}, v_{i+1})$ for the site approximation starting from a point $(\theta_{active}(p), \theta_{active}(p)+\varepsilon)$ close to the unstable fixed point. Behavior is shown for p=0.10 and $p=p_{eq}(S=\infty) \approx 0.2071$ (for which stationary profiles exist), and for p=0.22 (no stationary profile).

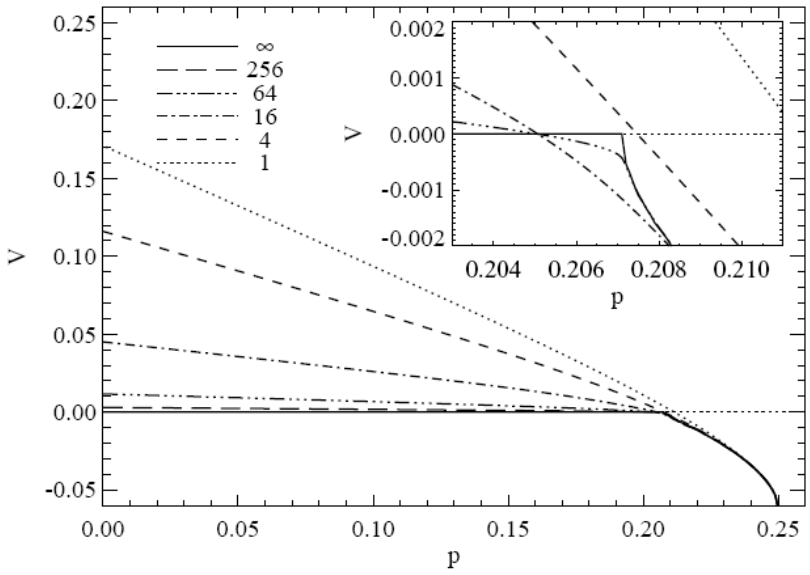

Figure 10. Predictions for V(S,p) versus p from the site approximation. Inset: Detailed view of behavior for p close to the equistability pressure for various interface orientations.

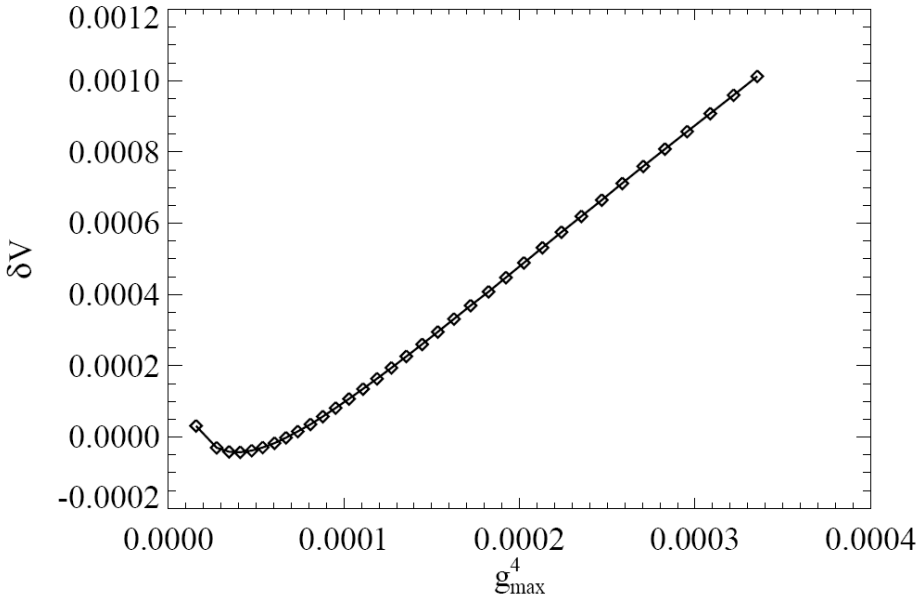

Figure 11. Difference δV = V(p, S=1)-V(p, S=2) versus the 4th power of a measure of the maximum gradient, $g_{max,}$ of the profile. Here g_{max} is taken as the maximum coverage difference between consecutive rows aligned with the interface.

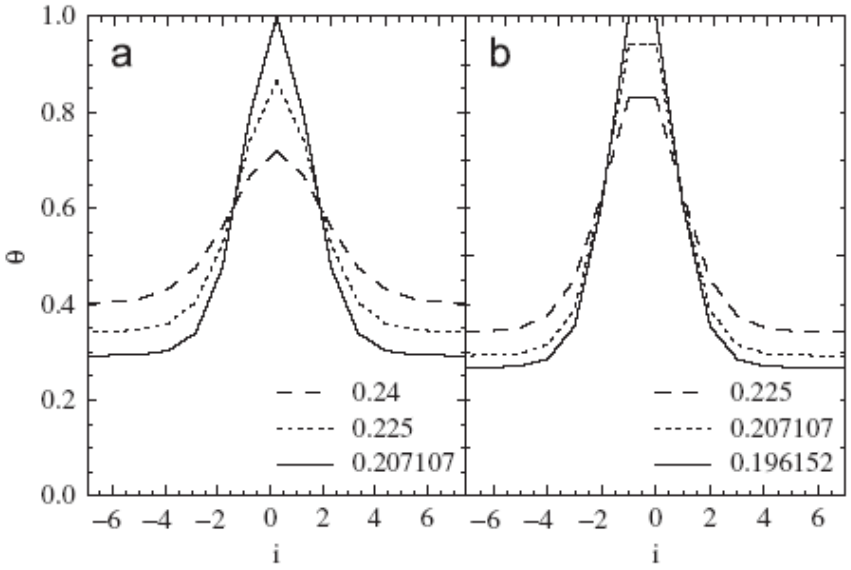

Figure 12. Site-approximation results for planar vertical critical perturbations: (a) perturbations symmetric about i=0 for $p=p_{eq}(S=\infty)\approx 0.2071$ and p=0.225; (b) perturbations symmetric about i=-1/2 for $p=p_{eq}(S=\infty)\approx 0.2071$ and p=0.225.

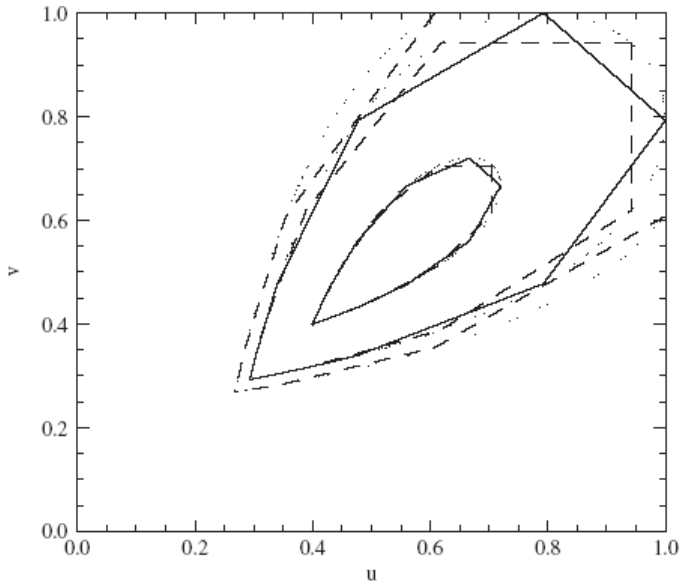

Figure 13. Characterization of planar vertical critical perturbations in terms of orbits of the iterated map for the site approximation.

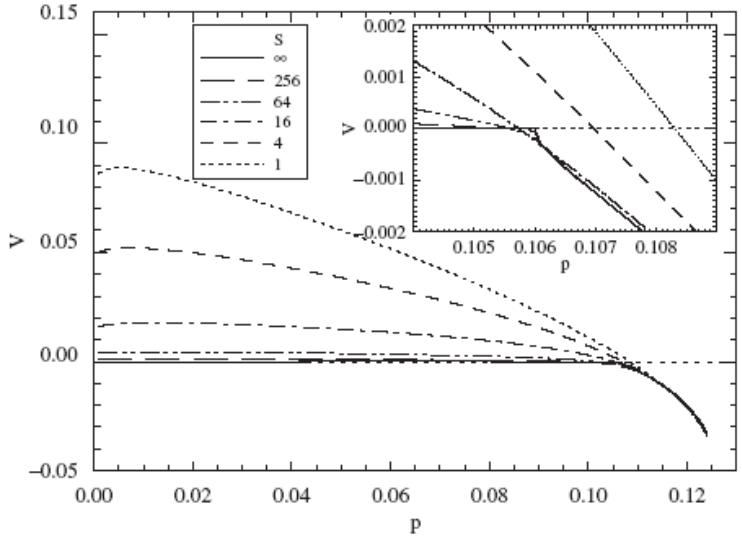

Figure 14. Predictions for V(S,p) versus p from the pair approximation. Inset: Detailed view of behavior for p close to the equistability pressure for various interface orientations.

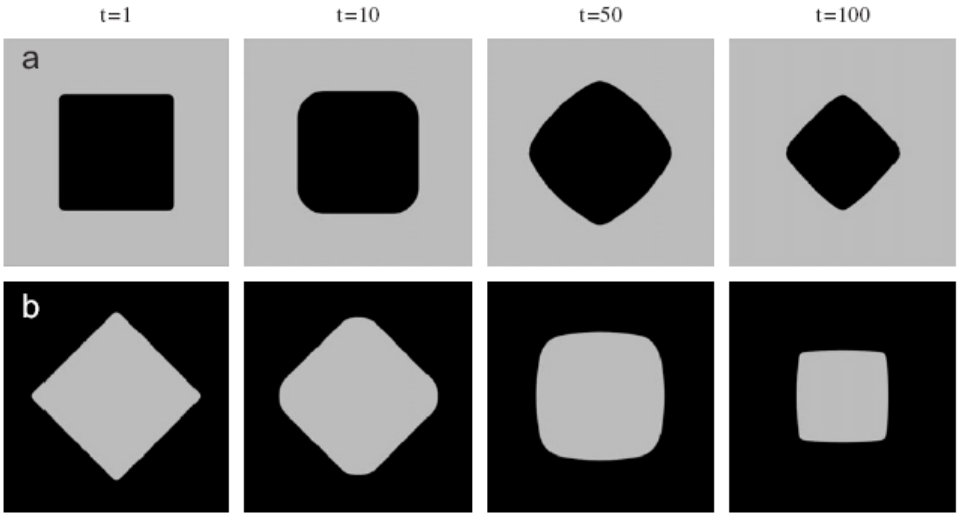

Figure 15. Dynamics of embedded droplets in the two-phase coexistence region as predicted by the site approximation: (a) poisoned square-shaped droplet in the active phase; (b) diamond-shaped empty or active droplet in the absorbing phase.

CHAPTER 4. SCHLOEGL'S SECOND MODEL FOR AUTOCATALYSIS WITH PARTICLE DIFFUSION: LATTICE-GAS REALIZATION EXHIBITING GENERIC TWO-PHASE COEXISTENCE

A paper published in the Journal of Chemical Physics

Xiaofang Guo[1,2,3], Da-Jiang Liu[1], and J.W. Evans[1,3]

Ames Laboratory – USDOE[1] and Departments of Physics & Astronomy[2] and Mathematics[3],

Iowa State University, Ames, Iowa 50011

Abstract

We analyze a discontinuous non-equilibrium phase transition between an active (or reactive) state and a poisoned (or extinguished) state occurring in a stochastic lattice-gas realization of Schloegl's second model for autocatalysis. This realization, also known as the Quadratic Contact Process, involves spontaneous annihilation, autocatalytic creation, and diffusion of particles on a square lattice, where creation at empty sites requires a suitable nearby pair of particles. The poisoned state exists for all annihilation rates $p>0$ and is an absorbing particle-free "vacuum" state. The populated active steady state exists only for p below a critical value, p_e. If p_f denotes the critical value below which a finite population can survive, then we show that $p_f < p_e$. This strict inequality contrasts a postulate of Durrett, and is a direct consequence of the occurrence of coexisting stable active and poisoned states for a finite range $p_f \le p \le p_e$ (which shrinks with increasing diffusivity). This so-called generic two-phase coexistence markedly contrasts behavior in thermodynamic systems. However,

one still finds metastability and nucleation phenomena similar to those in discontinuous equilibrium transitions.

PACS Numbers: 05.70.Fh, 02.50.Ey, 05.50.+q, 05.70.Ln

I. Introduction

Deterministic non-linear chemical kinetics and the corresponding bifurcations or phase transitions of non-equilibrium steady states for macroscopic reaction systems have traditionally been analyzed by mean-field rate equations[1,2]. The associated deterministic reaction front propagation and pattern formation have also been described by reaction-diffusion equations at the mean-field level[1,3,4]. In addition, there are numerous studies examining stochastic effects on chemical kinetics via mean-field master equations[1,5,6] and on associated pattern formation via multivariate master equations[1]. The latter can be recast utilizing time-dependent Ginzburg-Landau-type formulations to produce Langevin reaction-diffusion equations[6-8].

The deterministic mean-field analyses have been successfully applied to three-dimensional solution-phase, gas-phase, electrochemical and biochemical systems, with perhaps the best known study of pattern formation being for the Belousov-Zhabotinskii reaction[1,2]. Fluctuation effects have been considered particularly in the context of biochemical reactions[9]. Heterogeneous catalysis on extended single-crystal surfaces under low-pressure conditions has provided a remarkably rich variety of two-dimensional examples of deterministic non-linear dynamics[10] and pattern formation[11], even for mechanistically simple surface reactions. Again, mean-field analysis is traditionally applied. Fluctuation

effects have also been considered in surface reactions under conditions where they become more significant, e.g., for nanoscale systems[12,13] and under higher-pressure conditions[13,14].

However, it is natural to attempt to advance beyond mean-field-level descriptions of chemical reaction phenomena to statistical mechanical analyses of appropriate atomistic models for interacting particle systems. This is particularly relevant for situations where the reactants are not "well-stirred" or spatially randomized, as applies for surface reactions. Two of several possible modeling strategies are as follows. The first applies reactive lattice gas automata models where particles on a lattice are assigned velocities (generally subject to randomization) and move around colliding and reacting[15,16]. One can thereby describe reactive hydrodynamics and reaction-diffusion phenomena which might be analyzed via lattice Boltzmann equations. The second applies traditional stochastic lattice-gas models where the state of sites changes at specified rates associated with reaction, diffusion, etc. (akin to the Glauber model, except that the rates generally do not satisfying detailed-balance)[17]. These models are described by an exact hierarchy of master equations for multi-site probabilities which is amenable to approximate analysis. The current study and the following discussion focus on this second class of models.

Indeed, for stochastic lattice-gas "reaction" models, there has been considerable interest in non-equilibrium phase transitions. Most attention has been paid to universality in continuous transitions [17-19], with relatively little investigation of discontinuous transitions. One exception is studies of the Ziff-Gulari-Barshad (ZGB) model[20] for monomer-dimer surface reactions which exhibits a discontinuous transition to a monomer-poisoned absorbing state. Various related phenomena have been analyzed in some detail: propagation and fluctuation behavior of interfaces between active and poisoned states[20-22]; epidemic

properties of an active droplet embedded in the poisoned state[23,24]; and nucleation of droplets within the metastable active state[21,25]. While a realistic and predictive atomistic-level description of surface reactions generally requires far more complex models[26], simple ZGB-type models are invaluable for elucidating basic issues associated with non-equilibrium phase transitions in reaction systems. In fact, it is natural to search for even simpler single-component reaction models to explore remaining fundamental issues for discontinuous phase transitions.

This last observation motivates our consideration in this paper of a stochastic lattice-gas realization of a Schloegl's second model[3,27,28] for autocatalysis. This model for autocatalysis in a reactive system of particles, X, includes the following mechanistic steps[3,27,28]:

$$X \rightarrow \varnothing \text{ (spontaneous annihilation)}, \quad 2X \rightarrow 3X \text{ (autocatalytic creation)}, \tag{1}$$

and possibly particle diffusion. Spontaneous annihilation occurs at rate p, and autocatalytic creation occurs at a suitably prescribed rate subject to the requirement of at least one preexisting nearby pair of particles. A more general formulation also includes spontaneous creation $\varnothing \rightarrow X$, but this process is excluded in our study. Traditional off-lattice formulations also include the autocatalytic annihilation process $3X \rightarrow 2X$ in order to avoid population explosion[3,27,28]. However, in our stochastic lattice-gas formulation, autocatalytic particle creation requires an empty site $\varnothing$, and is thus more accurately represented as[29-31] $2X+\varnothing \rightarrow 3X$. This empty site requirement automatically limits population growth. It should also be noted that there exist lattice gas automata treatments of this model[15,16]. Of course, there is no Hamiltonian or detailed-balance constraint on the rates for lattice gas formulations this non-equilibrium model.

Both off-lattice and lattice formulations display cubic mean-field kinetics, i.e., the rate of change of particle concentration is a cubic function of concentration, C. Upon increasing the annihilation rate p, there is a bifurcation in the steady-states from bistability (where a stable active steady state with finite population C>0 coexists with the stable C=0 vacuum state) to monostability (where the C=0 vacuum state is the unique stable steady state)[27-31]. Consequently, this mean-field formulation of Schloegl's second model provided a non-equilibrium analogue of the van der Waals description of discontinuous liquid-gas equilibrium phase transitions in fluids.

The above characterization of mean-field steady-state behavior suggests that lattice gas realizations of Schloegl's second model might provide a prototype for a non-equilibrium discontinuous phase transition. If so, it is perhaps the most simple and natural model which could provide a fundamental understanding of such behavior. However, it turns out that behavior of this non-equilibrium model depends on the specific realization and on the lattice dimension. For two-dimensional lattices, one can find either continuous or discontinuous transitions[28,30]. Thus, in this contribution, we will restrict our attention to a specific stochastic lattice-gas model realization Schloegl's second model on a square lattice. This realization is also known as the Quadratic Contact Process (QCP)[29-31] and it does display a discontinuous transition.

In Sec.II, we describe in detail our QCP realization of Schloegl's second model with particle hopping on a square lattice, as well as outlining related fundamental concepts. We also review previous results for this model in the limiting cases of zero and infinite particle diffusion. Next, in Sec.III, we analyze the steady states and their relative stability which leads to a characterization the discontinuous phase transition in this model and demonstrates so-

called generic two-phase coexistence. We also analyze key aspects of the kinetics elucidating metastability associated with this transition. Generic two-phase coexistence in this model is tied to an orientation-dependence of the equistability of planar interfaces separating the active and poisoned states. Thus, in Sec.IV, we are motivated characterize both interface structure and propagation. Exploiting these insights, in Sec. V, we present a droplet analysis in order to characterize both phase stability in generic two-phase coexistence regime and the size and structure of critical droplets in the metastable regime. Concluding remarks are offered in Sec. VI.

II. Model Specification and Fundamental Concepts

A. Model Specification, Steady-States, and Critical Annihilation Rates

Our realization Schloegl's second model, or equivalently of the QCP, on a square lattice as a stochastic Markov process involves the following components[29-31]: **(i)** spontaneous particle annihilation occurring randomly at rate p; **(ii)** autocatalytic particle creation at an empty site requiring one or more diagonally adjacent pairs of occupied sites; specifically, the creation rate is given by k/4, where k is the number of such diagonally adjacent occupied pairs and thus can take the values k = 0, 1, 2,or 4; **(iii)** hopping of particles to any adjacent empty sites at rate h (per target site). See **Fig.1** for a schematic of these processes. A key variable is the particle density or concentration, C, i.e., the fraction of filled sites which satisfies $0 \leq C \leq 1$. In this paper, we shall focus exclusively on the properties of this model for an infinite square lattice. Of course, all kinetic Monte Carlo simulations are performed on a finite lattice (with periodic boundary conditions) and care must be taken to eliminate finite-size-effects.

It is immediately clear that for any p>0, the "vacuum state" with no particles (C=0) corresponds to an absorbing steady state for this model (to use the terminology of Markov processes) from which the system can never escape. This state could also be described as a poisoned or extinguished state. However, one also expects that at least for small p, there exists an active or reactive steady-state with a non-zero particle density for the model on an infinite lattice. (On a finite lattice, the system will always eventually evolve to the absorbing state.) Indeed, for $p<<1$, the lattice should be almost completely populated, so most empty sites are completely surrounded by particles and the associated particle creation rate is unity. Thus, in this regime, effectively one has random annihilation of particles at rate p and random creation of particles at empty sites at rate 1, so that the "equilibrium" steady-state concentration will trivially satisfy $C_{eq}(p) = 1-p + O(p^2)$.

It is appropriate to now introduce some basic quantities to be investigated for this model. First, we let $p_e(h)$ denote the critical value of the annihilation rate p such that an active steady state exists for $0 \leq p \leq p_e(h)$ on an infinite lattice[29]. Implicitly, the active steady state in this regime is stable against perturbations by vacuum state droplets, i.e., such vacuum droplets must perish. One expects that $C_{eq}(p)$ will decrease continuously with increasing p from a maximum value of $C_{eq}(0)=1$ to some minimum value $C_{eq}(p_e)$. The latter would be strictly positive if the model exhibits a discontinuous transition from the active to the vacuum state, and zero for a continuous transition. Second, we define another possibly distinct critical value, $p_f(h)$, of the annihilation rate p such that for $p_f(h) \leq p$ the vacuum state is stable against perturbations by active state droplets. Said differently[29], there is a non-zero probability of survival of particles starting from a finite set of populated sites for $p \leq p_f(h)$.

For a broad class of stochastic models, including the QCP with $h \geq 0$, general arguments demonstrate that $p_f(h) \leq p_e(h)$, i.e., survivability of a finite set of populated sites implies existence of an active steady state, but not necessarily the reverse[29,32]. The above discussion shows that the strict inequality $p_f < p_e$ is equivalent to generic two-phase coexistence[30,31,33-36] for $p_f(h) \leq p \leq p_e(h)$ where both the active and vacuum steady states are simultaneously stable.

B. Interface Propagation and Equistability

For $p \leq p_e(h)$, one can consider the propagation of planar interfaces separating the active and vacuum states with various orientations relative to the underlying square lattice[30,31]. We will label the slope of the interface by S, measured relative the principle lattice direction, so the corresponding angle giving the interface orientation is $\theta = \arctan S$. By rotational symmetry, behavior for orientations θ and $\theta \pm \pi/2$ are equivalent (e.g., S=0 and $S=\infty$ are equivalent). Let $V(p, h, S)$ denote the propagation velocity of this interface, where $V>0$ corresponds to the active state displacing the vacuum state, and $V<0$ the opposite case. Propagation occurs indefinitely for $p \leq p_e(h)$ since spontaneous nucleation of the active state within the absorbing vacuum state is not possible for any $p \geq 0$, and the active state is by definition stable. As a result, it follows that $V(p, h, S)$ is well-defined for all $p \leq p_e(h)$. This contrasts behavior in thermodynamic systems where interface propagation away from a single equistability point is transient.

In the absence of particle annihilation for p=0, $V(p=0, h, S)$ is strictly positive (except for h=S=0 as discussed below). Propagation for p=0 corresponds to expansion of a completely filled region of the lattice into a vacuum region by irreversible autocatalytic

creation of particles at the interface. Furthermore, one expects such V(p, h, S) to decrease with increasing p as the stability of the active state decreases relative to that of the vacuum state. We anticipate that active and vacuum states separated by a planar interface with slope S will be equistable, corresponding to a stationary interface, at a unique value the annihilation rate $p = p_{eq}(h, S)$. (One exception is for h=S=0.) For generality, we have allowed for the possibility that $p_{eq}(h, S)$ depends explicitly on S and that $p_{eq}(h, S) < p_e(h)$. In contrast, p_{eq} and p_e must be equal and independent of S in thermodynamic systems. In our general scenario, we have that $V(p, h, S) > 0$ for $p < p_{eq}(h, S)$, and $V(p, h, S) < 0$ for $p_{eq}(h, S) < p < p_e(h)$. For the QCP with $h \geq 0$, it is also reasonable to expect that typically V varies linearly with p close to equistability, so that in this regime one has

$$V(p, h, S) \approx -B(h,S)\delta p_{eq}(h, S), \text{ for small } \delta p_{eq}(h, S) = p - p_{eq}(h, S), \quad (2)$$

with B>0 (except for h=S=0).

In this general scenario, one also expects that the critical annihilation rates, $p_e(h)$ and $p_f(h)$, are related to the annihilation rates, $p_{eq}(h, S)$, for equistability via

$$p_e(h) = \max_{0 \leq S \leq \infty} p_{eq}(h, S) = p_{eq}(h, \max) \text{ and } p_f(h) = \min_{0 \leq S \leq \infty} p_{eq}(h, S) = p_{eq}(h, \min) \quad (3)$$

The first identity should hold since for any p smaller than $p_{eq}(h, \max)$, there exists a range of orientations such that an interface expands into the vacuum state creating a stable active state in its wake. For p above $p_{eq}(h, \max)$, an active droplet should be destroyed by the surrounding vacuum state encroaching on all sides, so the active state is not stable. For the second identity, a similar rationalization applies except that for h=0 there is some ambiguity in defining $p_{eq}(h=0, S=0)$. We will exploit the relationships (3) in our simulation analysis in Sec. III. Below, for convenience, we shall often leave implicit the h-dependence.

C. Dimensional Analysis

It will sometimes be instructive to utilize a simple dimensional analysis to elucidate the behavior of key quantities in terms of a suitably defined characteristic length, L_c, and characteristic time, τ_c. Since both particle annihilation and creation rates are of order unity in our model, the same applies for τ_c =O(1). One might expect that $(L_c)^2 \approx (L_r)^2 + (L_d)^2$, where L_r=O(1) is a "reaction range" which reflects spatial coupling in the particle creation process, and $L_d \approx (h\tau_c)^{1/2}$ is the diffusion length[21] . Then, one has that[21] $L_c \propto (a+h)^{1/2}$ where a=O(1). Equivalently, one can write $L_c \approx (D_{eff}\, \tau_c)^{1/2}$ in terms of an effective diffusion coefficient D_{eff} $\propto$ a + h. Some motivation for this form of D_{eff} comes from the so-called diffusion approximation in classical spatial contact models[37], and from the approximate analysis of the master equations for spatially non-uniform states in the QCP[38,39]. In terms of these characteristic quantities, one expects that

$$V \sim L_c/\tau_c \sim (D_{eff}/\tau_c)^{1/2}, \text{ so that } V \sim (a+h)^{1/2} \sim h^{1/2}, \text{ for large h.} \qquad (4)$$

A more complete representation of behavior near equistability (except for h=S=0) should be given by $V(p, h, S) \sim -(a+h)^{1/2}\, \delta p_{eq}(h, S)$ where again $\delta p_{eq}(h, S) = p - p_{eq}(h, S)$ (cf. Sec.II B). For large h, these predictions for the behavior of V(p, h, S) are confirmed by a mean-field reaction-diffusion equation analysis. See Ref. 3 and Sec. II D.

D. Model Behavior in Limiting Cases: h=0, h$\rightarrow\infty$

We briefly review previous analyses of the QCP with h=0 (i.e., no particle hopping) on an infinite square lattice. Simulation studies[30,31] indicate the existence of a discontinuous phase transition. Specifically, starting from a completely populated lattice, the system

evolves to an active state for $0 \le p \le p_e(h=0)=0.09443$ (± 0.00003), but instead to the "poisoned" $C_{eq}=0$ vacuum state for $p > p_e(h=0)$. The active steady-state value, $C_{eq}(p)$, of C decreases from $C_{eq} = 1$ for p=0 to $C_{eq} \approx 0.83$ as $p \to p_e(h=0)$. As might be anticipated based on mean-field modeling, the discontinuous transition behavior will be preserved for h>0. See Sec. III.

A remarkable feature[30,31] of the QCP with h=0 emerged from consideration of equistability of the active and vacuum states separated by a planar interfaces with various slopes S. The annihilation rate, $p_{eq}(S) = p_{eq}(h=0, S)$, corresponding to equistability does actually depend on interface orientation or slope, S, in marked contrast to a thermodynamic systems! Also, $p_{eq}(S)$ achieves a maximum value of $p_{eq}(max) = p_{eq}(S=1) = p_e$ for a diagonally oriented interface with slope S=1. For other orientations or slopes S, equistability occurs at lower $p = p_{eq}(S)$ with a minimum of $p_{eq}(S \to 0) = p_{eq}(S \to \infty) = 0.0869$ (± 0.0004) being achieved approaching horizontal or vertical interfaces with $S = 0$ or ∞.

One <u>special quirk</u> for this QCP with h=0 is that the vacuum state bordered by a vertical interface can never be populated for any p>0, i.e., this vacuum region can never shrink[30,31]. This follows from the rule for autocatalytic creation of particles noting that empty sites in a vertical vacuum strip never have diagonally adjacent occupied neighboring pairs. In an infinite system, one has that the interface is stationary $V(p, S=0 \text{ or } \infty) = 0$ for all $0 \le p \le p_{eq}(S \to 0) \approx 0.0869$. Expansion of the vacuum state into the active state[30,31] with $V(p, S=0 \text{ or } \infty) < 0$ <u>only</u> occurs for $p > p_{eq}(S \to 0) \approx 0.0869$. As a result, there is some ambiguity in defining $p_{eq}(min)$. The second identity in Eq. (2) only applies for h=0 if one sets $p_{eq}(min)=0$, as now discussed.

Another ramification of this quirk[29,30] for h=0 is that the critical value for survival of finite populations satisfies $p_f(h=0) = 0$. Given the special rule for autocatalytic creation of particles, for the QCP with h=0, a finite populated region can never expand outside of a rectangle inscribing the initial populated sites. As a result, all particles must eventually be annihilated based on the properties of finite-state Markov processes with absorbing states[5].

The QCP with h>0 avoids the above quirk. The vacuum state separated by a vertical interface from the active state can either expand or shrink depending on the value of p. Also, a finite set of populated sites can in principle expand and survive indefinitely. Durrett has postulated[29] that $p_f(h) = p_e(h)$ for the QCP with any h>0, which is no doubt a common expectation. However, the current work will in fact show that this Durrett postulate does not hold for h>0, and that this failure is a direct consequence of so-called generic two-phase coexistence.

Finally, we mention that for the QCP in the limit $h\rightarrow\infty$ of a well-stirred or randomized system, behavior is described exactly by a mean-field treatment[3,29,31]. Exact analysis based on the mean-field rate equation for the kinetics[3,31],

$$dC/dt = R(C) = -pC + C^2(1-C), \tag{5}$$

demonstrates bistability, i.e., coexistence of stable active and vacuum states, with the concentration in the active steady state satisfying[31]

$$C_{eq}(p) = ½ + ½(1-4p)^{1/2}, \text{ for } p_{s-}(h=\infty) = 0 \le p \le ¼ = p_{s+}(h=\infty). \tag{6}$$

Here, $p_{s\pm}(h)$ denote upper and lower spinodal points. Analysis of interface propagation based on a mean-field reaction-diffusion equation[3,31] demonstrates that for large h

$$V(p, h, S) \propto h^{1/2}[1-3(1-4p)^{1/2}], \text{ for } p_{s-}(h=\infty) = 0 \le p \le ¼ = p_{s+}(h=\infty), \tag{7}$$

independent of S, corresponding to equistability[31,33] when $p = p_e(h=\infty) = p_f(h=\infty) = 2/9$. Thus, the Durrett postulate[29] is satisfied in the $h=\infty$ mean-field limit.

III. Steady-States and Kinetics: Simulation Results

Conventional Kinetic Monte Carlo (KMC) simulation (for some selected constant p) of the general QCP for $h \geq 0$ can be used to follow evolution starting from a completely populated lattice to the final steady state. This allows determination of the active steady-state concentration, $C_{eq}(p)$, versus p, and thus estimation of $p_e = p_e(h)$. See **Fig.2** which displays this "equation of state" for h=0.001 revealing a discontinuous transition just as for h=0. However, one shortcoming of such a conventional KMC simulation analysis is that for p just slightly above $p_e(h)$, the system tends to get trapped for long times in a metastable active state before reaching the vacuum state. This leads to the potential for overestimation of $p_e(h)$. These general features of the non-equilibrium discontinuous transition, and the challenges for accurate determination of p_e, are analogous to those seen in the ZGB model[20,23,40]. This prompted development of an alternative approach[20,30,31] to determine p_e and related quantities which we adopt in Sec. III A.

A. Equistability of Active and Vacuum Steady-States

A comprehensive picture of the relative stability of active and vacuum states follows from consideration of the equistability of interfaces between these states with various orientations S. This analysis also leads to a reliable determination of the critical annihilation rate, p_e, for existence of an active state from the relation $p_e = \max_{0 \leq S \leq \infty} p_{eq}(S) = p_{eq}(\max)$, where we leave implicit the h-dependence. Our analysis for h>0 presented below indicates

that $p_{eq}(S)$ does depend on S, where the maximum is achieved for S=1 so that $p_e = p_{eq}(S=1)$ for all h>0 (just as for h=0). We also find that $p_f = p_{eq}(\min) = \min_{0\le S\le\infty} p_{eq}(S) = p_{eq}(S=0) = p_{eq}(S=\infty)$ is strictly below $p_e = p_{eq}(\max) = p_{eq}(S=1)$ for h>0, contrasting the Durrett postulate[29].

All of our results for $p_{eq}(S)$ were obtained from so-called constant-population ensemble simulations[30,41] involving the following steps: **(i)** a target population is selected (usually $C_t \approx ½$); **(ii)** at each step, a site is picked at random; **(iii)** with probability 4h*/(1+4h*), one attempts to hop in one of four randomly chosen directions (which requires the selected site to be occupied and the chosen adjacent site to be empty); **(iv)** with probability 1/(1+4h*), one attempts to either annihilate or create particles; if $C>C_t$ applies for the current value of C, then annihilation is attempted (occurring if the site is populated), and if $C<C_t$ then autocatalytic particle creation is attempted (occurring if the site is empty and with a probability $k/4 \le 1$); **(v)** we track the fraction, f, of attempts to annihilate particles in (iv). Then, the fraction of attempts to annihilate is 1-f and p :1 = f :1-f , so that p=f/(1-f). To match the correct relative rates for particle hopping and particle annihilation and creation in conventional simulation, one sets 4h*/1 = 4h/(1+p), so that h = (1+p)h*. Starting with a planar interface between completely filled and vacuum states with the selected S, the constant-population ensemble simulation preserves this planar interface geometry for $C_t \approx ½$ and the output pressure automatically corresponds to the desired $p_{eq}(S)$.

The S-dependence of $p_{eq}(S)$ described above is shown in the inset of **Fig. 2** for the case h=0.001. In our determination of $p_{eq}(S)$, we have also performed a finite-size scaling analysis[30] (not shown) revealing a weak dependence of our estimates on system size. For

h=0.001, we find that $p_e = p_{eq}(S=1) = 0.0958$ and that $p_f = p_{eq}(S=0 \text{ or } \infty) = 0.0941$ (obtained from interpolating constant coverage simulation results for h* close to 0.001). Based on the general arguments in Sec. 2A, one has stability of both the active and vacuum steady states for $p_f < p < p_e$. Thus, in the "equation of state" plot **Fig. 2**, we include two vertical lines at $p = p_e$ and $p = p_f$ to indicate the extent of regime of generic two-phase coexistence.

A more comprehensive set of results for the h-dependence of $p_e = p_{eq}(\max) = p_{eq}(S=1)$ and $p_f = p_{eq}(\min) = p_{eq}(S=0 \text{ or } \infty)$ are reported in **Table I** (obtained from interpolation of constant coverage simulation results for various h*). Note that p_e varies roughly linearly with small h, but p_f varies non-linearly quickly approaching p_e. Thus, the width $\Delta p_{eq} = p_e - p_f$ of the regime of generic two-phase coexistence decreases quickly with increasing h, and is below 0.0001 for h>0.01. From our simulations alone, we cannot rule out the possibility that Δp_{eq} becomes zero above some critical value h_c of h. See Sec. VI for further discussion of this point. The limiting behavior, $p_{eq}(S=1) = p_{eq}(S=0 \text{ or } \infty) = 2/9$ for h=∞, follows from (7). It should be noted that a similar shrinkage to the width of the generic two-phase coexistence region occurs upon introducing a spontaneous particle creation. In this case, two-phase coexistence (and the discontinuous transition) terminate at a critical point[30,42].

B. Metastable States, Spinodal Points, and Poisoning Kinetics

For the QCP with h≥0 on an infinite lattice, one finds evidence for a metastable extension of the active steady state into a regime $p_e \le p \le p_{s+}$. Here, p_{s+} denotes an effective upper spinodal point. However, just as for thermodynamic systems, the precise nature and even the existence of the metastable state and spinodal point in an infinite system is a subtle

issue. In fact, based on behavior for equilibrium Ising-type systems[43-45], there should not exist a unique analytic metastable extension of the active state steady state, but rather a family of C^{∞} metastable extensions[31]. Consequently, there is no natural unique definition of p_{s+}. However, from a more practical perspective, concepts of metastability and spinodal points are particularly valuable in characterizing the kinetics of non-equilibrium models in the vicinity of discontinuous transitions[21,25,31]. Indeed, analysis of the kinetics is likely the most effective way to define these quantities, a strategy which has been used for equilibrium systems[44]. Finally, we note that some studies of equilibrium systems have defined different types of spinodal points specific to finite systems[46]. These are distinct from p_{s+} specific to an infinite system considered here.

Here, we first consider determination of the location of the effective upper spinodal point through analysis of the "rapid" poisoning kinetics, i.e., evolution to the vacuum state, for $p>p_{s+}$. In later sections, we will present two distinct but complementary and consistent strategies to locate p_{s+}. We emphasize that there is some ambiguity in each of these strategies, so that one never achieves a precise and unambiguous determination of the spinodal point. In the regime $p>p_{s+}$, evolution is not nucleation-limited (cf. Sec. III C). The system should poison exponentially quickly as predicted by a mean-field theory[31,38], and the poisoning rate should depend strongly on the distance $\delta p_{s+} = p-p_{s+} >0$ above the upper spinodal. Specifically, one might anticipate that C(t) has the form $C \approx c(\delta p_{s+}t)$, so that curves for C(t) versus $\delta p_{s+}t$ for different p should collapse[21,31] for the appropriate choice of p_{s+}. Application of this idea requires selection a suitable regime of p in which to analyze the kinetics. We typically choose the lowest value corresponding to $\delta p_{s+} \approx 0.010$ and the width of

this regime as roughly 0.015. This procedure is illustrated for h=0.001 where optimum collapse is achieved with $p_{s+} \approx 0.102$ in **Fig. 3**.

Results for p_{s+} versus $h \geq 0$ are summarized in **Table I**. We should caution that results depend to some extent on the choice of the p-regime. Even for $h \rightarrow \infty$ where $p_{s+} = ¼$ is well-defined[29], the estimate from the above procedure deviates from ¼ when using a p-regime which is a significant finite distance from p_{s+}. Note that the width of the metastable regime, $\Delta p_{s+} = p_{s+} - p_e$, appears to shrink slightly as h becomes no zero, and is actually roughly constant for a significant range of h before increasing to its significantly larger $h \rightarrow \infty$ limiting value of 1/36.

Finally, we discuss the lower spinodal, $p_{s-} < p_{eq}(\text{min}) = p_f$. Previous analysis of kinetics at low p for the QCP indicated that[31] $p_{s-} = 0$ for h=0. Our simulations of the kinetics of the QCP for $h \geq 0$ (not shown) provide no evidence for existence of a non-trivial lower spinodal with p_{s-} greater than 0.The mean-field treatment described in Sec. I and higher-order dynamic cluster approximations of exact master equations[38,39] predict that $p_{s-} = 0$ for any $h \geq 0$. Thus, we anticipate that $p_{s-} = 0$ for our lattice-gas realization for the QCP with any $h \geq 0$.

C. Avrami Analysis of Nucleation-Mediated Poisoning Kinetics

Next, we analyze the nucleation-mediated poisoning kinetics, i.e., evolution to the vacuum state, for $p_e < p < p_{s+}$, which is much slower than and different in nature from the poisoning described above for $p > p_{s+}$. A detailed analysis of these kinetics for h=0 can be found in Ref. 31. Behavior for h>0 is qualitatively similar, and is analyzed here in the same way.

Just as for thermodynamic systems, the idea here is that there exists a critical size for droplets of the poisoned or vacuum state above which they will grow and below which they shrink. Poisoning is then controlled by the fluctuation-mediated formation and subsequent growth of such critical droplets. Key parameters are the nucleation rate of critical droplets, k_{nuc}, and the propagation velocity, V_{grow}, of selected interface orientations of the super-critical droplets. Following the postulate in Ref. 25 abd 31 for k_{nuc}, and adopting ideas from Sec. II C for V_{grow}, we propose that

$$k_{nuc} \propto \exp(-c_{nuc}/\delta p_{eq+}) \text{ and } V_{grow} \sim (a+h)^{1/2}\, \delta p_{eq+}, \text{ where } \delta p_{eq+} = p - p_e. \quad (8)$$

Also, based on a dimensional analysis or mean-field analysis, we expect that $c_{nuc}(h) \sim a+h$ for large h (cf. Sec. V D). Then, an Avrami formulation[47] demonstrates that the nucleation kinetics is controlled by the characteristic time $\tau_{nuc} \propto (V_{grow})^{-2/3}(k_{nuc})^{-1/3}$. Specifically, after a "short" transient period during which the system reaches the metastable active state with particle concentration C_m, the time evolution of the particle concentration should be given by[25,31]

$$C(t)/C_m \approx \exp[-A(t/\tau_{nuc})^3], \text{ choosing } \tau_{nuc} = (c_{nuc})^{-1/3}(\delta p_{eq+})^{-2/3}\exp[c_{nuc}/(3\delta p_{eq+})]. \quad (9)$$

Plotting $C(t)/C_m$ versus t/τ_{nuc} for various δp_{eq+} and fixed h and adjusting c_{nuc} to optimize collapse of this family of curves provides an estimate of $c_{nuc} = c_{nuc}(h)$. This analysis has already been successfully applied[31] to the QCP with h=0, but it extends to quantify the variation of $c_{nuc}(h)$ with h. Specifically, for each h, we choose the same set of values of δp_{eq+} = 0.0031 + 0.0005 m, with m = 0, 1, 2, and 3. Then, in **Fig.4**, we show both the 'raw' kinetics $C(t)/C_m$ versus t, as well as the optimum collapsed curves for four choices of h=0.001, 0.1, 0.2, and 0.4. Behavior for h=0.001 is essentially indistinguishable from that reported previously[31] for h=0. Interestingly, nucleation-mediated poisoning is significantly faster for

h=0.1 than for h=0.001 (or h=0). It is also somewhat faster for h=0.2, but slower for h=0.4 and becomes progressively slower for larger h. This trend is reflected in the estimated values of $c_{nuc} \approx 0.024$,[31] 0.023, 0.012, 0.021, and 0.048 for h = 0, 0.001, 0.1, 0.2, and 0.4, respectively. The non-monotonic variation of the lifetime of the metastable state with increasing h might be anticipated from the results in Sec. III B for the variation of the width of the metastable region.

Some theoretical underpinning for the above formulation of poisoning kinetics will follow from our analysis of the nature of critical droplets of the vacuum state embedded in the active state, and of the associated nucleation barrier, presented in Sec. V.

IV. Interface Structure and Propagation

As discussed in Sec. II and Sec. III, generic two-phase coexistence in our QCP realization of Schloegl's model is directly tied to an orientation-dependence of the equistability of planar interfaces separating the active and poisoned states. This motivates a more detailed analysis of interface structure and propagation in this section. The resulting insight will be invaluable for our analysis of critical droplets in Sec. V.

A. Coarse-Grained Kpz Description of Interface Structure

To elucidate the propagation and structure of the interface between active and vacuum states, it is natural to adopt a coarse-grained mesoscale picture. Here, the interface location at time t is described by a continuous "height" function, y(x, t), measured in a direction orthogonal to the global interface orientation for varying location, x, along the interface. Then, evolution of y is described by a suitable stochastic partial differential

equation. For the S=1 "high symmetry" orientation, this evolution equation should have[23,24] the Kardar-Parisi-Zhang (KPZ) form[48,49]

$$\partial y/\partial t = V_0 + \tfrac{1}{2}\lambda\,(\partial y/\partial x)^2 + \nu\,\partial^2 y/\partial x^2 + \ldots + \eta(x,t), \qquad (10)$$

in the regime of small slopes where $V_0 = V(p, h, S=1)$ and $\eta(x,t)$ represents a non-conserved noise term satisfying $\langle\eta(x,t)\rangle=0$ and $\langle\eta(x,t)\,\eta(x',t')\rangle = \gamma\,\delta(x-x')\delta(t-t')$. On the right hand side of (10), the kinetic coefficient $\lambda>0$ in the non-linear term can be estimated from simple geometric arguments[50]. The linear term provides stability by damping meandering of the interface, and the kinetic coefficient ν is discussed in further below. Description of interface propagation and structure is more complex for other orientations, but the corresponding evolution equation should have a linear stabilizing term with a possibly orientation-dependent ν.

Analysis of Eq. (10) reveals that for long times the interface achieves a stationary local structure <u>independent</u> of λ. The slopes $\partial y/\partial x$ adopt a Gaussian distribution with variance $\gamma/(2\nu)$, and a spatial correlation function satisfies[48]

$$G(x) = \langle[y(x+x',t)-y(x',t)]^2\rangle = \langle[y(x,t)-y(0,t)]^2\rangle \approx \gamma/(2\nu)\,|x|^{2\alpha} \text{ with } \alpha = \tfrac{1}{2}\,, \qquad (11)$$

provided that $|x|$ is not too large. Equivalently, the long-time stationary interface roughness, $W_{sat}(L)$, measured in a "small" finite window of width L satisfies[48,49]

$$W_{sat}(L)^2 = L^{-1}\int_{0<x<L} dx\,[y(x,t)-\langle y(t)\rangle_L]^2 \propto (\gamma/\nu)\,L^{2\alpha} \text{ with } \alpha = \tfrac{1}{2}, \qquad (12)$$

where $\langle y(t)\rangle_L$ denotes the average over the window. Thus, the ratio γ/ν measures the amplitude of interface wandering. Often α is referred to as the wandering or roughness exponent, and $\alpha = \frac{1}{2}$ corresponds to simple random walk behavior of the interface.

In general KPZ-type formulations of interface propagation, the kinetic coefficient ν is often referred to as an "effective line tension"[49]. However, this can be misleading. A more appropriate perspective comes from a coarse-grained formulation of equilibrium interface fluctuations via evaporation-condensation[51] which is described by Eq. (10) with $V_0=0$ and $\lambda=0$. In this case, the kinetic coefficient $\nu \propto \Gamma\, \tilde{\sigma} > 0$ is proportional to the product of a suitable mobility, Γ, and the interface stiffness or interface rigidity[51], $\tilde{\sigma}$. Also, as a result of the fluctuation-dissipation relation, $\gamma/(2\nu) = kT/\tilde{\sigma}$ is independent of Γ in the equilibrium case.

For our non-equilibrium application, ν might most appropriately be regarded as a product of an effective mobility, Γ_{eff}, and an effective stiffness, $\tilde{\sigma}_{eff}$. In fact, ν should not just be interpreted as an effective line tension since: (i) the interface stiffness and line tension coincide only when the interface properties are isotropic[51]; (ii) the presence of the mobility factor means that ν scales differently with h than either the stiffness or line tension (see Sec.V). On the latter issue, a dimensional analysis (cf. Sec. II C) indicates that the kinetic coefficient, ν, satisfies

$$\nu \sim (L_c)^2/\tau_c, \text{ so that } \nu \sim a + h \sim h \text{ for large h.} \qquad (13)$$

This prediction is confirmed by a mean-field reaction-diffusion equation analysis. See Ref. 3 and Sec. V.

B. Interface Stiffness

Motivated by the above discussion, we examine the structure of interfaces separating active and vacuum steady states at equistability for different interface orientations, θ =

arctan(S), and for various h. Direct inspection of simulation images provides insight into the dependence on θ and h of

$$G(x) \propto (|x|\,\gamma)/(\Gamma_{eff}\,\tilde{\sigma}_{eff}) \text{ or } W_{sat} \propto (L\,\gamma)/(\Gamma_{eff}\,\tilde{\sigma}_{eff}). \quad (14)$$

Fig. 5 compares behavior for interfaces with S=0 and S=1 when h*=h=0, and also for h*=0.001 and h*=0.1. A strong anisotropy in interface structure is evident for h*=h=0 with significantly greater roughness for S=1 than S=0. If we assume there is no strong θ-dependence of Γ_{eff}/γ, then one concludes that a maximum (minimum) in the effective interface stiffness, $\tilde{\sigma}_{eff}$, is achieved for S=0 (S=1) when h=0. Upon increasing h* or h to as little as 0.001, this anisotropy appears to be significantly reduced. For h*=0.1, interface behavior appears close to isotropic.

The other dramatic feature apparent in **Fig. 5** is that the interfaces roughness for S=0 increases dramatically as h is increased from h*=0 to h*=0.001 and further to h*=0.1. A similar, but less dramatic increase, is apparent for S=1. However, from the dimensional analysis above, eventually ν must grow with increasing h and thus eventually the interface roughness will decrease. If we assume that the ratio Γ_{eff}/γ is a non-decreasing function of h, then we are forced to conclude that the effective stiffness, $\tilde{\sigma}_{eff}$, at least initially decreases with increasing h>0. The decrease in is $\tilde{\sigma}_{eff}$ more dramatic for S=0 than for S=1. However, since $\nu \sim \Gamma_{eff}\,\tilde{\sigma}_{eff} \sim a + h \sim h$, for large h, it might be anticipated that $\tilde{\sigma}_{eff}$ will increase for large h, behavior confirmed in Sec. V. Thus, we conclude that $\tilde{\sigma}_{eff}$ varies non-monotonically with h. This proposal seems consistent with the observed non-monotonic variation with h of the lifetime of the metastable state described in Sec. III C. See Sec. V for further discussion.

To elucidate this proposed non-monotonic variation of $\tilde{\sigma}_{eff}$ with h, we recall that interface properties quickly become more isotropic as h increases above zero. Enhanced isotropy generally reduces stiffness in thermodynamic systems. Suppressing the dependence of various quantities on p, one can represent the dependence of stiffness on the angle, θ = arctan(S), defining the local orientation of the interface in this four-fold symmetric system via

$$\tilde{\sigma}_{eff}(\theta) \approx \tilde{\sigma}_1(h) + g(h)\,[\cos(2\theta)]^2, \qquad (15)$$

where g(h)>0 measures the strength of the anisotropy. Here, we just keep the lowest-order terms in the Fourier expansion, and we have recast[52] the conventional expansion in a form so that $\tilde{\sigma}_1(h)$ corresponds to the stiffness for an interface with S=1. The requirement that g(h)>0 ensures that the stiffness is maximum (minimum) for S= 0 and ∞ (S=1). We also anticipate that g(h) decreases quickly towards zero as h increases above zero resulting in the above-mentioned initial rapid decease in $\tilde{\sigma}_{eff}$ for S=0. The less dramatic initial decrease in $\tilde{\sigma}_{eff}$ for S=1 requires that $\tilde{\sigma}_1(h)$ also decreases initially as h increases above zero, although probably much less strongly than g(h). The strong variation of g(h) versus the weaker variation of $\tilde{\sigma}_1(h)$ is what motivated our choice of the form (15). The proposed non-monotonic behavior of $\tilde{\sigma}_{eff}$ requires that $\tilde{\sigma}_1(h)$ also vary non-monotonically, eventually increasing for large h.

C. Dependence of Interface Propagation Velocity on Annihilation Rate

Here, we consider the propagation velocity of planar interfaces separating the vacuum and both stable and metastable active states with slopes S=1 and S=0 (or S=∞) as a function

of p. As noted in Sec. II, interface propagation for any S is well-defined (i.e., it occurs indefinitely) for $p < p_e(h)$. For such well-defined propagation, V(p, h, S) can be readily determined by monitoring the linear variation with time of empty sites in a finite system with periodic boundary conditions by selecting an initial strip geometry for the vacuum state, say[31]. The increase or decrease in population corresponds to expansion or shrinkage of the vacuum state strip. To convert these variation rates into a velocity, one must also know the particle concentration in the active state[31]. Comparative results are shown for V(p, h, S=1) and V(p, h, S=0 or ∞) versus p for h=0 in **Fig. 6a** and h=0.001 in **Fig. 6b**. Note that these curves provide upper and lower bounds on the V(p, h, S) for all other S. Behavior is consistent with the general comments in Sec. II B.

In contrast, for $p > p_e(h)$, it is <u>not</u> possible to sustain indefinite interface propagation with the vacuum state displacing the metastable active state since spontaneous nucleation of the vacuum state occurs within the metastable active state. More technically, there will not exist an analytic extension of the well-defined V(p, h, S) from[31] $p < p_e(h)$ to $p > p_e(h)$. For example, one does not have a well-defined extension of $V(p, S=1)>0$ for $p < p_{eq}(S=1) = p_e$ to $V(p, S=1) < 0$ for $p > p_e$. Interestingly, for S=0 (or ∞), interface propagation is well-defined for not just $p < p_{eq}(S=0 \text{ or } \infty)$ where $V(p, S=0) > 0$, but also for the regime $p_{eq}(S=0) < p < p_e$ above the relevant equistability pressure where $V(p, S=0) < 0$. Thus, one expects V(p, S=0) to be an analytic function at $p = p_{eq}(S=0)$, where $V(p, S=0) = 0$, and also up to p_e (but not for $p > p_e$).

Despite these complications, it is instructive to explore the behavior of $V(p, h, S) < 0$ for $p_e(h) < p < p_{s+}$ as estimated from transient propagation. In fact, we will see that such an analysis provides an unconventional second strategy to estimate the upper spinodal, p_{s+}.

However, there are practical issues in the determination of V(p, h, S) which should be addressed before discussing simulation results. The major challenge is that we wish to determine V(p, h, S) approaching the upper spinodal where interface motion becomes more transient and less robust since spontaneous nucleation of the vacuum state within the active state regions becomes more facile. The latter leads an additional decrease in the particle population not associated with expansion of the vacuum strip, potentially leading to overestimation of the magnitude of $V<0$. We partly ameliorate this problem[53] by determining the size of the vacuum strip counting only those empty sites which are connected to the strip, and excluding those which are part of disconnected isolated vacuum clusters or droplets within the active state. See **Fig. 7**.

Results for transient interface propagation for $p>p_e(h)$ are also presented in **Fig. 6**. A tendency for the V(p, h, S) curves for different S to merge, and for their slopes, dV/dp, to diverge, as $p \to p_{s+}$ might be anticipated noting results from any of: **(i)** a mean-field reaction-diffusion equation analysis (7) for large h; **(ii)** a more complex analysis of interface propagation based on non-uniform master equations[38,39]; or **(iii)** previous simulations[31] for the QCP with h=0. Indeed, when viewed over a broad range of p, these V(p, h, S)-curves in **Fig. 6** do appear to merge and their slopes increase strongly as $p \to p_{s+}$ (based on the estimates of p_{s+} in Sec.4A). However, an expanded view near this upper spinodal, where there is considerable ambiguity in determining V(p, h, S), does not show complete merging and the slopes do not diverge.

D. Dependence of Interface Propagation Velocity on Hop Rate

The independence of p_{eq} on S in the limit as $h\to\infty$ is a consequence of the more general feature that V(p, h, S) becomes "independent" of orientation, S, for this mean-field reaction-diffusion regime (noting that particle diffusion is isotropic). By "independent", we mean that differences in V for different S become insignificant relative to the magnitude of V. In fact, a stronger condition applies, as described below. To illustrate this behavior of V(p, h, S), we determine the dependence on h of both V(p=0, h, S=1) and V(p=0, h, S=0 or ∞). The "large" difference between these velocities for h=0, where[30,31] V(p=0, h=0, S=1) = $1/(8\sqrt{2}) \approx 0.0884$ (in units of lattice constants per unit time) and V(p=0, h=0, S=0 or ∞) = 0 quickly shrinks upon increasing h. Similar behavior is observed for p>0. See **Fig. 8** for behavior when p=0 and p=0.05. Anticipating that $V \sim (a+h)^{1/2}$ (cf. Sec. II C), we plot the square of V versus h in **Fig. 8** producing a near-linear variation, $V(p, h, S)^2 \approx e(p, S)^2 + d(p)^2 h + O(h^{-n})$ with n>0. Thus, one has that

$$V(p, h, S) \approx [d(p)\, h^{1/2} + \tfrac{1}{2}\, e(p, S)^2\, d(p)^{-1}\, h^{-1/2} + O(h^{-n-1/2})], \text{ for large h,} \qquad (16)$$

so that differences in V for different S decrease like $h^{-1/2}$ if e(p,S) depends explicitly on S, or faster otherwise. Close to equistability, one has that $e(p, S) \approx e(S)\, \delta p_{eq}(h,S)$ and $d(p) \approx d \cdot \delta p_{eq}(h,S)$, so that $V(p, h, S) \approx d\, [d^{-2}\, e(S)^2 + h]^{1/2}\, \delta p_{eq}(h,S)$, where $\delta p_{eq}(h, S) = p - p_{eq}(h, S)$.

V. Droplet Structure and Evolution

In this section, we consider droplets of a stable phase embedded in a distinct stable or metastable phase. These studies elucidate both the feature of generic two-phase coexistence, as well as nucleation mediated poisoning kinetics.

A. Droplet Analysis of Phase Stability

In **Fig. 9**, we summarize a droplet analysis of phase stability[44] demonstrating generic two-phase coexistence for the QCP with h=0.001 in the regime $p_f = 0.0941 \leq p \leq p_e = 0.0958$.

First, we discuss stability of the vacuum state for h=0.001. In **Fig. 9a**, we show the fate of a large diagonal droplet of occupied sites embedded in the vacuum state for p=0.0950. This droplet quickly converts to a diagonal droplet of the active state. Initially, the sides expand since $p < p_{eq}(S=1)$. Indeed, the initial diagonal shape was chosen to maximize this initial growth rate. However, these faster growing diagonal facets quickly "grow out" converting the droplet to a square shape with horizontal and vertical facets which then shrink since $p > p_{eq}(S=0) = p_{eq}(S=\infty)$. Thus, the active droplet ultimately disappears no matter how large the initial size, showing that the vacuum state is stable for p = 0.0950. In contrast, for $p = 0.0920 < p_f$, such a diagonal active droplet converts to a square shape and thereafter expands since $p < p_{eq}(S=0) = p_{eq}(S=\infty)$, i.e., the vacuum state is not stable. See **Fig. 9b**.

Next, we explore stability of the active state for h=0.001. In **Fig. 9c**, we show the fate of a large square droplet of the vacuum state embedded in a sea of an initially completely populated lattice for p = 0.0950. This surrounding sea quickly converts to the active state. Initially, the droplet sides expand since $p > p_{eq}(S=0) = p_{eq}(S=\infty)$, the initial square shape being chosen to maximize this initial growth rate. However, these faster growing horizontal and vertical facets quickly grow out converting the droplet to a diamond shape with diagonal facets which shrink since $p < p_{eq}(S=1)$. Thus, the vacuum droplet ultimately disappears no matter how large the initial size, showing that the active state is stable for p = 0.0950. In

contrast for p = 0.0970 > p_e, such a square vacuum droplet converts to a diagonal shape and thereafter expands since p > p_{eq}(S=1), i.e., the active state is not stable. See **Fig. 9d**.

The qualitative picture described in detail above for h=0.001 applies for all h>0. Our analysis of droplet evolution also extends to the more general case and corresponds to a kinematic Wulff construction of "growth shapes"[48,49]. The above type of droplet analysis also clarifies the feature that critical value for survival of finite populated regions, $p_f = p_{eq}$(min), is strictly below the critical value for existence for an active state, $p_e = p_{eq}$(max), for h>0, in contrast to the Durrett postulate[29].

B. Critical Droplets: Basic Formulation

The concept of a critical droplet of a stable state embedded within a metastable state is quite general. The idea is that stable droplets which are smaller than some critical size will shrink due their high edge curvature. However, those above the critical size will grow. In the regime $p_e < p < p_{s+}$, nucleation-limited poisoning is controlled by the spontaneous fluctuation-mediated creation of droplets of the vacuum state with the critical size or larger embedded in the metastable active state. Growth of these supercritical droplets will spread the vacuum state across the system.

Since the vacuum state is an absorbing state, fluctuation-mediated evolution to the active state is not possible for any p. However, consider evolution starting from a state with a low density of randomly distributed particles. Then, a type of nucleation-limited evolution to the stable active state should occur for $p_{s-} < p < p_f$ (provided that[31] h>0). This follows since the initial state includes a low concentration of critical and supercritical active droplets

whose growth will spread the active state across the system. As noted in Sec. III B, we expect that $p_{s-} = 0$.

The above observations prompt a detailed analysis of both vacuum and active critical droplets. More precisely, we will define a critical droplet as the smallest droplet of the stable state embedded in the metastable state which is just as likely to grow as to shrink. Thus, a slightly larger droplet is more likely to grow. Three additional comments are appropriate. **(i)** One must sample over all possible droplet shapes for anisotropic systems where critical droplets are not circular. **(ii)** The probabilistic aspect of our definition reflects the feature that the evolution of small droplets is stochastic. Indeed, even droplet survival or disappearance is generally ambiguous (see below). **(iii)** For droplet sizes which are large enough, evolution is however effectively deterministic and the critical size and shape are unambiguous.

To provide insight into critical size behavior, it is instructive to consider first the simpler scenario of reaction model with <u>isotropic</u> interface properties where $p_e = p_f = p_{eq}(S)$ for all S. Here, critical droplets are circular with a critical radius, R_c, determined by the condition that the curved interface must be stationary. We have proposed that the normal velocity of the planar interface, V_0, satisfies $V_0 \propto (a+h)^{1/2}\, \delta p_{eq}$ for small $\delta p_{eq} = p - p_e = p - p_f$ and the kinetic coefficient, ν, satisfies $\nu \sim a+h$ (see Sec.2C and Sec.4A). Then, based on a KPZ formulation (10), the velocity of an interface with non-zero curvature κ, or radius of curvature $R=1/\kappa$, has the form

$$V(R) \approx |V_0| - \nu\cdot\kappa \approx |V_0| - \nu/R, \text{ so that} \tag{17}$$

$$\kappa_c \approx |V_0|/\nu \text{ and } R_c \approx \nu/|V_0| \propto (a+h)^{1/2}/|\delta p_{eq}|. \tag{18}$$

One caveat in the application of this analysis for critical droplets of the vacuum state where $p>p_e$ is that V_0 is strictly not well-defined and must be extracted from studies of transient interface propagation (cf. Sec. IV B). This form (18) of R_c can be confirmed in the isotropic regime of large h based on a mean-field reaction-diffusion equation analysis[3]. However, this variation of R_c with δp_{eq} could be obscured[21,23] for systems where ν and $\tilde{\sigma}_{eff}$ decrease strongly to small values with decreasing δp_{eq}.

Analysis of critical droplets for anisotropic systems, such as the QCP with finite $h \geq 0$, is more complicated. The shape of the critical droplet will not be circular due to anisotropy in both the interface propagation velocity and the interface stiffness. The relationship $\kappa_c \approx |V_0|/\nu$ can still be used to determine the direction dependent κ_c, and thus the shape of the critical cluster: **(i)** For active droplets when $p<p_f$, the smaller $|V_0|$ for S = 0 or ∞ should produce critical clusters which tend to be facetted with smaller κ_c in the horizontal and vertical directions, i.e., square-shaped critical active droplets. This effect should be amplified by the larger $\tilde{\sigma}_{eff}$ and ν for S=0 or ∞ (relative to S=1). **(ii)** For vacuum droplets when $p>p_e$, the effect of the smaller $|V_0|$ for S=1 (relative to other S) should be to produce critical clusters which tend to be facetted with smaller κ_c in the diagonal direction. However, this effect should be offset to some degree by the smaller interface stiffness, $\tilde{\sigma}_{eff}$, and smaller ν, for S=1 (relative to S=0).

Finally, we consider the p-dependence of the critical size. For critical vacuum droplets as $p \to p_{eq}(S=1) = p_e$ from above, the curvature of diagonal edges vanishes which one anticipates will force divergence of the critical droplet size. For critical active droplets as

$p \to p_{eq}(S=0) = p_f$ from below, the curvature of horizontal and vertical edges vanishes which one anticipates will force divergence of the critical droplet size.

C. Critical Droplets: Simulation Results

One can perform conventional constant-p simulations for different initial droplet sizes to assess the survival probability as a function of size, and thereby determine the critical size (for various p)[21,23]. However, simulations using the constant-population ensemble provide a way to more directly or "automatically" assess the critical size[21,41]. Here, one chooses an initial droplet-type configuration and appropriate target concentration, C_t. Constant-population ensemble simulation stabilizes this droplet configuration while allowing conversion to the appropriate critical droplet structure. The simulation outputs the annihilation rate, p, corresponding to the selected critical size. Inverting this data gives critical size versus p. All results shown below are obtained from this approach. One caution is while constant-population ensemble simulations must recover results for constant-p simulations for large systems, our results for small critical sizes use somewhat small systems in order to help stabilize the droplet. As an aside, our critical size analysis provides a third strategy for estimating spinodal point locations from the condition that the critical size should be of order unity at the spinodal. Below R_c will denote a measure of the critical linear size of the generally non-spherical clusters.

First, we present simulation results for the behavior of the critical size of vacuum droplets embedded in the metastable active state in the regime $p_e \le p \le p_{s+}$ for the QCP with $h \ge 0$. As for thermodynamic systems, there is some ambiguity in assessing droplet survival since new droplets of the vacuum state can always be spontaneously nucleated in the

surrounding metastable active state. Results for the variation of the critical linear dimension, R_c, of vacuum droplets with $p>p_e$ are shown in **Fig. 10** for h*=0.001 (so that $h \approx 0.0011$) . Here, the relevant variable is $\delta p_{eq} = \delta p_{eq+} = p - p_e > 0$. Results in the inset to **Fig. 10** are consistent with the dependence $R_c \propto 1/\delta p_{eq+}$. Estimating an effective spinodal point, p_{s+}, from the condition that $R_c = O(1)$ at $p=p_{s+}$, indicates that $p_{s+} \approx 0.103\text{-}0.104$ for h*=0.001. In addition, a similar analyses (not shown) indicates that $p_{s+} \approx 0.102\text{-}0.103$ for h*=h=0, and for h*=0.1 indicates that $p_{s+} \approx 0.152\text{-}0.155$. In the former case, R_c measured as a function of δp_{eq} is essentially identical to results for h*=0.001. These estimates for p_{s+} are consistent with those reported in **Table I** from an analysis of the kinetics in Sec. III B.

Second, we analyze the critical size of active state droplets embedded in the vacuum state when $p \leq p_f$ for the QCP with h>0 (but not with h=0). For h=0, the previously mentioned quirk of the QCP means that droplets never survive[29,30]. For h>0, one can precisely define the critical size of active droplets based on a survival probability of 0.5 since survival of such droplets in a background of an absorbing state is unambiguous[21,23]. This contrasts the case of vacuum droplets described above, and also the traditional case of droplets in thermodynamic systems. Results for the variation of the critical linear dimension, R_c, of active droplets with $p < p_f$ are shown in **Fig. 10** for h*=0.001. Now, the relevant variable is now $\delta p_{eq} = \delta p_{eq-} = p - p_f < 0$ (appropriately modifying the above definition), and again it seems that behavior of R_c is reasonably described by the form $R_c \propto 1/|\delta p_{eq-}|$. However, the average or effective value of ν for active droplets may be different from that for vacuum droplets for the same h. Our results appear consistent with the identification $p_{s-}=0$, as estimated from the condition that $R_c = O(1)$ when $p=p_{s-}$.

Finally, we describe results for the shape and structure of critical droplets derived from the above simulations. **Fig. 11a** shows critical active droplets of ~10^4 populated sites for h*=0.001 and h*=0.1. For small h* or h, the perimeter of the droplet tends to be facetted along horizontal and vertical directions and the effective stiffness of the interface between active and vacuum states is high. This behavior is consistent with our analysis in Sec. V B. For larger h* or h, the cluster is less faceted, and the interface less stiff. **Fig. 11b** shows critical vacuum droplets of ~10^4 empty sites for h*=0, h*=0.01, and h*=0.1. Again the interface at the perimeter of the droplets clearly becomes less stiff with increasing h. Note that the shape of the critical vacuum droplets is much less facetted than that of the active droplets for the same small h*=0.001, again consistent with our analysis in Sec. V B. As noted in Sec. V A, interface stiffness will eventually increase with increasing h, and critical droplets will become circular due to reduced anisotropy.

D. Critical Droplets: Thermodynamic Analogy

The predicted variation of R_c with δp_{eq} from a "kinetic" analysis described in Sec. V B and Sec. V C can also be extracted from a heuristic quasi-thermodynamic analysis[44,54]. For simplicity, we first present this analysis for isotropic systems. One introduces an effective free energy advantage per unit area, δU, for the stable state (relative to the metastable state) which is assumed to satisfy $\delta U \approx A|\delta p_{eq}|$ with $A>0$ at most weakly dependent on h. In addition, one introduces an effective line tension, σ_{eff}, for the interface between active and vacuum states. Then, the effective free energy of a droplet of radius R of the stable state embedded in the metastable state satisfies

$$F(R) = -\pi R^2 \delta U + 2\pi R \sigma_{eff}, \quad (19)$$

and critical droplets correspond to maximizing F. Thus, the critical radius, R_c, and the effective barrier for nucleation of critical droplets, $E_{nuc} = F(R_c)$, satisfy[44,54]

$$R_c = \sigma_{eff}/\delta U = A^{-1}\sigma_{eff}/|\delta p_{eq}| \text{ and } E_{nuc} = \pi(\sigma_{eff})^2/\delta U = \pi A^{-1}(\sigma_{eff})^2/|\delta p_{eq}|, \quad (20)$$

The result for R_c is consistent with the analysis (18) above in Sec. V B provided that $\sigma_{eff} \sim (a+h)^{1/2}$ for large h. The feature that $\sigma_{eff} \sim (a+h)^{1/2}$ is confirmed below, and also highlights an issue raised in Sec. IV B: the effective interface stiffness or line tension, $\tilde{\sigma}_{eff} = \sigma_{eff}$ for an isotropic system (see below), can have different scaling with h than the kinetic coefficient $\nu \propto \Gamma \tilde{\sigma}_{eff} \sim a+ h$. The discrepancy is due to the behavior of the effective mobility $\Gamma_{eff} \sim (a+h)^{1/2}$.

The expression for E_{nuc} allows assessment of the rate, k_{nuc}, for spontaneous nucleation of critical clusters of the vacuum state embedded in the metastable active state assuming the form[25,31] $k_{nuc} \propto \exp(-bE_{nuc})$ for some constant b>0. Comparing this expression for k_{nuc} with the form $k_{nuc} \propto \exp(-c_{nuc}/\delta p_{eq+})$ adopted in Sec. III C for our Avrami analysis of nucleation-mediated poisoning, we conclude that

$$c_{nuc}(h) = \pi b A^{-1}(\sigma_{eff})^2 \sim a+h, \text{ for large h.} \quad (21)$$

The numerical results that $c_{nuc}(h) \approx 0.024$, 0.023, 0.012, 0.021, and 0.048 for h = 0, 0.001, 0.1, 0.2, and 0.4, respectively, indicates that σ_{eff} varies non-monotonically with h.

This thermodynamic analysis of R_c involves the effective line tension, σ_{eff}, of the interface between active and vacuum states, whereas the kinetic analysis in the preceding sections involved the stiffness, $\tilde{\sigma}_{eff}$, through the relation $\nu \propto \Gamma \tilde{\sigma}_{eff}$. For general anisotropic thermodynamic systems, these quantities are related by[51] $\tilde{\sigma}_{eff} = \sigma_{eff} + d^2\sigma_{eff}/d\theta^2$. Thus, $\tilde{\sigma}_{eff}$

and σ_{eff} are equivalent only for isotropic systems, as noted above. If we assume that the same relation applies for anisotropic non-equilibrium systems, then adopting the expression (15) for $\tilde{\sigma}_{eff}(\theta)$, it follows that[52]

$$\sigma_{eff}(\theta) \approx \sigma_1(h) - g(h)[\cos(2\theta)]^2/15, \text{ where } \sigma_1(h) = \tilde{\sigma}_1(h) + 8g(h)/15. \quad (22)$$

Given the reduced amplitude of terms involving the presumed rapidly decreasing function g(h) compared with (12) (cf. Sec. IV B), the non-monotonic variation of σ_{eff} with increasing h should be weaker than the presumed strong non-monotonicity of $\tilde{\sigma}_{eff}$. This is consistent with the numerical results for $c_{nuc}(h)$ presented above.

E. Ginzburg-Landau Type Formulation

Finally, we note that it is possible to provide a solid basis for the above quasi-thermodynamic analysis if one restricts attention to the regime of large h where mean-field description of kinetics and spatiotemporal behavior applies. In this regime, the reaction kinetics can be formulated in terms of a local effective free energy density[3],

$$U(C) = \tfrac{1}{2}\, pC^2 - 1/3\, C^3 + \tfrac{1}{4}\, C^4, \text{ satisfying } R(C) = -d/dC\, U(C), \quad (23)$$

where R(C) is given in (5). U(C) has a double-well form for $0=p_{s-} < p<p_{s+}=1/4$, and the difference in well depths is $\delta U \approx 2/9\, \delta p_{eq}$ for small $\delta p_{eq} = p-p_e = p-2/9$.

Spatiotemporal behavior can be described in terms of an associated Ginzburg-Landau-type effective free energy (or Lyapunov) functional[3],

$$F = \int d\underline{x}\, [U(C(\underline{x})) + \tfrac{1}{2}\, h|\nabla C(\underline{x})|^2] \,. \quad (24)$$

The mean-field reaction diffusion equations for the QCP with large h then take the form of a deterministic Cahn-Allen equation[3,55]. Thus, it is also possible to explicitly evaluate σ_{eff} =

$\tilde{\sigma}_{eff} \propto h^{1/2}$ (independent of θ) from the value (per unit length) of F integrated across an interface between active and vacuum states[55]. In fact, this result follows from a simple scaling analysis noting that the width of the interface scales like $h^{1/2}$, and thus the magnitude of ∇C like $h^{-1/2}$. Consequently, one finds that $R_c = \sigma_{eff}/\delta U \propto h^{1/2}/|\delta p_{eq}|$, a result reported above which can also be obtained from a more direct analysis of the mean-field reaction-diffusion equations[3].

Finally, it should also be noted that stochastic aspects of nucleation mediated poisoning for large h in this regime $2/9 = p_e < p < p_{s+} = ¼$ can be treated within the framework of the appropriate Langevin version of the above reaction-diffusion or Cahn-Allen equation[8,54-56],

$$\partial C/\partial t = -\delta F[C]/\delta C + \zeta = R(C) + h\nabla^2 C + \zeta, \qquad (25)$$

but with non-trivial multiplicative noise[8,55,56], ζ. Here, $\zeta = \zeta_{ac} + \zeta_{diff}$ has contributions from non-conserved particle annihilation-creation noise and conserved particle diffusion noise[55,56]. A detailed analysis will be reported in a separate paper[55].

VI. Conclusions

Our realization of Schloegl's second model for autocatalysis including particle diffusion with hop rate $h \geq 0$ on a square lattice has revealed a non-equilibrium discontinuous phase transition between an active state and an absorbing vacuum state. The critical annihilation rate for existence of an active state, $p_e(h)$, strictly exceeds that for survival of a finite population, $p_f(h)$, for $h>0$ contrasting the postulate of Durrett[29]. This feature is a direct consequence of a dependence on orientation of the annihilation rate $p_{eq}(h, S)$ for equistability of a planar interface separating the active and vacuum states, as previously identified[30,31] for

the case h=0. This orientation-dependence in turn leads to generic two-phase coexistence which is quite distinct from behavior in thermodynamic systems. Nonetheless, one does still find existence of a metastable state just above the discontinuous transition and associated nucleation phenomena exhibiting features quite analogous to discontinuous phase transitions in equilibrium systems.

As noted in Sec. III A, from simulation data alone, we cannot rule out the existence of a critical value, h_c, of h such that $p_e = p_f$ for $h \geq h_c$, i.e., generic two-phase coexistence disappears but the discontinuous transition persists in this regime. However, in our realization of the QCP on a square lattice modified to include spontaneous particle creation[30], and in Toom's noisy North-East-Center voting model[32-35], generic two-phase coexistence does persist until disappearance of the discontinuous transition at a critical point. Also, analysis based on approximate truncation of the exact mater equations[39] for the QCP with $h \geq 0$ indicate that $p_e > p_f$ for all $h < \infty$.

It is natural to ask whether the features displayed by this model apply more broadly for non-equilibrium models displaying discontinuous phase transitions? We do expect that interface orientation dependent propagation and equistability, as well as generic two-phase coexistence, do occur more generally. However, the orientation-dependence may often be very weak and the regime of two-phase coexistence may be narrow and as a consequence difficult to detect[57].

Acknowledgements

This work was supported by the Division of Chemical Sciences and by the SciDAC Computational Chemistry program of the U.S. Department of Energy (Basic Energy

Sciences). It was performed at Ames Laboratory which is operated for the USDOE by Iowa State University under Contract No. DE-AC02-07CH11358.

References

[1] G. Nicolis and I. Prigogine, *Self-Organization in Non-Equilibrium Systems* (Wiley, New York, 1977).
[2] P. Gray and S.K. Scott, *Chemical Oscillations and Instabilities* (Clarendon, Oxford, 1994).
[3] A.S. Mikhailov, *Foundations of Synergetics I* (Springer, Berlin, 1990).
[4] *Chemical Waves and Patterns*, R. Kapral and K. Showalter, ed.s (Kluwer, Amsterdam, 1995).
[5] N.G. Van Kampen, *Stochastic Processes in Physics and Chemistry* (North Holland, Amsterdam, (1981).
[6] A.S. Mikhailov and A.Yu. Loskutov, *Foundations of Synergetics II* (Springer, Berlin, 1996).
[7] J. Garcia-Ojalvo and J.M. Sancho, *Noise in Spatially Extended Systems* (Springer, Berlin, 1999).
[8] M. Hildebrandt, A.S. Mikhailov, and G. Ertl, Phys. Rev. Lett. **81**, 2602 (1998).
[9] D.T. Gillespie and L. Petzold, in *System Modeling in Cellular Biology*, Z. Szallasi et al., ed.s (MIT Press, Cambridge, 2006), p.331.
[10] R. Imbihl, Prog. Surf. Sci. **44**, 185 (1993).
[11] R. Imbihl and G. Ertl, Chem. Rev. **95**, 697 (1995).
[12] Y. Suchorksi, J. Beben, E.W. James, J.W. Evans, and R. Imbihl, Phys. Rev. Lett. **82**, 1907 (1999).
[13] D.-J. Liu and J.W. Evans, J. Phys.: Cond. Matt. **19**, 065129 (2007).
[14] J. Starke, C. Reichert, M. Eiswirth, H.H. Rotermund, and G. Ertl, Europhys. Lett. **73**, 820 (2006).
[15] D. Dab, A. Lawniczak, J.P. Boon and R. Kapral, Phys. Rev. Lett. **64**, 2462 (1990).
[16] J.P. Boon, D. Dab, R. Kapral, and A. Lawniczak, Phys. Rep. **273**, 55 (1996).
[17] J. Marro and R. Dickman, *Nonequilibrium Phase Transitions in Lattice Models* (Cambridge UP, Cambridge, 1999).
[18] H. Hinrichsen, Adv. Phys. **49**, 815 (2000).
[19] G. Odor, Rev. Mod. Phys. **76**, 663 (2004).
[20] R.M. Ziff, E. Gulari, and Y. Barshad, Phys. Rev. Lett. **56**, 2553 (1986).
[21] J.W. Evans and T.R. Ray, Phys. Rev. E, **50**, 4302 (1994).
[22] R. H. Goodman, D. S. Graff, L. M. Sander, P. Leroux-Hugon, and E. Clément Phys. Rev. E **52**, 5904 (1995).
[23] J.W. Evans and M.S. Miesch, Phys. Rev. Lett. **66**, 833 (1991).
[24] E. Loscar and E.V. Albano, Rep. Prog. Phys. **66**, 1343 (2003).
[25] E. Machado, G.M. Buendia, and P.A. Rikvold, Phys. Rev. E **71**, 031603 (2005).
[26] D.-J. Liu and J.W. Evans, Surf. Sci., in press (2009) (Ertl Issue).
[27] F. Schloegl, Z. Phys. **253**, 147 (1972).
[28] P. Grassberger, Z. Phys. B Cond. Matt. **47**, 365 (1982).

[29] R. Durrett, SIAM Rev. **41**, 677 (1999).
[30] D.-J. Liu, X. Guo, and J.W. Evans, Phys. Rev. Lett., **98**, 050601 (2007).
[31] X. Guo, D.-J. Liu, and J.W. Evans, Phys. Rev. E, **75**, 061129 (2007).
[32] C. Bezuidenhout and L. Gray, Ann. Prob. **22**, 1160 (1994).
[33] A.L. Toom, in *Multicomponent Random Systems*, edited by R.L. Dobrushin and Y.G. Sinai (Marcel Dekker, New York, 1980).
[34] C.H. Bennett and G. Grinstein, Phys. Rev. Lett. **55**, 657 (1985).
[35] G. Grinstein, IBM J. Res. Dev. **48**, 5 (2004).
[36] M.A. Munoz, F. de los Santos, and M.M.T. da Gama, Euro. Phys. J. B **43**, 73 (2005).
[37] D. Mollison, J. Roy. Stat. Soc. B, **39**, 283 (1977).
[38] X. Guo, J.W. Evans, and D.-J. Liu, Physica A **387**, 177 (2008).
[39] X. Guo, D.-J. Liu, and J.W. Evans, Physica A, to be submitted (2009).
[40] Interchange the role of particles and empty sites in the QCP [32,33]. Then, one has spontaneous creation of particles at empty sites, and their autocatalytic removal given suitable empty pairs of sites. The former mimics monomer adsorption in the ZGB model, and the latter mimics reactive monomer removal (which requires empty pairs sites to allow dimer adsorption).
[41] R.M. Ziff and B.J. Brosilow, Phys. Rev. A **46**, 4630 (1992).
[42] D.-J. Liu, J. Stat. Phys., submitted (2008).
[43] R.H. Schonmann and S.B. Shlosman, Comm. Math. Phys. **194**, 389 (1998).
[44] S. Shlosman, Physica A **263**, 180 (1999).
[45] S. Friedli and C.-E. Pfister, Phys. Rev. Lett. **92**, 015702 (2004).
[46] P.A. Rikvold, H. Tomita, S. Miyashita, and S.W. Sides, Phys. Rev. E **49**, 5080 (1994). This study described the spinodal associated with an infinite Ising system as the "mean-field spinodal point" (MFSP), although it cannot be assessed with a simple mean-field theory.
[47] M. Avrami, J. Chem. Phys. **7**, 1103 (1939); **8**, 212 (1940); **9**, 177 (1941).
[48] J. Krug and H. Spohn, in *Solids Far from equilibrium: Growth, Morphology and Defects*, C. Godreche ed. (Cambridge UP, Cambridge, 1991).
[49] A.-L. Barabasi and H.E. Stanley, *Fractal Concepts in Surface Growth* (Cambridge UP, Cambridge, 1995).
[50] For a planar interface with small slope $\partial y/\partial x$ measured relative to S=1, the normal velocity is denoted $V(S=1+\partial h/\partial x)$. By a Pythagorean construction, the velocity in the y-direction is $\partial y/\partial t = V(S=1+\partial h/\partial x)[1+(\partial h/\partial x)^2]^{1/2} \approx V_0 + \delta V + 1/2\ V_0\ (\partial h/\partial x)^2$, where $V_0 = V(S=1)$, and $\delta V = V(S=1+\partial h/\partial x) - V(S=1) \approx C(\partial h/\partial x)^2$ (Ref. 31). Thus, one has $\lambda = 2C + V_0$.
[51] H.-C. Jeong and E.D. Williams, Surf. Sci. Rep. **34**, 171 (1999).
[52] Writing $\widetilde{\sigma}_{eff}(\theta) \approx \sigma_{av}(h) + f(h)\cos(4\theta)$, it follows that $\sigma_{eff}(\theta) \approx \sigma_{av}(h) - f(h)\cos(4\theta)/15$. These identities are equivalent to (15) and (22) noting that $\widetilde{\sigma}_1(h) = \sigma_{av}(h) - f(h)$ and $g(h) = 2f(h)$.
[53] An increasing number of vacuum clusters which nucleate just ahead of the interface can be incorporated into the advancing interface as time progresses corrupting estimation of V.
[54] J.D. Gunton and M. Droz, *Introduction to the Theory of Metastable and Unstable States*, Springer Lecture Notes in Physics Vol. 183 (Springer, Berlin, 1983).
[55] A. Matzavinos, X. Guo, D.-J. Liu, and J.W. Evans, to be submitted (2009). Here, $\zeta_{ac} \propto C^{1/2}(p+C-C^2)^{1/2}\xi_{ac}$ is the non-conserved particle annihilation-creation noise, and

$\zeta_{diff} \propto \nabla[h^{1/2}C^{1/2}(1-C)^{1/2}\xi_{diff}]$ is the conserved particle diffusion noise. ξ_{ac} and ξ_{diff} are independent white noises.

[56] M. Hildebrand and A.S. Mikhailov, J. Phys. Chem. **100**, 19089 (1996).
[57] D.-J. Liu and J.W. Evans., to be submitted (2009).

Table I. KMC simulation results for the QCP with particle hopping for the annihilation rates corresponding to equistability of horizontal or vertical interfaces, peq(S=0 or ∞) = pf, and for diagonal interfaces, peq(S=1) = pe, between active and vacuum states, and for the upper spinodal, ps+. Note that Δpeq = pe-pf < 0.0001 for h ≥0.02 and Δps+ = ps+-pe varies non-monotonically.

	p_f	p_e	Δp_{eq}	p_{s+}	Δp_{s+}		$p_f \approx p_e$	p_{s+}	Δp_{s+}
h=0	0.0869	0.0944	0.0075	0.101	0.007	h=0.02	0.1145	0.120	0.005
h=0.001	0.0941	0.0958	0.0017	0.102	0.006	h=0.05	0.1304	0.135	0.005
h=0.002	0.0962	0.0973	0.0011	0.103	0.006	h=0.2	0.1650	0.170	0.005
h=0.005	0. 1006	0.1010	0.0004	0.107	0.006	h=0.5	0.1863	0.193	0.007
h=0.01	0.1061	0.1062	0.0001	0.111	0.005	h=1	0.1990	0.208	0.009
						h=4	0.2150	0.227	0.012
						h=∞	0.2222	0.250	0.028

Figures

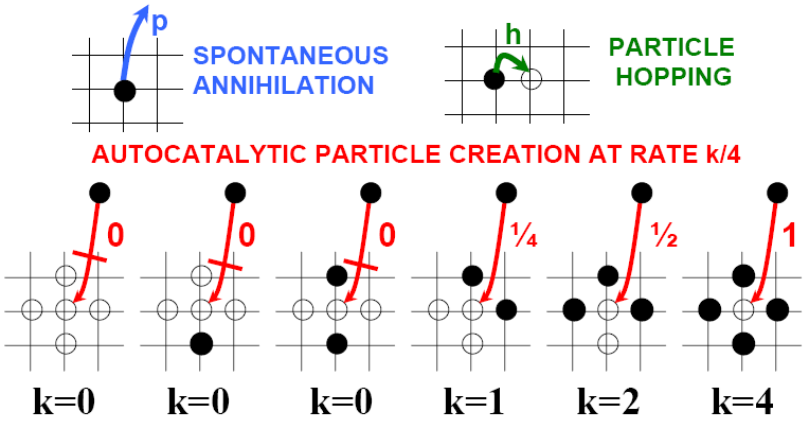

Figure 1. Schematic of particle annihilation, autocatalytic creation, and hopping processes in Schloegl's second model or the QCP on a square lattice. Here particles are denoted by filled circles (•) and empty sites by open circles (o). Rates for the various processes are also indicated, and the bar through the arrow indicates that the process is not allowed.

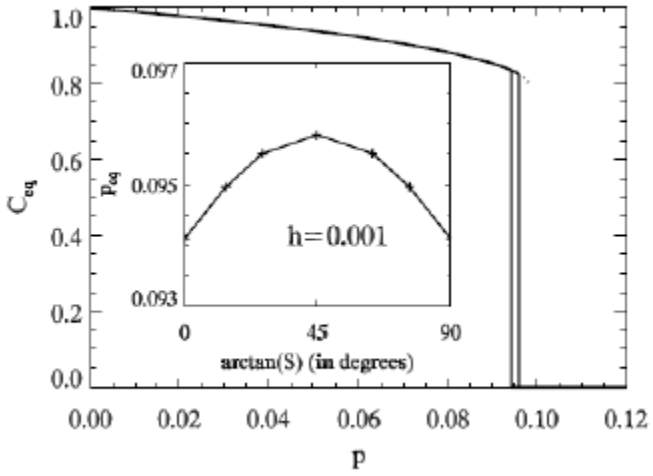

Figure 2. Steady-state concentration, C_{eq}, versus particle annihilation rate, p, in the QCP with h=0.001. The vertical lines indicate $p = p_f = 0.0941$ and $p = p_e = 0.0958$ bordering the regime of generic two-phase coexistence for h=0.001. The dotted line indicates the metastable active state. Inset: Dependence of annihilation rate, $p_{eq}(S)$, for interface equistability on interface slope, S, for h=0.001.

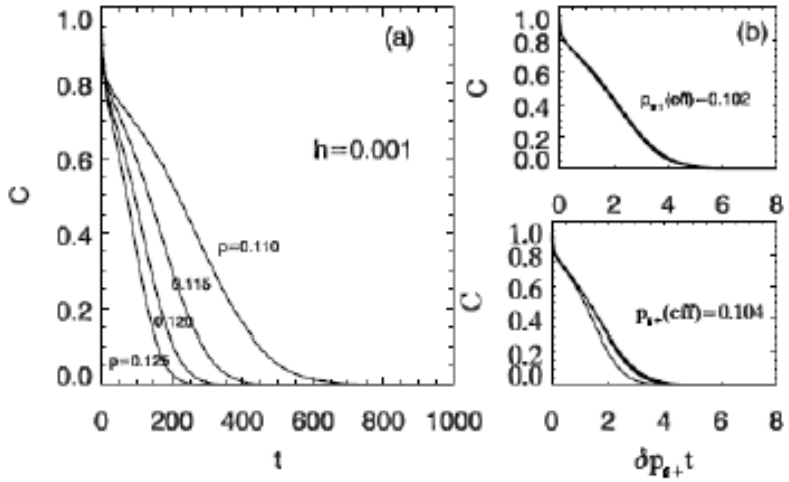

Figure 3. KMC simulation results for evolution of the particle concentration in the QCP with h=0.001: (a) C(t) versus time, t, for evolution from a completely populated lattice (C=1) to the vacuum state (C=0) for various annihilation rates, p (shown), above the effective upper spinodal, p_{s+}; (b) C(t) versus scaled time, $\delta p_{s+} t$, where $\delta p_{s+} = p - p_{s+}$ for the optimum choice of $p_{s+} = 0.102$ to achieve collapse; (c) C(t) versus scaled time, $\delta p_{s+} t$, for a less than optimum $p_{s+}=0.104$.

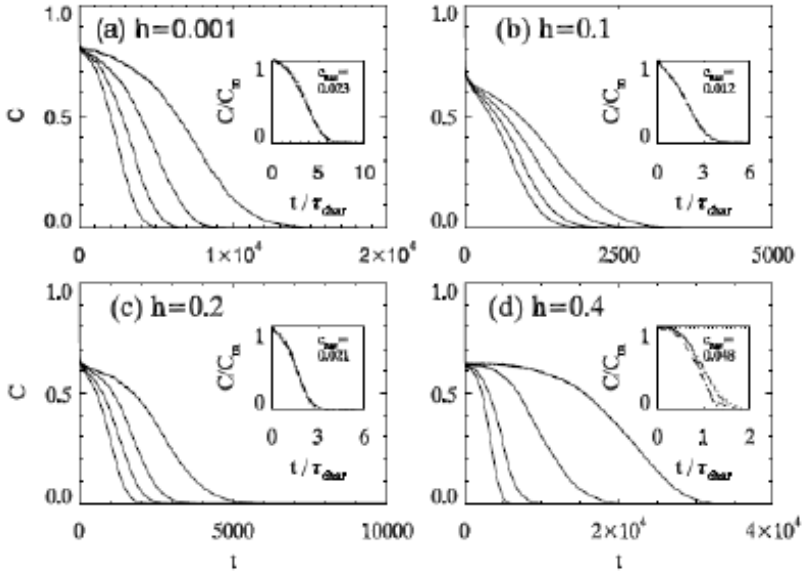

Figure 4. Nucleation-mediated poisoning kinetics for $p_e < p < p_{s+}$. Results are shown for h=0.001 (a), 0.1 (b), 0.2 (c), and 0.4 (d). In all cases, we consider four values of p corresponding to $\delta p_{eq+} = p - p_e = 0.0031 + 0.0005$ m, with m = 0, 1, 2, and 3. We show both the 'raw' kinetics $C(t)/C_m$ versus t in the main plot, where the curve with the most (least) rapid decay corresponds to the largest (smallest) p and δp_{eq+}. The insets show the optimum collapsed curves leading to estimates of $c_{nuc}(h)$, as described in the text.

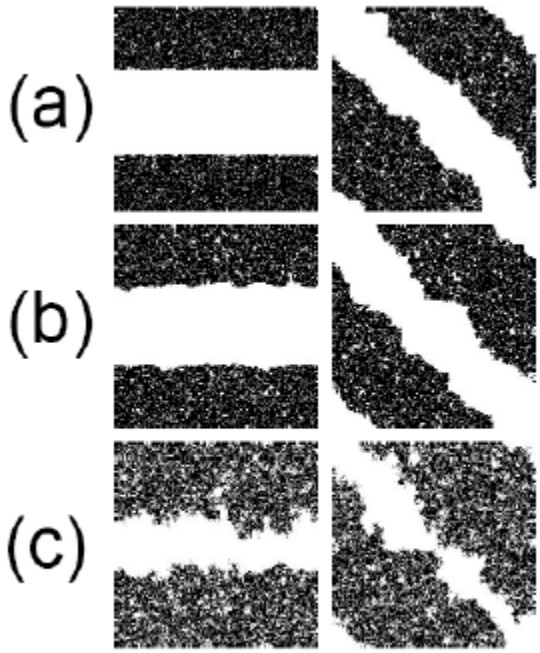

Figure 5. Structure of interfaces between the active state and poisoned state at equistability. Particles are black and empty sites are white (so the poisoned vacuum state is completely white). Left column: S=0. Right column: S=1. Top (a), middle (b), and bottom (c) frames correspond to h*=0, h*=0.001, and h*=0.1, respectively. System size is 256×256 sites.

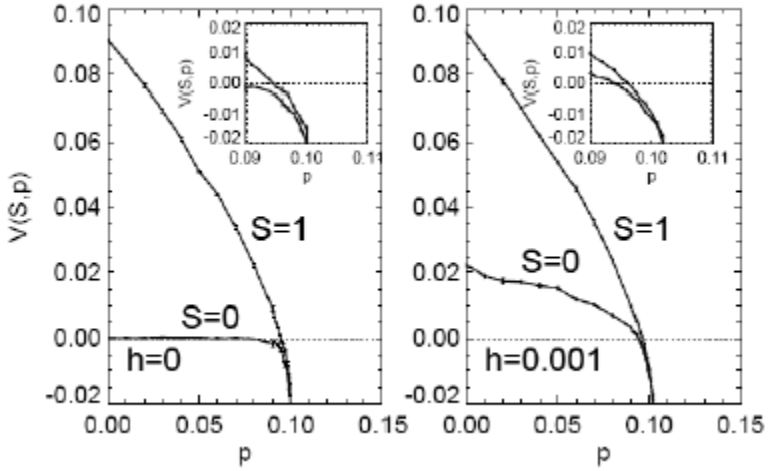

Figure 6. KMC simulation results for V(p, h, S=1) and V(p, h, S=0 or ∞) versus p for the QCP with: (a) h=0; and (b) h=0.001. Insets show behavior close to the upper spinodal point p_{s+} ≈0.101 (0.102) for h=0 (0.001). Note that the p-value where V(p, h, S=1) = 0 corresponds to p = p_e(h) where p_e = 0.0944 for h=0, and p_e = 0.0958 for h=0.001.

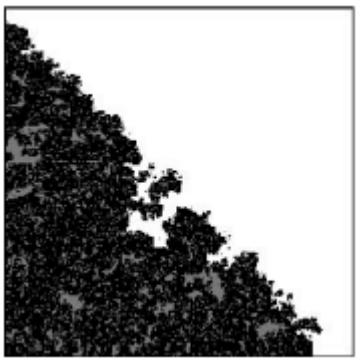

Figure 7. KMC simulation image of interface propagation of the vacuum state (upper right) into the active state (lower left) for h=0 and p=0.100 (above p_e = 0.0944 and close to p_{s+} ≈ 0.101). Image size: 256×256 sites. The image was taken ~800 Monte Carlo steps after the initiation of propagation from a straight interface separating completely filled and empty regions. The image distinguishes empty sites within and connected to the vacuum state (white) from disconnected empty sites and clusters interior to the active state (grey). Occupied sites are black. Note that spontaneous nucleation of the vacuum state occurs within the active state, so that the interior (grey) vacuum clusters grow in time.

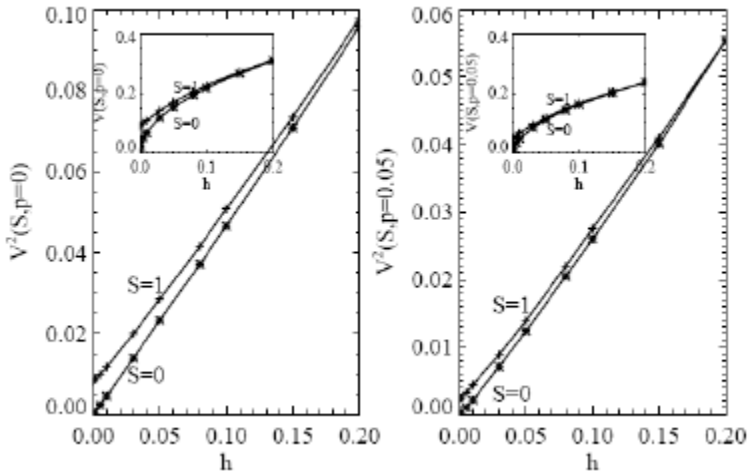

Figure 8. KMC simulation results for the square of the propagation velocities, V(p, h, S=1) (upper curve) and V(p, h, S=0) (lower curve) versus h for planar interfaces separating active and vacuum states. Insets show V(p, h, S) versus h. Left frame (a): p=0. Right frame (b): p=0.05.

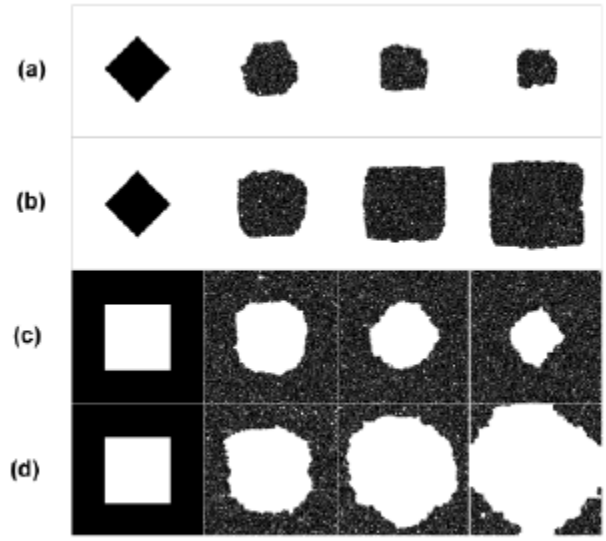

Figure 9. KMC simulations of droplet evolution for the QCP with h=0.001. Evolution of an initially diamond-shaped filled droplet (embedded in the vacuum state) quickly converting to an active droplet and: (a) shrinking for p=0.0950 within the two-phase coexistence (2PC) region; (b) growing for p=0.0920 below the 2PC region. Evolution of an initially square-shaped vacuum droplet (embedded in the completely occupied state which quickly converts to the active state) and: (c) shrinking for p=0.0950 within the 2PC region; and (d) growing for p=0.0970 above the 2PC region. Initial occupied droplet sizes are $128\sqrt{2}\times128\sqrt{2}$ sites in (a) and (b). Initial vacuum droplet sizes are 256×256 sites in (c) and (d). Images are shown at 0, ~8000, ~24000, and ~40000 Monte Carlo steps. In all cases, occupied sites are black and empty sites are white.

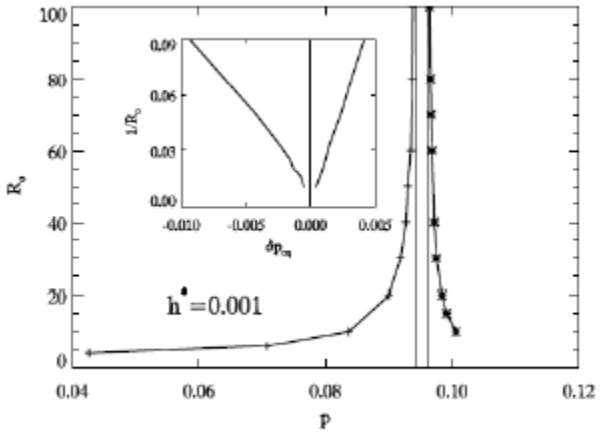

Figure 10. Critical linear size, R_c, in lattice constants for the QCP with h*=0.001 for vacuum droplets versus $p > p_e = 0.0959$ (right portion of plot), and for droplets of the active state versus $p < p_f = 0.0943$ (left portion of plot). Vertical lines indicate p_f and p_e. Insets: $1/R_c$ versus $\delta p_{eq} = p - p_f$ (left portion) or $p - p_e$ (right portion) revealing near-linear proportionality. Here R_c was determined in a simple fashion, e.g., by identifying $(R_c)^2$ as the number of occupied sites for active droplets.

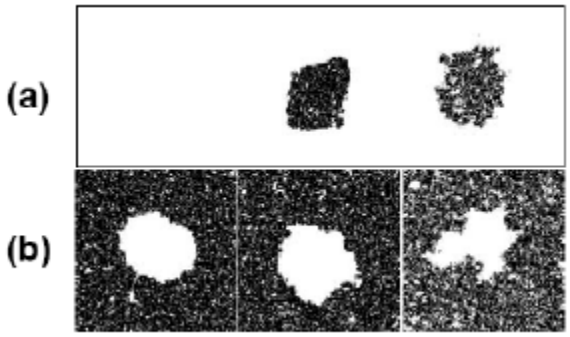

Figure 11. (a) Critical droplets of the active state of ~10^4 populated sites for the QCP with h*=0.001 and p = 0.0938 so $\delta p_{eq} = -0.0005$ (middle), and for h*=0.1 and p=0.1506 so $\delta p_{eq} = -0.0003$ since $p_f \approx 0.1509$ (right). Note the somewhat facetted square shape for h*=0.001. (b) Critical vacuum droplets of ~10^4 empty sites for h*=0 and p = 0.0948 so $\delta p_{eq} = 0.0004$ (left), h*=0.001 and p = 0.0964 so $\delta p_{eq} = 0.0005$ (middle), and h*=0.1 and p = 0.1514 so $\delta p_{eq} = 0.0005$ since $p_e \approx 0.1509$ (right). In all cases, occupied sites are black and empty sites are white.

CHAPTER 5. METASTABILITY IN SCHLOEGL'S SECOND MODEL FOR AUTOCATALYSIS: LATTICE-GAS REALIZATION WITH PARTICLE DIFFUSION

Xiaofang Guo and J.W. Evans

Ames Laboratory – USDOE and Department of Mathematics,

Iowa State University, Ames, Iowa 50011

Abstract

We analyze metastability associated with a discontinuous non-equilibrium phase transition in a stochastic lattice-gas realization of Schloegl's second model for autocatalysis. This realization involves spontaneous annihilation, autocatalytic creation, and diffusion of particles on a square lattice, where creation at empty sites requires an adjacent diagonal pair of particles. This model, also known as the Quadratic Contact Process, exhibits discontinuous transition between a populated active state and a particle-free "vacuum" poisoned state, as well as generic two-phase coexistence. The poisoned state exists for all annihilation rates $p>0$ and is an absorbing state in the sense of Markov processes. The active or reactive steady state exists just for p below a critical value, p_e, but a metastable extension appears for a range of higher p up to an effective upper spinodal point, p_{s+}. We assess the location of p_{s+} (above p_e) and by characterizing associated poisoning kinetics and interface propagation behavior for various hop rates.

PACS Numbers: 05.70.Fh, 02.50.Ey, 05.50.+q, 05.70.Ln

1. Introduction

There has been long-standing interest in discontinuous equilibrium phase transitions in thermodynamic systems, and particularly in associated metastability and nucleation phenomena [1,2]. For example, in the mean-field van der Waals description of a fluid below the critical temperature for phase separation, the low-density (high-density) metastable state exists for pressures above (below) the equistability pressure, determined by the Maxwell construction, up to a well-defined upper (lower) spinodal point [3]. However, in contrast, statistical mechanical analyses indicate a dependence of spinodal behavior on system size [1,2]. Furthermore, for the equilibrium Ising model for an infinite system [4-6], it has been shown that there not exist a unique analytic metastable extension of the active state steady state. It is possible to generate a family of C^{∞} metastable extensions by running the dynamics from a suitable initial state for a period of time increasing exponentially with the distance from the transition point [4-6]. However, this family of extensions does not provide much insight into the location of the effective spinodal point for an infinite system, and in fact there is no natural unique definition.

Non-equilibrium systems actually provide a richer variety of non-equilibrium phase transition or bifurcation behavior [7,8]. Bistability of steady states is the analogue of phase separation in the van der Waals model, its disappearance at a cusp bifurcation being the non-equilibrium analogous of a critical point [8,9]. A natural goal is to advance beyond mean-field-level to statistical mechanical analyses. Recent studies of non-equilibrium phase transitions in lattice-gas models have focused on universality in continuous transitions [10-12]. However, increasing attention is being paid to analysis of various phenomena in

reaction-diffusion type models exhibiting discontinuous transitions: propagation and fluctuation behavior of interfaces between active and poisoned states [13-18]; epidemic properties of an active droplet embedded in the poisoned state [19,20]; and nucleation of droplets within the metastable active state [14,18,21].

It is well recognized that reaction-diffusion models with discontinuous transitions exhibit metastability [9]. However, just as for equilibrium systems, one does not expect the existence of a unique analytic extension of stable states beyond transition points, and thus one does not expect spinodal points to be uniquely or well-defined for infinite systems [24,25]. Nonetheless, the concept of a spinodal provides a valuable tool for interpretation of model dynamics, so further analysis is appropriate. Interestingly, for non-equilibrium systems, there exist both additional challenges and advantages relative to equilibrium systems. The challenge derives from the feature that there does not exist a thermodynamic framework for analysis of these systems, e.g., critical droplets within the metastable state cannot be describe in terms of a free energy functional [1]. On the other hand, for models exhibiting mean-field bistability, one can recover true bistability in the statistical mechanical model in the regime of rapid particle hopping [9,22], in which case spinodal points are well-defined.

In this study, we consider Schloegl's second model for autocatalysis in a reactive system of particles, X, which traditionally includes the following mechanistic steps [8,16-18,23-27]:

$$X \rightarrow \varnothing \text{ (spontaneous annihilation)}, \quad 2X \rightarrow 3X \text{ (autocatalytic creation)}, \tag{1}$$

and possibly particle diffusion. Annihilation occurs at rate p, and autocatalytic creation occurring at a suitably prescribed rate requires existing nearby pairs of particles. The most general formulation also includes spontaneous creation $\varnothing \rightarrow X$, but this process is excluded in our study. Traditional off-lattice formulations also include the autocatalytic annihilation process $3X \rightarrow 2X$ in order to avoid population explosion [8,23]. However, in lattice formulations, autocatalytic particle creation requires an empty site $\varnothing$, and is thus more accurately represented as $2X+\varnothing \rightarrow 3X$ [16-18,26,27]. This empty site requirement automatically limits population growth.

Both off-lattice and lattice formulations display cubic mean-field kinetics, i.e., the rate of change of particle concentration is a cubic function of concentration, C [8,18,23,27]. Upon increasing the annihilation rate p, there is a bifurcation in the steady-states from bistability (where a stable active steady state with finite population $C>0$ coexists with the stable $C=0$ vacuum state) to monostability (where the vacuum state is the unique stable steady state) [18]. In this contribution, we will restrict our attention to a specific realization Schloegl's second model on a square lattice, also known as the Quadratic Contact Process (QCP) [16-18,27], which displays a discontinuous transition from an active state to the vacuum state when p exceeds p_e. One also finds evidence for a metastable extension of the active steady state into a regime $p_e \leq p \leq p_{s+}$, where, p_{s+} denotes an effective upper spinodal point of central interest in this study. Our interest here is exclusively in behavior in the limit of infinite system size, rather than considering finite systems where a variety of approaches to defining spinodals have been considered [1,28].

In Sec.2, we describe in detail the realization of the QCP analyzed in this paper, as well as presenting the hierarchical form of the exact master equations for this model. In

Sec.3, we present simulation results for "moderate" hop rate for poisoning kinetics in the vicinity of the effective spinodal point. Next, in Sec.4, we present an analysis of model behavior within the pair-approximation to the exact master equations. This actually facilitates interpretation of the simulation results. Finally, in Sec.5, we present a coarse-grained continuum Langevin reaction-diffusion equations describing the model, but based on the pair-approximation rather than a traditional mean-field site-approximation. Conclusions are provided in Sec.6.

2. Model Specification and Master Equations

Our realization Schloegl's second model, or equivalently of the QCP, on a square lattice as a stochastic Markov process involves the following components [26-18,27]: **(i)** particle annihilation occurring randomly at rate p; **(ii)** particle creation at empty sites requiring one or more diagonally adjacent pairs of occupied sites; specifically, the creation rate is given by k/4, where k is the number of adjacent diagonal occupied pairs and thus can take the values k = 0, 1, 2, or 4; **(iii)** hopping of particles to any adjacent empty sites at rate h (per target site). **Fig.1** provides a schematic of these processes. Again C denotes the particle concentration, i.e., the fraction of filled sites. For any p>0, the "vacuum state" with C=0 corresponds to an absorbing steady state from which the system cannot escape. However, there also exists an active or reactive steady-state with $C=C_{eq}(p)>0$ for $0<p\le p_e$. Indeed, for $p<<1$, the lattice is almost completely populated with $C_{eq}(p) = 1-p + O(p^2)$ independent of h.

While kinetic Monte Carlo (KMC) simulation will be utilized below to provide precise results for the evolution of C, it is instructive to present the exact master equations for the QCP with $h\ge 0$ in the form of an infinite coupled hierarchy. It will be instructive to

explore the predictions of truncation approximations to these equations. Here, we only present the main results. For details of the formulation, see Ref. [29] which analyzed the QCP with h=0.

First, consider spatially homogeneous states of the QCP with h≥0 on an infinite square lattice. We let "x" denote an occupied site and "o" an empty site. Then, P[x] = C denotes the probability of a occupied site, P[o] = 1-C the probability of an empty site, P[x x] the probability of an adjacent occupied pair, P[o o] the probability of an adjacent empty pair, etc.. Conservation of probability ensures that all configurational probabilities can be written as combinations of such probabilities for configurations with just empty sites, e.g., P[x] = 1 - P[o], P[x o] = P[o] - P[o o], P[xx] = 1-2P[o]+P[oo], etc. [30], or instead with just occupied-site configurations. For the QCP, we favor empty site configurations when developing the master equations. A similar situation applies for models which just include irreversible cooperative creation of particles and no annihilation or hopping, usually referred to as "cooperative sequential adsorption" models [30]. The exact form of the first two such hierarchical master equations in an infinite coupled set becomes

$$d/dt\ P[o] = p\ P[x] - P\begin{bmatrix} x & \\ o & x \end{bmatrix}, \quad \text{and} \tag{2a}$$

$$d/dt\ P[o\ \ o] = 2p\ P[o\ \ x] - P\begin{bmatrix} & x & \\ x & o & o \\ & & \end{bmatrix} + 2h\ P[o\ \ -\ \ o] + 4h\ P\begin{bmatrix} o & \\ - & o \end{bmatrix} - 6h\ P[o\ \ o]. \tag{2b}$$

The first gain term in (1a,b) corresponds to particle annihilation, the second loss term to autocatalytic creation, and the last three terms in the P[o o]-equation to particle hopping. Particle hopping terms are absent in the P[o]-equation since hopping preserves particle number. The autocatalytic creation terms equations are obtained by exact reduction of

contributions from multiple configurations after exploiting the specific form of the creation rates [29]. The hopping terms incorporate an exact simplification applicable for particle hopping with simple site exclusion [31]. We also exploited rotational symmetries to identify equivalent contributions.

For a more complete analysis of model behavior, one can extend the above hierarchical master equations to consider spatially non-uniform or inhomogeneous states in an infinite system [29]. In particular, one can use these generalized equations to analyze the propagation of planar interfaces separating vacuum and active states for various slopes, S, to determine annihilation rates, $p=p_{eq}(S)$, corresponding to stationarity of these interfaces.

To this end, we introduce location-dependent probabilities for specific configurations of sites, e.g., $P[o_{i,j}]$ for the probability that site (i,j) is empty, $P[o_{i,j}\ o_{i+1,j}]$ for the probability that the adjacent pair of sites (i,j) and (i+1,j) are both empty, an analogous quantity for the probability of a vertical pair of empty sites, etc.. Then, the first two equations in the exact set of hierarchical master equations describing the evolution of these quantities have the form

$$d/dt\ P[o_{i,j}] = p\ P[x_{i,j}] - \frac{1}{4} P\begin{bmatrix} x_{i,j+1} & \\ o_{i,j} & x_{i+1,j} \end{bmatrix} - \ldots$$

$$+ h\,(P[o_{i+1,j}] + P[o_{i-1,j}] + P[o_{i,j+1}] + P[o_{i,j-1}] - 4P[[o_{i,j}]\ ), \qquad (3a)$$

$$d/dt\ P[o_{i,j}\quad o_{i+1,j}] = p\ P[o_{i,j}\quad x_{i+1,j}] + p\ P[x_{i,j}\quad o_{i+1,j}] - \frac{1}{4} P\begin{bmatrix} & x_{i,j+1} & \\ x_{i-1,j} & o_{i,j} & o_{i+1,j} \\ & & \end{bmatrix} - \ldots$$

$$+ h\,(P[o_{i-1,j}\quad -\quad o_{i+1,j}] + P\begin{bmatrix} o_{i,j+1} & \\ - & o_{i+1,j} \end{bmatrix} + \ldots - 6\,P[o_{i,j}\quad o_{i+1,j}]\ ). \qquad (3b)$$

See Ref.[29], which treats the QCP with h=0, for the complete set of autocatalytic particle creation terms. For the QCP with h>0, additional terms corresponding to hopping in both the $P[o_{i,j}]$ and $P[o_{i,j}\ o_{i+1,j}]$ equations have been simplified by exact reduction [31,32]. For vertical interfaces, $S=\infty$, probabilities are independent of j leading to significant simplification of (3); a different simplification applies for diagonal interfaces with slope S=1 (cf. Ref.[29]).

In the regime $h\to\infty$ where the system is well-stirred, all multi-site configuration probabilities factorize in terms of single-site probabilities. This implies that behavior is described exactly as $h\to\infty$ by the mean-field reaction-diffusion equation [18,27]

$$dC/dt = R(C) + D\,\nabla^2 C \qquad (4)$$

with cubic mean-field kinetics $R(C) = -pC + C^2(1-C)$, and where $D=a^2\,h$ denotes the diffusion coefficient for lattice constant 'a'. One finds a stable active steady state satisfying $p=C(1-C)$, so that $C_{eq} = \frac{1}{2} + \frac{1}{2}(1-4p)^{1/2}$ for $0 \le p \le p_{s+}$, as well as a stable vacuum steady-state C=0. Here, p_{s+} denotes the (mean-field) upper spinodal. Note that one can write

$$R(C) = -d/dC\ U(C) \text{ with } U(C) = \tfrac{1}{2}\,pC^2 - 1/3\,C^3 + \tfrac{1}{4}\,C^4. \qquad (5)$$

The effective free energy density, U(C), has a double-well form for $0 \le p < p_{s+} = \frac{1}{4}$, and reduces to $U(C) = \frac{1}{4}\,C^2(2/3 - C)^2$ at equistability $p = p_e = 2/9$ with equal well heights [18,27]. Correspondingly, the velocity with which the active state displaces the vacuum state in the bistable region satisfies $V(p) \propto D^{1/2}[3(1-4p)^{1/2} - 1]$ for $0 \le p \le p_{s+} = \frac{1}{4}$ and vanishes at $p = p_e = 2/9$ [3,18].

3. Simulation Results: Spinodal Points; Poisoning Kinetics; Interface Propagation

We perform conventional KMC simulations to determine the poisoning kinetics for our realization of Schloegl's model. In these simulations, processes are implemented with probabilities in proportion to the physical rates. Simulations become less efficient for increasing h, as most time is spent on hopping of a high concentration of mobile particles. This scenario applies for both idealized and realistic atomistic models of reaction-limited models.

Of particular interest in this study is the poisoning kinetics of the QCP for moderate hop rate h for $p>p_e$ and specifically around the effective spinodal point. As $p>p_e$ increases, one should find a transition from slow poisoning mediated by nucleation and growth of supercritical vacuum droplets to a faster poisoning associated with spinodal decomposition [17,18]. Thus, direct inspection of simulation images for various p should give some insight into the spinodal location. Previous simulation studies have determined the variation with h of the annihilation rate, $p_e = p_e(h)$, below which a stable active steady state exists [18]. In addition, these studies determine a distinct annihilation rate, $p_f = p_f(h)$, such that $p_f < p_e$ and both active and vacuum states are stable against local perturbations by the other state in the regime $p_f < p < p_e$, i.e., the model exhibits generic two-phase coexistence [16-18]. Specifically, these simulations have shown that $p_e = 0.0944$, 0.1967, 0.2150, and $0.2222^{\bullet}$ for h=0, 1, 4, and ∞ [18]. See **Table I**. In addition, the width of the generic two-phase coexistence region satisfies $p_e - p_f = 0.0075$ for h=0+, quickly decreasing to $p_e - p_f < 0.0001$ for $h \geq 0.02$ [18].

In **Fig.2**, we show evolution in the QCP with h=1 from a completely filled lattice for various $p>p_e(h=1) \approx 0.197$. In **Fig.2a-b** for $p \leq 0.210$, it is clear that poisoning occurs via nucleation and growth of vacuum droplets. However, as p increases to 0.214, **Fig.2c-e** suggest a transition in the mechanism of poisoning. Tentatively, we assign an effective spinodal point of $p_{s+}(h=1) \approx 0.213$. In **Fig.3**, we show the analogous evolution for the QCP with h=4 for various $p>p_e(h=4) \approx 0.215$. **Fig.3a-b** for $p \leq 0.234$ reveal nucleation-mediated poisoning, but **Fig.3c-e** suggest a transition to a different mechanism for higher p. Tentatively, we assign an effective spinodal point of $p_{s+}(h=4) \approx 0.236$. See **Table I**.

A more detailed characterization of nucleation-mediated poisoning for $p_e < p < p_{s+}$ is possible utilizing concepts from Avrami theory [33] combined with recent postulates for the nucleation rate in these non-equilibrium systems [17,18,21]. We propose that the nucleation rate for supercritical droplets of the vacuum state has the form $k_{nuc} \propto \exp(-c_{nuc}/\delta p_e)$, where $\delta p_e = p-p_e$, and that thereafter these droplets grow with a velocity scaling like $V_{grow} \propto \delta p_e$. Then, nucleation kinetics is controlled by a characteristic time $\tau_{nuc} \propto (V_{grow})^{-2/3}(k_{nuc})^{-1/3}$. Specifically, after a transient where the concentration reaches a metastable state value C_m, one has that [33]

$$C(t)/C_m \approx \exp[-A(t/\tau_{nuc})^3] \text{ choosing } \tau_{nuc} = (\delta p_e)^{-2/3} \exp[c_{nuc}/(3\delta p_e)]. \quad (6)$$

Fig.4 confirms this behavior for nucleation-mediated poisoning kinetics for the QCP with h=1 for p=0.208-0.211 above $p_e(h=1)=0.197$ and below $p_{s+}(h=1) \approx 0.213$. We extract an estimate of $c_{nuc}(h=1) \approx 0.14$-$0.15$ which reflects the magnitude of the effective barrier for nucleation of supercritical vacuum droplets [18]. Note that significantly smaller values of c_{nuc} were obtained previously for h=0 – 0.4 [18]. We have performed a similar analysis of

nucleation-mediated poisoning kinetics with h=4 for p=0.233-0.235 above $p_e(h=1)=0.215$ and below $p_{s+}(h=1) \approx 0.236$. As expected [18], we extract an even higher estimate of $c_{nuc}(h=4) \approx 0.36\text{-}0.37$.

Another strategy to assess the location of effective spinodal point is based on the idea that the rate of rapid poisoning in the regime $p>p_{s+}$ should depend primarily on the distance, $\delta p_{s+} = p-p_{s+} >0$, above an effective spinodal. Specifically, C should have the form $C \approx c(\delta p_{s+} t)$, so that curves for C versus $\delta p_{s+} t$ for different p should collapse for the appropriate choice of p_{s+} [14,17,18]. Application of this idea requires selection a suitable regime $p_{min} < p < p_{max}$ in which to analyze the kinetics. In fact, we choose two different regimes for higher or lower $\Delta = p_{min} - p_{s+}$ based on the above estimates of p_{s+} to assess the dependence of our new estimates of p_{s+} on Δ. **Fig.5a** shows poisoning kinetics in the QCP for h=1 for a range of p=0.220-0.235 ($\Delta \approx 0.007$) above $p_e(h=1)=0.197$ suggesting $p_{s+}(h=1) = 0.207\text{-}0.208$, but **Fig.5b** for p=0.215-0.225 ($\Delta \approx 0.002$) suggests that $p_{s+}(h=1) = 0.209\text{-}0.210$. A similar analysis of poisoning kinetics in the QCP for h=4 for a range of p=0.245-0.270 ($\Delta \approx 0.009$) above $p_e(h=4)=0.215$ suggesting $p_{s+}(h=4) = 0.226\text{-}0.227$, but for p=0.240-0.260 ($\Delta \approx 0.004$) suggests that $p_{s+}(h=4) = 0.228\text{-}0.229$. Thus, the estimate of p_{s+} appears to increase as Δ becomes smaller. In Sec.4, with the aid of the analytic pair-approximation for model kinetics, we will discuss how to obtain a refined estimate of p_{s+} accounting for this dependence on Δ.

As an aside, we remark that for h=0 where previous studies have indicated very weak metastability, inspection of images of evolution during poisoning does not reveal such a clear distinction between nucleation-mediated poisoning and spinodal decomposition. See **Fig.6**. Analysis of rapid poisoning kinetics for $p>p_{s+}$ suggests that perhaps $p_{s+} = 0.100\text{-}0.101$.

Finally, we comment on another strategy to provide insight into the effective p_{s+}. This is motivated by the observation that mean-field results suggest that the velocity of propagation, $V(p)<0$, of the vacuum state displacing the metastable active state for $p>p_e$ might have unusual behavior approaching p_{s+}. One complication is that such propagation is transient as the metastable active state eventually poisons. This becomes more problematic for p approaching p_{s+} where spontaneous nucleation of the vacuum state becomes more facile. To partly ameliorate this problem, we previously adopted a percolation-theoretic approach defining the interface as empty sites with filled neighbors connected to the bulk vacuum state. This allowed us to ignore possibly large droplets of the vacuum state nucleated ahead of the front in the metastable active state. However, eventually the vacuum droplets embedded in the active state percolate causing an artificial divergence of the interface velocity.

To avoid this complication, here we adopt a different simpler definition of the interface as well as its location and thus velocity. We initialize the (large finite) system with a sharp interface separating the vacuum state on one side and a completely filled lattice on the other. Then, we determine the subsequent mean location of this interface by matching to that of a reference sharp interface with the vacuum state on one side and a uniform state on the other which poisons starting from an initially completely filled state. See the schematic **Fig.7**. This strategy gives a well-defined interface location even for $p>p_{s+}$ where the non-vacuum state poisons rapidly. To interpret simulation results, two observations should be made regarding this definition of interface location and velocity in the context of a mean-field model: (i) as $p\rightarrow p_{s+}$ from below, it takes longer to reach the true asymptotic velocity

(which is non-analytic at p_{s+}); (ii) for $p>p_{s+}$, the propagating front accelerates (with changing shape).

Corresponding results for the interface velocity, V(p), versus p in the QCP with h=1 are shown in **Fig.8** where V(p) is determined as the difference in interface location at initial time $t_i \approx 60$ from that at a range of final times, t_f. The result is largely independent of t_f up to $p \approx 0.212$, but |V(p)| becomes larger for longer t_f for higher p, consistent with acceleration of the front for $p>p_{s+}$. This suggests that $p_{s+}(h=1) \approx 0.212$, reasonably consistent with the estimate from **Fig.2**.

4. Pair-Approximation Results: Spinodal Points; Poisoning Kinetics; Interface Propagation

The lowest-order site-approximation (cf. Sec.2) fails to capture the h-dependence of the reaction kinetics which is of primary interest here. However, this dependence is incorporated in the higher-order approximations. Here, we consider only the pair-approximation [29,34]. In the hierarchical master equations for uniform states (2), this approximation factorizes multi-site probabilities in the particle creation terms as products of the m constituent pair probabilities and divides by $P[o]^{m-1}$ to avoid over-counting of the shared central empty site. One thereby obtains a closed set of equations for single-site and pair probabilities. In addition, hopping terms involving the probabilities of separated pairs of empty sites are factorized as $P[o]^2$. Since P[x]=1-P[o] and P[xo]=P[o]-P[oo], the pair-approximation yields the closed equations

$$dt\ P[o] = pP[x] - P[xo]^2/P[o] = p(1-P[o]) - (P[o]-P[oo])^2/P[o], \text{ and}$$

$$d/dt\ P[oo] = 2pP[xo] - P[xo]^2P[oo]/P[o]^2 + 6h(P[o]^2 - P[oo]) \qquad (7)$$

$$= 2p(P[o]-P[oo]) - (P[o]-P[oo])^2P[oo]/P[o]^2 + 6h(P[o]^2 - P[oo]).$$

Below it is convenient to let K = P[xo]/P[o] denote the conditional probability or concentration of finding a particle adjacent to a prescribed empty site. Due to spatial correlations, K is distinct from the concentration C = P[x] = 1-P[o]. Then, noting that P[xo] = K(1-C) and P[o o] = (1-K)(1-C), the pair-approximation then yields the kinetic equations

$$d/dt\ C = -pC + K^2(1-C) \text{ and } d/dt\ K + (1-K)(1-C)^{-1}\ d/dt\ C = [-2p + K(1-K)]K - 6h(K-C)\ . \quad (8)$$

The hopping term in the second equation of (7) forces $K \to C$, as $h \to \infty$, thus correctly recovering mean-field behavior. Solving (8) in the steady-state determines C_{eq} and K_{eq} versus p in the pair-approximation including their h-dependence. For example, one finds that

$$C_{eq} = 1-p +O(p^2) \text{ and } K_{eq} = 1- (2+6h)(1+6h)^{-1}p + O(p^2). \quad (9)$$

The differing linear terms show that spatial correlations persist even for small p when $h<\infty$. One can also eliminate p from steady-state form of (8) to obtain K_{eq} as a function of C_{eq}. One thus obtains

$$K_{eq} \approx C_{eq}[1-C_{eq}(1-C_{eq})/(6h)] \text{ and } p_{s+}(\text{pair}) \approx 1/4 -1/(48h), \text{ for } h>>1. \quad (10)$$

Similarly, one obtains

$$K_{eq} \approx C_{eq}(2-C_{eq})^{-1}[1-6h(2-C_{eq})(1-C_{eq})/C_{eq}]^{-1} \text{ and } p_{s+}(\text{pair}) \approx 1/8 + h, \text{ for } h<<1. \quad (11)$$

Next, we utilize numerical analysis of the pair-approximation equations to provide additional insight into the cases h=1 and h=4 considered by simulations in Sec.3. Specifically, we analyze the rapid poisoning kinetics for $p>p_{s+}$ choosing ranges of $p_{min} < p < p_{max}$ for the same distance $\Delta = p_{min} - p_{s+}$ above p_{s+} as in the simulation studies. Exact steady-state analysis indicates that $p_{s+}(\text{pair}) \approx 0.2329$ for h=1, and $p_{s+}(\text{pair}) \approx 0.2451$ for h=4. See **Table I**. However, **Fig.9a** shows pair-approximation kinetics in the QCP for h=1 for a range

of p=0.240-0.255 ($\Delta\approx0.007$) suggesting that $p_{s+}(h=1)$ = 0.224-0.225, and **Fig.9b** shows p=0.235-0.245 ($\Delta\approx0.002$) suggesting that $p_{s+}(h=1)$ = 0.229-0.230. Thus, even the latter estimate is about 0.003 below the correct value. If this correction is applied to the simulation estimate in **Fig.5b**, one obtains $p_{s+}(h=1) \approx 0.213$ (consistent with direct analysis from **Fig.2**). Similar pair-approximation analysis of kinetics in the QCP for h=4 for a range of p=0.254-0.279 ($\Delta\approx0.009$) suggests that $p_{s+}(h=4)$ = 0.234-0.235, but for p=0.249-0.269 ($\Delta\approx0.004$) suggests that $p_{s+}(h=4)$ = 0.239-0.240. The latter is 0.005 below the exact value, a correction if applied to simulation results for h=4 give the estimate of $p_{s+}(h=4) \approx 0.235$ (consistent with direct analysis from **Fig.2**).

Finally, we discuss extension of the pair-approximation to the description of spatially non-uniform states. In particular, we wish to analyze the propagation of an interface between the active and vacuum states to determine the equistability pressure, p_e, and also the characteristics of interface propagation for $p>p_e$ and particularly for $p\approx p_{s+}$ (just as in Sec.3). The truncation procedure based on factorization of probabilities naturally extends to the infinite hierarchy (3) for spatially non-uniform states either at the level of the site- or pair-approximation. In either case, the result is a set of discrete reaction-diffusion type equations. An example of this procedure for a lattice-gas reaction model at the level of the site approximation is found in Ref. [35], and for the QCP with h=0 at the level of the site- and pair-approximations is found in Ref. [29]. Extension of the latter analysis to include diffusion terms is straightforward. We present results at the pair-approximation level based on analysis of coupled discrete reaction-diffusion equations (RDE's) for single-site and pair probabilities

which vary with location (i.e., lattice site). For special cases of vertical or diagonal interfaces, these can be simplified as in Ref.[29].

We have noted previously that the QCP for $h \geq 0$ exhibits generic two-phase coexistence [16-18]. This feature derives from the property that the equistability or stationarity point for a planar interface separating active and vacuum states depends on the orientation of the interface. This property is preserved in the pair-approximation. **Table II** shows the dependence of the annihilation rates for stationarity of vertical (or horizontal) interfaces ($S=\infty$ or 0) and diagonal interfaces ($S=1$) as a function of h. There are some complications associated with propagation failure of vertical interfaces [29,36] which will be discussed elsewhere. However, the main observation here is that pair-approximation predicts that the orientation-dependence of interface propagation and equistability quickly diminishes with increasing h (although not as quickly as actual model behavior determined from simulations [18]).

However, our primary interest here is in analyzing the variation of velocity of propagation, $V(p)<0$, of an interface between a vacuum state and a state which is initially a filled lattice, i.e., the analogue of the interface propagation analyzed by simulation in **Fig.8**. Within the pair-approximation, this corresponds to the vacuum state displacing the metastable active state for $p_e<p<p_{s+}$ or displacing a poisoning state for $p>p_{s+}$. Results for V(p) versus p in the QCP with h=1 are shown in **Fig.10** where V(p) is determined as the difference in interface location at initial time $t_i=300$ from that at a range of final times, t_f. The result is largely independent of t_f up to $p \approx 0.232$ just below $p_{s+}=0.233$, but $|V(p)|$ becomes larger for longer t_f for higher p, consistent with acceleration of the front for $p>p_{s+}$. Thus, behavior is entirely analogous to that in **Fig.8**.

5. Continuum RDE's Based on the Pair-Approximation

Mean-field continuum Langevin reaction-diffusion equations (RDE's) [37,38] have provided a useful conceptual framework for analysis of fluctuation effects in reaction-diffusion systems, where the hop rate is sufficiently large to ensure effective mixing (and thus mean-field reaction kinetics), but no so large as to completely quench fluctuations [9]. However, for our analysis of the QCP with moderate particle hop rates, there are significant deviations from mean-field reaction kinetics as reflected in the shift of the spinodal points from its $h \to \infty$ mean-field value of ¼. Consequently, we are motivated to incorporate a higher-level pair-approximation description of reaction kinetics into a continuum RDE formulation. One strategy to derive continuum RDE's without noise terms is to coarse-grain the discrete RDE's which follow from the exact hierarchical master equations after applying the appropriate factorization approximation (cf. Ref. [38]). This analysis will not yield noise terms might come from consideration of suitable birth-death master equations for discrete populations of relevant "species" in an array of spatial cells [1,37,38].

To coarse-grain the discrete RDE's, we start with the factorized form of (3) for the probabilities of empty sites and adjacent empty pairs at specific locations. We then rewrite these in terms of coarse-grained continuum variables to describe their spatial variation after applying suitable Tayor expansions (cf. Ref.[39]). Note that concentration gradients can induce different nearest-neighbor correlations in horizontal and vertical directions, so we use two corresponding variables. The complete set of variables are:

$U(\underline{r} = (i,j)a) = P[o_{i,j}]$, $V(\underline{r} = (i+½,j)a) = P[o_{i,j}\, o_{i+1,j}]$, and $W(\underline{r} = (i,j+½)a) = P[o_{i,j}\, o_{i,j+1/2}]$, (12)

where again ‘a’ is the lattice constant. Examples of required Taylor expansions are:

$$P[o_{i\pm1,j}] = U(\underline{r}) \pm a\, U_x(\underline{r}) + \tfrac{1}{2} a^2 U_{xx}(\underline{r}) + \ldots \text{ for } \underline{r} = (i,j)a,$$

$$P[o_{i+1,j}\, o_{i+2,j}] = V(\underline{r}) + a\, V_x(\underline{r}) + \tfrac{1}{2} a^2 V_{xx}(\underline{r}) + \ldots \text{ for } \underline{r} = (i+\tfrac{1}{2},j)a \qquad (13)$$

$$P[o_{i+1,j}\, o_{i+1,j\pm1}] = W(\underline{r}) + \tfrac{1}{2} a\, W_x(\underline{r}) \pm \tfrac{1}{2} a\, W_y(\underline{r}) + 1/8\, a^2 W_{xx}(\underline{r}) + 1/8\, a^2 W_{yy}(\underline{r}) \pm \tfrac{1}{4} a^2 W_{xy}(\underline{r}) + \ldots$$

again for $\underline{r} = (i+\tfrac{1}{2},j)a$. Thus (3) becomes:

$$\partial/\partial t\, U = p(1-U) - U^{-1}(U-V)(U-W) + 1/8\, a^2 (U-V)W_{yy} + 1/8\, a^2 (U-W)V_{xx} + a^2 h (U_{xx}+U_{yy}), \qquad (14)$$

$$\partial/\partial t\, V = 2p(U-V) - U^{-2} V(U-V)(U-W) + 6h(U^2-V) + a^2 h\, U(7/2\, U_{xx} + \tfrac{1}{2} U_{yy}) + \tfrac{1}{4} a^2 p\, U_{xx} + \text{other}$$

where ‘other’ denotes additional $O(a^2)$ terms , and the W-equation follows from that for V by rotational symmetry. Note that for a spatially uniform system where V=W, (14) recovers to the spatially-uniform pair-approximation kinetics (7).

Addition of noise terms to the above RDE’s would allow simulation of metastability and nucleation-mediated poisoning as described in Sec.3 (see Fig.4). Standard procedures are available at the mean-field level to generate such noise terms which include non-conserved contributions due to reaction (summing separate contributions from particle annihilation and creation for our model) and conserved contributions due to diffusion [18,37,38]. For the above formulation at the level of the pair-approximation, it is necessary to start with master equations describing the evolution of discrete populations of both empty sites and empty pairs for a finite region. One then generates the coarse-grained Fokker-Planck equations from which the form of multiplicative noise terms can be deduced. Details will be presented elsewhere [40].

6. Conclusions

Our stochastic realization of Schloegl's second model for autocatalysis with particle diffusion on a square lattice, aka the Quadratic Contact process, provides an ideal testing ground to explore issues related to discontinuous phase transitions and associated metastability phenomena in non-equilibrium reaction-diffusion models. Based on analysis for equilibrium Ising-type models, one does not expect that an unambiguous precise definition is possible for the spinodal point in our non-equilibrium model for an infinite lattice. Nonetheless, the concept of a spinodal appears to provide a useful tool for analyzing poisoning kinetics, particularly for moderate or large hop rates. Our combination of simulation and pair-approximation analysis is effective in determining the location of the effective spinodal point as a function of particle hop rate.

Acknowledgements

JWE thanks Da-Jiang Liu for discussions on poisoning dynamics, and Y. De Decker for discussions on coarse-grained reaction-diffusion equations. XG and JWE were supported for this work by the Division of Chemical Sciences of the U.S. Department of Energy (Basic Energy Sciences). It was performed at Ames Laboratory which is operated for the USDOE by Iowa State University under Contract No. DE-AC02-07CH11358.

References

[1] J.D. Gunton and M. Droz, *Introduction to the Theory of Metastable and Unstable States*, Springer Lecture Notes in Physics Vol. 183 (Springer, Berlin, 1983).
[2] J.D. Gunton, M. San Miguel, and P.S. Sahni, in *Phase Transitions and Critical Phenomena*, edited by J.L. Lebowitz and C. Domb (Academic Press, London, 1983).
[3] H.E. Stanley, *Introduction to Phase Transitions and Critical Phenomena* (Oxford University Press, Oxford, 1971).

[4] R.H. Schonmann and S.B. Shlosman, Comm. Math. Phys. **194**, 389 (1998).
[5] S. Shlosman, Physica A **263**, 180 (1999).
[6] S. Friedli and C.-E. Pfister, Phys. Rev. Lett. **92**, 015702 (2004).
[7] G. Nicolis and I. Prigogine, *Self-Organization in Non-Equilibrium Systems* (Wiley, New York, 1977).
[8] A.S. Mikhailov, *Foundations of Synergetics I* (Springer, Berlin, 1990).
[9] J.W. Evans, D.-J. Liu, and M. Tammaro, Chaos **12**, 131 (2002).
[10] J. Marro and R. Dickman, *Nonequilibrium Phase Transitions in Lattice Models* (Cambridge UP, Cambridge, 1999).
[11] H. Hinrichsen, Adv. Phys. **49**, 815 (2000).
[12] G. Odor, Rev. Mod. Phys. **76**, 663 (2004).
[13] R.M. Ziff, E. Gulari, and Y. Barshad, Phys. Rev. Lett. **56**, 2553 (1986).
[14] J.W. Evans and T.R. Ray, Phys. Rev. E, **50**, 4302 (1994).
[15] R. H. Goodman, D. S. Graff, L. M. Sander, P. Leroux-Hugon, and E. Clément Phys. Rev. E **52**, 5904 (1995).
[16] D.-J. Liu, X. Guo, and J.W. Evans, Phys. Rev. Lett., **98**, 050601 (2007).
[17] X. Guo, D.-J. Liu, and J.W. Evans, Phys. Rev. E, **75**, 061129 (2007).
[18] X. Guo, D.-J. Liu, and J.W. Evans, J. Chem. Phys. **130**, 074106 (2009).
[19] J.W. Evans and M.S. Miesch, Phys. Rev. Lett. **66**, 833 (1991).
[20] E. Loscar and E.V. Albano, Rep. Prog. Phys. **66**, 1343 (2003).
[21] E. Machado, G.M. Buendia, and P.A. Rikvold, Phys. Rev. E **71**, 031603 (2005).
[22] M. Tammaro, M. Sabella, and J.W. Evans, J. Chem. Phys. **103**, 10277 (1995).
[23] F. Schloegl, Z. Phys. **253**, 147 (1972).
[24] P. Grassberger, Z. Phys. B Cond. Matt. **47**, 365 (1982).
[25] J.P. Boon, D. Dab, R. Kapral, and A. Lawniczak, Rep. Mod. Phys. **273**, 55 (1996).
[26] S. Prakash and G. Nicolis, J. Stat. Phys. **86**, 1289 (1997).
[27] R. Durrett, SIAM Rev. **41**, 677 (1999).
[28] P.A. Rikvold, H. Tomita, S. Miyashita, and S.W. Sides, Phys. Rev. E **49**, 5080 (1994).
[29] X. Guo, J.W. Evans, and D.-J. Liu, Physica A **387**, 177 (2008).
[30] J.W. Evans, Rev. Mod. Phys. **65**, 1281 (1993).
[31] J.W. Evans and D.K. Hoffman, Phys. Rev. B **30**, 2704 (1984).
[32] R. Kutner, Phys. Lett. **81A**, 239 (1981).
[33] M. Avrami, J. Chem. Phys. **7**, 1103 (1939); **8**, 212 (1940); **9**, 177 (1941).
[34] R. Dickman, Phys. Rev. A **34**, 4246 (1986).
[35] P. Fischer and U.M. Titulaer, Surf. Sci. **221**, 409 (1989).
[36] D.-J. Liu, X. Guo, and J.W. Evans, in preparation (2009).
[37] M. Hildebrand and A.S. Mikhailov, J. Phys. Chem. **100**, 19089 (1996).
[38] M. Hildebrand, A.S. Mikhailov, and G. Ertl, Phys. Rev. Lett. **81**, 2602 (1998).
[39] Y. De Decker, G.A. Tsekouras, A. Provata, Th. Erneux, and G. Nicolis, Phys. Rev. E **69**, 036203 (2004).
[40] Y. De Decker, X. Guo, and J.W. Evans, in preparation (2009).

Tables

Table I. KMC simulation and pair-approximation results for p_e, p_{s+}, and the width of the metastable regime $\Delta p_{s+} = p_{s+} - p_e$ in the QCP with particle hop rate $h \geq 0$. *From KMC simulation, one finds that $p_e = 0.09443$ and $p_f = 0.0869$ for $h=0$, but $p_f - p_e < 0.0001$ for $h > 0.02$.

	p_e	p_{s+}	Δp_{s+}
h=0 KMC	0.094*	0.101	0.007
h=0 PAIR	0.1083	0.1250	0.0167
h=1 KMC	0.199	0.213	0.014
h=1 PAIR	0.2079	0.2329	0.0250
h=4 KMC	0.215	0.236	0.021
h=4 PAIR	0.2181	0.2451	0.0270
h=∞ EXACT	$0.2222^{\bullet}$	0.2500	0.2780

Table II. Pair-approximation results for the QCP with particle hop rate h. Values of p for equistability of vertical interfaces, $p_{eq}(S=\infty)$, and diagonal interfaces, $p_{eq}(S=1)$, between active and vacuum states, and for the upper spinodal, p_{s+}.

PAIR APPROX.	$p_{eq}(S=\infty$ or 0)	$p_{eq}(S=1)=p_e$	p_{s+}
h=0	0.1060	0.1083	1/8 = 0.1250
h=0.01	0.11759	0.11863	0.13429
h=0.05	0.14335	0.14368	0.15997
h=0.10	0.16018	0.16035	0.17828
h=0.20	0.17776	0.17784	0.19801
h=0.50	0.197546	0.197573	0.22078
h=1.0	0.207900	0.207909	0.23292

Figures

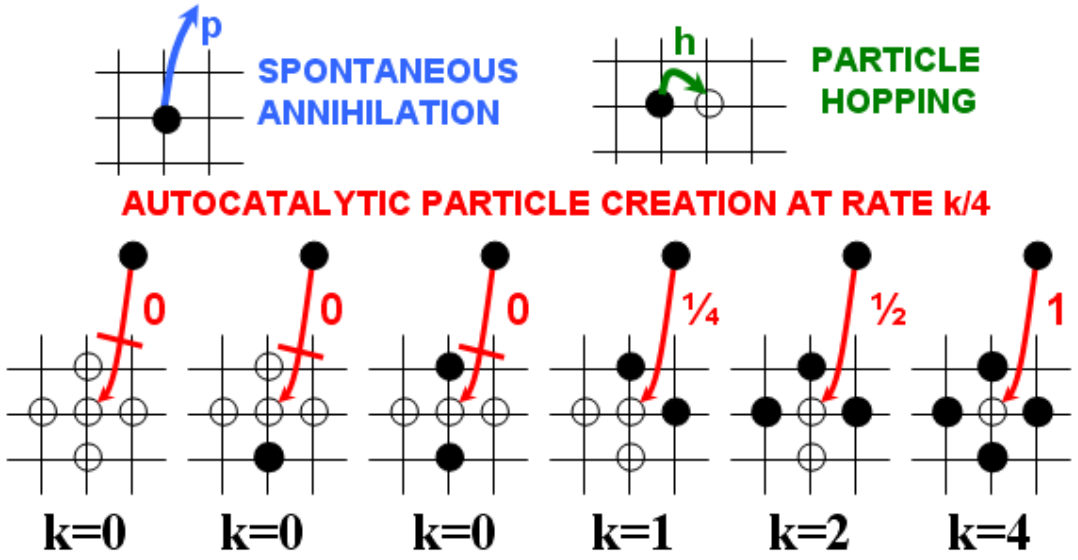

Figure 1. **Schematic of particle annihilation, autocatalytic creation, and hopping processes in Schloegl's second model or the QCP on a square lattice. Here particles are denoted by filled circles (•) and empty sites by open circles (o). Rates for the various processes are also indicated, and the bar through the arrow indicates that the process is inactive.**

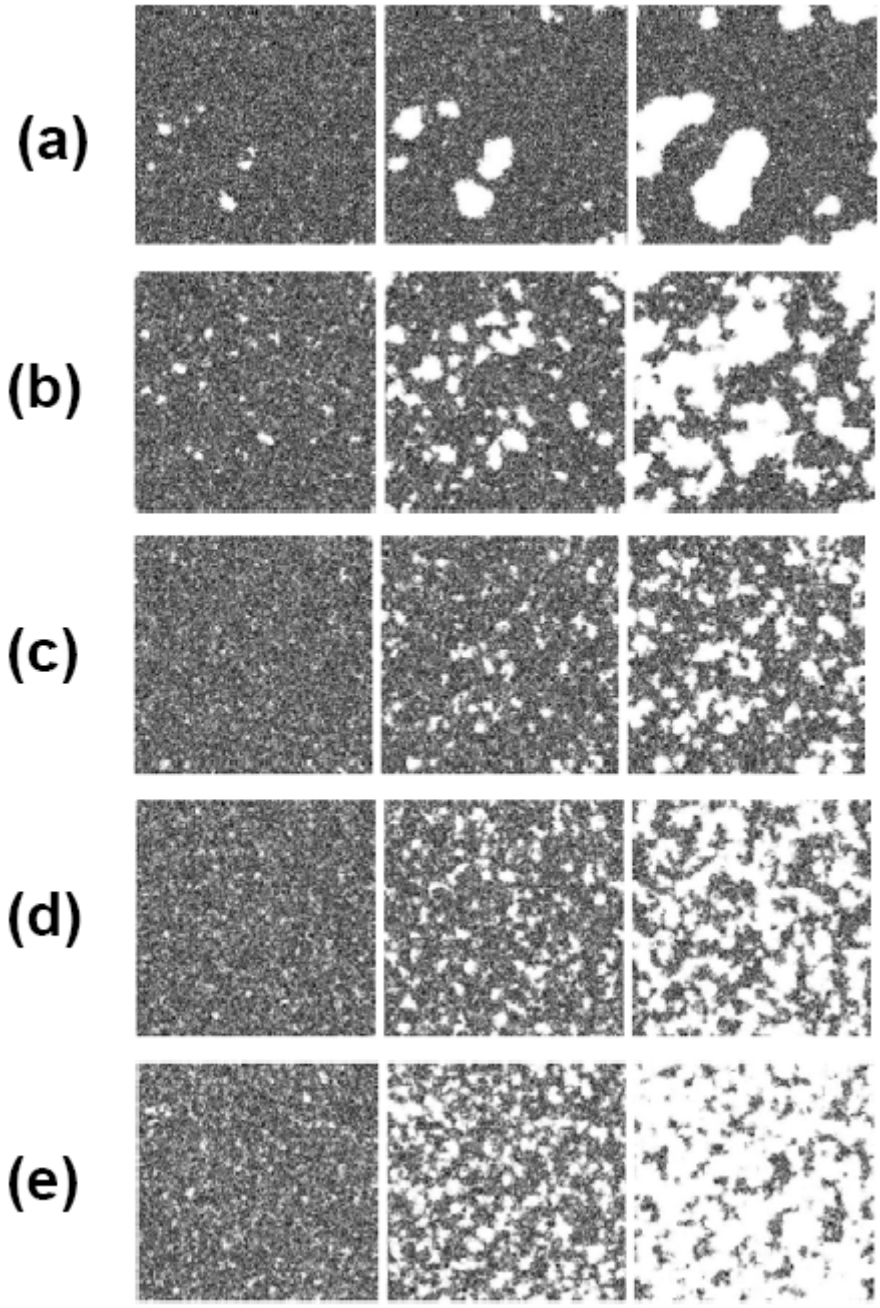

Figure 2. **Simulated evolution in the QCP with h=1 starting from a filled 1024×1024 site lattice (which quickly evolves to a metastable active state) for: (a) p=0.208; t= 480, 960, 1440; (b) p=0.210 t= 240, 480, 720; (c) p=0.212; t= 96, 192, 288; (d) p=0.213; t= 96, 192, 288; (e) p=0.214; t= 96, 192, 288.**

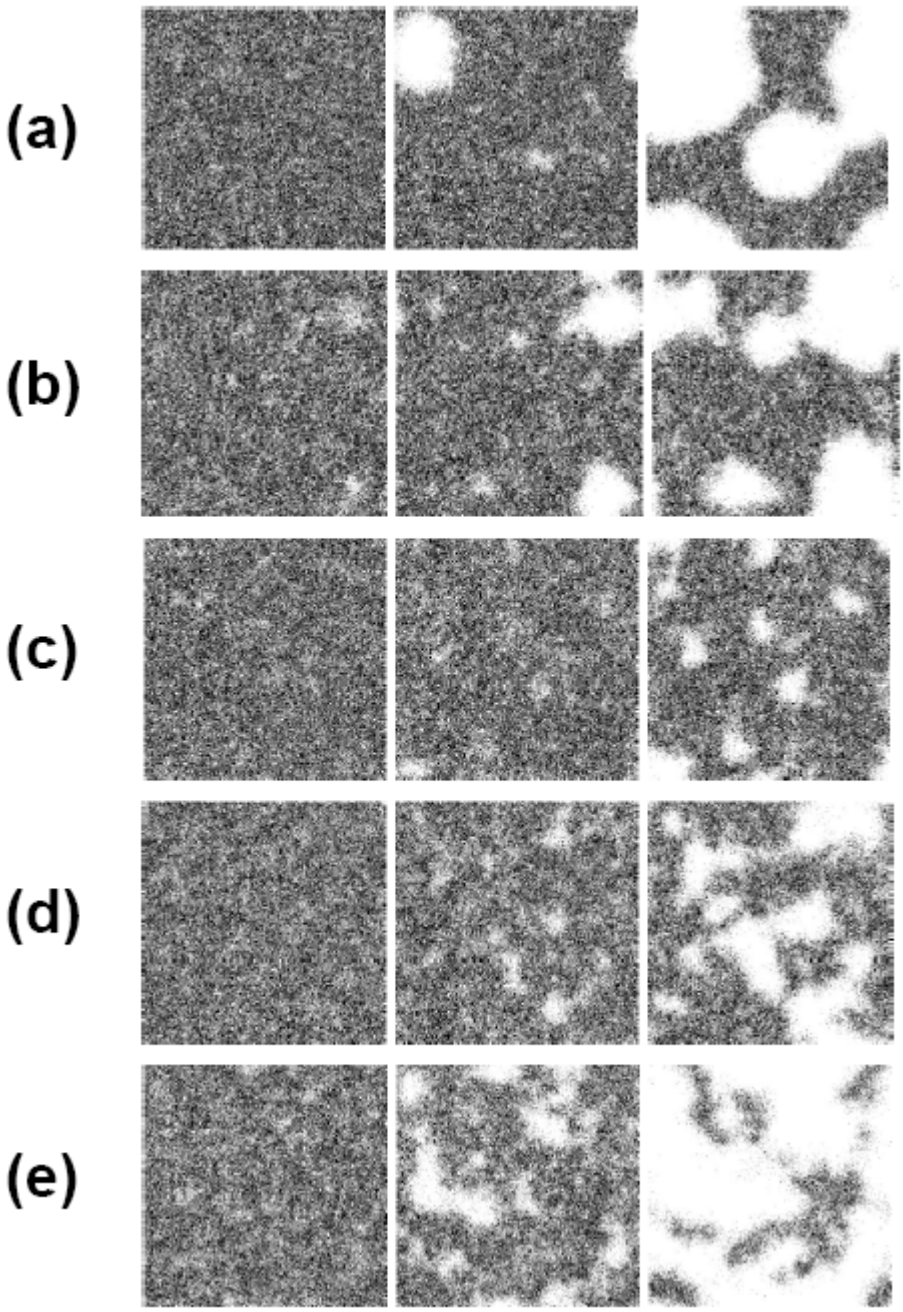

Figure 3. Simulated evolution in the QCP with h=4 starting from a filled 512×512 site lattice (which quickly evolves to a metastable active state) for: (a) p=0.232; t= 290, 580, 870; (b) p=0.234 t= 116, 232, 348; (c) p=0.235; t= 58, 116, 174; (d) p=0.236; t= 58, 116, 174; (e) p=0.237; t= 58, 116, 174.

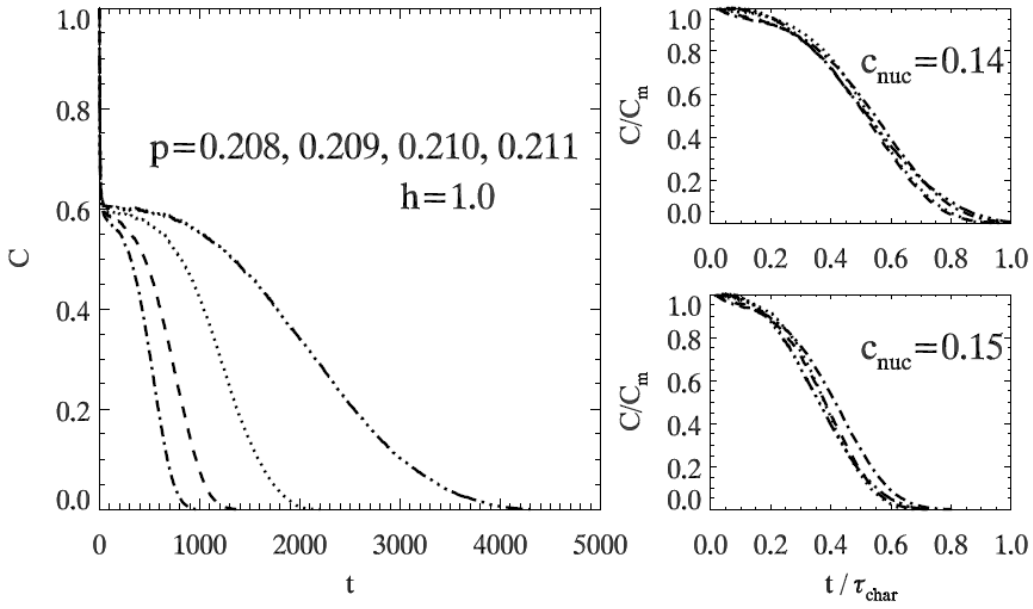

Figure 4. **Simulation results for nucleation-mediated poisoning kinetics in the QCP for h=1 for p=0.208-0.211 between $p_e(h=1)=0.197$ and $p_{s+}(h=1) \approx 0.213$. The parameter c_{nuc} is extracted from the characteristic time for nucleation τ_{nuc} in (6). It reflects the magnitude of the effective barrier to nucleation, and is significantly larger than values for h=0-0.4 determined previously [18].**

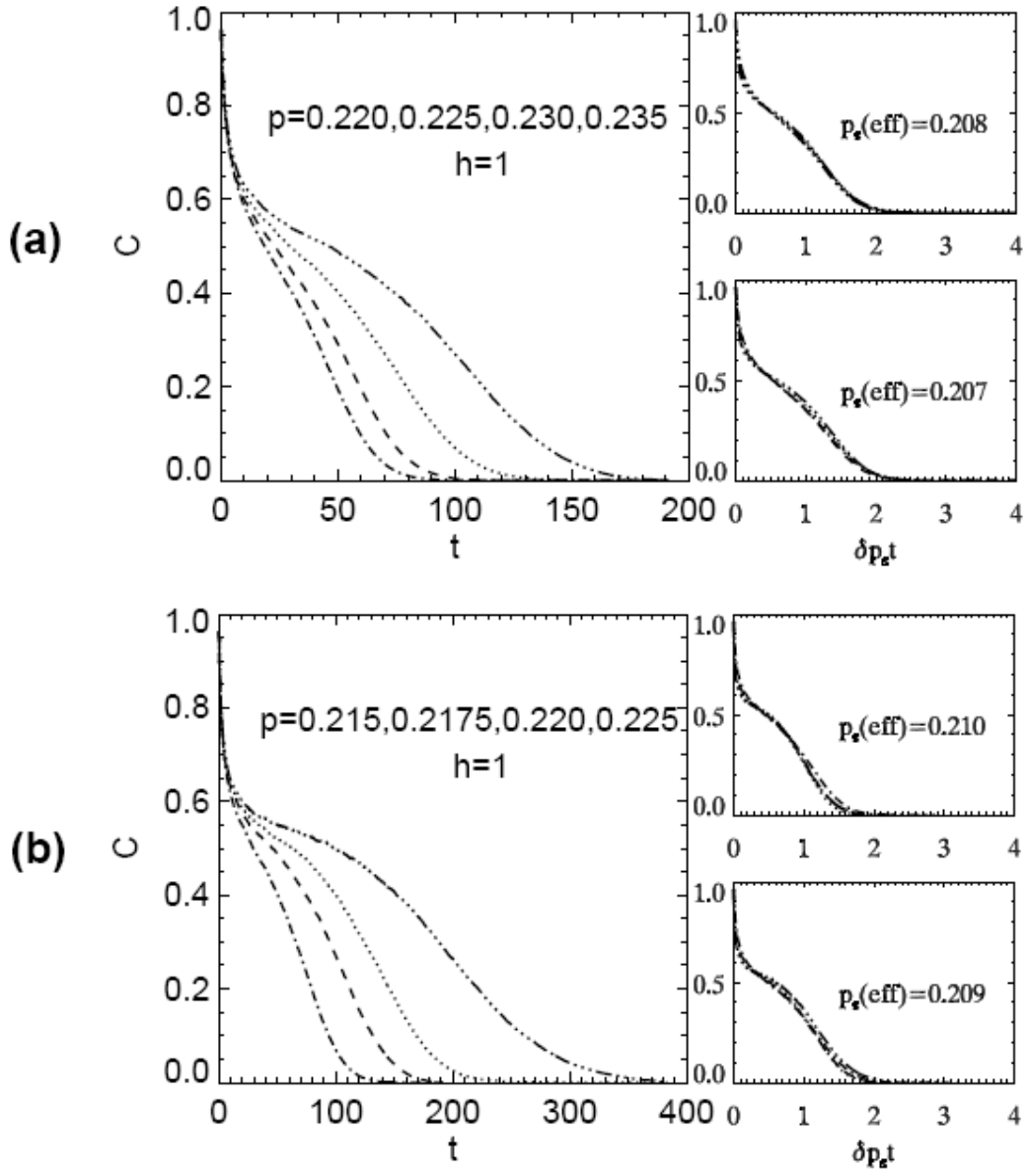

Figure 5. Simulation results for the poisoning kinetics in the QCP for h=1 for: (a) p=0.220-0.235 data suggesting that $p_{s+}(h=1)$ = 0.207-0.208; (b) p=0.215-0.225 data suggesting that $p_{s+}(h=1)$ = 0.209-0.210.

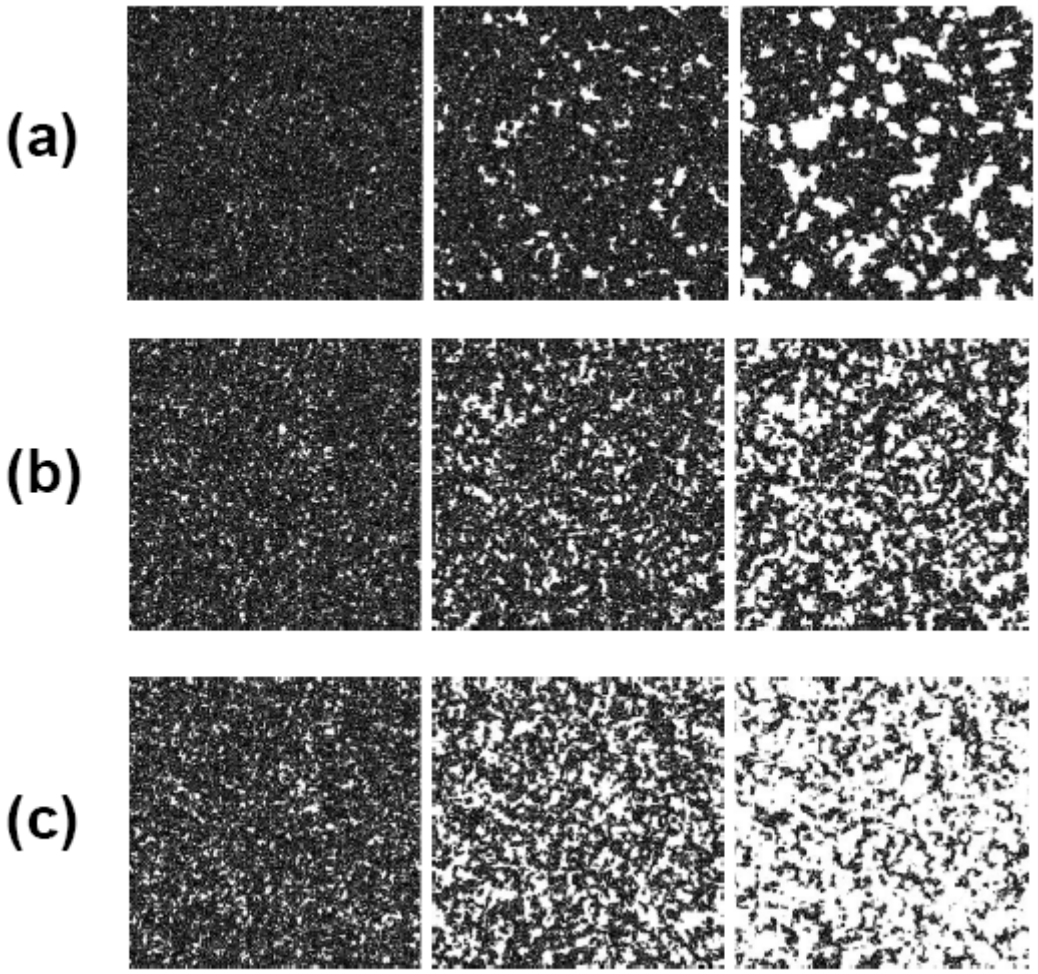

Figure 6. Simulated evolution in the QCP with h=0 starting from a filled 1024×1024 site lattice (which quickly evolves to a metastable active state) for: (a) p=0.098; t= 455, 2275, 4090; (b) p=0.100 t= 455, 910, 1365; (c) p=0.101; t= 455, 910, 1365.

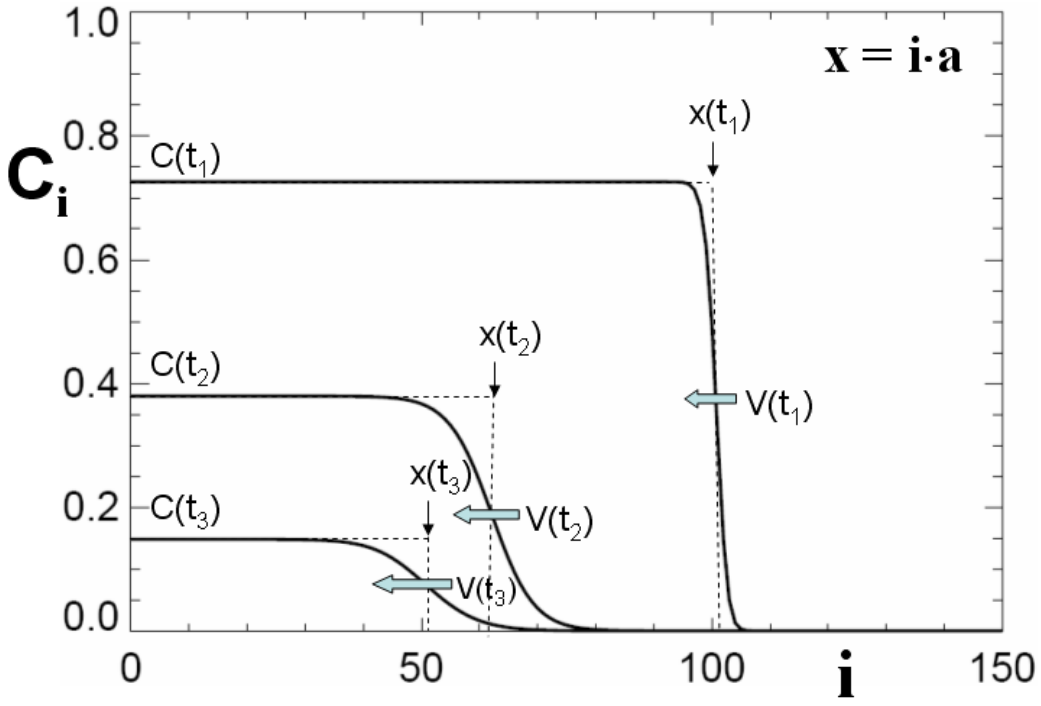

Figure 7. Schematic for determination of the location, x(t), of a vertical interface between the vacuum state and an initially filled "poisoning state" from the concentration profiles in the QCP for $p>p_e$. Profiles are shown as solid curves passing through discrete average concentrations, $C_i = \langle C_{i,j} \rangle_j$ for columns i, where (i,j) is the site label on the square lattice. x(t) matches the location of the reference sharp interface (dashed curves) so that $\sum_i C_i(t) = \sum_{i<x(t)} C(t)$, where $C(t) \to 0$ as $t \to \infty$ denotes the concentration of a uniform initially filled state. Profiles shown are taken from pair-approximation simulations with h=1 and p=0.235 exceeding $p_{s+} \approx 0.233$. An analogous definition is possible for other interface orientations.

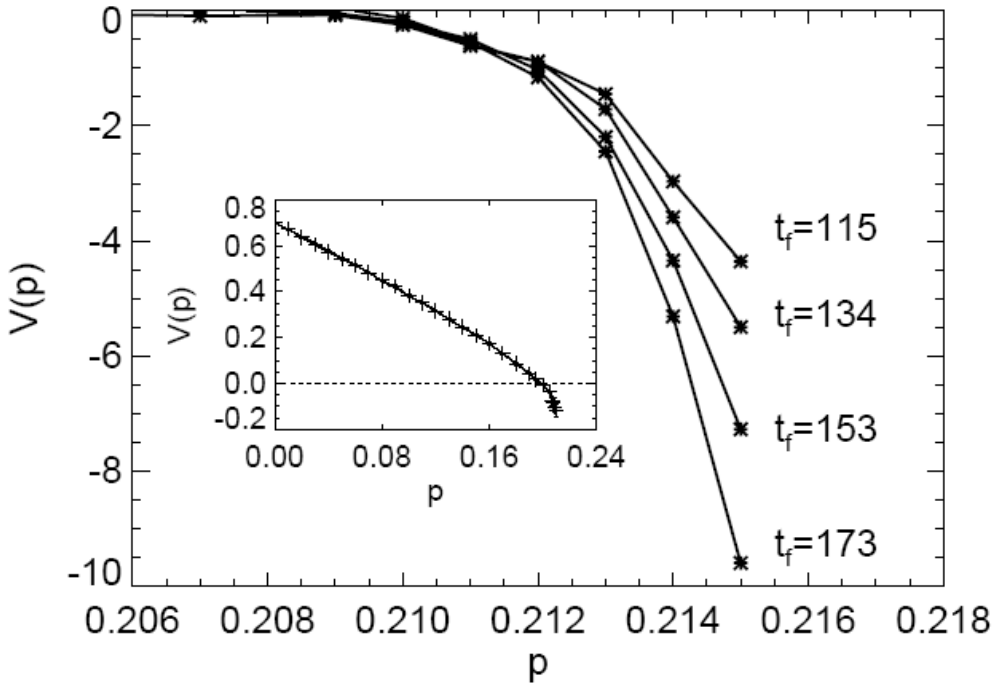

Figure 8. **Simulation results for the propagation velocity, V(p), for an interface between vacuum and poisoning states in the QCP with h=1 defined as in Fig.6 where velocity is measured as the difference in location between time $t_i = 60$ and t_f (shown). Results depend on t_f just below and above $p = p_{s+} \approx 0.213$. Inset: V(p) over a broader range of p.**

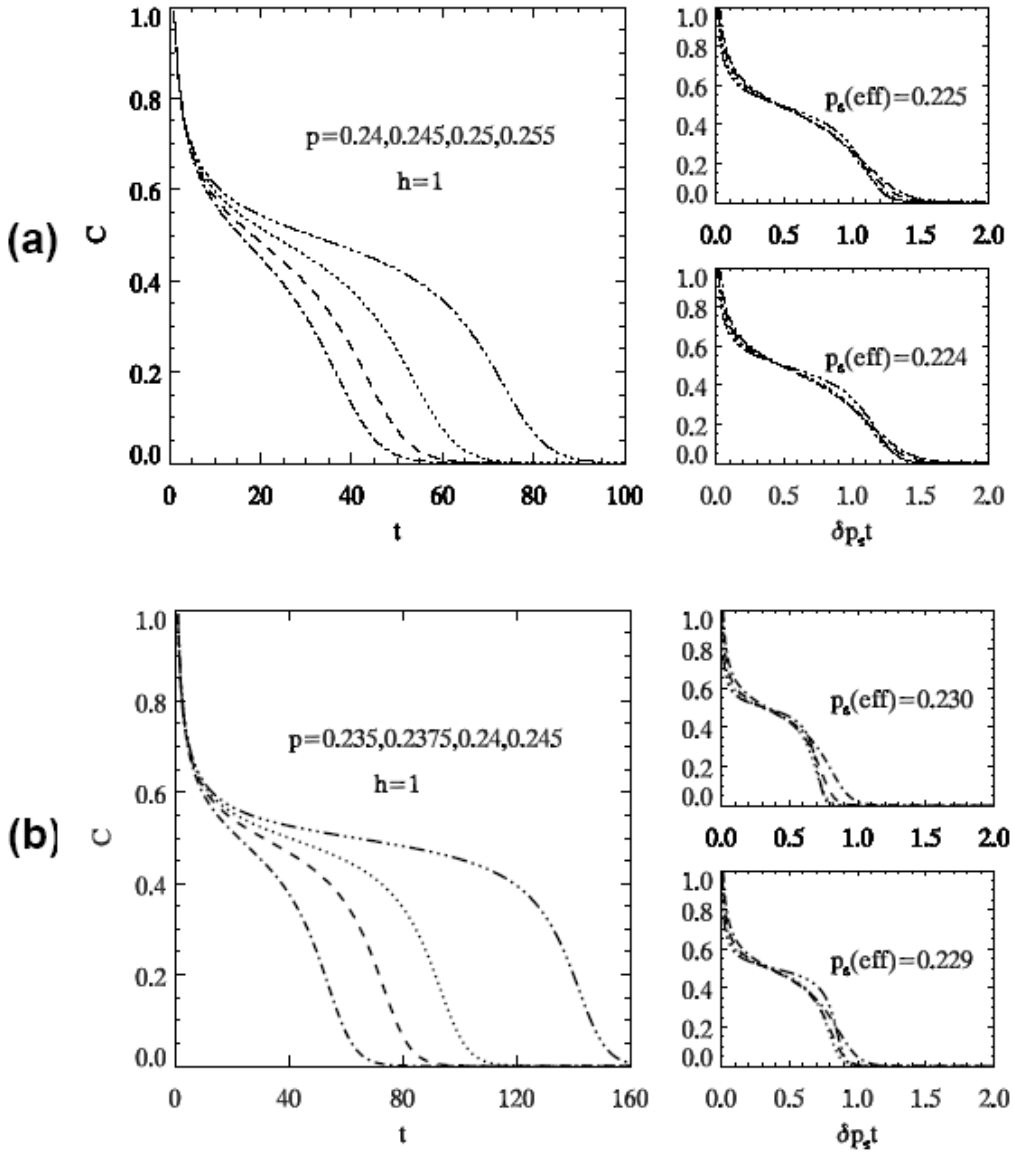

Figure 9. Pair-approximation results for the poisoning kinetics in the QCP for h=1 for: (a) p=0.240-0.255 data suggesting that $p_{s+}(h=1)$ = 0.224-0.225; (b) p=0.235-0.245 data suggesting that $p_{s+}(h=1)$ = 0.229-0.230.

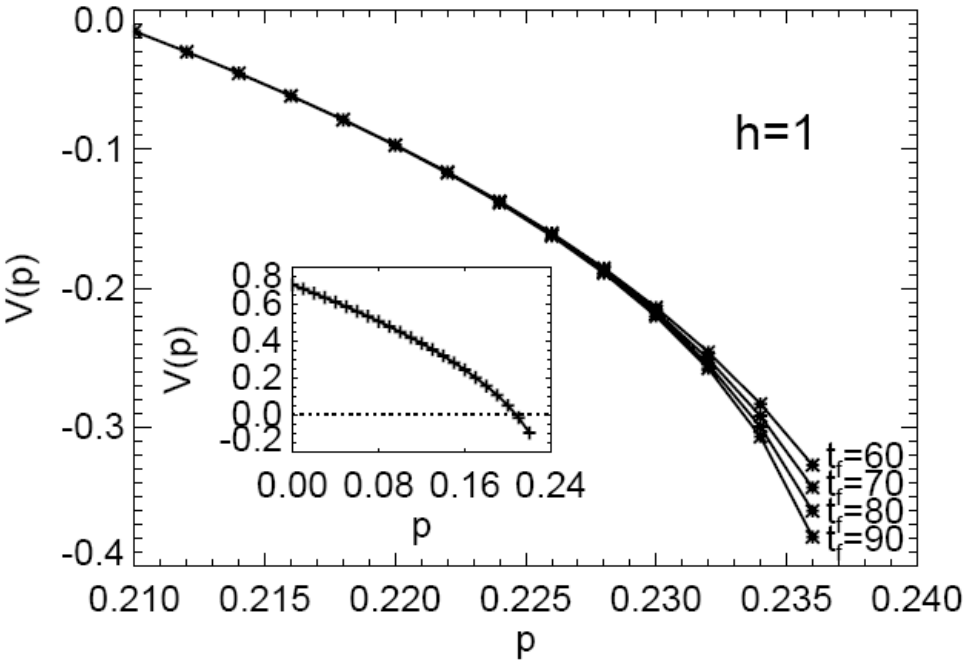

Figure 10. Pair-approximation results for the propagation velocity, V(p), for an interface between vacuum and poisoning states in the QCP with h=1 defined as in Fig.7 where velocity is measured as the difference in location between time t_i = 60 and t_f (shown). Results depend on t_f just below and above $p = p_{s+} \approx 0.233$. Inset: V(p) over a broader range of p. Note the semi-quantitative agreement with simulation results in the inset to Fig.8.

CHAPTER 6. TRICRITICALITY IN A GENERALIZED SCHLOEGL MODEL FOR AUTOCATALYSIS: LATTICE-GAS REALIZATION WITH PARTICLE DIFFFUSION

Xiaofang Guo[1,2], Daniel Unruh[1], Da-Jiang Liu[1], and J.W. Evans[1,2]

Ames Laboratory – USDOE[1] and Department of Mathematics[2],

Iowa State University, Ames Iowa 50011

Abstract

We analyze a lattice-gas version of a model for autocatalysis with particle diffusion which incorporates both the mechanisms of Schloegl's first and second models. Adjusting the relative strength of these mechanisms induces a crossover between continuous and discontinuous transitions, as suggested by a mean-field analysis. Kinetic Monte Carlo simulations are used to map out corresponding tricritical line as a function of particle hop rate, and a detailed analysis is provided of the tricritical "epidemic exponent" for the case of no hopping. The complete phase diagram is also recovered reasonably accurately by applying the pair-approximation to the exact hierarchical form of the master equations for this model.

1. Introduction

Non-equilibrium systems are well known to provide a richer variety of phase transition or bifurcation behavior than traditional equilibrium systems [1,2]. However, there are also many similarities in behavior. At the mean-field level of analysis, bistability of steady states is the analogue of phase separation in the van der Waals model, its disappearance at a cusp bifurcation being the non-equilibrium analogous of a critical point

[2-4]. It is also straightforward to construct non-equilibrium systems also exhibit continuous phase transitions at the mean-field level. However, a natural goal is to advance beyond mean-field-level to statistical mechanical analyses of these non-equilibrium models. Such recent studies of non-equilibrium phase transitions in lattice-gas models have focused on universality in continuous transitions [5-7]. However, increasing attention is being paid to analysis of various phenomena in reaction-diffusion type models exhibiting discontinuous transitions [8-14]. Consequently, it is natural to also explore the crossover between continuous and discontinuous transition behavior, i.e., to assess tricritical behavior in non-equilibrium systems [15]. To achieve this goal, it is natural to consider a generalized or hybrid version of Schloegl's first and second models for autocatalysis, which are described below.

In the traditional off-lattice mean-field context, special cases of Schloegl's first (n=1) and second (n=2) models of relevance here have the mechanism [2,14,16-22]:

$X \to \varnothing$ (spontaneous annihilation), $nX \to (n+1)X$ (autocatalytic creation).

Thus, spontaneous annihilation occurs at rate p, and autocatalytic creation occurring at a suitably prescribed rate requires existing nearby particle in the first model (n=1), or nearby pair of particles in the second model (n=2). The most general formulation also includes spontaneous particle creation $\varnothing \to X$, but this process is excluded in our study. Traditional off-lattice formulations also include the autocatalytic annihilation process $(n+1)X \to nX$ in order to avoid population explosion [2,16]. Implicitly, the models are usually assumed to include particle diffusion. These models display quadratic (cubic) mean-field kinetics for n=1 (n=2), i.e., the rate of change of particle concentration is a quadratic (cubic) function of concentration, C [2,16-19]. Upon increasing the annihilation rate p, there is a bifurcation in

the steady-states from a regime with a stable active steady state with finite population C>0 to one where the vacuum state with C=0 is the unique stable steady state [5,22]. For n=1, this transition is continuous, but for n=2 it is discontinuous.

In this work, we will consider exclusively lattice-gas formulations where autocatalytic particle creation requires an empty site ∅, and is thus more accurately represented as $nX+\varnothing\rightarrow(n+1)X$ [14,19-22]. This empty site requirement automatically limits population growth. However, the mean-field treatment of these models has essentially the same features as the traditional off-lattice formulation. The lattice-gas formulation of Schloegl's models might also be described as the standard Contact Process (SCP) for the first model (n=1), and as the Quadratic Contact Process (QCP) for the second model (n=2) [5,14,20-22]. The former provides the prototype for a continuous phase transition to an absorbing vacuum state which is in the universality class of directed percolation or Reggeon field theory [5]. The second, at least with a suitable choice of rates, provides an example of a discontinuous phase transition actually displaying generic two-phase coexistence.

In this work we shall consider a lattice-gas realization of a hybrid version of Schloegl's first and second models (or equivalently of the SCP and QCP) with particle hopping. Our focus is on analysis of tricritical behavior associated with the conversion between continuous and discontinuous transitions. For the most part, we focus on the regime where the QCP is "perturbed" by adding a "small amount" of the SCP mechanism. From this perspective, the generalized model could provide additional insight into the behavior of the pure QCP, particularly for small particle hop rate where unusual generic two-phase coexistence is observed.

In Sec.2, we describe in detail the realization of the hybrid QCP+SCP model analyzed in this paper, as well as presenting the hierarchical form of the exact master equations for this model. Mean-field behavior is also briefly described. In Sec.3, we present simulation results focusing on determination of the tricritical point as a function of hop rate. A more detailed analysis of tricriticality is also provided for the case of no hopping. Next, in Sec.4, we present an analysis of model behavior within the pair-approximation to the exact master equations. This approximation reasonably describes behavior observed in simulation studies. Conclusions are provided in Sec.5.

2. Model Specification and Master Equations

Our realization the generalized or hybrid Schloegl model, or equivalently of the QCP+SCP, on a square lattice as a stochastic Markov process involves the following components (cf. Ref.[14,20-22]): **(i)** particle annihilation occurring randomly at rate p; **(ii)** particle creation at empty sites requiring one or more diagonally adjacent pairs of occupied sites (the QCP mechanism); specifically, the creation rate is given by k/4, where k is the number of adjacent diagonal occupied pairs and thus can take the values k = 0, 1, 2, or 4; **(iii)** a separate pathway for particle creation at empty sites requiring just one or more adjacent occupied sites (the SCP mechanism); specifically, the creation rate is given by $j \cdot \delta$, where j is the number of adjacent occupied sites and thus can take the values j = 0-4; **(iv)** hopping of particles to any adjacent empty sites at rate h (per target site). **Fig.1** provides a schematic of these processes. Again C denotes the particle concentration, i.e., the fraction of filled sites. For any p>0, the “vacuum state” with C=0 corresponds to an absorbing steady state from which the system cannot escape. However, there also exists an active or reactive steady-state

with $C=C_{eq}(p)>0$ at least for small p. Indeed, for $p<<1$, the lattice is almost completely populated with $C_{eq}(p) = 1-(1+4\delta)^{-1}p + O(p^2)$ independent of h.

While kinetic Monte Carlo (KMC) simulation will be utilized below to provide precise results for the steady-state variation of C with p (i.e., the equation of state) for various δ and h. In particular, we will determine the tricritical value of $\delta_{tc}=\delta_{tc}(h)$ of δ, such that the model for a specific h exhibits a discontinuous transition to a vacuum state for $\delta<\delta_{tc}$, and a continuous transition for $\delta>\delta_{tc}$. However, it is also instructive to present the exact master equations for the QCP+SCP with $h\geq 0$ in the form of an infinite coupled hierarchy. It will be instructive to explore the predictions of truncation approximations to these equations.

First, we consider spatially homogeneous states of the QCP+SCP with $h\geq 0$ on an infinite square lattice. We let "x" denote an occupied site and "o" an empty site. Then, P[x] = C denotes the probability of a occupied site, P[o] = 1-C the probability of an empty site, P[x x] the probability of an adjacent occupied pair, P[o o] the probability of an adjacent empty pair, etc.. Conservation of probability ensures that all configurational probabilities can be written as combinations of such probabilities for configurations with just empty sites, e.g., P[x] = 1 - P[o], P[x o] = P[o] - P[o o], P[xx] = 1-2P[o]+P[o o], etc. [23], or instead with just occupied-site configurations. For the QCP, we favor empty site configurations when developing the master equations. A similar situation applies for models which just include irreversible cooperative creation of particles and no annihilation or hopping, usually referred to as "cooperative sequential adsorption" models [23]. The <u>exact</u> form of the first two such hierarchical master equations in an infinite coupled set becomes (cf. Ref.[24])

$$d/dtP[o] = p\cdot P[x] - \left(4\cdot\frac{1}{4}\cdot P\begin{bmatrix} & x & \\ o & o & x \\ & o & \end{bmatrix} + 4\cdot\frac{1}{2}\cdot P\begin{bmatrix} & x & \\ o & o & x \\ & x & \end{bmatrix} + 1\cdot 1\cdot P\begin{bmatrix} & x & \\ x & o & x \\ & x & \end{bmatrix} \right)$$

$$-\delta\cdot\left(4\cdot 1\cdot P\begin{bmatrix} & o & \\ o & o & x \\ & o & \end{bmatrix} + 4\cdot 2\cdot P\begin{bmatrix} & x & \\ o & o & x \\ & o & \end{bmatrix} + 2\cdot 2\cdot P\begin{bmatrix} & o & \\ x & o & x \\ & o & \end{bmatrix} + 4\cdot 3\cdot P\begin{bmatrix} & x & \\ x & o & x \\ & o & \end{bmatrix} + 1\cdot 4\cdot P\begin{bmatrix} & x & \\ x & o & x \\ & x & \end{bmatrix} \right)$$

$$= p\cdot P[x] - P\begin{bmatrix} x & \\ o & x \end{bmatrix} - 4\delta\cdot P[o \quad x] \qquad (1)$$

$$d/dtP[o \quad o] = 2p\cdot P[o \quad x] - 2\cdot\left(2\cdot\frac{1}{4}\cdot P\begin{bmatrix} & x & \\ o & o & x \\ & o & \end{bmatrix} + 1\cdot\frac{1}{2}\cdot P\begin{bmatrix} & x & \\ o & o & x \\ & x & \end{bmatrix} \right)$$

$$-2\delta\cdot\left(3\cdot 1\cdot P\begin{bmatrix} & o & \\ o & o & x \\ & o & \end{bmatrix} + 2\cdot 2\cdot P\begin{bmatrix} & x & \\ o & o & x \\ & o & \end{bmatrix} + 1\cdot 2\cdot P\begin{bmatrix} & x & \\ o & o & o \\ & x & \end{bmatrix} + 1\cdot 3\cdot P\begin{bmatrix} & x & \\ o & o & x \\ & x & \end{bmatrix} \right)$$

$$+2h\cdot\left(P[o \quad x \quad o] + 2\cdot P\begin{bmatrix} & o \\ o & x \end{bmatrix} - P[o \quad o \quad x] - 2\cdot P\begin{bmatrix} & x \\ o & o \end{bmatrix} \right)$$

$$= 2p\cdot P[o \quad x] - P\begin{bmatrix} & x & \\ o & o & x \end{bmatrix} - 2\delta\cdot P[o \quad o \quad x] - 4\delta\cdot P\begin{bmatrix} & x \\ o & o \end{bmatrix}$$

$$+2h\cdot\left(P[o \quad - \quad o] + 2\cdot P\begin{bmatrix} & o \\ o & - \end{bmatrix} - 3\cdot P[o \quad o] \right) \qquad (2)$$

where again probabilities of configurations involving filled sites can be rewritten in terms of those just involving empty sites. The first gain terms in (1) and (2) (proportional to p) correspond to particle annihilation, the second group of loss terms to autocatalytic creation via the QCP mechanism, the third group (proportional to δ) to autocatalytic creation via the SCP mechanism, and the last three terms in the P[o o]-equation (proportional to h) to particle hopping. Particle hopping terms are absent in the P[o]-equation since hopping preserves particle number. After the second equality, we have implemented an exact summation and simplification of terms associated with particle creation for both QCP and SCP mechanisms.

Likewise, the hopping terms incorporate an exact cancellation and simplification applicable for the special case of particle hopping with simple site exclusion [25,26]. We also exploited rotational symmetries to identify equivalent contributions.

One can extend the above exact hierarchy to treat spatially non-uniform states [24]. Here, one introduces the probabilities $P[x_{i,j}] = C_{i,j}$ that site (i,j) is occupied, $P[o_{i,j}] = 1-C_{i,j}$ that site (i,j) is empty, $P[o_{i,j}\, o_{i+1,j}]$ that both sites (i,j) and (i+1,j) are empty, etc.. The form of the hierarchy naturally extends (1) and (2) above, but now hopping terms appear in the equation for the single-site quantity of the form [24] $d/dt\, P[o_{i,j}]|_{hop} = h(P[o_{i+1,j}]+P[o_{i,j+1}]+P[o_{i-1,j}]+P[o_{i,j-1}]-4P[o_{i,j}])$.

It is instructive to provide a mean-field analysis for the above QCP+SCP model. This corresponds to ignoring all spatial correlations, so probabilities of multi-site configurations factor as a product of constituent single-site probabilities. This treatment describes exactly behavior in the limit $h\rightarrow\infty$ where the system is "well-stirred" by rapid particle diffusion. We apply this procedure to the spatially non-uniform version of (1), and writing the result in terms of the possibly spatially varying particle concentration $C(\underline{r}=(i,j)a) = C_{i,j}$ at coarse-grained position $\underline{r}$ for lattice constant 'a'. One then obtains the mean-field reaction-diffusion equation (RDE)

$$\partial C/\partial t = R(C) + D\,\nabla^2 C \text{ with } R(C) = -p\cdot C + C^2(1-C) + 4\delta\cdot C(1-C), \qquad (3)$$

and where $D=a^2 h$ denotes the particle diffusion coefficient. One finds a stable uniform active steady state satisfying $p=C(1-C)+4\delta(1-C)$ for certain p, as well as a vacuum steady-state C=0.

A schematic of steady-state behavior (i.e., the equation of state) for $h\rightarrow\infty$ is presented in **Fig.2**. When $\delta < \delta_{tc} = ¼$, the model displays bistability of an active populated and vacuum state provided that $p_{s-}(\delta) < p < p_{s+}(\delta)$. The upper and lower spinodals satisfy

$p_{s-}(\delta) = 4\delta$ and $p_{s+}(\delta) = (1+4\delta)^2/4 = 4\delta + (1-4\delta)^2/4$. (4)

For $p<p_{s-}$ ($p>p_{s+}$), only the active (vacuum) state is stable. Bistability disappears at $\delta = \delta_{tc}$. For $\delta>\delta_{tc}$, one instead finds a continuous transition at $p=p_c(\delta) =4\delta$ from a unique stable active steady-state exists for $p<p_c(\delta)$ to a unique stable vacuum state for $p>p_c(\delta)$ [27].

Additional insight into steady-state behavior comes from writing

$R(C) = -d/dC\ U(C)$ with $U(C) = ½\ (p-4\delta)C^2 – 1/3\ (1-4\delta)C^3 + ¼\ C^4$. (5)

The effective free energy density, U(C), has a double-well form when $\delta < \delta_{tc}$ for $p_{s-}(\delta) < p < p_{s+}(\delta)$, and reduces to $U(C) = ¼\ C^2(2/3-8\delta/3 -C)^2$ with equal well heights when $p = p_{eq}(\delta) = 4\delta+(2/9)(4\delta–1)^2$. Insight into the significance of $p=p_{eq}(\delta)$ comes from analysis based on the RDE (3) for the evolution of an interface separating the stable active state from the stable vacuum state in the bistable region. One finds that the interface is stationary at $p = p_{eq}(\delta)$, i.e., this corresponds to the equistability point for the active and vacuum states within the bistable region.

Fig. 3 shows the phase diagram in the p-δ plane for the mean-field QCP+SCP including the spinodal lines, $p=p_{s\pm}(\delta)$, and the equistability line, $p=p_{eq}(\delta)$, for $\delta<\delta_{tc}$ which merge at $\delta=\delta_{tc}$. The continuation of these lines for $\delta>\delta_{tc}$ is given by $p=p_c(\delta)$ corresponding to the continuous transition. In a stochastic or statistical mechanical version of the model, $p_{eq}(\delta)$ would correspond to the location of a discontinuous transition. Thus, it is natural to introduce a general transition $p = p_{tr}(\delta)$ which would correspond to a discontinuous transition $p_{tr}(\delta) = p_{eq}(\delta)$ for $\delta<\delta_{tc}$ and a continuous transition $p_{tr}(\delta) = p_c(\delta)$ for $\delta>\delta_{tc}$. Thus, $\delta = \delta_{tc}$ would correspond to a tricritical point.

3. Simulation Results: Tricritical Behavior in the QCP+SCP

As δ increases from zero in the QCP+SCP for fixed particle hop rate $h<0$ (including $h=0$), one expects to observe a conversion from a discontinuous to a continuous transition upon reaching a tricritical value $\delta=\delta_{tc}(h)$. Our primary goal here is to apply kinetic Monte Carlo simulations to determine $\delta=\delta_{tc}(h)$. One complication is that the QCP for $\delta=0$ exhibits generic two-phase coexistence: stable active and vacuum states coexist not just for a single value of p (which would correspond to the location of the unique discontinuous transition for a thermodynamic system), but rather for a finite range $p_f(\delta) < p < p_e(\delta)$. The origin of this behavior is that the annihilation rate for equistability of active and vacuum states separated by a planar interface depends on the orientation of the interface, p_e (p_f) corresponds to diagonal (horizontal or vertical) interfaces. Thus, both $p_e(\delta)$ and $p_f(\delta)$ can be regarded as corresponding to special cases of equistability points, $p_{eq}(\delta)$. Previous analysis for the QCP with $\delta=0$ revealed that $p_e=0.0944$ and $p_f=0.0869$ when $h=0$, but that $\Delta p_{eq} = p_e - p_f$ decreases very quickly with increasing h from $\Delta p_{eq}=0.0075$ when $h=0$ to $\Delta p_{eq}<10^{-4}$ when $h=0.02$. Similarly, for fixed $h\geq 0$, we expect that generic two-phase coexistence persists for $\delta>0$, but that Δp_{eq} decreases quickly with increasing δ and vanishes at $\delta = \delta_{tc}$. New results for $h=0$ and increasing $\delta>0$ are shown in **Table I** confirming the very rapid decrease of Δp_{eq} with increasing δ [28].

Thus, as a practical matter, except very close to $(\delta, h)=(0, 0)$, one has that $p_e(\delta) \approx p_f(\delta)$ in the QCP+SCP for $\delta<\delta_{tc}$ and some fixed h corresponding to equistability of the two phases and to the location of a discontinuous transition $p_{tr}(\delta) = p_{eq}(\delta)$. For $\delta>\delta_{tc}$, the discontinuous transition is replaced by a continuous transition at $p = p_{tr}(\delta) = p_c(\delta)$.

Our initial goal for analysis of the QCP+SCP for fixed h (including h=0) and varying δ is to determine the value of $p= p_{tr}(\delta)$ of the transition as a function of δ. Rather than conventional "constant-p" simulations, it is more convenient to utilize "constant concentration (CC)" simulations [29]. In the former, one selects p and then decides whether to annihilate or create a particle at a randomly selected site based on this value. For the latter CC simulations [29], one selects a target particle concentration C_t and annihilates (creates) a particle and a randomly selected site if the actual concentration satisfies $C>C_t$ ($C<C_t$). The p-value associated with C_t is then determined from the fraction of attempts to annihilate a particle. The constant-p and the constant concentration simulations should be consistent for a large system. However, the latter are particularly convenient for determining the locations of discontinuous and continuous transitions, our initial objective here (as well as the regime of generic two-phase coexistence). These simulation results also provide an estimate of the location $\delta=\delta_{tc}$ of the conversion from a discontinuous to a continuous transition.

Fig.4a provides results from CC simulations for p versus C in the QCP+SCP with h=0 and various $\delta>0$. From these results, we extract precise estimates of the transition location $p=p_{tr}(\delta)$ versus $\delta>0$ shown in **Table II**. In addition, analysis of this data to determine $dp/dC|_{C=0}$ versus δ reveals a sudden transition from small positive to substantial negative values as δ exceeds $\delta_{tc}(h=0) \approx 0.032$. A refined determination of $\delta_{tc}(h=0)$ will be provided immediately below. These results for $p_{tr}(\delta)$ versus δ, the estimate of $\delta_{tc}(h=0)$, and also more detailed results for $p_e(\delta)$ and $p_f(\delta)$ versus δ from **Table I**, are summarized in **Fig.4b**.

For a more detailed characterization of behavior at the transition point $p=p_{tr}(\delta)$ and in particular at the tricritical point, $\delta=\delta_{tc}$, for the QCP+SCP with h=0, we perform an epidemic

analysis to assess the evolution of a patch of filled sites or of the active state embedded in the vacuum state. Of particular interest is the behavior at $p=p_{tr}(\delta)$ of survival probability, $P_s(t)$, versus t. For a continuous transition when δ exceeds δ_{tc}, one has that $P_s(t) \sim t^{-\zeta}$, as $t\to\infty$, where the exponent $\zeta = \zeta_{DP} \approx 0.451$ adopts the value of the directed percolation universality class [5,15]. However, exactly at the tricritical point, $\zeta = \zeta_{tc}$ will adopt a distinct value associated with the universality class of tricritical points, and for which we shall see that $\zeta_{tc} > \zeta_{DP}$. Furthermore, close to $\delta=\delta_{tc}$, the effective value of ζ would plausibly be controlled by ζ_{tc} rather than ζ_{DP}. For a discontinuous transition when $\delta<\delta_{tc}$, one expects that asymptotically $P_s(t)\to 0$ exponentially as $t\to\infty$ (at least for finite effective line tension of the interface between active and vacuum states). However, in practice, simulation data might mimic algebraic decay with a larger exponent ζ. The inset to **Fig.5** shows behavior of $P_s(t)$ versus t for the QCP+SCP with h=0 at $p=p_{tr}(\delta)$ for a broad range of δ=0.01-0.07 which is consistent with the above picture.

The above observations indicate that the effective ζ will evolve from values smaller than ζ_{tc} to values larger than ζ_{tc} as δ increases through δ_{tc}. Consequently, a plot of $\ln[P_s(t)]$ versus $\ln[t]$ should evolve from positive to negative curvature as δ increases through δ_{tc}. See the main part of **Fig.5** which shows higher quality data for a restricted range of δ around δ_{tc}. With this in mind, it is natural to fit simulation data for a suitable range of t to the form

$$\ln[P_s(t)] \approx - \zeta_0 - \zeta_1 \ln[t] - \zeta_2 (\ln[t])^2. \qquad (6)$$

Then, ζ_2 should evolve from negative values for $\delta<\delta_{tc}$ to positive values for $\delta>\delta_{tc}$. Thus, the optimum estimate of δ_{tc} should come from the value of δ when $\zeta_2=0$, and the optimum estimate of ζ_{tc} should come from the value of ζ_1 at this point. Thus, the simulation

data shown in **Fig.5**, and the associated ζ_1 and ζ_2 values reported in **Table III** from the range t=1000-8000 indicate that $\delta_{tc} \approx 0.034$ and $\zeta_{tc} \approx 1.24$ for the QCP+SCP with h=0.

Finally in this section, we briefly assess the location of the tricritical point in the QCP+SCP with finite h>0. Here, we just perform a CC analysis for various h>0 to determine $p_{tr}(\delta)$ versus δ, and the value of $\delta=\delta_{tc}(h)$. Results for C versus p with h=0.5 are shown in **Fig.6**, and an analysis of $dp/dC|_{C=0}$ versus δ reveals a sudden transition to negative values as δ exceeds $\delta_{tc}(h=0.5) \approx 0.032$. Results for $\delta_{tc}(h)$ from a similar analysis for other finite h, together with the exact result for $h=\infty$ from the mean-field analysis in Sec.2, are plotted to show the entire tricritical line in **Fig.7**.

4. Pair-Approximation Analysis: Tricritical Behavior in the QCP+SCP

First, we consider an approximate analysis of the exact master equations for spatially uniform states. The lowest-order mean-field site-approximation (which ignores all spatial correlations) fails to capture the h-dependence of the reaction kinetics which is of interest here. However, this dependence is incorporated in the higher-order approximations. Here, we consider only the pair-approximation [24,30]. In the hierarchical master equations for uniform states (1), this approximation factorizes multi-site probabilities in the particle creation terms as products of the m constituent pair probabilities and divides by $P[o]^{m-1}$ to avoid over-counting of the shared central empty site. One thereby obtains a closed set of equations for single-site and pair probabilities. In addition, hopping terms involving the probabilities of separated pairs of empty sites are factorized as $P[o]^2$. Thus, the pair-approximation yields the equations

$$d/dt\, P[o] = p\cdot P[x] - P[o\,x]^2/P[o] + 4\delta\cdot P[o\,x]\,, \text{ and}$$

$$d/dt\, P[o\,o] = 2p\cdot P[o\,x] - P[o\,x]^2\, P[o\,o]/P[o]^2 - 6\delta\cdot P[o\,o]P[o\,x]/P[o] + 6h(P[o]^2 - P[o\,o]), \quad (7)$$

which can be closed using P[x] = 1-P[o] and P[xo] = P[o]-P[oo].

Below it is convenient to introduce the conditional probability or concentration, K = P[xo]/P[o], of finding a particle adjacent to a prescribed empty site. Due to spatial correlations, K is distinct from the concentration C = P[x] = 1-P[o]. Then, noting that P[xo] = K(1-C) and that P[o o] = (1-K)(1-C), the pair-approximation then yields the kinetic equations

$$\begin{aligned}(1-C)^{-1}\, d/dt\, C &= p\cdot C/(1-C) - K^2 - 4\delta\cdot K, \text{ and}\\ (1-C)^{-1}\, d/dt\,[(1-K)(1-C)] &= [2p - K(1-K) - 6\delta(1-K)]K + 6h(K-C).\end{aligned} \quad (8)$$

The hopping term in the second equation of (8) forces $K\to C$ as $h\to\infty$, thus correctly recovering mean-field behavior corresponding to the absence of spatial correlations.

Our primary interest is in the analysis of steady-state behavior where dC/dt=dK/dt=0. Eliminating C from the steady-state form of (8) yields

$$[2p-K(1-K)-6\delta(1-K)][p+K^2+4\delta K] + 6h[p-K(1-K)-4\delta(1-K)] = 0. \quad (9)$$

The motivation for selecting K as the natural variable over C is particularly clear for the case h=0, which we now discuss in some detail (analogous to our simulation treatment).

For the QCP+SCP with h=0, the steady-state relation (9) reduces to $2p-K(1-K)-6\delta(1-K)=0$. Thus, analysis of tricritical behavior is no more difficult than for the mean-field treatment corresponding to $h\to\infty$. It is readily shown that when $\delta < \delta_{tc} = 1/6$, the model displays bistability of an active populated and vacuum state provided that $p_{s-}(\delta) < p < p_{s+}(\delta)$. The upper and lower spinodals predicted from the pair-approximation satisfy

$$p_{s-}(\delta) = 3\delta \text{ and } p_{s+}(\delta) = (1+6\delta)^2/8 = 3\delta + (1-6\delta)^2/8. \quad (10)$$

For $p<p_{s-}$ ($p>p_{s+}$), only the active (vacuum) state is stable. Bistability disappears at $\delta = \delta_{tc}$. For $\delta>\delta_{tc}$, one instead finds a continuous transition at $p=p_c(\delta)=3\delta$ from a unique stable active steady-state exists for $p<p_c(\delta)$ to a unique stable vacuum state for $p>p_c(\delta)$ [27]. A more complete analysis of pair-approximation predictions for steady-state behavior when h=0 is shown in **Fig.8**. This is the analogue of **Fig.2** for mean-field behavior where $\delta_{tc} = ¼$ for $h=\infty$.

For a comprehensive analysis of pair-approximation behavior and comparison with simulation predictions for h=0 (or any finite h>0), it is necessary to determine equistability values for p in the bistable region when $\delta<\delta_{tc}$. This requires consideration of spatially non-uniform states, specifically the evolution of planar interfaces separating stable active and vacuum states. To this end, it is necessary to apply the pair-approximation to the spatially-non-uniform version of the hierarchical master equations (1) and (2) which were discussed briefly in Sec.2. This yields a coupled set of discrete RDE's for site dependent particle concentration, $C_{i,j}$, and related pair probabilities. (For a development of such equations in the pair-approximation for the QCP, see Ref.[24] for h=0 and Ref.[31] for h>0. For lower-level site-approximation developments of such equations for other reaction-diffusion models, see Ref.[32-33].) Analysis of interface propagation described by these equations reveals a dependence on orientation, just as seen in simulation studies of the QCP+SCP. Specifically, we find that the equistability value of p depends on interface orientation, corresponding to generic two-phase coexistence.

For the QCP+SCP with h=0, results for the equistability p versus δ for horizontal (or vertical) and for diagonal interfaces predicted from the pair-approximation are shown in **Table IV**. These values quickly merge with increasing δ, just as do p_e and p_f in the simulation analysis for h=0 (although merging of the latter is even faster; cf. Table I). **Fig. 9** shows pair-approximation prediction for the phase diagram in the p-δ plane for the QCP+SCP model with h=0 including the spinodal lines, $p=p_{s\pm}(\delta)$, and the equistability line, $p=p_{eq}(\delta)$, for $\delta<\delta_{tc}$ which merge at $\delta=\delta_{tc}$. The continuation of these lines for $\delta>\delta_{tc}$ is given by $p=p_c(\delta)$ corresponding to the continuous transition. The mean-field analogue of this plot is provided by **Fig.3**, and the analogue from simulation studies is provided by **Fig.4b** (but without the spinodal lines).

Finally, for the general QCP+SCP with h≥0, Fig.10 presents the results of a pair-approximation steady-state analysis based on (9) to determine the tricritical line δ_{tc} versus h. The analogue of this plot from simulation studies is provided by **Fig.7**. In both cases, δ_{tc} increases monotonically with h reaching the same mean-field value of $\delta_{tc} = ¼$ for $h=\infty$. However, the pair-approximation is not able to accurately predict the value of δ_{tc}, and thus its variation for small h.

5. Conclusions

In summary, we have provided a comprehensive analysis of tricritical behavior in a lattice-gas realization of a hybrid version of Schloegl's first and second models for autocatalysis with particle diffusion. This models also corresponds to a combination of the standard Contact Process (SCP) and Quadratic Contact process (QCP) on a square lattice. Of

particular focus in our study was mapping out of the tricritical line as a function of hop rate showing convergence to the mean-field value in the limit of rapid hopping. In addition, we provided a detailed analysis of trictitical behavior for the special case of the model without particle hopping, specifically determining an “epidemic exponent”. It should be noted that a previous study considered a modified version of this hybrid model on various lattices without particle hopping obtaining a number of other exponents related to tricritical behavior [15].

Acknowledgements

This work was supported by the Division of Chemical Sciences of the U.S. Department of Energy (Basic Energy Sciences). It was performed at Ames Laboratory which is operated for the USDOE by Iowa State University under Contract No. DE-AC02-07CH11358. DU was also supported by NSF REU Grant CHE-0453444.

References

[1] G. Nicolis and I. Prigogine, *Self-Organization in Non-Equilibrium Systems* (Wiley, New York, 1977).
[2] A.S. Mikhailov, *Foundations of Synergetics I* (Springer, Berlin, 1990).
[3] H. Malchow and L. Schimanski-Geier, *Noise and Diffusion in Bistable Nonequilibrium Systems* (Teubner, Berlin, 1985).
[4] J.W. Evans, D.-J. Liu, and M. Tammaro, Chaos **12**, 131 (2002).
[5] J. Marro and R. Dickman, *Nonequilibrium Phase Transitions in Lattice Models* (Cambridge UP, Cambridge, 1999).
[6] H. Hinrichsen, Adv. Phys. **49**, 815 (2000).
[7] G. Odor, Rev. Mod. Phys. **76**, 663 (2004).
[8] R.M. Ziff, E. Gulari, and Y. Barshad, Phys. Rev. Lett. **56**, 2553 (1986).
[9] J.W. Evans and M.S. Miesch, Phys. Rev. Lett. **66**, 833 (1991).
[10] J.W. Evans and T.R. Ray, Phys. Rev. E, **50**, 4302 (1994).
[11] R. H. Goodman, D. S. Graff, L. M. Sander, P. Leroux-Hugon, and E. Clément Phys. Rev. E **52**, 5904 (1995).
[12] E. Loscar and E.V. Albano, Rep. Prog. Phys. **66**, 1343 (2003).
[13] E. Machado, G.M. Buendia, and P.A. Rikvold, Phys. Rev. E **71**, 031603 (2005).
[14] D.-J. Liu, X. Guo, and J.W. Evans, Phys. Rev. Lett. **98**, 050601 (2007).

[15] S. Luebeck, J. Stat. Phys. 123, 193 (2006).
[16] F. Schloegl, Z. Phys. **253**, 147 (1972).
[17] P. Grassberger, Z. Phys. B Cond. Matt. **47**, 365 (1982).
[18] J.P. Boon, D. Dab, R. Kapral, and A. Lawniczak, Rep. Mod. Phys. **273**, 55 (1996).
[19] S. Prakash and G. Nicolis, J. Stat. Phys. **86**, 1289 (1997).
[20] R. Durrett, SIAM Rev. **41**, 677 (1999).
[21] X. Guo, D.-J. Liu, and J.W. Evans, Phys. Rev. E, **75**, 061129 (2007).
[22] X. Guo, D.-J. Liu, and J.W. Evans, J. Chem. Phys. **130**, 074106 (2009).
[23] J.W. Evans, Rev. Mod. Phys. **65**, 1281 (1993).
[24] X. Guo, J.W. Evans, and D.-J. Liu, Physica A **387**, 177 (2008).
[25] R. Kutner, Phys. Lett. **81A**, 239 (1981).
[26] J.W. Evans and D.K. Hoffman, Phys. Rev. B **30**, 2704 (1984).
[27] In either regime, the active steady-state coverage satisfies $2C_{eq} =(1-4d)+[(1-4d)^2-4(p-4d)]^{1/2}$.
[28] The decrease of Δp_{eq} with δ is very similar to that for a related model where the SCP mechanism is replaced by spontaneous creation at empty sites at rate δ. See D.-J. Liu, J. Stat. Phys. **135**, 77 (2009). Note that for a high-concentration active state, there should not be much difference between the SCP mechanism and spontaneous creation.
[29] R.M. Ziff and B.J. Brosilow, Phys. Rev. A **46**, 4630 (1992).
[30] R. Dickman, Phys. Rev. A **34**, 4246 (1986).
[31] X. Guo and J.W. Evans, Phys. Rev. E, submitted (2009).
[32] P. Fischer and U.M. Titulaer, Surf. Sci. **221**, 409 (1989).
[33] Y. De Decker, G.A. Tsekouras, A. Provata, Th. Erneux, and G. Nicolis, Phys. Rev. E **69**, 036203 (2004).

Table

Table I. Values of p_e and p_f versus δ for the QCP+SCP with h=0.

δ	p_f	p_e
0	0.0869	0.09443
0.0001	0.0901	0.09456
0.0002	0.0910	0.09503
0.0005	0.0929	0.09549
0.001	0.0947	0.09622
0.002	0.0974	0.09798

Table II. Location of the transition $p=p_{tr}(\delta)$ for the QCP+SCP with h=0.

δ	p_{tr}
0.01	0.11554
0.02	0.13622
0.03	0.15669
0.04	0.17787
0.05	0.19941
0.06	0.22203
0.07	0.24490

Table III. Values of parameters ζ_1 and ζ_2 versus δ for the QCP+SCP with h=0.

δ	ζ_1	ζ_2
0.030	1.47357	-0.06994
0.032	1.50569	-0.07333
0.034	1.20198	0.01006
0.036	1.04131	0.02397
0.038	0.92689	0.04320
0.040	0.77899	0.09712

Table IV. Pair-approximation prediction of equistability points in the QCP+SCP with h=0.

δ	p_{eq}(horizontal/ vertical)	p_{eq}(diagonal)
0.0	0.1060	0.1083
0.01	0.12530	0.12607
0.02	0.14416	0.14447
0.03	0.16342	0.16356
0.04	0.18329	0.18336
0.10	0.31772	0.31772
1/6	1/2	1/2

Figures

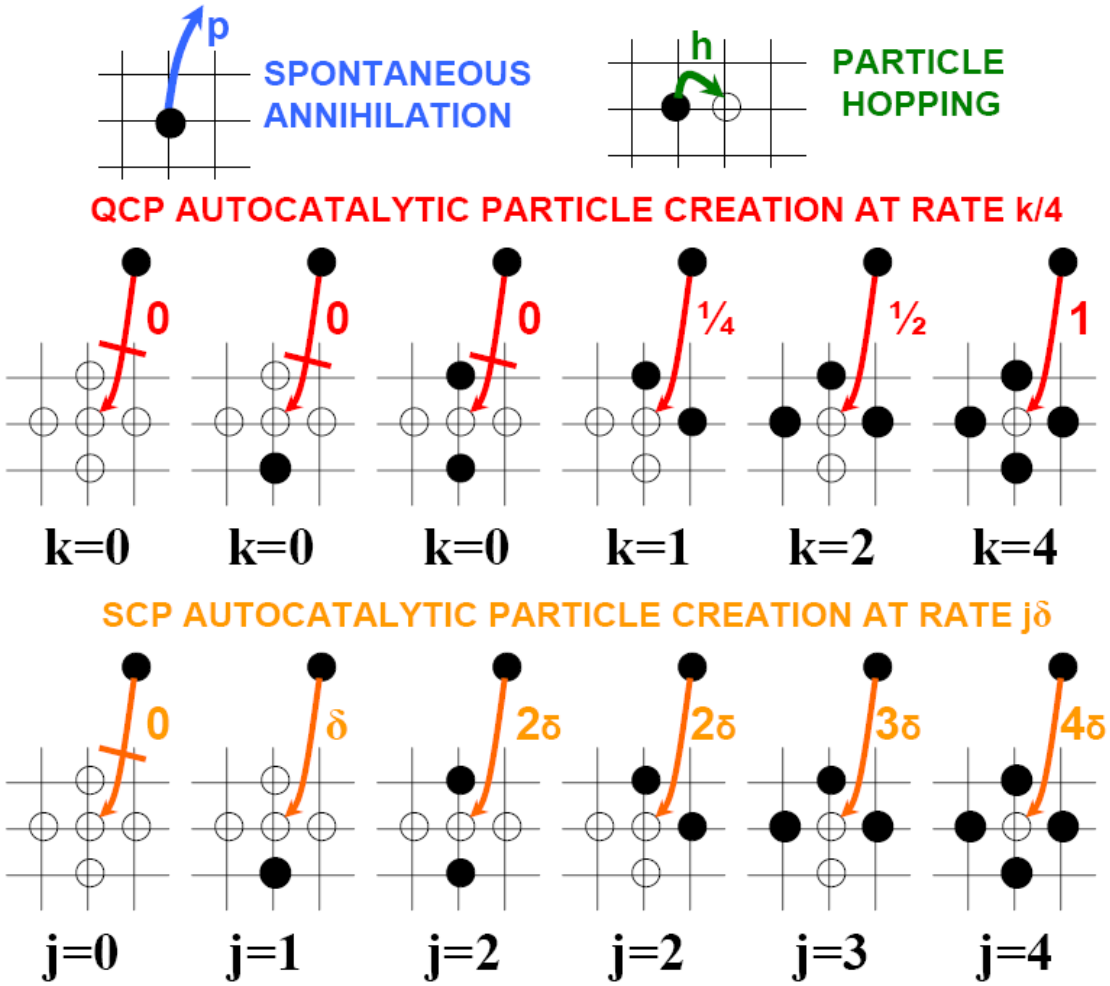

Figure 1. Schematic of particle annihilation, autocatalytic creation, and hopping processes in our generalized Schloegl model (QCP+SCP) on a square lattice. Here particles are denoted by filled circles (•) and empty sites by open circles (o). Rates for the various processes are also indicated, and the bar through the arrow indicates that the process is inactive.

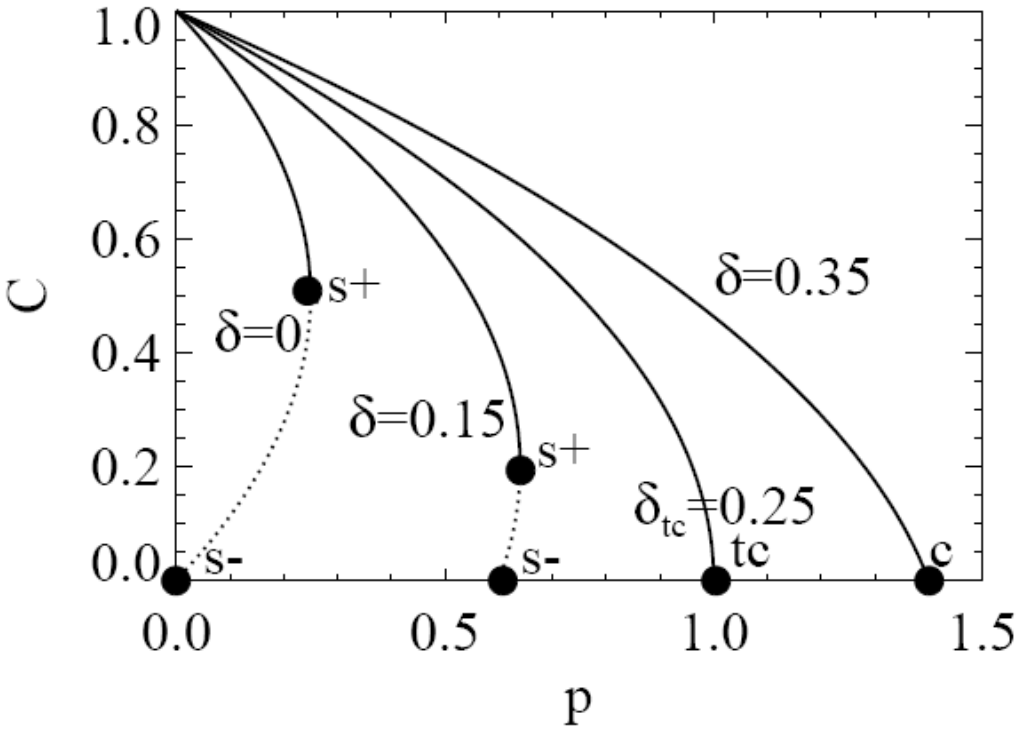

Figure 2: Mean-field steady-state behavior for particle concentration, C, versus p in the QCP+SCP. For $\delta<\delta_{tc}$ = ¼ below the tricritical point (tc), we show upper (s+) and lower (s-) spinodals bordering the region of bistability. For $\delta<\delta_{tc}$, we show the location of the continuous transition (c) to the vacuum state.

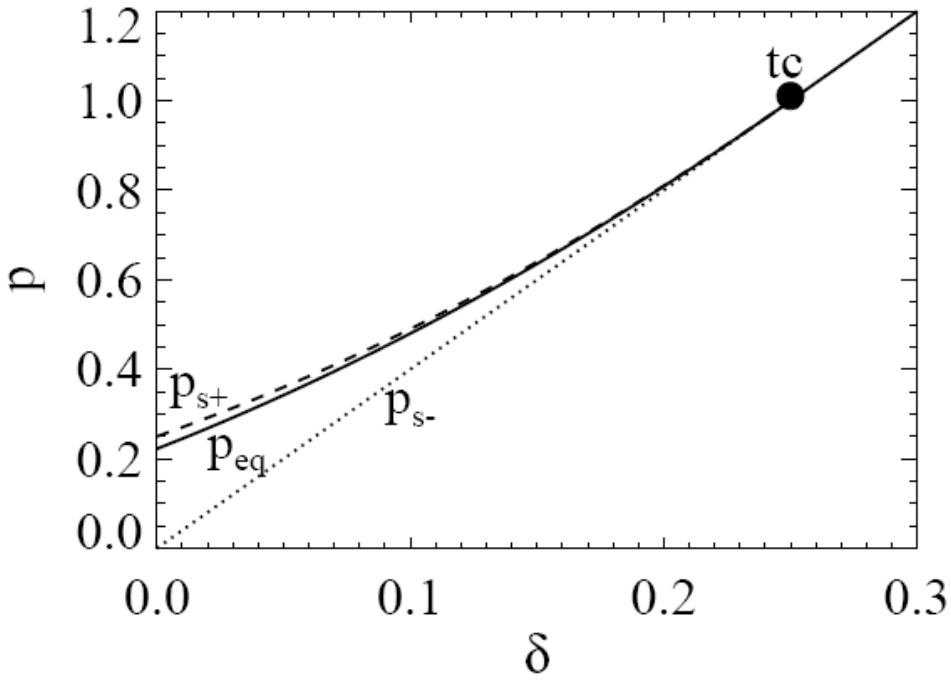

Figure 3: Phase diagram in the p-δ plane for the mean-field QCP+SCP including the spinodal lines, $p=p_{s\pm}(\delta)$, and the equistability line, $p=p_{eq}(\delta)$, for $\delta<\delta_{tc}$ below the tricritical point (tc) which merge at $\delta=\delta_{tc}$. The continuation of these lines for $\delta>\delta_{tc}$ is given by $p=p_c(\delta)$ corresponding to the continuous transition.

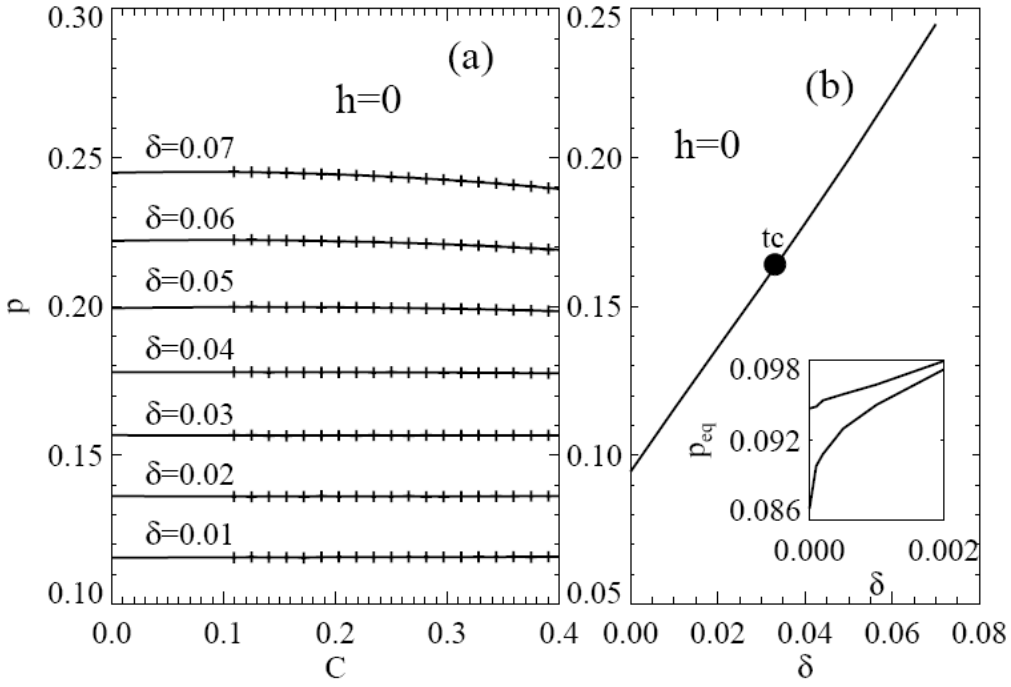

Figure 4: Simulation analysis of the QCP+SCP for h=0: (a) Results of CC simulations for p versus $C=C_t$ used to determine $p_{tr}(\delta)$ versus δ by extrapolation of C(p) versus p to C=0; (b) Plot of results for $p_{tr}(\delta)$ versus δ obtained from (a), also showing the tricritical point (tc). The inset shows p_e (lower curve) and p_f (upper curve) versus δ for a range of very small δ where they are significantly different.

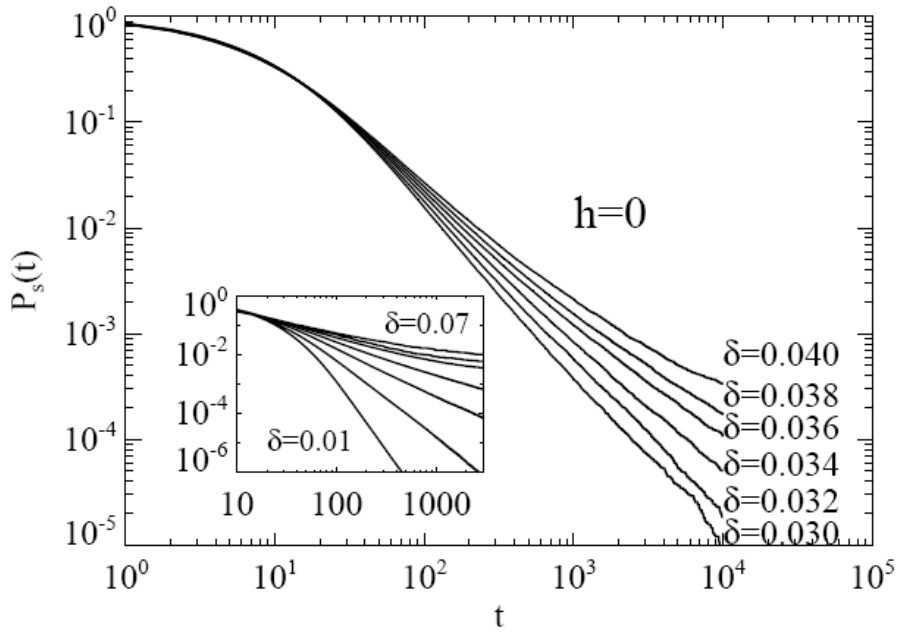

Figure 5: Epidemic analysis for the QCP+SCP with h=0. Survival probability, $P_s(t)$, versus time, t, for a single occupied site embedded in the vacuum state for various δ choosing $p=p_{tr}(\delta)$ with values given in Table II. The inset shows behavior for a broad range of δ varying between 0.01 and 0.07 in increments of 0.01. The main plot shows high-quality data in the vicinity of the tricritical point used to estimate $\delta_{tc} \approx 0.034 \pm 0.001$ and $\zeta_{tc} \approx 1.24$.

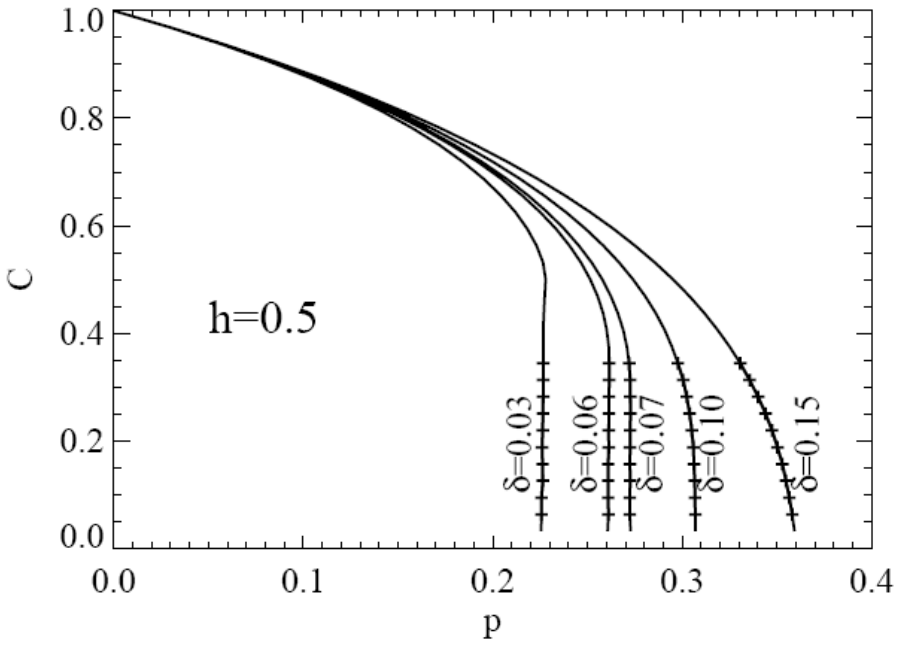

Figure 6: CC simulation results for the QCP+SCP with h=0.5 showing p versus C (or equivalently C versus p) for various δ. This data is used to estimate $\delta_{tc}(h=0.5) \approx 0.070$.

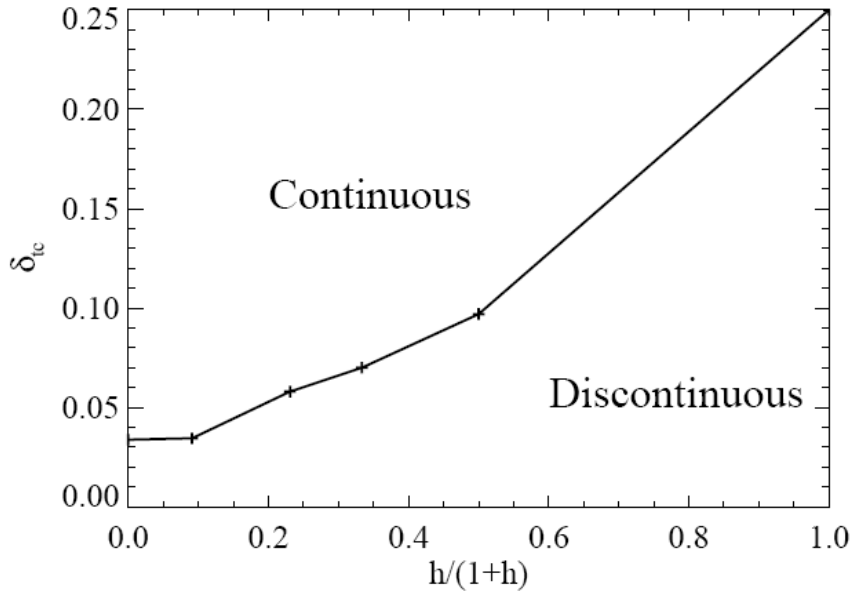

Figure 7: Simulation results for the tricritical line, $\delta_{tc}(h)$, versus h for the general QCP+SCP with $h \geq 0$. This line separates regions of discontinuous (below) and continuous (above) transitions.

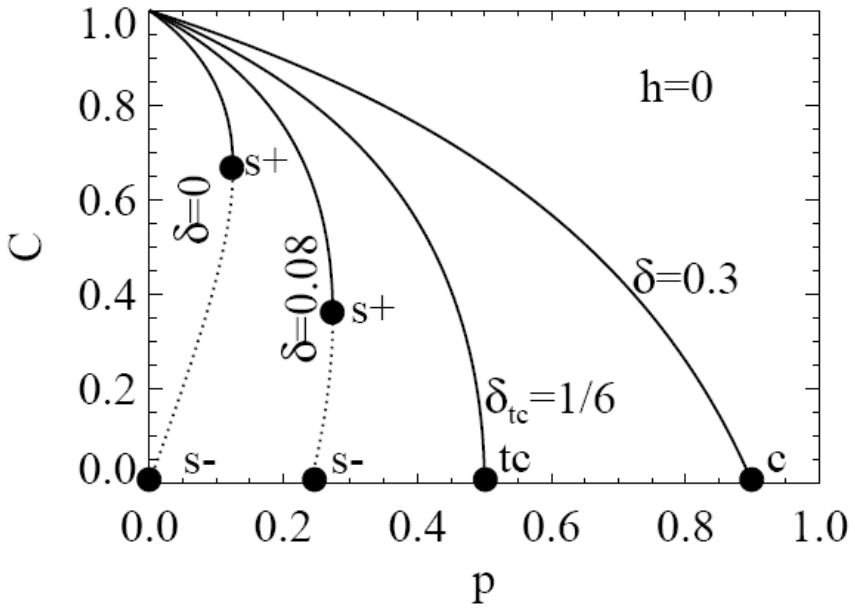

Figure 8: Pair-approximation predictions for steady-state behavior for particle concentration, C, versus p in the QCP+SCP with h=0. For $\delta<\delta_{tc} = 1/6$ below the tricritical point (tc), we show upper (s+) and lower (s-) spinodals bordering the region of bistability. For $\delta<\delta_{tc}$, we show the location of the continuous transition (c) to the vacuum state.

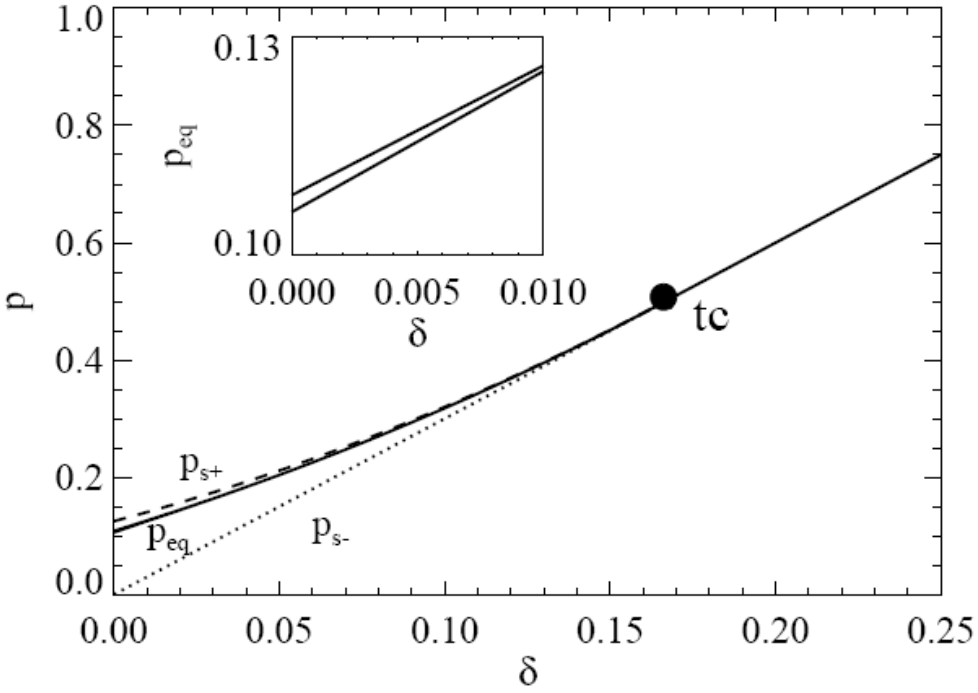

Figure 9: Pair-approximation predictions for the phase diagram in the p-δ plane for the mean-field QCP+SCP with h=0. including the spinodal lines, $p=p_{s\pm}(\delta)$, and the equistability line, $p=p_{eq}(\delta)$, for $\delta<\delta_{tc}$ below the tricritical point (tc) which merge at $\delta=\delta_{tc}$. The continuation of these lines for $\delta>\delta_{tc}$ is given by $p=p_c(\delta)$ corresponding to the continuous transition. The inset shows distinct values for p_{eq} for horizontal or vertical interafces (lower curve) and for diagonal interfaces (upper curve) versus δ for a range of very small δ where they are significantly different.

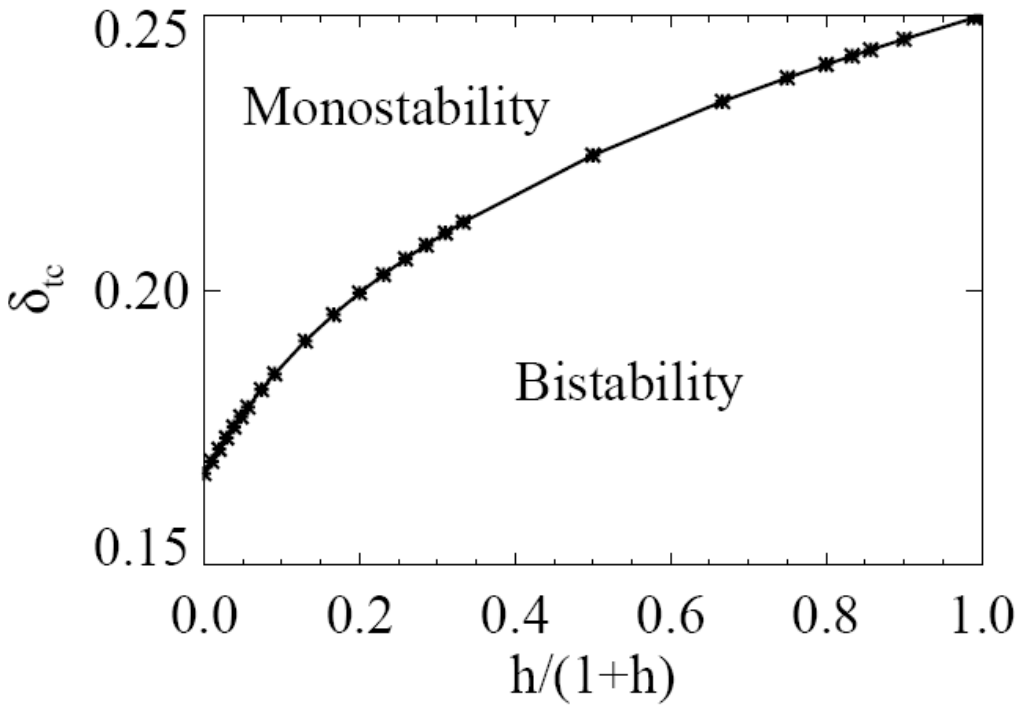

Figure 10: Pair-approximation predictions for the tricritical line, $\delta_{tc}(h)$, versus h for the general QCP+SCP with $h \geq 0$. This line separates regions of bistability (below) and monostability (above).

CHAPTER 7. GENERAL CONCLUSIONS

The studies in this thesis have focused on analysis of a non-equilibrium statistical mechanical model for reactions, specifically a realization of Schloegl's second model for autocatalysis on a square lattice (also known as the Quadratic Contact process). While this model, and similar models, exhibit some features which are similar to equilibrium models described by a Hamiltonian (e.g., discontinuous phase transitions and associated metastability and nucleation phenomena), there are also fundamental differences. Perhaps most significant is the discovery for the QCP of generic two-phase coexistence, i.e., two distinct stable phases or states in the reaction model can coexist for a finite range of control parameter. This contrasts behavior in equilibrium systems which phases can coexist only at a single point in parameter space (where the chemical potentials of the two phases are equal). The various chapters in the thesis present a detailed analysis of this novel phenomenon for the QCP and its variations or generalizations. One related topic of particular interest was the analysis of metastability phenomena in these non-equilibrium systems where the standard tools and concepts of thermodynamics are not available to facilitate understanding. Indeed this type of issue has been highlighted in the report of the Basic Energy Sciences Advisory Committee (BESAC) of the US Department of Energy as one of five Science Grand Challenge Areas. We have also made significant progress on analyzing such metastability phenomena.

In closing, to summarize the developments and discoveries from the work presented in this thesis, we present a bulleted list of the main highlights:

*Discovery utilizing kinetic Monte Carlo simulation of generic two-phase coexistence (2PC) in a stochastic realization of Schloegl's second model for autocatalysis, or equivalently the Quadratic Contact process.

*Demonstration of the failure of the Durrett hypothesis pertaining to the above model with particle diffusion (as a direct consequence of 2PC).

*Development of exact master equations and approximate hierarchical truncations to provide an effective (semi-quantitative) treatment of the above models.

*Development and analysis of discrete reaction-diffusion equations for spatially inhomogeneous states associated with the above approximations, together with development and application of a novel iterated map strategy for their analysis.

*Detailed analysis of metastability associated with the discontinuous phase transition in the above models. Development and application of appropriate concepts to describe nucleation phenomena in these non-equilibrium models.

*Development of hybrid or generalized Schloegl's models which exhibit tricritical behavior, and analysis of this behavior using constant concentration simulations and epidemic analysis.

*Analysis of critical and stationary droplets in the above models at the level of the site-approximation to the master equations for spatially non-uniform states. Discovery of a new phenomenology of stationary droplets with a range of sizes (contrasting the traditional picture of critical droplets).

*Extension of the QCP and related models to a variety of lattices (other than the square lattice).

This work was supported by the Division of Chemical Sciences and also by the SciDAC Computational Chemistry Program of the U.S. Department of Energy (Basic Energy Sciences). It was performed at Ames Laboratory which is operated for the USDOE by Iowa State University under Contract No. DE-AC02-07CH11358.

APPENDIX A: FINITE-SIZE SCALING ANALYSIS

Here, we provide some additional discussion of the type of simulation analysis presented in Chapter 2 and Chapter 4 for the Quadratic Contact Process potentially with particle hopping. Specifically, we check for finite-size effects in these simulations, i.e., a dependence of key quantities on the size of the simulation system. In principle, any finite system must evolve to the absorbing state. However, in practice for larger systems, the time-scale for this evolution is far longer than assessed by simulation. Nonetheless, there can be some dependence of key quantities on system size. Our intent here is to assess this dependence.

To this end, for $h \geq 0$, we perform constant-coverage (CC) simulations in rectangular $L_x \times L_y$ site systems with $L_y = SL_x$ starting from an initial filled strip of slope S of the absorbing state for target coverage $\theta=0.5$. The goal is to assess the equistability pressure, p_{eq}, for an interface of slope S. Here, we show the cases of h=0 and h=0.001. Simulations indicate clear slope dependence as discussed in previous chapters.

For h=0 and S>0, p_{eq} depends only very weakly on L_y (i.e., very weak finite-size effects) with $p_{eq}(L_y \rightarrow \infty) = 0.09443$, 0.09400, and 0.09283, for S=1, 2, and 4, respectively [1]. See Fig. 1(a). For h=0 and for the special case S=0(∞) [1], there is particular concern regarding finite-size effects and the adsorbing state cannot shrink. In fact, it could "grow artificially" even for small p in any finite system, thus potentially corrupting the estimate of p_{eq}. For this reason, we perform we perform CC simulations for a sequence of systems with $L_y = 2^n L_x$ containing a vertical interface of length $2^n L_x$, and extrapolate behavior $n \rightarrow \infty$ for

different simulation times (in order obtain the most accurate estimate of behavior for $n \to \infty$) [1]. See Fig. 1(b).

For h=0.001, we find a slightly stronger dependence of p_{eq} on L_y (with differing behavior for different S) with $p_{eq}(L_y \to \infty)$ = 0.09592, 0.09563, 0.09496, and 0.0944, for S=1, 2, 4, and 0(∞), respectively. See Fig.2.

References

[1] D.-J. Liu, Xiaofang Guo, and J. W. Evans, Phys. Rev. Lett. 98, 050601 (2007).

Figures

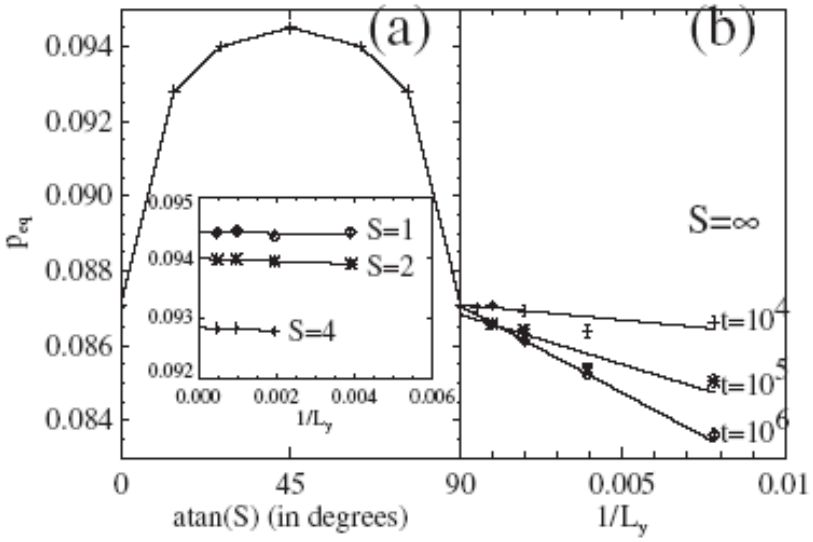

Figure 1. Quadratic Contact Process for h=0. (a) Dependence of p_{eq} on interface slope S. Inset shows CC simulation analysis of system size effects for S = 1, 2, and 4, (b) Analysis of effect of system size and CC simulation time on estimates for p_{eq} (S=∞).

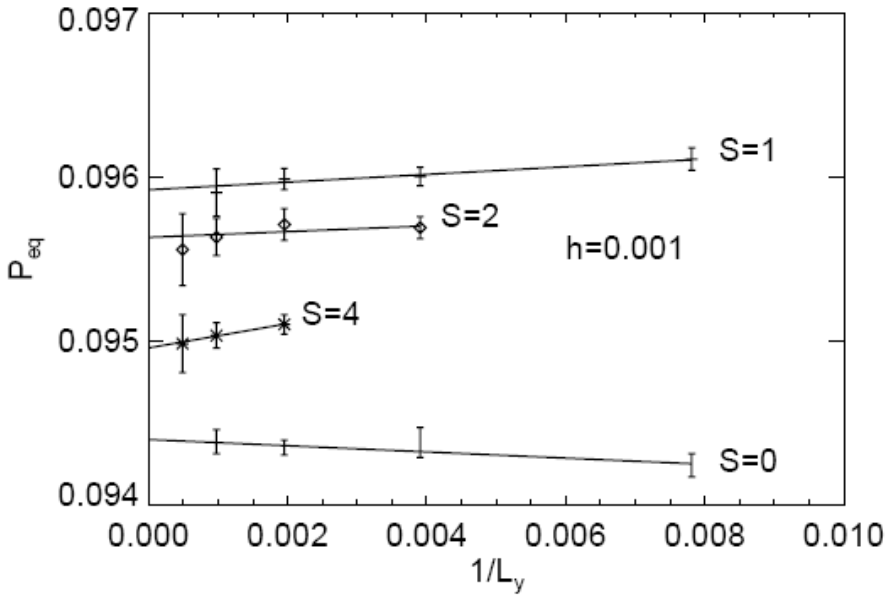

Figure 2. Quadratic Contact Process for h=0.001. CC simulation analysis of system size effects on p_{eq} for S=0, 1, 2, and 4.

APPENDIX B: PAIR-APPROXIMATION FOR INTERFACE EVOLUTION IN A LG ADSORPTION-DESORPTION MODEL REALIZATION OF THE 2D ISING MODEL

In a lattice-gas (LG) adsorption-desorption model realization of the Ising model, the adsorption rate is proportional to p, and desorption rate is proportional to α^n, $0 \le \alpha \le 1$, n is the number of filled nearest-neighbor (NN) sites. For a spatially uniform system, the first entry in the hierarchical form of the master equations has the form

$$\begin{aligned} d/dt\ P[x] = p \cdot P[o] - \binom{4}{0} \cdot P\begin{bmatrix} & o & \\ o & x & o \\ & o & \end{bmatrix} - \alpha \cdot \binom{4}{1} \cdot P\begin{bmatrix} & o & \\ x & x & o \\ & o & \end{bmatrix} - \alpha^2 \cdot \binom{4}{2} \cdot P\begin{bmatrix} & x & \\ x & x & o \\ & o & \end{bmatrix} \\ - \alpha^3 \cdot \binom{4}{3} \cdot P\begin{bmatrix} & x & \\ x & x & x \\ & o & \end{bmatrix} - \alpha^4 \cdot \binom{4}{2} \cdot P\begin{bmatrix} & x & \\ x & x & x \\ & x & \end{bmatrix} \end{aligned} \tag{1}$$

where x denotes a filled site, and o denotes an empty site.

Here we consider the simplest mean-field site approximation which ignores all spatial correlations. Then, above equation can be written as

$$\frac{d\theta}{dt} = p(1-\theta) - \theta(1-\theta+\alpha\cdot\theta)^4 \tag{2}$$

where we introduce the notation θ=P[x].

For steady-state, we have

$$\frac{d\theta}{dt} = 0 \Rightarrow p = \frac{\theta(1-\theta+\alpha\cdot\theta)^4}{1-\theta} \tag{3}$$

There exists a critical value, $\alpha_c = 0.36$, for the parameter α, such that the steady-states exhibit bistability for $\alpha < \alpha_c$. Fig.1 illustrates this feature. We can also determine the upper

and lower limits, P_{s+} and P_{s-}, for the regime of bistability. See Fig.2. Table 1 lists P_{s+} and P_{s-} values for various α.

To determine the equistability pressure, we analyze the propagation of interfaces separating stable coexisting stable states or phases. To perform this analysis, we need to extend the master equation formulation to treat spatially non-uniform states. We consider the vertical interfaces with S=∞, and the diagonal interfaces with S=1 separating active and absorbing states for p<p_s(site) and $\alpha < \alpha_c$. In the site approximation, for the case S=∞ (vertical interfaces), we have

$$dP_x^i/dt = p \cdot P_o^i - \left(P_o^{i-1} + \alpha \cdot P_x^{i-1}\right)^2 \left(P_o^{i+1} + \alpha \cdot P_x^{i+1}\right)^2 P_x^i \qquad (4)$$

For the case S=1 (diagonal interfaces), we have

$$dP_x^i/dt = p \cdot P_o^i - \left(P_o^i + \alpha \cdot P_x^i\right)^2 \left(P_o^{i+1}P_o^{i-1} + \alpha \cdot (P_x^{i-1}P_o^{i+1} + P_o^{i-1}P_x^{i+1}) + \alpha^2 P_x^{i-1}P_x^{i+1}\right)P_x^i \qquad (5)$$

Results within the site approximation for the interface propagation velocity, V (p, S, α) versus p with fixed α=0.05 and α=0.3 are shown in Fig. 3. These results are obtained from numerical analysis of (4) and (5) for vertical and diagonal interfaces. We find that V(p) = 0 for vertical interface not just at a single point, but for finite range of p which crosses the point $V(p_{eq}, S=1) = 0$, i.e., one has propagation failure for a finite region. As α approaches to α_c, this propagation failure region becomes narrow. For α = 0.05, this range is 0.0084-0.0147, and for s=1 p_{eq} is around 0.0112-0.0113. For α = 0.3, the width of the propagation failure region is neglibible, so $p_{eq}(s=1) \approx p_{eq}(s=\infty) = 0.1643$.

Table 1. p_{s-} and p_{s+} for different α

α	P_{s-}	P_{s+}
0.05	0.00110593	0.113027
0.10	0.00082088	0.12182
0.15	0.00055279	0.132208
0.20	0.00052786	0.144721
0.25	0.00075314	0.160205
0.30	0.00149854	0.180175
0.35	0.00205853	0.208279

Figures

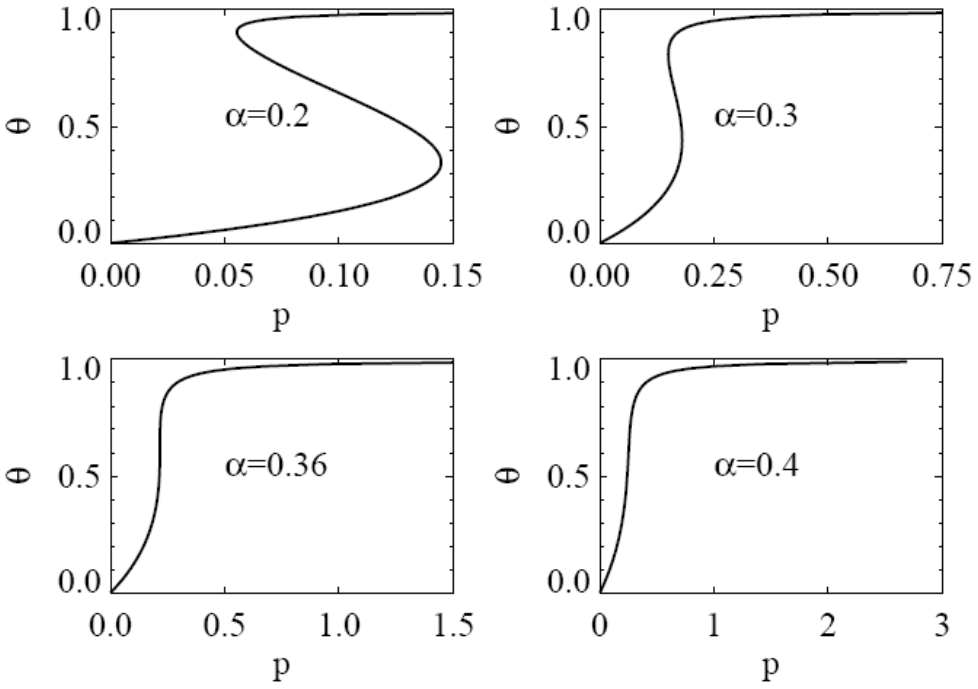

Figure 1. Steady-state coverage behavior for fixed value α

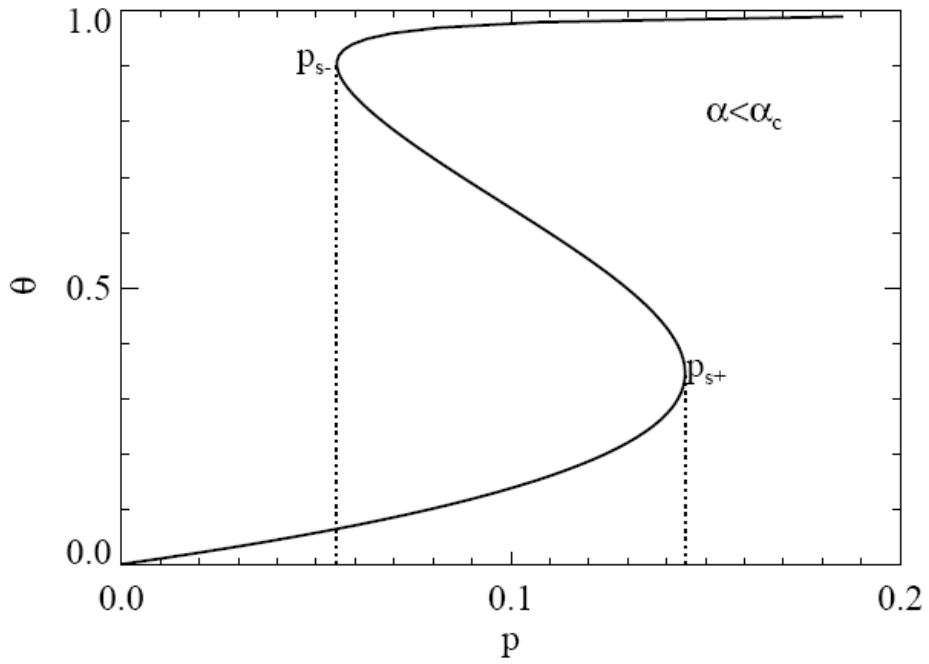

Figure 2. Schematic showing p_{s+} and p_{s-}

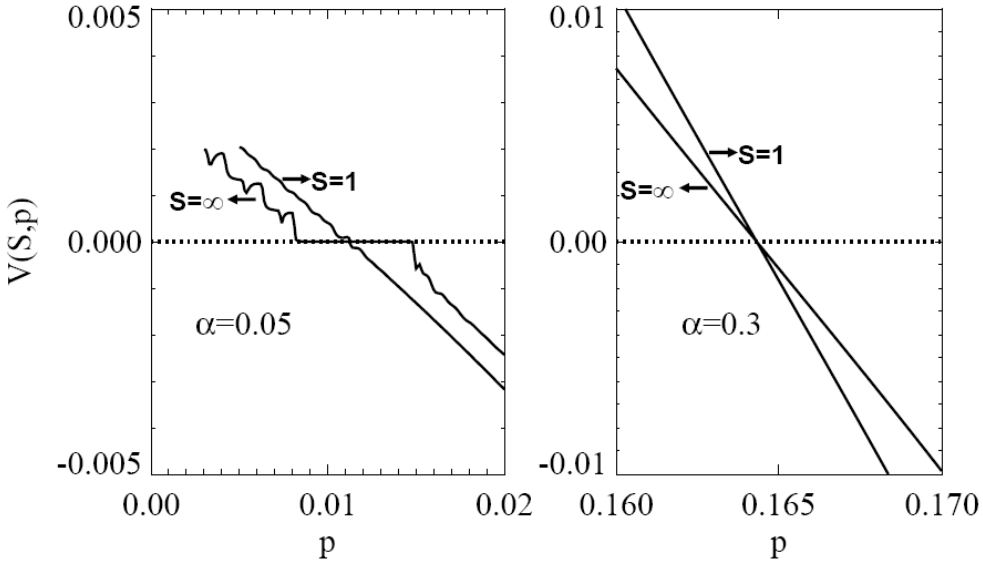

Figure 3. V (p, S) versus p from site approximation for S=1 and S=∞ with fixed α

APPENDIX C: SUPPLEMENTARY RESULTS FOR QCP WITH PARTICLE HOPPING

In this Appendix, we provide some additional results from KMC simulation and from analysis of the pair approximation for QCP with particle hopping. These results supplement those presented in Chapter 5.

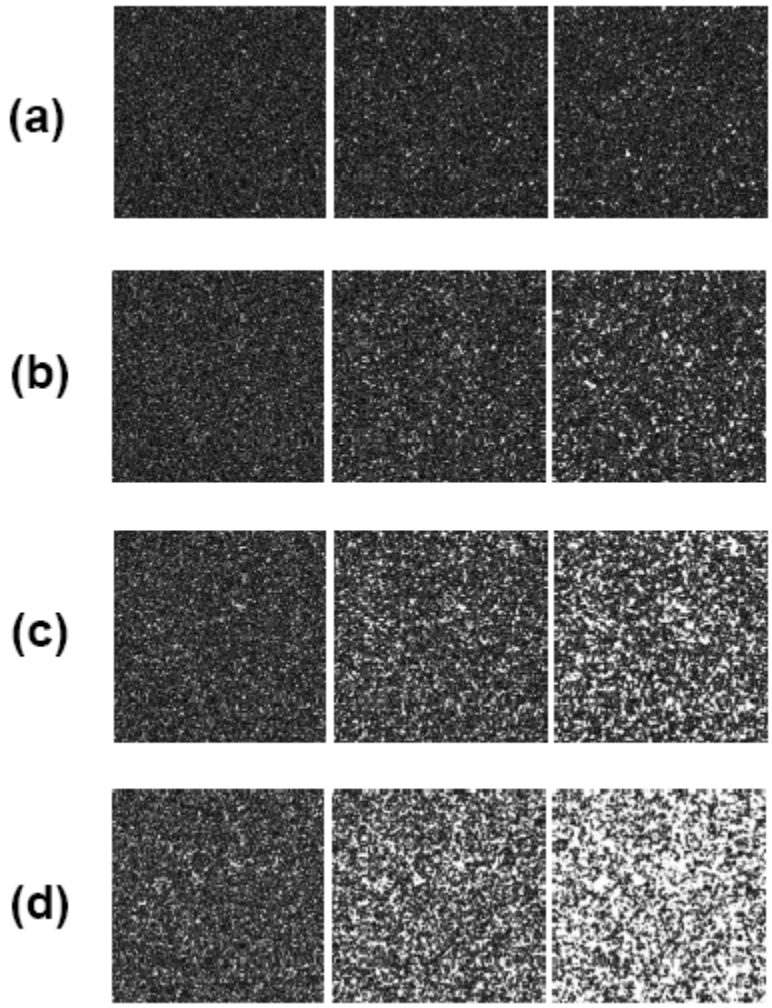

Figure 1. Simulated evolution in the QCP with h=0 starting from a filled 1024×1024 site lattice (which quickly evolves to a metastable active state) in the vicinity of $p=p_{s+}$. (a) p=0.098 (b) p=0.100 (c) p=0.102 (d) p=0.104; t= 182, 364, 546;

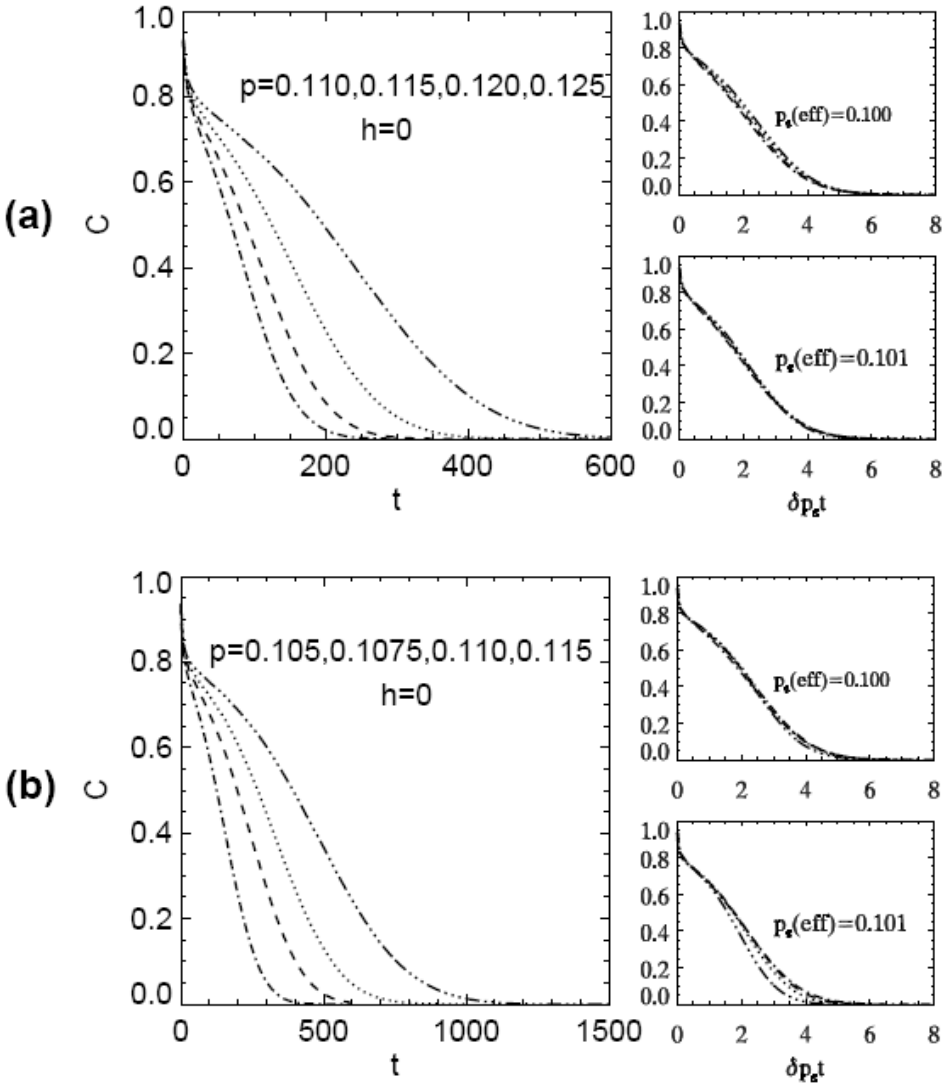

Figure 2. Simulation results for poisoning kinetics in the QCP when h=0 for p=0.110-0.125 yielding the estimate p_{s+}=0.100-0.102 (a). A second range of p from p=0.105-0.115 gives a similar estimate p_{s+} =0.099-0.101 (b).

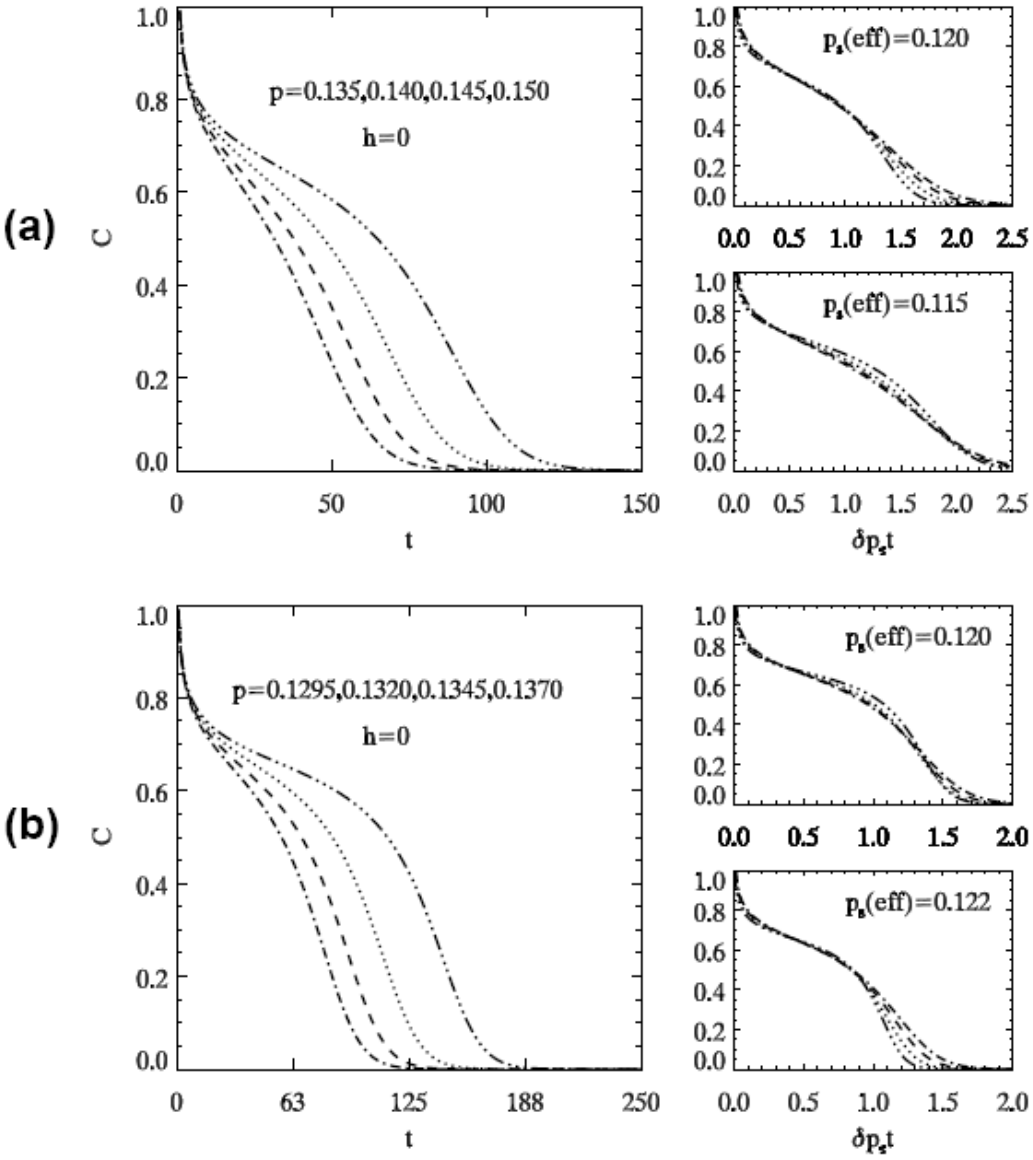

Figure 3. Pair-approximation results for poisoning kinetics in the QCP when h=0 for p=0.135-0.150 yielding p_{s+}=0.115-0.120 (a) (cf. the exact result p_{s+}=0.125). A second range of p from p=0.1295-0.1370 gives an estimate p_{s+} =0.120-0.122 (b).

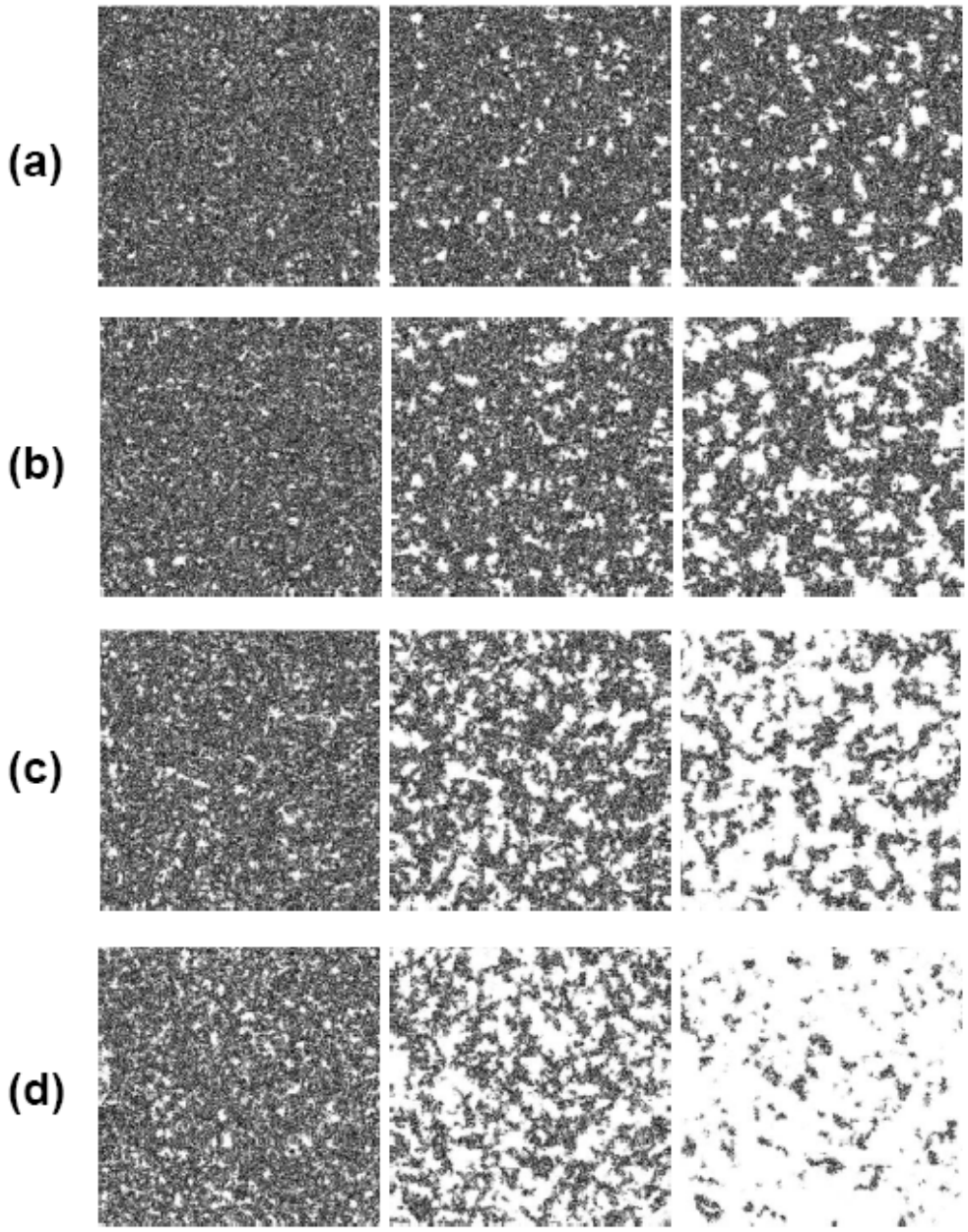

Figure 4. Simulated evolution in the QCP with h=0.4 starting from a filled 1024×1024 site lattice (which quickly evolves to a metastable active state) in the vicinity of $p=p_{s+}$: (a) p=0.188 (b) p=0.189 (c) p=0.190 (d) p=0.191. Times are t=280, 560, 840.

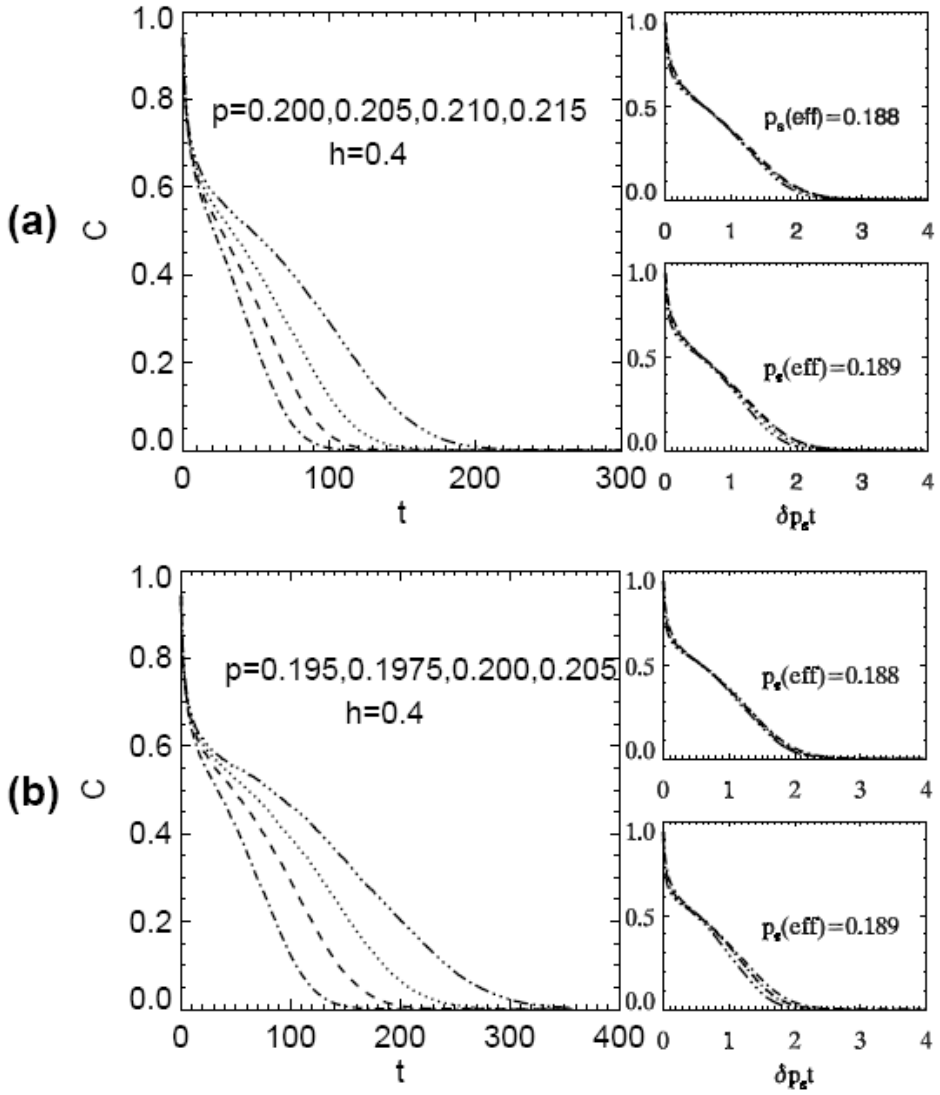

Figure 5. Simulation results for poisoning kinetics in the QCP when h=0.4 for p=0.200-0.215 yielding the estimate p_{s+}=0.188-0.189 (a). A second range of p from p=0.195-0.205 gives a similar estimate p_{s+} =0.188-0.189 (b).

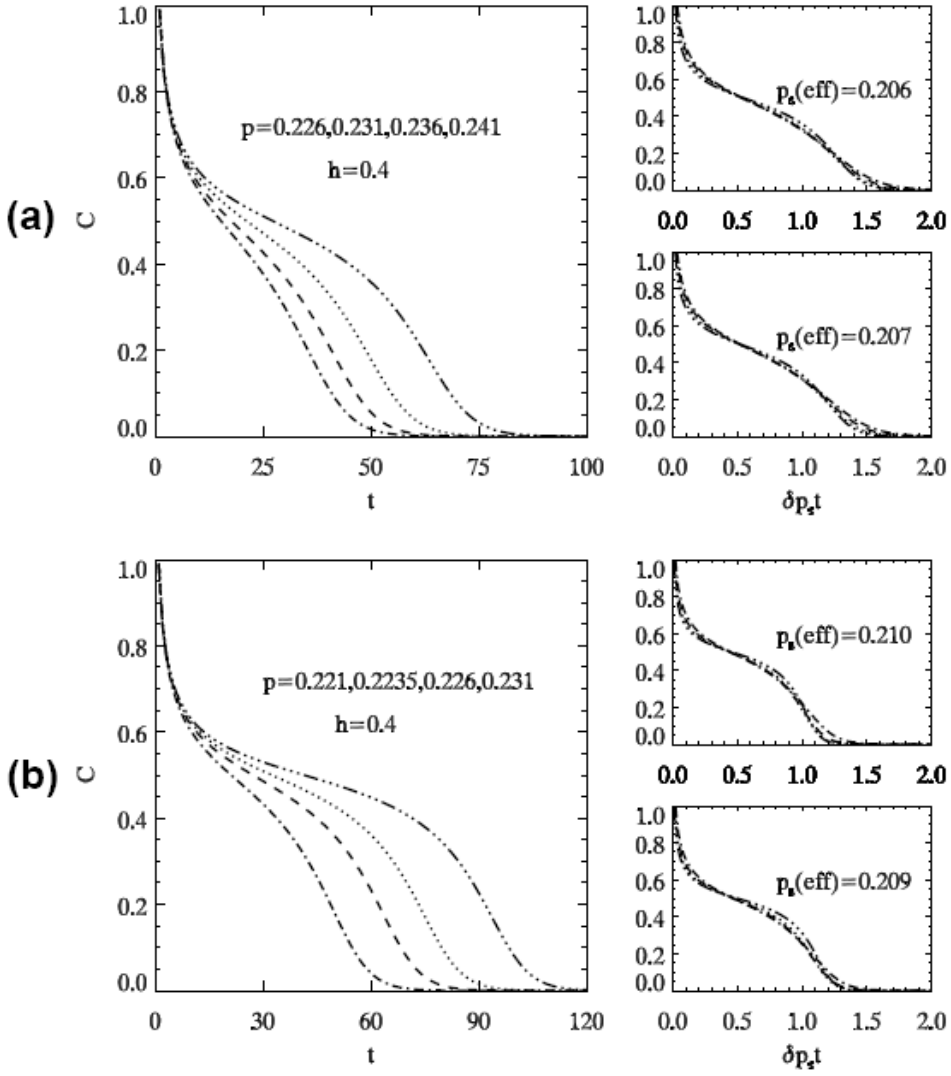

Figure 6. Pair-approximation results for poisoning kinetics in the QCP when h=0.4 for p=0.226-0.241 yielding the estimate p_{s+}=0.206-0.207 (a). A second range of p from p=0.221-0.231 gives an estimate p_{s+} =0.209-0.210 (b).

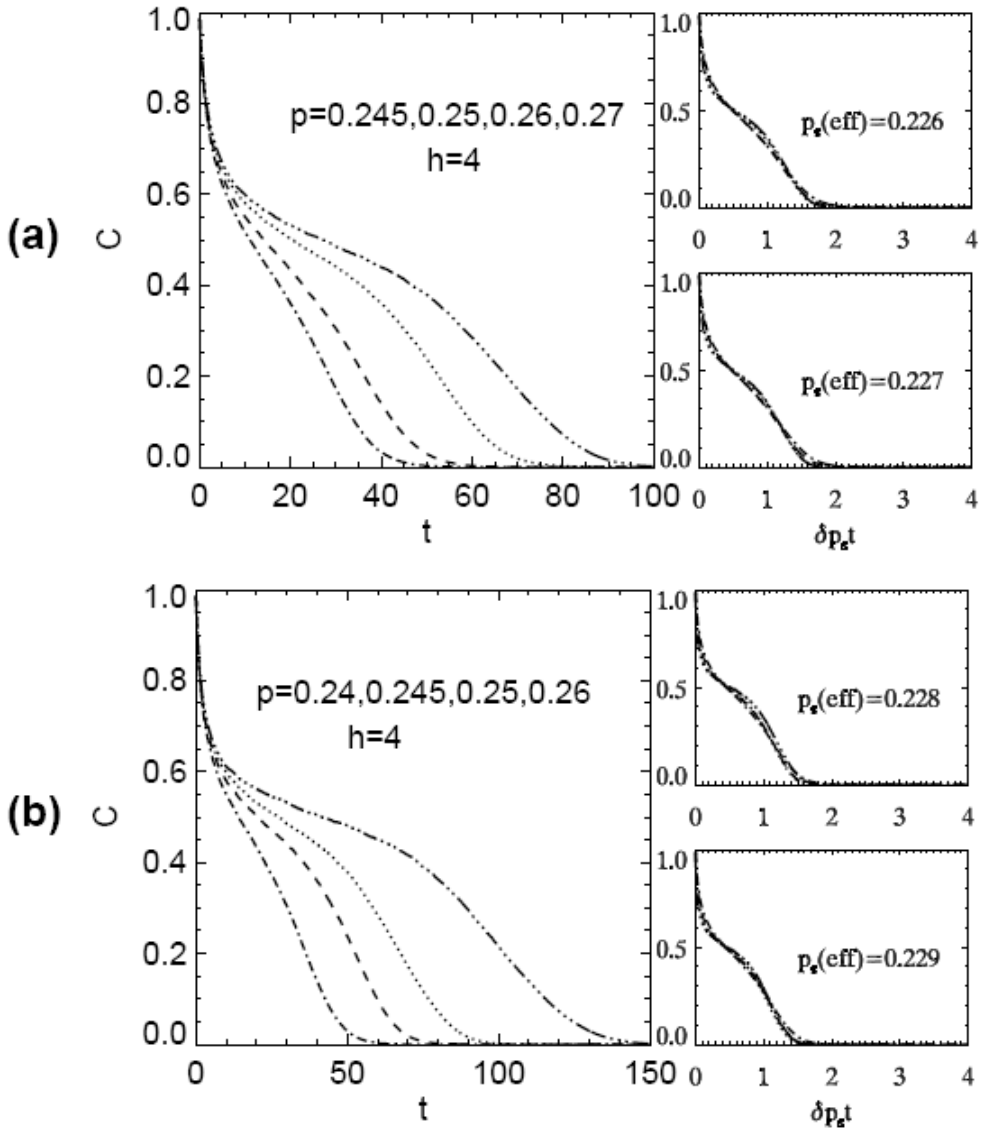

Figure 7. Simulated poisoning kinetics in the QCP for h=4 for a range of p=0.245-0.270 above $p_e(h=4)=0.215$ suggesting $p_{s+}(h=4)$ = 0.226-0.227 (a) Data for p=0.240-0.260 suggests that $p_{s+}(h=4)$ = 0.228-0.229 (b).

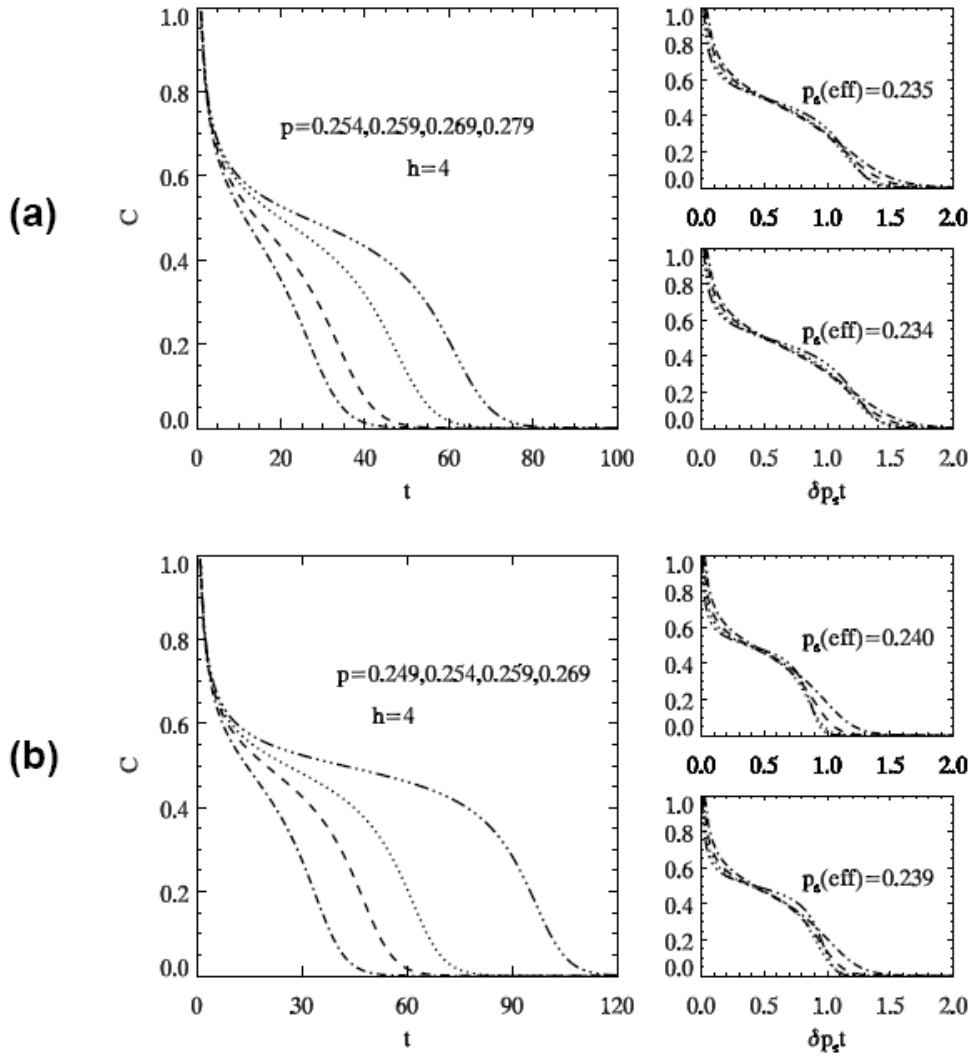

Figure 8. Pair-approximation analysis of poisoning kinetics in the QCP for h=4 for a range of p=0.254-0.279 suggesting $p_{s+}(h=4)$ = 0.234-0.235 (a) Data for p=0.249-0.269 suggests that $p_{s+}(h=4)$ = 0.239-0.240 (b).

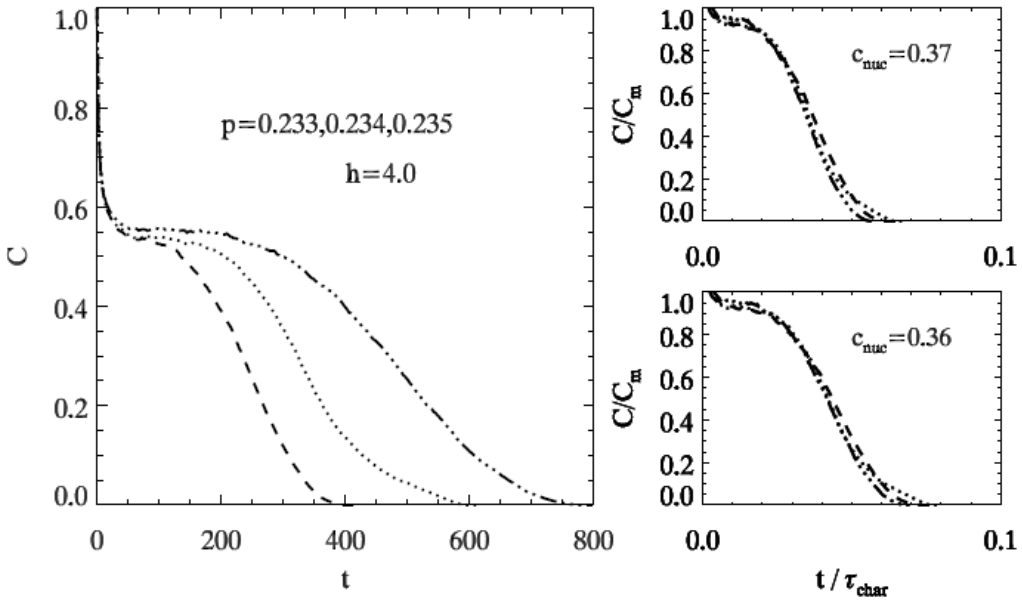

Figure 9. Simulation results for nucleation-mediated poisoning kinetics in the QCP for h=4 for p=0.233-0.235 between $p_e(h=4)=0.215$ and $p_{s+}(h=4) \approx 0.236$. The parameter c_{nuc} is extracted from the characteristic time for nucleation τ_{nuc}. It reflects the magnitude of the effective barrier to nucleation, and is significantly larger than values for h=0-1 determined previously.

APPENDIX D: TRICRITICALITY IN A HYBRID QCP+MCP MODEL

The hybrid QCP+SCP model described in Sec.2 (Ch.6) includes particle creation via two distinct "parallel" mechanisms at empty sites with k≥1 adjacent diagonal occupied pairs. Creation occurs via the QCP mechanism with rate k/4. However, creation also occurs at rate j·δ via the SCP mechanism, where j=2 for k=1, j=3 for k=2, and j=4 for k=4. See Fig.1 in Ch.6. It is natural to consider modifying the model replacing the SCP mechanism with a SCP-like particle creation mechanism that is not operative for those configurations where the QCP is operative. We naturally choose this SCP-like mechanism such that particle creation occurs with rate δ, say, only at empty sites with exactly one filled neighboring site. We will describe this SCP-like particle creation mechanism as the modified Contact Process (MCP). Thus, the hybrid QCP+MCP model considered here one has: (i) particle annihilation ate rate p: (ii) particle hopping to adjacent empty sites at rate h (per direction); and (iii) particle creation via both the QCP and MCP mechanisms.

Note that in the QCP+MCP (QCP+SCP) models, the total particle creation rate at an empty site completely surrounded by four filled sites is given by 1 (1+4δ). As a result for annihilation rate p<<1 where the lattice is almost completely populated in the active steady-state, the steady-state particle population satisfies $C_{eq}(p) = 1-p + O(p^2)$ for the QCP+MCP, versus $C_{eq}(p) = 1-(1+4\delta)^{-1}p + O(p^2)$ for the QCP+SCP, in both cases independent of h. On the other hand, in an active state where C_{eq} is small and spatial correlations are weak, most empty sites have just one filled neighbor, so the particle creation rate at those sites is δ for both models.

For spatially uniform states, the exact form of the first hierarchical master equations, after exact reduction of the QCP and hopping terms described previously, becomes

$$d/dt\ P[o] = p \cdot P[x] - P\begin{bmatrix} x & \\ o & x \end{bmatrix} - 4\delta \cdot P\begin{bmatrix} & o & \\ o & o & x \\ & o & \end{bmatrix} \tag{1}$$

$$d/dt\ P[o\quad o] = 2p \cdot P[o\quad x] - P\begin{bmatrix} & x & \\ o & o & x \end{bmatrix} - 2\delta \cdot P\begin{bmatrix} & o & \\ o & o & x \\ & o & \end{bmatrix} - 4\delta \cdot P\begin{bmatrix} & x & \\ o & o & o \\ & o & \end{bmatrix}$$

$$+ 2h \cdot \left(P[o\quad -\quad o] + 2 \cdot P\begin{bmatrix} & o \\ o & - \end{bmatrix} - 3 \cdot P[o\quad o] \right) \tag{2}$$

and where P's in the two MCP loss terms in (2) are equivalent so these terms can be combined.

Next, we present a mean-field analysis of the QCP+MCP model starting with the generalized version of the above exact master equations for spatially non-uniform states. For a coarse-grained particle concentration, C=C(r=(i,j)a), where 'a' denotes the lattice constant, this analysis yields the reaction-diffusion equation (RDE)

$$\partial C/\partial t = R(C) + D\ \nabla^2 C \text{ with } R(C) = -p \cdot C + C^2(1-C) + 4\delta \cdot C(1-C)^4, \tag{3}$$

and where $D=a^2 h$. One finds a stable uniform active steady state satisfying $p=C(1-C)+4\delta(1-C)^4$ for certain p, as well as a vacuum steady-state C=0. However, steady-state bifurcations are significantly more complex in this model than in the QCP+SCP.

One can identify a number of distinct steady-state bifurcation values for δ. **Fig.A** illustrates the steady-state dependence of C on p for selectedδ. These are chosen to best illustrate the bifurcation behavior which is summarized schematically in **Fig.B** and in the following:

(i) For small $\delta \geq 0$, a high-C stable active state exists for $0 \leq p \leq p_{s+}(\delta)$, and a stable vacuum state exists for $p \geq p_{s1-}(\delta)$, so the model exhibits bistability in the regime $p_{s1-}(\delta) \leq p \leq p_{s+}(\delta)$. This is analogous to behavior in the QCP+SCP. Here, one has $p_{s1-}(\delta) = 4\delta$ (just as in the QCP+SCP), and $p_{s+}(\delta) = ¼ + ¼\ \delta + O(\delta^2)$ which increases smoothly with δ. See Fig.A(a).

(ii) When δ increases above $\delta_{cts} = 1/16 = 0.0625$, a stable low-C active state develops which coexists with the above stable high-C active state. This low-C state exists for $p_{s2-}(\delta) \leq p \leq p_{cts}(\delta)$, where $p_{s2-}(\delta) = ¼ + 4(\delta - 1/16) – 256(\delta - 1/16)^2 + \ldots = 4\delta - 256(\delta - 1/16)^2 + \ldots$ for $\delta \geq 1/16$. Also, $p_{cts}(\delta) = 4\delta$ corresponds to a continuous transition from the stable low-C active state to the stable vacuum state. Thus, bistability exists in the regime $p_{s2-}(\delta) \leq p \leq p_{s+}(\delta)$. See Fig.A(b) and (c).

(iii) For $\delta > \delta_{cts}$, $p_{cts}(\delta)$ increases faster than $p_{s+}(\delta)$, so soon both $p_{s2-}(\delta)$ and $p_{s+}(\delta)$ are below $p_c(\delta)$. As δ increases further to reach a critical point $\delta_{cp} = 2/27 \approx 0.0741$, $p_{s2-}(\delta)$ and $p_{s+}(\delta)$ merge and bistability disappears. At this critical point, we find that $C_{cp} = ¼$ and $p_{cp} = 9/32 \approx 0.2813$. Also when $\delta = \delta_{cp}$, the continuous transition to the vacuum state persists, but occurs at a slightly higher p-value of $p_{cts} = 4\delta_{cp} = 8/27 \approx 0.2963$. See Fig.A(d).

For a more complete characterization of mean-field behavior, we also note the following. For δ below or just above δ_{cts}, one can determine $p = p_{eq}(\delta)$ corresponding to equistability between the high-C active and vacuum states, where $p_{s-}(\delta) \leq p_{eq}(\delta) \leq p_{s+}(\delta)$ [1]. This equistability point is determined from analysis of the effective potential U(C) defined by $R(C) = -dU/dC$, analogous to the treatment for the QCP+SCP. As δ increases above δ_{cts}, one finds that $p_{cts}(\delta) = 4\delta$ increases more quickly that $p_{eq}(\delta)$, and consequently $p_{cts}(\delta)$ and $p_{eq}(\delta)$ will intersect. This occurs at a $\delta = \delta_{eq} \approx 0.068$ (between δ_{cts} and δ_{cp}). See **Fig.B**.

Based on the above mean-field analysis, we describe behavior in the QCP+MCP lattice-gas model with large h for various regimes of δ: **(a)** For $0 \le \delta < \delta_{eq}$, one expects a discontinuous transition from a high-C active state to a vacuum state when p increases above $p_{eq}(\delta)$. **(b)** For $\delta_{eq} < \delta < \delta_{cp}$, one expects the discontinuous transition to persist, but instead to occur between the high-C active state and a low-C active state when p increases above $p_{eq}(\delta)$. This low-C active state then undergoes a continuous transition to the vacuum state as p increases to $p_{cts}(\delta)$ which is above $p_{eq}(\delta)$. As δ increases to δ_{cp}, the discontinuous transition disappears at this critical point. **(c)** For $\delta \ge \delta_{cp}$, the continuous transition from an active state to the vacuum state persists. Thus, to summarize behavior for the QCP+MCP with large h, a discontinuous transition for small δ converts to coexisting discontinuous and continuous transitions when δ increases above $\delta_{eq} \approx 0.068$. Then, the discontinuous transition disappears at a critical point soon after when δ increases to $\delta_{cp} \approx 0.074$, leaving just the continuous transition. In contrast for the QCP+SCP with large h, the discontinuous transition converts directly to a continuous transition as δ increases above the tricritical value $\delta_{tc} = ¼$.

The pair-approximation to the exact master equations described above can be applied in an attempt to describe behavior for finite $h \ge 0$ (including h=0). Here, we consider exclusively the case h=0. It is convenient to introduce the natural variable K = P[x o]/P[o] which denotes the conditional probability of finding a filled site next to a specified empty site. Then, the pair-approximation produces the steady-state condition $p = ½ K(1-K) + 6\delta(1-K)^3$ or K=0. Behavior is actually qualitatively distinct to that seen in mean-field treatment of the QCP+MCP, and more like that in for the QCP+SCP. Specifically, the pair approximation for h=0 predicts a direct transition from bistability to a continuous transition at a tricritical

point $\delta_{cp} = 1/18$. However, in contrast to the general situation for tricitical points (and that for the QCP+SCP), the curvature $d^2C/dp^2|_{tc} = 0$ vanishes at the tricritical point (just like at a critical point). Also when $\delta \geq \delta_{tc}$, the continuous transition to the vacuum state occurs at $p_{cts}(\delta) = 3\delta$. See **Fig.C**.

Next, we present the results of a simulation study for the QCP+MCP with h=0. We caution that the quality of the data in this study is not as high as that for the QCP+SCP. **Fig.D** show the results of CC simulations to determine the variation of p with C, but plotted to show C(p) versus p, for a range of δ around what appears to be a tricritical point, $\delta=\delta_{tc}$. From this data, we extract $p_{tr}(\delta) = \lim_{C\to 0} p(C)$, which corresponds the location of the discontinuous transition for $\delta<\delta_{tc}$ (noting that the two-phase coexistence region will have negligible width except for very small δ), and to the location of the continuous transition $p_{cts}(\delta)$ for $\delta>\delta_{tc}$. We also determine $dp/dC|_{C=0}$ versus δ which is around zero or slightly positive for small δ, but makes a transition to significant negative values as δ increases above $\delta_{tc} \approx 0.026$-$0.028$. In addition, we have performed an epidemic analysis to assess the evolution of a single occupied site embedded in the vacuum state. Specifically, we determine the behavior at the transition point, $p=p_{tr}(\delta)$, of the survival probability, $P_s(t)$, versus t, fitting data to the form $P_s(t) \sim t^{-\zeta}$, as $t\to\infty$. For $\delta_{ct} \approx 0.026$-$0.028$, one obtains $\zeta_{tc} = 1.40$-1.58. It is clear that ζ_{tc} adopts larger (smaller) values for δ significantly smaller (larger) than δ_{tc}, consistent with our discussion for the QCP+SCP. See **Fig.E**. This value of δ_{tc} seems somewhat above that for the QCP+SCP, perhaps reflecting the coincidence of tricritical and critical behavior in the pair-approximation treatment.

In summary, simulation studies of the QCP+MCP for h=0 indicate that a discontinuous transition for low δ converts directly to a continuous transition as δ increases above a tricritical value of $\delta_{tc} \approx 0.026\text{-}0.028$. Interestingly, the pair-approximation for h=0 also predicts such behavior despite the contrasting mean-field behavior for the QCP+MCP. The latter displays indirect conversion from a discontinuous to continuous transition via a region of coexistence of both transitions (with the discontinuous transition disappearing at a critical point). Finally, we briefly describe anticipated behavior in the QCP+MCP model as a function of h. No doubt the model will exhibit a tricritical point for a range of $h \geq 0$. However, for large enough h, mean-field behavior must be realized. Thus, the tricritical line in the (h,δ)-plane emanating from $(h, \delta) \approx (0, 0.027)$ propagates for a range of h before expanding into a region of finite width (in δ) corresponding to coexistence of discontinuous and continuous transitions.

References

[1] $p_{s\text{-}}(\delta)$ corresponds to $p_{s1\text{-}}(\delta)$ and $p_{s2\text{-}}(\delta)$ for $\delta<\delta_{cts}$ and $\delta>\delta_{cts}$, respectively.

Figures

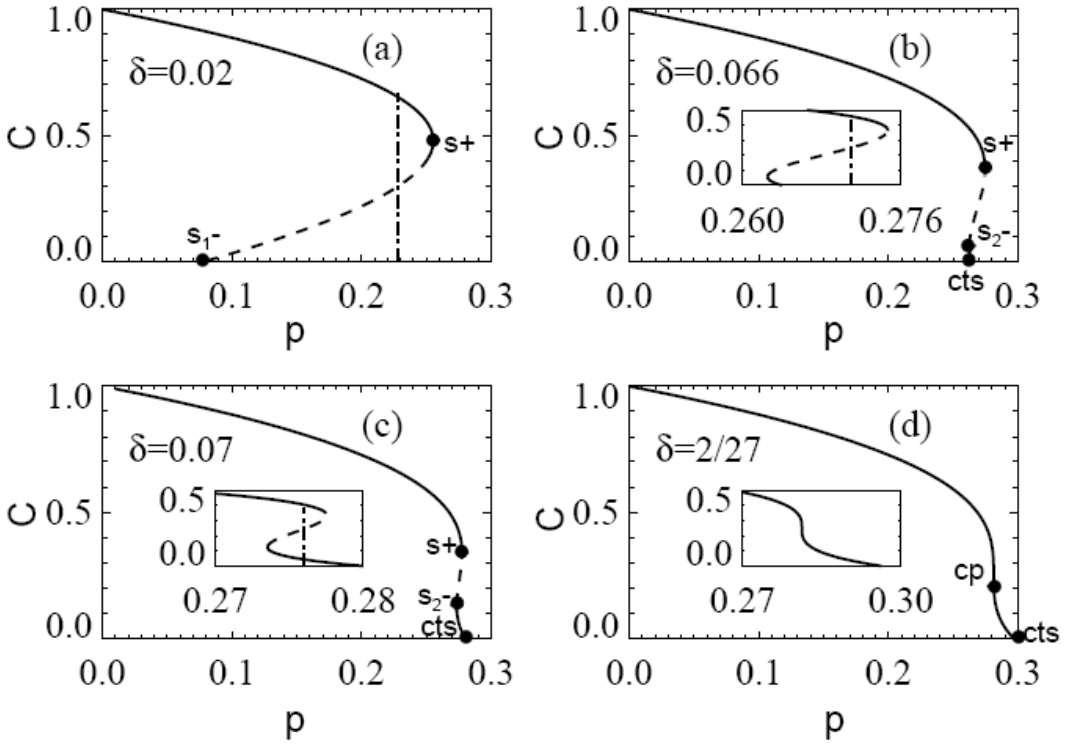

Figure A. Mean-field variation of steady-state C(p) with p in the QCP+MCP: (a) $\delta<\delta_{cts}$; (b) $\delta_{cts} < \delta < \delta_{eq}$; (c) $\delta_{eq} < \delta < \delta_{cp}$; (d) $\delta = \delta_{cp}$. The notation s+ and si- indicate upper and lower spinodals, respectively; cp indicates the critical point, and cts the continuous transition.

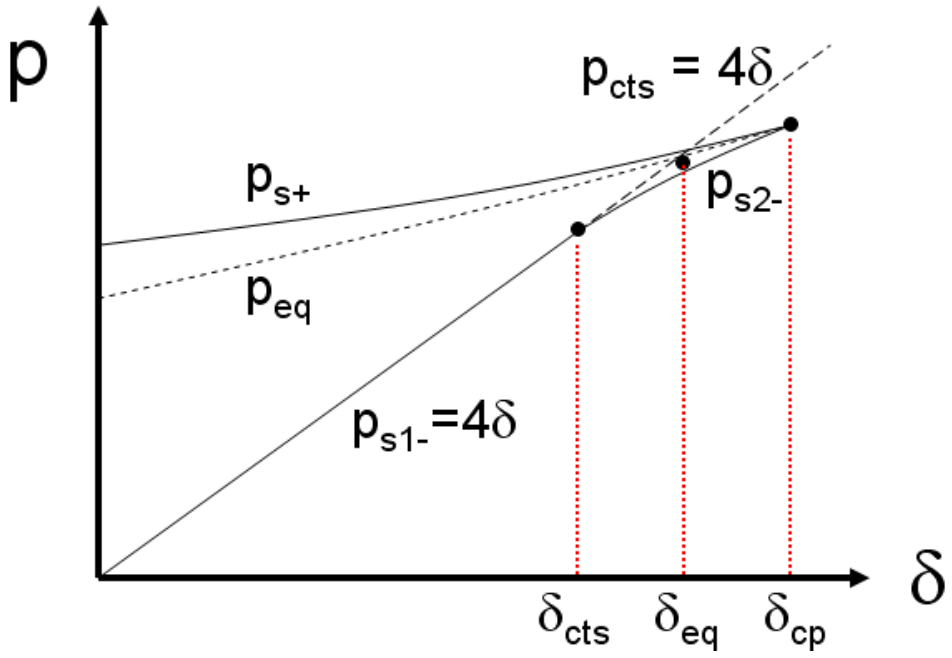

Figure B. Schematic of the mean-field phase-diagram in the p-δ plane for the QCP+MCP. This is distorted from quantitative behavior described in the text in order to show clearly different regions.

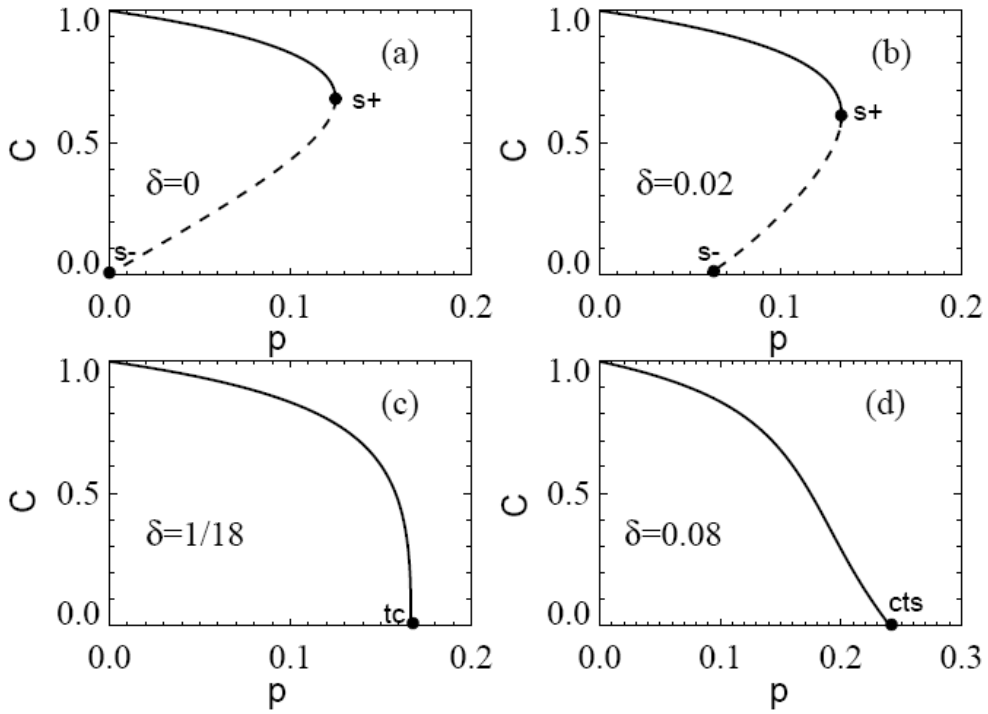

Figure C. **Pair-approximation prediction for variation of steady-state C(p) with p in the QCP+MCP with h=0: (a) δ=0; (b) $0 < \delta < \delta_{tc}$; (c) $\delta = \delta_{tc} = 1/18$; (d) $\delta > \delta_{tc}$. The notation s+ and s- indicate upper and lower spinodals, respectively; tc indicates the tricritical point, and cts the continuous transition.**

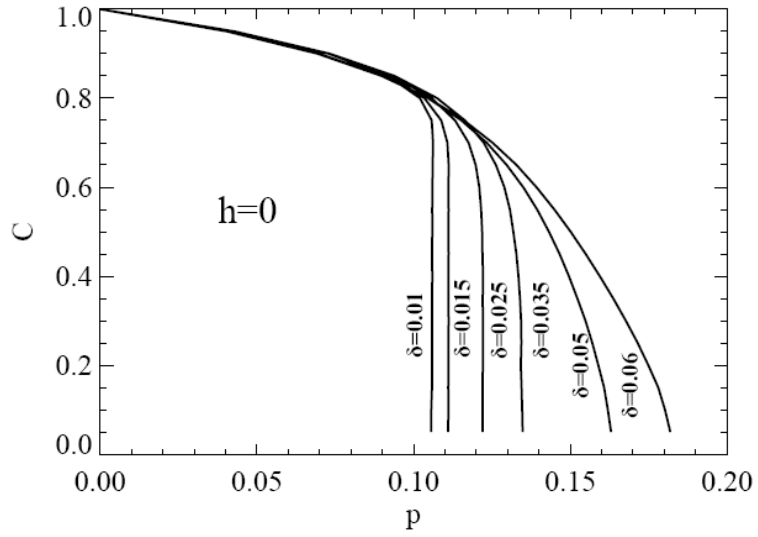

Figure D. CC simulation results for steady-state behavior in the QCP+MCP with h=0 for various δ. From this data, we estimate that $\delta_{ct} \approx 0.026$-$0.028$.

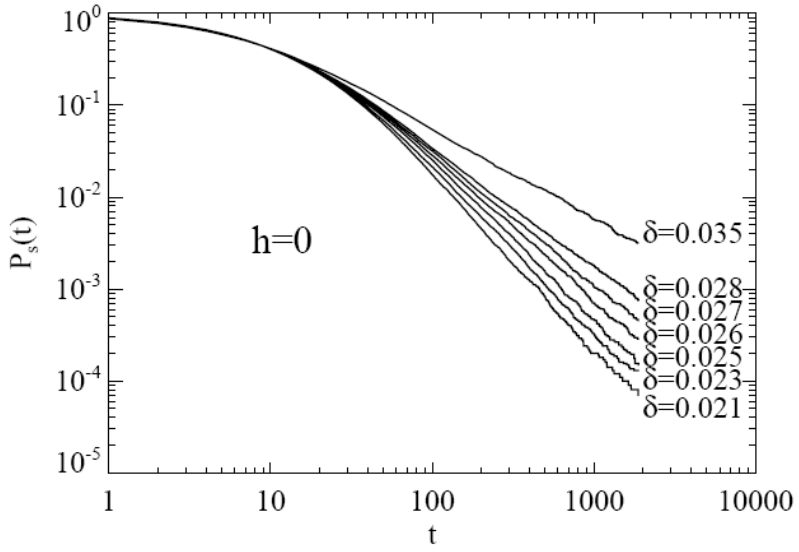

Figure E. Epidemic analysis for the QCP+MCP with h=0. Survival probability, $P_s(t)$, versus time, t, for a single occupied site embedded in a vacuum state for various δ from 0.021 to 0.035, and choosing $p = p_{tr}(\delta)$. For $\delta_{ct} \approx 0.026$-$0.028$, one obtains $\zeta_{tc} = 1.40$-1.58.

APPENDIX E: DISCRETE RDE ANALYSIS OF FRONTS AND DROPLETS FOR THE SITE-APPROXIMATION TO THE QUADRATIC CONTACT PROCESS WITH HOPPING

We consider the adsorption-desorption realization of the quadratic contact process on a square lattice where particles adsorb at empty sites at rate p and desorb at from sites with $k\geq 1$ adjacent diagonal empty pairs at rate k/4, as in Ch.3. However, here we also allow particles to hop to adjacent empty sites at rate h. Within the site-approximation (ignoring all spatial correlations) the coverage, $\theta_{i,j}$, at site (i,j) for spatially non-uniform states satisfies the discrete reaction-diffusion equations (RDE's)

$$d/dt\ \theta_{i,j} = p(1-\theta_{i,j}) - ¼\ \theta_{i,j}(2-\theta_{i+1,j} -\theta_{i-1,j})(2-\theta_{i,j+1} -\theta_{i,j-1}) + h(\theta_{i+1,j} + \theta_{i-1,j} +\theta_{i,j+1} + \theta_{i,j-1} -4\theta_{i,j}) \quad (1)$$

For uniform states, these equations recover bistability between a low-θ active steady state, $\theta=\theta_{eq}(p) = ½[1- (1-4p)^{1/2}]$, and a poisoned state with $\theta=1$, for $0\leq p\leq p_{s+}=1/4$.

The above equations (1) for non-uniform states predict that planar interfaces between these states in the bistable regime will generally evolve with constant velocity, where: **(i)** the active state displaces the less stable poisoned state for low $p\geq 0$; **(ii)** the poisoned state displaces the less stable active state for higher $p\leq p_{s+}$. However, this evolution depends on interface orientation or slope S (relative to the principal lattice direction). We focus on diagonal interfaces (S=1) where $\theta_{i,j} = \theta(i-j)$, and vertical interfaces ($S=\infty$) where $\theta_{i,j} = \theta(i)$. Note that behavior for vertical and horizontal (S=0) interfaces is equivalent by rotational symmetry. For S=1 and all $h\geq 0$, there appears to be a unique a $p = p_{eq}(S=1)$ for which there is a stationary interface corresponding to equistability of the two states. For S=0 or ∞ and $h>0$, we find that there is a finite window of $p=p_{eq}(S=0 \text{ or } \infty)$ of stationary interfaces or of

equistability, which might also be described as a regime or “propagation failure”. Note, however, that this window quickly shrinks in width with increasing h>0. The extreme case for h=0 is discussed in Ch.3. All these cases of equistability or stationary interfaces correspond to non-trivial time-independent solutions of (1).

For the simpler case with S=1 with a unique equistability $p=p_{eq}(S=1)$, we make some additional observations. For $p_{eq}(S=1)<p<p_{s+}$ where the poisoned state is more stable, one might expect a planar perturbation of the active state by the poisoned state [where $\theta_{i,j} = \theta_{eq} + \delta\theta(i-j)$ with small $\delta\theta\geq 0$] would grow spreading the poisoned state across the entire system. However, this is only true for a perturbation above a critical size. This “critical planar perturbation” of the active state by the poisoned state corresponds to another non-trivial steady-state solution of (1). Likewise, for $0<p<p_{eq}(S=1)$ where the active state is more stable, one might expect a planar perturbation of the poisoned state by the active state [where $\theta_{i,j} = 1 - \delta\theta(i-j)$ with small $\delta\theta\geq 0$] would grow spreading the active state across the entire system. However, again this is only true above a critical size and the associated “critical planar perturbation” is yet another non-trivial steady-state solution of (1).

In addition to non-trivial planar steady-state solutions of (1), it is natural to consider “droplet-like” steady state solutions. Indeed, nucleation theory which considers the fluctuation-induced formation of a more stable steady-state from a less stable one is based on consideration and analysis of such “critical droplets”. The following two subsections consider both planar and droplet-like steady-state solutions of (1).

A. Planar Steady-State Solutions of the Discrete RDE’s

For this analysis, we find that it is convenient to recast the steady-state form of (1) as an iterated map. The form of this iterated map depends on the orientation of the planar interface or perturbation. However, the general idea is as follows. Let θ(i) denote the coverage at all sites in the diagonal row for S=1 or horizontal row for S=0, or vertical column for S=∞. Then, the iterated map adopts the notation $(u_i, v_i) = (\theta(i-1), \theta(i))$ where the map is $(u_i, v_i) \rightarrow (u_{i+1}, v_{i+1})$. Below we separately describe this mapping and procedure in detail for S=1 and S=0 or ∞.

A1. Iterated Map for Vertical Interfaces

Assume that $\theta_i(p) = \theta_{active}(p) + c\lambda^i$. For h=0, we obtain $\lambda = \frac{1-\sqrt{1-r^2}}{r}$ with $r = \theta_{active}/(1-\theta_{active})$ and $\theta_{active} = \frac{1-\sqrt{1-4p}}{2}$, and $u_{i+1} = v_i, v_{i+1} = 2 - u_i - 2\frac{p}{v_i}$

For h > 0, we obtain $\lambda = r - \sqrt{r^2 - 1}$ with $r = \frac{(1-\theta_{active})^2 + 2h}{\theta_{active}(1-\theta_{active}) + 2h}$

and $\theta_{active} = \frac{1-\sqrt{1-4p}}{2}$, and $u_{i+1} = v_i, v_{i+1} = \frac{v_i(1-v_i)(2-u_i)/2 - p(1-v_i)/v_i - h(u_i - 2v_i)}{h + v_i(1-v_i)/2}$

To perform our numerical analysis of this iterated map, we start at point $(u,v) = (\theta_{active} + \varepsilon, \theta_{active} + \varepsilon')$ or $(u,v) = (1+\varepsilon, 1+\varepsilon')$ (where $\varepsilon'/\varepsilon = \lambda$) slightly perturbed from the fixed point $(u,v) = (\theta_{active}, \theta_{active})$ and iterate. Points from these different iterations together generate a continuous curve.

A2. Iterated Map for Diagonal Interfaces

Assume again that $\theta_i(p) = \theta_{active}(p) + c\lambda^i$. For h=0, we obtain $\lambda = \frac{1-\sqrt{1-4\theta_{active}}^2}{2\theta_{active}}$

with $\theta_{active} = \frac{1-\sqrt{1-4p}}{2}$, and $u_{i+1} = v_i, v_{i+1} = 2 - u_i - 2\frac{\sqrt{p(1-v_i)}}{\sqrt{v_i}}$

For h > 0, we obtain $\lambda = r - \sqrt{r^2 - 1}$ with $r = \frac{1+4h-\theta_{active}}{4h+2\theta_{active}(1-\theta_{active})}$

and $\theta_{active} = \frac{1-\sqrt{1-4p}}{2}$, and $u_{i+1} = v_i, v_{i+1} = 2 - u_i - \frac{-4h+2\sqrt{4h^2+(p+4h)v_i(1-v_i)}}{v_i}$

To perform the iterated map analysis, the same strategy is applied as above.

First, we apply the iterated map procedure to obtain accurate estimates of $p_{eq}(s=1)$ and $p_{eq}(S=0 \text{ or } \infty)$ by searching for loci of the map which directly connect (u, v) = (θ_{eq}, θ_{eq}) to (u, v) = (1, 1). These loci correspond to stationary interfaces between the two steady states. An example of such an interfaces, and several examples of such loci will be shown in the figures below for S=1. The results for p_{eq} are shown in **Table I**.

Next, we show numerical results for the stationary interface (with $p=p_{eq}$), and planar critical perturbations of the poisoned state (for $p<p_{eq}$) and of the active steady-state (for $p>p_{eq}$) for S=1 and h=0 in **Fig.A**. The orbits of the iterated map for the same three p-values are shown in **Fig.B**. Corresponding orbits for the stationary interface (with $p=p_{eq}$), and planar critical perturbations of the poisoned state (for $p<p_{eq}$) and of the active steady-state (for $p>p_{eq}$) for S=1 are shown in **Fig.C** for h=0.01 and in **Fig.D** for h=1.

B. Steady-State Droplet Solutions of the Discrete RDE's

First, we consider the case for the QCP with h=0.01 of poisoned droplets embedded in the active state for higher p where $p_{eq}(S=1)=0.2128 < p < p_{s+} = ¼ = 0.250$. In this regime,

the poisoned state is more stable. Thus, a traditional "nucleation theory" perspective would suggest that there exists a critical size for the poisoned droplets below which they will shrink and above which they will grow spreading the poisoned state across the system. Simulations for fixed p starting with square poisoned droplets of various sizes embedded in an empty lattice do indeed find this behavior. Examples of this evolution are shown in **Fig.E**. The existence of a size which appears to be stable, so the droplet survives for long times without growing or shrinking, is less clear. The results of this analysis for the critical droplet size versus p are shown in **Fig.F**. The size appears to diverge as p approaches $p_{eq}(S=1)$ from above, analogous to behavior in traditional nucleation theory. (For simplicity the plotted size R_s is just the square root of the initial number of filled sites). It appears that $1/R_c$ goes to zero non-linearly approaching $p=p_{eq}(S=1)$ from above.

The situation for active droplets embedded in the poisoned state for lower p around and below $p_{eq}(S=0 \text{ or } \infty)$ can be significantly more complicated due to occurrence of a regime of "propagation failure" for horizontal or vertical interfaces. This suggests the possibility of a finite range of sizes where active droplets are stationary, i.e., they neither grow nor shrink. (Perhaps such a narrow regime of sizes could even exist for vacuum droplets at higher p.) A schematic of the proposed complex behavior is shown in **Fig.G**.

To provide a reasonably comprehensive analysis of active droplets for h=0.01, consider first the choice p=0.2070 below $p_{eq}(S=0)=0.2081$. It is certainly the case that large enough active droplets grow, small enough active droplets shrink, and now it appears easier to find stable droplets for sizes in between. See **Fig.H**. A more detailed analysis for this p=0.2070 actually reveals three distinct sizes for stationary droplets. See **Fig.I**.

We have repeated the above analysis for various p. For example, **Fig.J** shows a broader range of sizes for stationary droplets exists for a slightly higher p=0.2075. A summary of such analyses for various p just showing the maximum and minimum stationary sizes is shown in **Fig.K**. This behavior is consistent with that proposed in the schematic **Fig.G**.

Table

Table I. Equistability points for diagonal (S=1) and horizontal or vertical (S=0 or ∞) interfaces.

h	p_{eq}(S=1)	p_{eq}(S=0 or ∞)
0	0.2114	0-0.2071
0.01	0.2128	0.2081-0.2097*
0.1	0.2177	0.2172
1	0.2215	0.2215
∞ (mean-field limit)	2/9	2/9

Figure

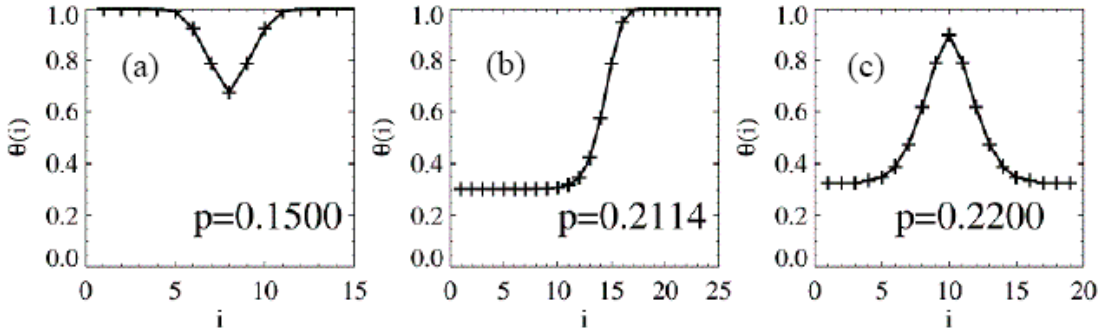

Figure A. Numerical results for the stationary interface (with p=peq=0.2114), and planar critical perturbations of the poisoned state (for $p<p_{eq}$) and of the active steady-state (for $p>p_{eq}$) for S=1 and h=0

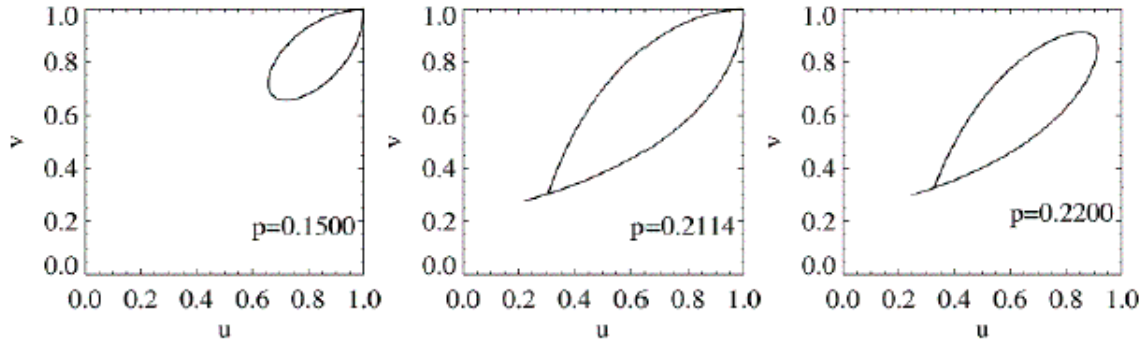

Figure B. Orbits of the iterated map for S=1 and h=0 for $p<p_{eq}$, $p=p_{eq}=0.2114$, and p>peq (the same three p values as shown in Figure A.)

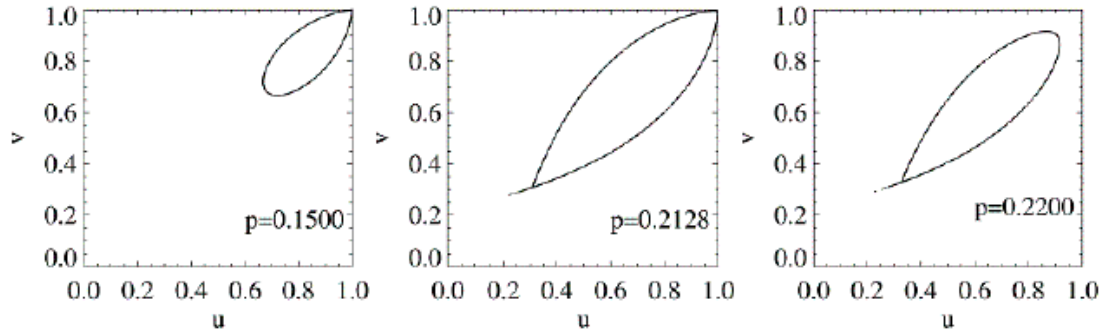

Figure C. Orbits of the iterated map for S=1 and h=0 for $p<p_{eq}$, $p=p_{eq}=0.2114$, and $p>p_{eq}$.

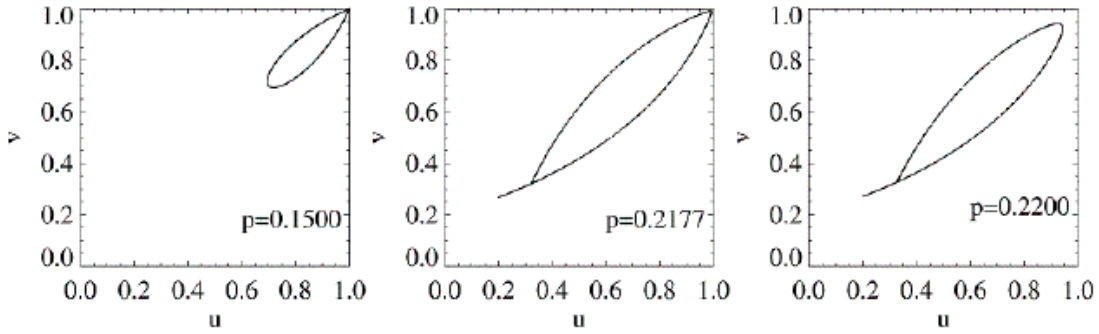

Figure D. Orbits of the iterated map for S=1 and h=1 for $p<p_{eq}$, $p=p_{eq}=0.2177$, and $p>p_{eq}$.

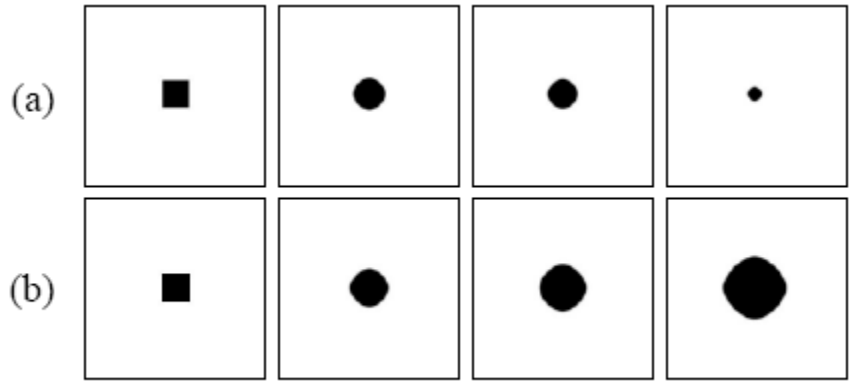

Figure E. Evolution of poisoned droplets of different initial sizes R_i embedded in the active steady state for p=0.2145: a. R_i=36 b. R_i=38

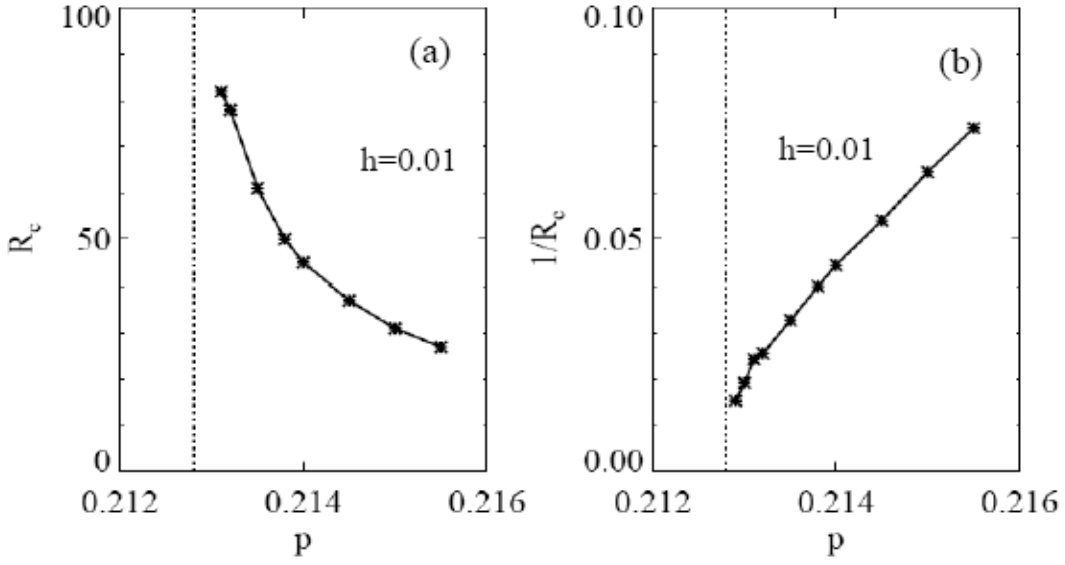

Figure F. Dependence of the critical size of poisoned droplets on p

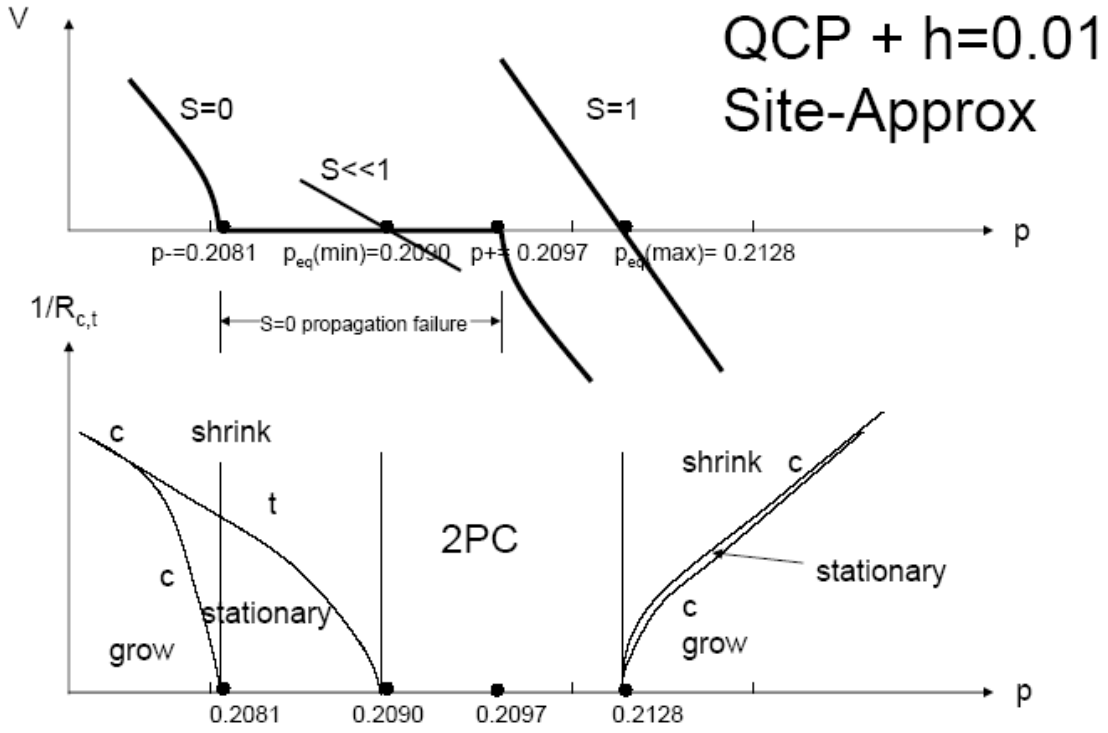

Figure G. Schematic of proposed behavior for active droplets (bottom) and the associated interface propagation velocities V (top).

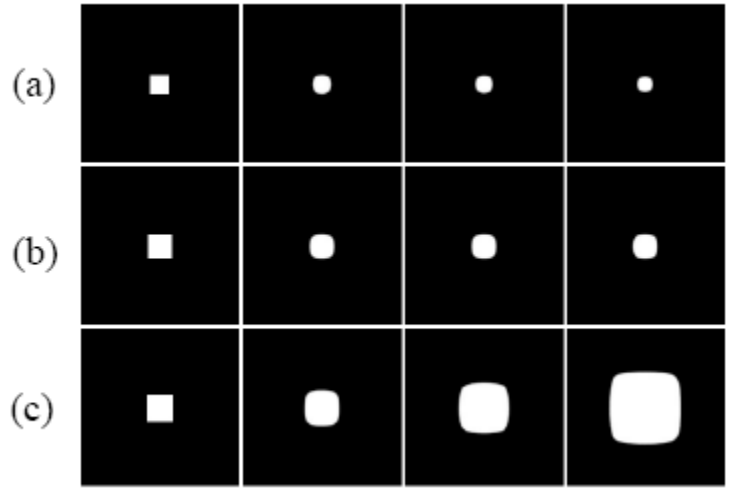

Figure H. Evolution of active droplets of different initial sizes R_i embedded in the poisoned state for p=0.2070, a. Ri=30, b.R_i=38, c.R_i=42

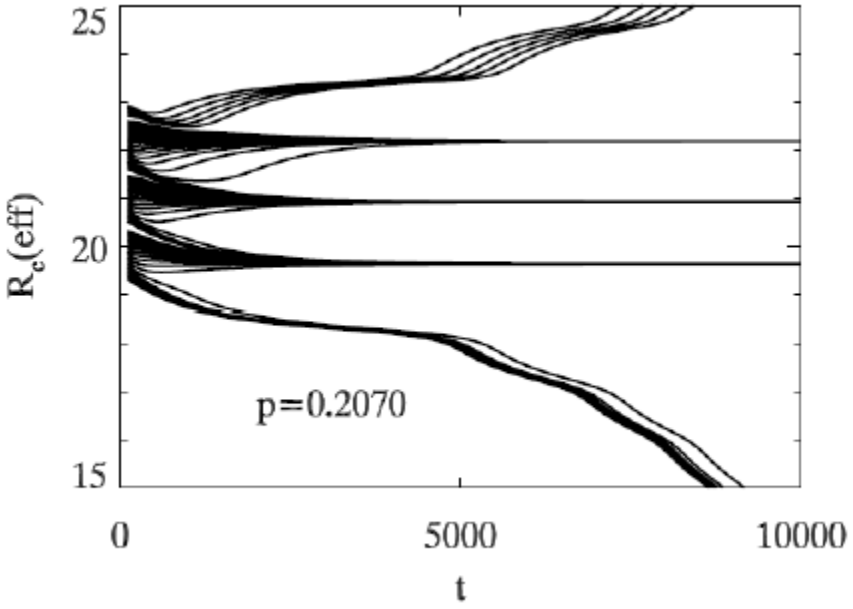

Figure I. Evolution of active droplets of various initial sizes and selection of various stationary sizes for p=0.2070.

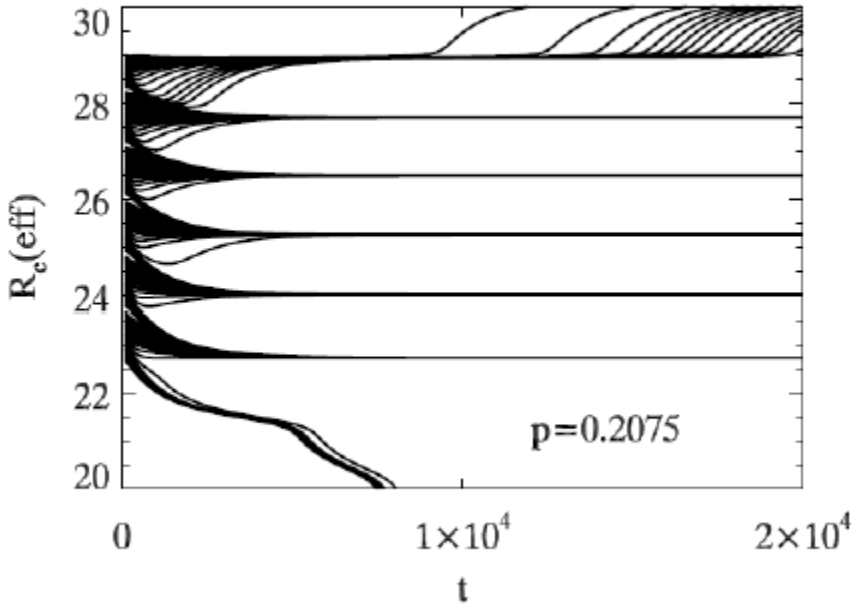

Figure I. Evolution of active droplets of various initial sizes and selection of various stationary sizes for p=0.2075.

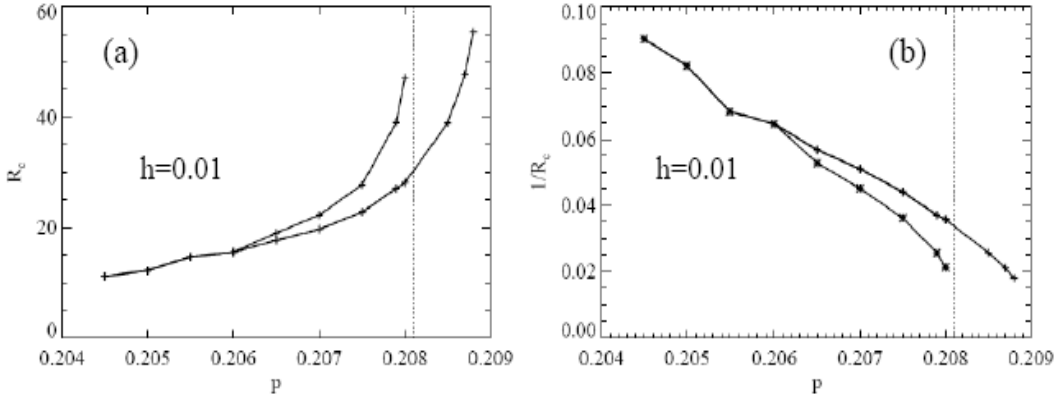

Figure K. Dependence of the maximum and minimum size of stationary active droplets on p

APPENDIX F: SCHLOEGL'S SECOND MODEL AND ITS VARIANTS (QUADRATIC AND CUBIC CONTACT PROCESSES) ON VARIOUS LATTICES

A. Quadratic Contact Process

We first provide a general definition and also some basic analysis of Schloegl's second model for autocatalysis, aka the Quadratic Contact process (QCP), on various lattices. Specifically, we will consider square, triangular, and cubic lattices. In the QCP, particles undergo random spontaneous annihilation at fixed rate p. Particles are also created autocatalytically at empty sites at a rate proportional to the number of "suitably connected filled pairs" on sites neighboring the empty site. It is convenient to choose a normalization for these creation rates so that the mean-field kinetics for the model will be independent of lattice type. We shall see that this goal is achieved by the choice of creation rate as k/k_{max}, where k is the number of suitably connected filled pairs, and k_{max} is the maximum number of such filled pairs. Note that "suitably connected filled pairs" corresponds to diagonal neighboring pairs on the square and cubic lattices, and to neighboring filled pairs on the triangular lattice. Thus, we have k_{max} = 4, 6, and 12 for square, triangular, and cubic lattices, respectively. **Fig.1-3** provide schematics of particle annihilation and creation rules and rates for the QCP on the square, triangular, and cubic lattices, respectively.

Next, we present the mean-field kinetics of the particle concentration, C, for the QCP. These kinetics are obtained by ignoring all spatial correlations, so that the probability of multi-site configurations is simply given by a product of the relevant single site probabilities. For a square lattice, we obtain the kinetic equation:

$$\frac{dC}{dt} = -pC + \left[1\times\frac{4}{4}C^4(1-C) + 4\times\frac{2}{4}C^3(1-C)^2 + 4\times\frac{1}{4}C^2(1-C)^3 \right]. \quad (1)$$

The various contributions to the positive creation (gain) term on the RHS of eq.(1) correspond to different k as enumerated in **Fig.1**. For a triangular lattice, we obtain the kinetic equation:

$$\frac{dC}{dt} = -pC + \left[\begin{array}{l} 1\times\frac{6}{6}C^6(1-C) + 6\times\frac{4}{6}C^5(1-C)^2 + \left(6\times\frac{3}{6} + 9\times\frac{2}{6}\right)C^4(1-C)^3 \\ + \left(6\times\frac{2}{6} + 12\times\frac{1}{6}\right)C^3(1-C)^4 + 6\times\frac{1}{6}C^2(1-C)^5 \end{array} \right]. \quad (2)$$

The various contributions to the positive creation (gain) term on the RHS of eq(2) correspond to different k as enumerated in **Fig.2**. For a cubic lattice, we obtain the kinetic equation:

$$\frac{dC}{dt} = -pC + \left[\begin{array}{l} 1\times\frac{12}{12}C^6(1-C) + 6\times\frac{8}{12}C^5(1-C)^2 + \left(12\times\frac{5}{12} + 3\times\frac{4}{12}\right)C^4(1-C)^3 \\ + \left(12\times\frac{2}{12} + 8\times\frac{3}{12}\right)C^3(1-C)^4 + 12\times\frac{1}{12}C^2(1-C)^5 \end{array} \right]. \quad (3)$$

The various contributions to the positive creation (gain) term on the RHS of eq.(3) correspond to different k as enumerated in **Fig.3**. The first integer factor corresponds to the configurational degeneracy, and the second fractional factor to k/12.

Each of Eq. (1-3) can be simplified to the same equation:

$$dC/dt = -pC + C^2(1-C) \quad (4)$$

i.e., the same mean-field kinetics apply for the QCP on any lattice.

Perhaps, a more significant feature of our rate choice (than universal mean-field kinetics) is that it facilitates an exact reduction of the master equations which specify the exact dynamics of the QCP. (This reduction actually applies for both for spatially uniform

and non-uniform states, although here we consider only the former.) Furthermore, this exact reduction not only immediately allows recovery of the lattice-independent mean-field kinetics, but also allows ready generation of higher-order approximations for the kinetics. We demonstrate the latter for the so-called pair-approximation (whereas mean-field kinetics corresponds to the site-approximation).

The exact master equations for the QCP form an infinite coupled hierarchy for the evolution of the probability of a single filled site, a filled pair, etc. (or equivalently, one can consider empty configurations). It will be convenient to introduce the following notation. Let x (o) denote a filled (empty) site, and let P's denote probabilities of various configurations of such sites. For example, P[x]=C and P[xx] denote the probabilities of a single filled site and a filled pair, respectively. Similarly, P[o]=1-C and P[oo] denote the probability of a single empty site and empty pair, respectively. Conservation of probability implies that P[x]+P[o]=1, P[xo]+P[oo]=P[o], P[xx]+P[xo]=P[x], P[xx]+2P[xo]+P[oo]=1, etc. Then, in terms of probabilities for empty configurations, the exact master equations have the form

$$d/dt\ P[o] = p \cdot P[x] - \text{particle creation terms}, \quad (5)$$

$$d/dt\ P[oo] = 2p \cdot P[xo] - \text{particle creation terms, etc.} \quad (6)$$

The particle creation terms in each equation correspond to a sum over various relevant configurations multiplied by the appropriate rates. As an aside, we favor empty configurations in writing these equations by analogy with irreversible cooperative creation processes (i.e., processes without particle annihilation) where empty site configuration probabilities have certain special spatial Markov properties.

A schematic enumeration of the creation terms for eq.(5) is provided by **Fig.1-3** for the square, triangular, and cubic lattices, respectively. Similar to eq.(1-3), an exact reduction

is possible for these various terms. One can show that eq.(5) always reduces exactly to the simple and intuitive equation

$$d/dt\ P[o] = p \cdot P[x] - P[o + 2x], \tag{7}$$

where the term P[o+2x] represents the probability of an empty site with a suitably connected filled pair on neighboring sites.

An enumeration of the creation terms for eq.(6) is straightforward for the square and cubic lattices, but rather lengthy for the triangular lattice. **Fig.4a,c** provides a complete enumeration for the square and cubic lattices. **Fig.5a** provides only a partial enumeration for the triangular lattice. For the square and cubic lattices, one can consider creation of a particle on one of the two empty sites enumerating all possible configurations of neighbors of just that one empty site. Then, the total creation rate comes from doubling this result. For the triangular lattice, the empty sites in the pair share two neighbors, so one must enumerate configurations of all neighbors of both empty sites. One then determines the total rate of creation of particles at either site in the empty pair for each such configuration. An exact reduction of these desorption terms is also possible in all cases, although the form of these terms depends on the lattice type. For a square lattice, one obtains

$$d/dt\ P[o\ o] = 2p \cdot P[x\ o] - P[2o+2x], \tag{8}$$

where the terms P[2o+2x] represents the probability of a empty pair where one site in this pair has a suitably connected filled pair on neighboring sites. See **Fig.4b**. (Note that there is only one such configuration for the square lattices.) For a hexagonal lattice, one obtains

$$d/dt\ P[o\ o] = 2p \cdot P[x\ o] - 2/3\ P[2o+2xE] - 2/3\ P[2o+2xS], \tag{9}$$

where the terms P[2o+2xE] and P[2o+2xS] represents probabilities of an empty pair where one site in this pair has a neighboring filled pair. There are two such distinct configurations,

one where the filled pair is at the end of the empty pair (with probability denoted P[2o+2xE]), and the other where the filled pair is on the side of the empty pair (with probability denoted P[2o+2xS]). See **Fig.5b**. Similarly, for a cubic lattice, one obtains

$$d/dt\ P[o\ o] = 2p\cdot P[x\ o] - 2/3\ P[2o+2xL] - 2/3\ P[2o+2xB], \quad (10)$$

where the terms P[2o+2xL] and P[2o+2xB] represents probabilities of an empty pair where one site in this pair has a diagonal filled pair on neighboring sites. There are two such distinct configurations, one where the empty pair and one filled site form a linear triple (with probability denoted P[2o+2xL]), and the other both empty sites form a bent triple with the filled pair (with probability denoted P[2o+2xB]). See **Fig.4d**.

Finally, we implement the pair-approximation to the above exact master equations for the QCP on various lattices. For this approximation, for square and cubic lattices, we obtain:

$$d/dt\ P[o] = p\cdot P[x] - P[x\ o]^2/P[o] = p\cdot P[x] - (P[x\ o]/P[o])^2\ P[o], \text{ and} \quad (11)$$

$$d/dt\ P[o\ o] = 2p\cdot P[x\ o] - c\ P[o\ o]\ P[x\ o]^2/P[o]^2$$

$$= [2p - c\ (P[o\ o]/P[o])\ (P[x\ o]/P[o])]\ (P[x\ o]/P[o])\ P[o]. \quad (12)$$

where c = 1 (4/3) for a square (cubic) lattices. To close these equations, we can use P[x] = 1 - P[o] and P[x o] = P[o] – P[o o] (where the latter follows from P[x o] + P[o o] = P[o]). However, it is more instructive to reformulate (11) and (12) by introducing the conditional probability, Q = P[o o]/P[o] and noting that P[x o]/P[o] = 1-Q. This leads to the equations

$$d/dt\ C = -p\ C + (1-Q)^2(1-C)\ , \text{ and} \quad (13)$$

$$d/dt\ [\ (1-C)Q\ ] = [2p - c\ Q(1-Q)](1-Q)(1-C), \quad (14)$$

Consequently, one obtains the steady-state relations:

$$pC - (1-Q)^2(1-C)\ = 0 \text{ and } c\ Q(1-Q) = 2p\ \text{ for active states,} \quad (15)$$

or C = 0 and Q =1 for the absorbing state. From Eq, (15), it follows that the bistability regime in the pair-approximation exists for $0 < p < p_s(\text{pair}) = c/8$ (the upper spinodal). Thus, one has $p_s(\text{pair}) = 1/8$ (1/6) for the square (cubic) lattices.

For the hexagonal lattice, the form of the equations in the pair-approximation differs since the sites in the "suitable connected filled pair" are neighboring sites. This introduces extra factors of P[x x] in the numerator in the pair approximation for P[o+2x], P[2o+2xE], and P[2o+2xS] (as well as compensating additional factors of P[x] in the denominator). We do not discuss this case further.

Finally, we discuss simulation results for the QCP on various lattices, and compare these with results from the above pair-approximation analysis. In general, appearance of bistability in a mean-field site-approximation or higher-order pair-approximation is suggestive of a discontinuous transition in a lattice-gas model. In the case of the QCP, this would correspond to a transition from a high-concentration active state for $0 \le p \le p_e$ to a particle-free "vacuum" or poisoned state for $p>p_e$. Note that the latter is an absorbing state. Since these models do not include particle diffusion, one expects relatively weak metastability. Consequently, the discontinuous transition at $p=p_e$ should occur only at a slightly lower p than the upper spinodal point $p=p_s$ (where one might anticipate that p_s can be predicted relatively accurately by the pair-approximation).

It should be noted that the situation can be more complex than suggested above. First, even when mean-field and higher-order approximations exhibit bistability, it is possible that fluctuations can "destroy" the discontinuous transition in the lattice-gas model. Second, if the QCP lattice-gas model does exhibit a discontinuous transition, previous studies for the square lattice suggest that there will be generic two-phase coexistence. This means that for a

finite range $p_f < p < p_e$, one can find an orientation varying continuously with p such that a planar interface separating active and vacuum state is stationary (i.e., an orientation-dependent version of equistability).

Previous simulation results for the QCP on a square lattice indicate a discontinuous transition with $p_e = 0.0944$. This p_e-value should be compared with $p_s(\text{pair}) = 1/8 = 0.125$ (and a simulation estimate of $p_s = 0.11$). In contrast, previous simulation results for the QCP on a hexagonal lattice reveal the absence of a discontinuous transition (presumably due to fluctuation effects). Instead, one finds a continuous transition at $p \approx 0.177$. Finally, we present new results for the QCP on a cubic lattice. Direct simulation reveals the existence of a stable active state for $0 \leq p \leq p_e$ where $p_e \approx 0.148$. See **Fig.6**. This p_e-value should be compared with $p_e(\text{pair}) = 1/6 = 0.166^{\bullet}$.

B. CUBIC CONTACT PROCESSES

We first provide a general definition and also some basic analysis of what might be viewed as a third version of Schloegl's model for autocatalysis on various lattices. We will however focus on analysis for the hexagonal lattice. This model might also be regarded as a Cubic Contact Process (CCP). In the CCP, particles undergo random spontaneous annihilation at fixed rate p. Particles are also created autocatalytically at empty sites at a rate proportional to the number of "suitably connected filled triples" on sites neighboring the empty site. It is convenient to choose a normalization for these creation rates so that the mean-field kinetics for the model will be independent of lattice type. We shall see that this goal is achieved by the choice of creation rate as k/k_{max}, where k is the number of suitably connected filled triples, and k_{max} is the maximum number of such filled triples. Note that "suitably connected filled pairs" corresponds to diagonal neighboring filled triples on the

square lattice, and to neighboring filled triples on the triangular lattice. Thus, we have k_{max} = 4 and 6 for square and triangular lattices, respectively.

However, the CCP is trivial on a square lattice since once a cluster of more than one empty site is formed, it can never shrink. This implies that the vacuum state is the only stable steady-state for all p>0. However, the model is non-trivial on a triangular lattice, supporting an active steady-state for a finite range of p. Thus, below we consider only this case. **Fig.7** provides a schematic of particle annihilation and creation rules and rates for the CCP on a triangular lattice.

Next, we present the mean-field kinetics of the particle concentration, C, for the CCP. These kinetics are obtained by ignoring all spatial correlations, so that the probability of multi-site configurations is simply given by a product of the relevant single site probabilities. For a triangular lattice, we obtain the kinetic equation:

$$\frac{dC}{dt} = -pC + \left[\begin{array}{l} 1\times\frac{6}{6}C^6(1-C) + 6\times\frac{3}{6}C^5(1-C)^2 \\ +\left(6\times\frac{2}{6}+6\times\frac{1}{6}\right)C^4(1-C)^3 + 6\times\frac{1}{6}C^3(1-C)^4 \end{array} \right]. \qquad (16)$$

The various contributions to the positive creation (gain) term on the RHS of eq.(16) correspond to different k as enumerated in **Fig.7**. Eq. (16) can be simplified to:

$$dC/dt = -pC + C^3(1-C). \qquad (17)$$

A significant feature of our rate choice is that it facilitates an exact reduction of the master equations which specify the exact dynamics of the CCP. Furthermore, this exact reduction not only immediately allows recovery of the lattice-independent mean-field kinetics, but also allows ready generation of higher-order approximations for the kinetics. We

demonstrate the latter for the so-called pair-approximation (whereas mean-field kinetics corresponds to the site-approximation).

The exact master equations for the CCP form an infinite coupled hierarchy for the evolution of the probability of a single filled site, a filled pair, etc. (or equivalently, one can consider empty configurations). Below, we let x (o) denote a filled (empty) site, and let P's denote probabilities of various configurations of such sites. For example, P[x]=C and P[xx] denote the probabilities of a single filled site and a filled pair, respectively. Similarly, P[o]=1-C and P[oo] denote the probability of a single empty site and empty pair, respectively. Conservation of probability implies that P[x]+P[o]=1, P[xo]+P[oo]=P[o], P[xx]+P[xo]=P[x], P[xx]+2P[xo]+P[oo]=1, etc. Then, in terms of probabilities for empty configurations, the exact master equations have the form

$$d/dt\ P[o] = p\cdot P[x] - \text{particle creation terms}, \tag{18}$$

$$d/dt\ P[oo] = 2p\cdot P[xo] - \text{particle creation terms, etc.} \tag{19}$$

The particle creation terms in each equation correspond to a sum over various relevant configurations multiplied by the appropriate rates. As an aside, we favor empty configurations in writing these equations by analogy with irreversible cooperative creation processes (i.e., processes without particle annihilation) where empty site configuration probabilities have certain special spatial Markov properties.

A schematic enumeration of the creation terms for eq.(18) is provided by **Fig.7** for the triangular lattices. Similar to eq.(16), an exact reduction is possible for these various terms. One can show that eq.(18) reduces exactly to the simple and intuitive equation

$$d/dt\ P[o] = p\cdot P[x] - P[o + 3x], \tag{20}$$

where the term P[o+3x] represents the probability of an empty site with a neighboring filled triple.

An enumeration of the creation terms for eq.(19) is rather lengthy for the triangular lattice. A partial listing is provided in **Fig.8a**. The empty sites in the pair share two neighbors, so one must enumerate configurations of all neighbors of both empty sites. One then determines the total rate of creation of particles at either site in the empty pair for each such configuration. An exact reduction of these desorption terms is also possible and yields for a triangular lattice

$$d/dt\ P[o\ o] = 2p\cdot P[x\ o] - 2/6\ P[2o+3xE] - 4/6\ P[2o+3xS], \qquad (21)$$

where the terms P[2o+3xE] and P[2o+3xS] represents probabilities of an empty pair where one site in this pair has a neighboring filled triple. There are two such distinct configurations, one where the filled triple is at the end of the empty pair (with probability denoted P[2o+3xE]), and the other where the filled triple is on the side of the empty pair (with probability denoted P[2o+3xS]). See **Fig.8b**.

Finally, we implement the pair-approximation to the above exact master equations for the QCP on various lattices. For this approximation, we obtain:

$$d/dt\ P[o] = p\cdot P[x] - (P[x\ \ o]^3\ P[x\ x]^2)/(P[o]^2\ P[x]^4) \text{ and} \qquad (22)$$

$$d/dt\ P[o\ o] = 2p\cdot P[x\ \ o] - 2/6\ (P[o\ o]\ P[x\ \ o]^3\ P[x\ x]^2)/(P[o]^2\ P[x]^4)$$

$$- 4/6\ (P[o\ o]\ P[x\ \ o]^4\ P[x\ x]^2)/(P[o]^3\ P[x]^5) \qquad (23)$$

To close these equations, we can use P[x] = 1 - P[o], P[x o] = P[o] – P[o o] (which follows from P[x o] + P[o o] = P[o]), and P[x x] = 1 – 2P[o] + P[oo] (which follows from P[x x] + P[x o] = P[x]).

Figures

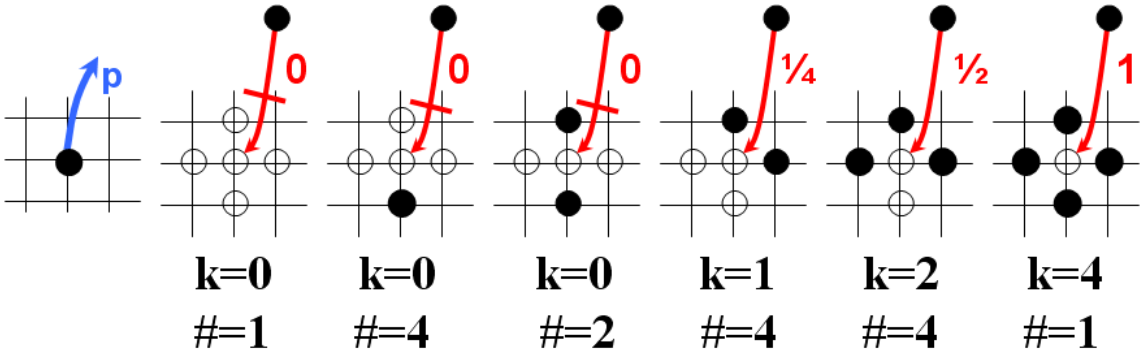

Figure 1. Schematic of particle annihilation and creation rules and rates (p and k/4) for the QCP on a square lattice. The configurational degeneracy (#) is also indicated.

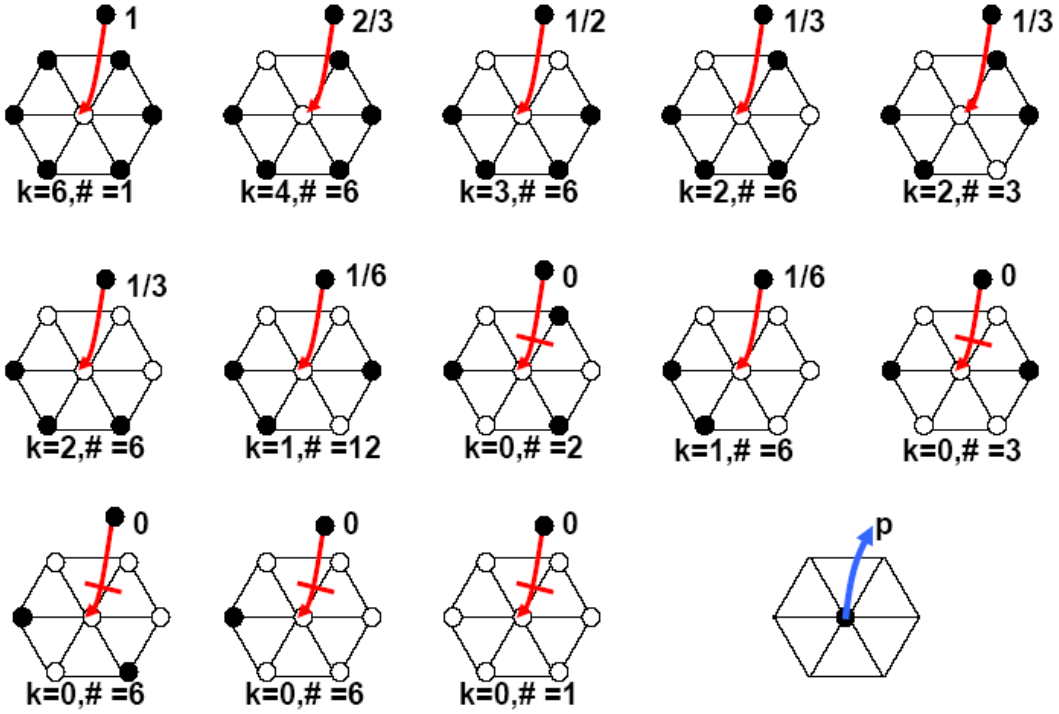

Figure 2. Schematic of particle annihilation and creation rules and rates (p and k/6) for the QCP on a triangular lattice. The configurational degeneracy (#) is also indicated.

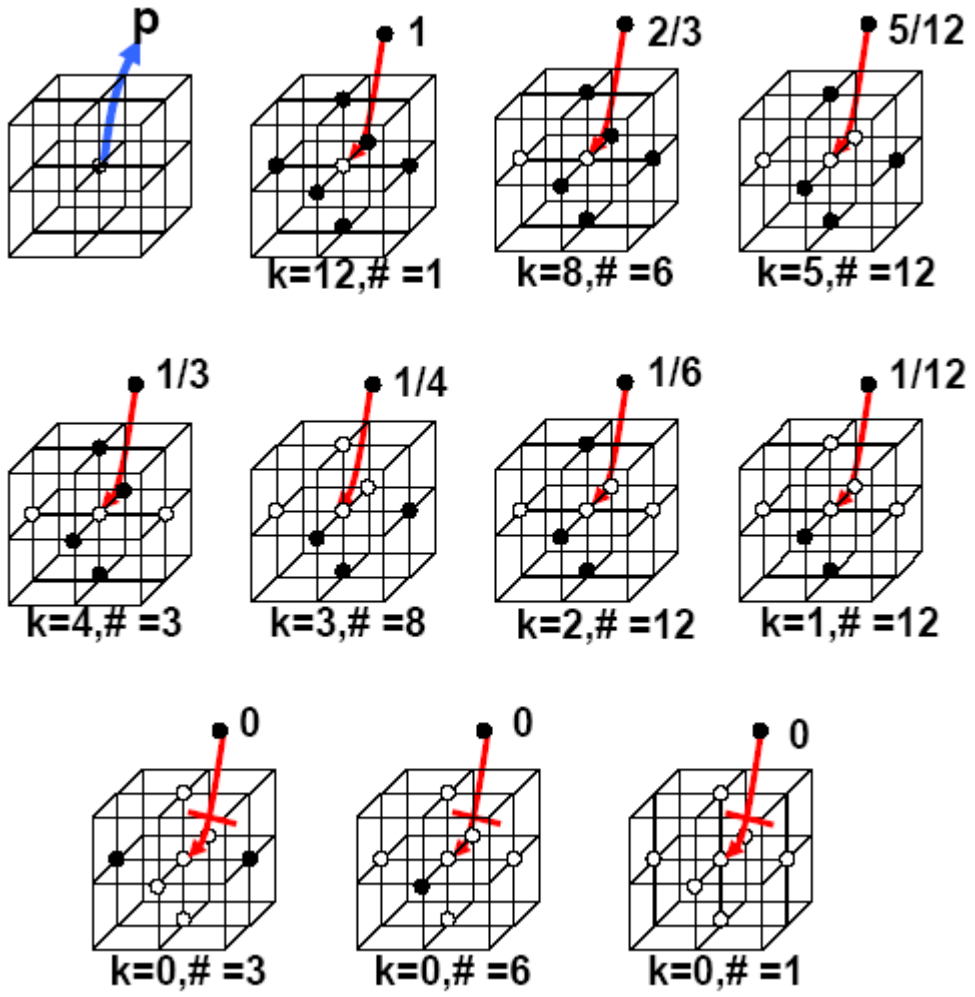

Figure 3. Schematic of particle annihilation and creation rules and rates (p and k/12) for the QCP on a cubic lattice. The configurational degeneracy (#) is also indicated.

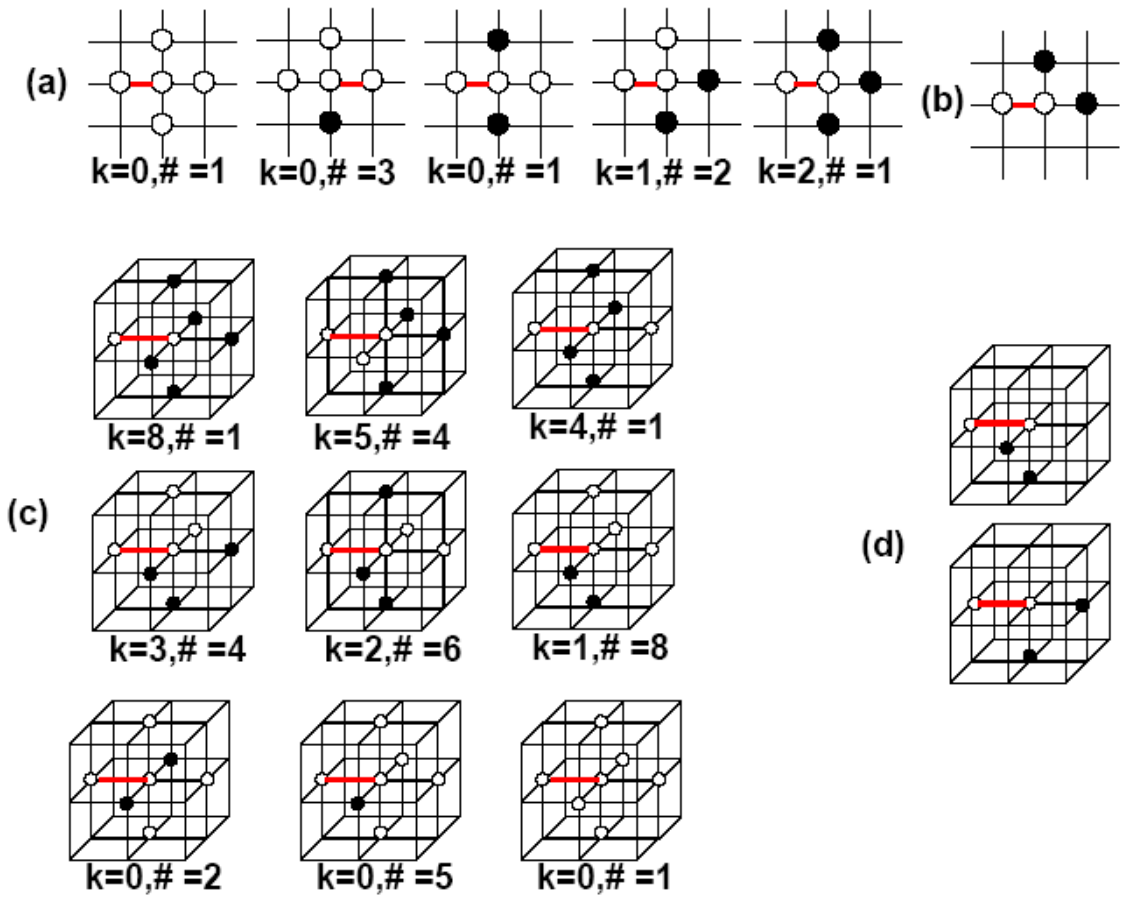

Figure 4. Configurations relevant for particle creation in the d/dt P[o o]-equation for the QCP on square (a) and cubic (c) lattices. Here, a thicker bond is drawn to indicate the empty pair on which we are considering particle creation. Also, k indicates creation rate and # the configurational degeneracy. The reduced form from summing these terms is also shown for the square (b) and cubic (d) lattice.

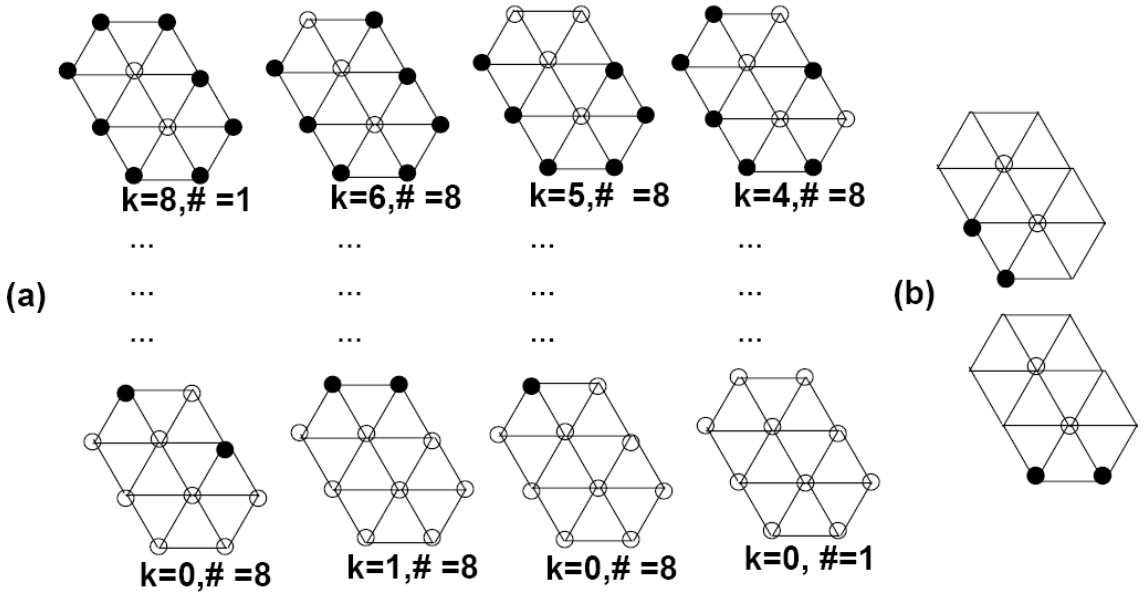

Figure 5. Partial listing of configurations relevant for particle creation in the d/dt P[o o]-equation for the QCP on triangular lattice (a). Here, it is the central empty pair on which we are considering particle creation. Also, k indicates creation rate and # the configurational degeneracy. The reduced form from summing these terms is also shown in (b).

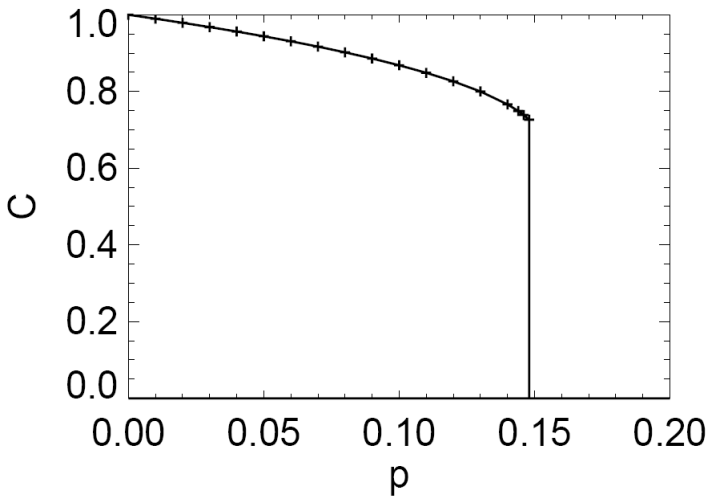

Figure 6. Simulation results for the steady-state particle concentration, C, versus annihilation rate, p, in the active state for the QCP on a cubic lattice. It follows that $p_e \approx 0.148$.

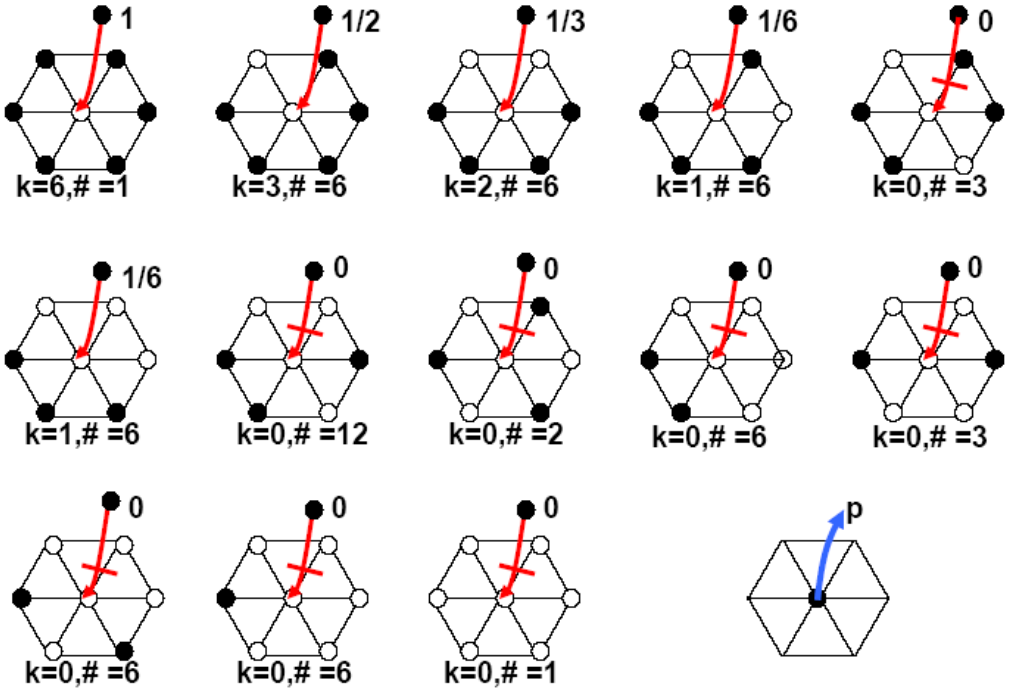

Figure 7. Schematic of particle annihilation and creation rules and rates (p and k/6) for the CCP on a triangular lattice. The configurational degeneracy (#) is also indicated.

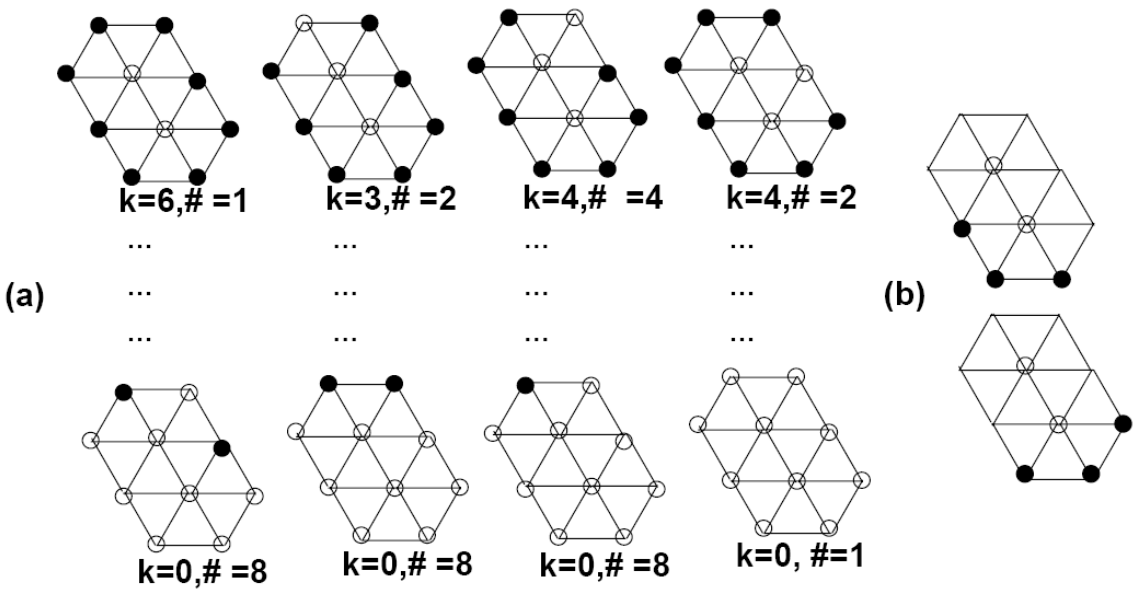

Figure 8. Partial listing of configurations relevant for particle creation in the d/dt P[o o]-equation for the CCP on triangular lattice (a). Here, it is the central empty pair on which we are considering particle creation. Also, k indicates creation rate and # the configurational degeneracy. The reduced form from summing these terms is also shown in (b).

ACKNOWLEDGEMENTS

I would like to take this opportunity to express my sincere thanks to Professor Jim Evans for his support, guidance, and encouragement throughout my graduate study and my life in Ames. I also would like to express my sincere gratitude to Dr. Da-jiang Liu for the guidance that he has given me along the way.

I also wish to thank my committee members for their efforts and contributions to this work: Professor Alex Travesset, Professor Ryan Martin, Professor Michael Smiley and Professor Edward Yu.

Finally, I am especially grateful for my parents, sisters and little brother for their constant support and encourage.